Multi-Energy Systems: Optimisation, Coordination, Offshore Applications and Techno-Economic Assessment

Miaorui Ma

Submitted in fulfilment of the requirements for the
Degree of Doctor of Philosophy

School of Engineering
College of Science and Engineering
University of Glasgow

February 2026

Abstract

The increasing penetration of renewable energy presents significant challenges to modern power systems due to the intermittency, uncertainty, and vulnerability to extreme weather conditions. Existing studies often address uncertainty modelling, system coordination, and offshore energy applications separately, with limited consideration of integrated optimisation frameworks that simultaneously improve operational flexibility, renewable energy utilisation, and long-term techno-economic performance under realistic environmental conditions. This thesis develops novel frameworks for modelling, optimisation, and techno-economic assessment of integrated multi-energy systems, with a focus on selected potential operational scenarios of microgrids, transmission–distribution coordination, and offshore energy islands, which are all tuned for the challenging renewable energy utilisation.

First, a multi-energy microgrid operational framework is proposed to integrate combined heat and power with renewable energy resources. A data-driven distributionally robust optimisation approach is adopted to address uncertainties in generation and demand. By combining day-ahead hourly scheduling with intra-day 15-minute dispatch, the framework enhances renewable utilisation, reduces operational costs, and achieves measurable carbon emission reduction by 10.6%.

Second, a coordinated optimisation model for transmission and distribution networks is developed, incorporating hydrogen-based energy storage. A mixed-integer linear programming formulation captures both physical characteristics and economic interactions, demonstrating improved flexibility and increased system revenues, which is 9.3% higher compared with uncoordinated cases. This coordination allows distributed energy resources contributing to higher-level system operations.

Third, the thesis investigates the techno-economic performance of offshore energy islands under coupled wind–wave conditions. High-fidelity OPENFAST simulations are applied to analyse power output and hydrogen production under varying wind speeds, revealing the sensitivity of revenues to extreme environmental conditions. Furthermore, a surrogate modelling approach based on Kriging is developed for floating energy islands, enabling efficient assessment of power generation and fatigue damage. Results highlight that optimal site selection can increase life-cycle profits by over 40%, demonstrating the significant impact of coupled environmental conditions on

the techno-economic performance of floating offshore energy islands.

Overall, this thesis contributes knowledge in: (1) advancing the optimisation of multi-energy microgrids subject to uncertainties, (2) proposing a coordinated transmission–distribution framework with hydrogen integration, and (3) developing techno-economic methodologies for offshore and floating energy islands. The findings provide theoretical and practical insights for the transition toward low-carbon, reliable, and sustainable energy systems.

Abbreviation List

ADMM	Alternating Direction Method of Multupliers
ANN	Artificial Neural Networks
AOP	Adaptive Overcurrent Protection
BS	Battery Storage
CB	Circuit Breaker
CFD	Computational Fluid Dynamics
CG	Controllable/Dispatchable Generator
CGs	Controllable Generators
CHP	Combined Heat And Power
CP	Carbon Penalty
C&CG	Column-And-Constraint Generation Algorithm
CSP	Concentrated Solar Power
CTI	Coordinated Time Interval
DK2	East Denmark Area
DR	Demand Response
DSO	Distribution System Operators
DRO	Distributionally Robust Optimisation
EH	Energy Hubs
ET	Energy Turbine
FOWT	Floating Offshore Wind Turbine
GT	Gas Turbine
IPSO	Improved Particle Swarm Optimization
IEA	International Energy Agency
IESs	Integrated Energy Systems
LCA	Life Cycle Analysis
LCP	Life Cycle Profit
LB	Lower Bound
LCOE	Levelized Cost Of Energy

LR	Lagrangian Relaxation
LV	Low-Voltage
MAE	Mean Absolute Error
MES	Multi-energy System
MILP	Mixed-Integer Linear Programming
MINLP	Mixed-Integer Non-Linear Programming
MPC	Model Predictive Control
MP	Main Problem
MV	Medium-Voltage
MRE	Mean Relative Error
MMG	Multi-Energy Microgrid
MMGs	Multi-Energy Microgrids
NMAE	Normalised Mean Absolute Error
NREL	National Renewable Energy Laboratory
OWT	Offshore Wind Turbine
PV	Photovoltaic Cells
P2H	Power-To-Hydrogen
P2G	Power-To-Gas
PSO	Particle Swarm Optimization
RES	Renewable Energy Source
RO	Robust Optimisation
SDDP	Stochastic Dual Dynamic Programming
SO	Stochastic Optimisation
SOC	State-Of-Charge
SP	Sub-Problem
TSOs	Transmission System Operators
TLBO	Teaching Learning-Based Optimisation
TLP	Tension-Leg Platform
UB	Upper Bound
WAMS	Wide-area Measurement Systems
WTs	Wind Turbines

Contents

Abstract i

Abbreviation List iii

Acknowledgements xii

Declaration xiii

1 Introduction 1

1.1 Background and Motivation 1

1.2 Research Objectives and Major Contributions 6

1.2.1 Chapter 3: Data-Driven Decarbonising Scheduling of Multi-Energy Microgrids 7

1.2.2 Chapter 4: Coordinated Scheduling of Transmission and Distribution Networks 10

1.2.3 Chapter 5: Application and Techno-Economic Framework for Offshore Energy Island Design Considering Wind-Wave Conditions 10

1.3 Structure of the Thesis 12

1.4 List of Publications 16

2 Literature Review 17

2.1 Robust Scheduling for Multi-Energy Microgrids 17

2.1.1 Multi-Energy Systems 17

2.1.2 Mathematical Optimisation and Decomposition Methods 18

2.1.3 Comparison of Optimisation Problems with Uncertainties 23

2.1.4 Deterministic Operations of Microgrid Systems 24

2.1.5 Multi-Energy Operations Considering Uncertainties 26

2.1.6 Low-Carbon Performance with Uncertainties Considered 27

2.1.7 Research Gap 27

2.2 Coordinated Scheduling of Integrated Energy Systems . . . 28
2.2.1 Transmission and Distribution System Operators (TSOs and DSOs) . . . 29
2.2.2 Renewable Integration in Transmission Networks . . . 30
2.2.3 Multi-Energy Optimisation of Distribution Networks . . . 32
2.2.4 Research Gap . . . 32
2.3 Operation of Offshore Energy Islands under Extreme Weather Conditions . . . 33
2.3.1 Offshore Wind Systems and Floating Offshore Energy Islands . . . 33
2.3.2 Economic Optimisation of Offshore Wind System . . . 36
2.3.3 OpenFAST Framework and Applications . . . 36
2.3.4 Research Gap . . . 39
2.4 Techno-Economic Optimisation of Offshore Wind Systems . . . 41
2.4.1 Offshore Energy Islands - State-of-the-Art . . . 41
2.4.2 Offshore Wind Turbines . . . 42
2.4.3 Related Research on Offshore Wind Energy Life Cycle Economics and Fatigue Assessment . . . 44
2.4.4 Research Gap . . . 46
2.5 Summary . . . 47

3 Robust Scheduling for Multi-Energy Microgrids 49
3.1 System Description and Modelling . . . 50
3.1.1 Configuration of the MMG . . . 50
3.1.2 Component modelling . . . 50
3.2 Uncertainty Characterisation and DRO Formulation . . . 56
3.2.1 Mathematical Model of Day-Ahead Scheduling Problem . . . 56
3.2.2 Confidence Set of Day-Ahead Scheduling Model . . . 57
3.3 Mathematical Model of 2-Step Scheduling . . . 59
3.3.1 First Step: C&CG Method for Day-Ahead Scheduling . . . 59
3.3.2 Second Step: MPC Method for Intra-Day Scheduling . . . 60
3.4 Case Study Setup and Simulation Results . . . 63
3.4.1 DRO Uncertainty Modelling and Settings . . . 65
3.4.2 Day-Ahead Results and Discussion . . . 68
3.4.3 Result Comparison with RO/SO Methods . . . 70
3.4.4 Effects of Employing EH . . . 71
3.4.5 Impacts of Carbon Penalty . . . 73
3.4.6 Intra-Day Results and Discussions . . . 77
3.5 Discussions . . . 79

3.5.1 Interpretation of Key Findings . . . 79
3.5.2 Methodological Reflection . . . 80
3.5.3 Practical Implications for Low-Carbon Operation . . . 80
3.5.4 Limitations and Future Outlook . . . 81
3.6 Conclusions . . . 81

4 Coordinated Scheduling of Electricity and Hydrogen 83
4.1 Modelling of Hydrogen Components and Power Network Coordination . . . 84
4.1.1 Transmission Network Modelling . . . 86
4.1.2 Distribution Network Modelling . . . 89
4.1.3 Model Coupling and Coordination Strategy . . . 91
4.2 Case Study . . . 93
4.2.1 Description of Datasets and Simulation Settings . . . 93
4.2.2 Parameter Setting . . . 94
4.3 Numerical Results . . . 96
4.3.1 Hydrogen System Dynamics . . . 97
4.3.2 Economic Evaluation . . . 98
4.4 Discussions . . . 102
4.4.1 Practical Implications for Power-Hydrogen Integration . . . 102
4.4.2 Model Limitations and Future Extensions . . . 103
4.5 Conclusion . . . 104

5 Multi-Energy Island Optimal Operation under Extreme Weather 106
5.1 Optimal Operation of Offshore Energy Islands under Extreme Weather Conditions 106
5.1.1 Modelling Framework under Extreme Conditions . . . 107
5.1.2 Case Study and Engineering Insights . . . 110
5.1.3 Result Analysis . . . 117
5.1.4 Discussion of Key Findings and the Need for Long-term Evaluation . . . 122
5.2 Life-Cycle Analysis: Techno-Economic Optimisation and Evaluation of Offshore Wind Systems . . . 124
5.2.1 Fatigue Damage Assessment under Coupled Wind-Wave Conditions . . . 125
5.2.2 Economic Assessment of Energy Islands . . . 132
5.2.3 Techno-Economic Evaluation Methodology . . . 135
5.2.4 Case Study and Simulation Results . . . 137
5.2.5 Discussions . . . 152
5.2.6 Conclusions . . . 153

6 Conclusions and Future Research **155**

6.1 Cross-Chapter Synthesis and Discussion 155

6.1.1 Thematic Connection Across the Four Studies 155

6.1.2 Methodological and Policy-Level Reflections 156

6.2 Summary of Main Contributions 159

6.3 Limitations and Lessons Learned 160

6.4 Future Research Directions 161

6.5 Closing Remarks 162

List of Tables

2.1 Comparison of Mathematical Optimisation and Decomposition Methods for Multi-Energy Systems 21
2.2 Relationship Between Decomposition Algorithms and Uncertainty Modelling Paradigms 22
2.3 Comparison of Optimisation Approaches for Uncertainty Modelling 25
2.4 Comparison among Different Research Works on Management Strategies of MMGs 28
2.5 Comparison of Transmission and Distribution System Operators (TSOs and DSOs) 31
2.6 Comparison of Offshore Wind Systems and Floating Offshore Energy Islands . . . 35
2.7 Summary of OpenFAST Modules and Key Applications 40
2.8 Comparison of Fixed-bottom and Floating Offshore Wind Turbines 45

3.1 Generation and Load Power Ratings 65
3.2 Probabilities of Scenarios 66
3.3 Setting of Case Study Parameters 66
3.4 Result Comparison of Solving Methods 71
3.5 Cost and Carbon Impacts of CHP 73
3.6 Cost and Carbon Impacts of CP 74
3.7 Carbon Penalty of Power and Gas under Different Cases 74
3.8 Comparison between Time-Varying and Constant Carbon Prices 77
3.9 Intra-day Carbon Penalty Impact 79

4.1 Case Study Parameters 95
4.2 Comparison between Two Hydrogen Storage Placements 99

5.1 NREL 5MW OC3-Spar Hywind Parameters. 113
5.2 Case Study Parameters. 113
5.3 Comparison between Two Hydrogen Storage Placements. 121
5.4 TLP Parameters in OpenFAST Settings. 136
5.5 25-year Costs and Profit of Energy Islands for Three Platforms. 137

List of Figures

1.1 Global energy transition indicators under the 1.5°C scenario (adapted from IRENA, 2024). 2
1.2 Total installed cost, capacity factor and LCOE trends by technology, 2010 and 2023. 4
1.3 Major Objectives and Contributions of Chapters. 8

3.1 Framework of the 2-Step Approach and Research Methodology. 50
3.2 A Representative MMG Configuration. 51
3.3 Flow Chart of Day-ahead and Intra-day Scheduling. 62
3.4 33-Bus MMG System. 63
3.5 Internal Configuration of an EH. 64
3.6 Bus Voltage Variation Over 24 Hours. 65
3.7 10 Clustered Scenarios of RES. 67
3.8 Electricity Price Setting (P). 68
3.9 Day-Ahead Prediction Results. 69
3.10 Day-Ahead DRO Scheduling Results. 70
3.11 Robust and Stochastic Scheduling Results. 72
3.12 Internal Configuration of EH without CHP. 73
3.13 Day-Ahead Scheduling Results Comparison Under Conditions With And Without Carbon Penalty. 75
3.14 Carbon Penalty Impacts over 5 Cases. 76
3.15 Comparison between Day-ahead and Intra-day Power and Load Prediction. 78
3.16 Intra-day Optimal Scheduling Results. 79

4.1 Internal Configuration of Transmission and Distribution of Integrated Power and Hydrogen System 85
4.2 Reconstructed Transmission and Distribution Network Case 94
4.3 Energy Exchange between Distribution Networks 100
4.4 State-of-Charge of Three Hydrogen Storage Systems 101

5.1 Internal Configuration of Distribution of Integrated Power and Hydrogen System . 108
5.2 Construction of NREL 5MW OC3 Spar Hywind Model. 112
5.3 Cut-in Wind Condition: Time-Varying Parameters. 115
5.4 Rated Wind Condition: Time-Varying Parameters. 116
5.5 Cut-out Wind Condition: Time-Varying Parameters. 118
5.6 Power Output under Three Cases. 120
5.7 Time history of streamwise shear, transverse shear, vertical axial stress. 128
5.8 LHS data sets. 131
5.9 Energy island configuration. 132
5.10 Framework of the Dual Economic and Damage Assessment and Research Methodology. 138
5.11 The Location of Three Platforms. 139
5.12 Configuration of NREL TLP. 140
5.13 Short-term Damage of Environmental Data Sets. 141
5.14 Fatigue Damage Kriging Model Performance. 142
5.15 The Relationship between Wind, Wave, and Fatigue Damage. 144
5.16 1979-2003 Wind Rose. 145
5.17 1979-2003 Distribution of the Environmental Input Variables. 146
5.18 Three Wind Platforms 1979-2003 Joint Probability. 147
5.19 Wind Power Output of Environmental Data Sets. 148
5.20 Wind Turbine Life Cycle Profit vs Life Cycle Damage. 148
5.21 Wind Power Kriging Model Performance. 149
5.22 Three Wind Platforms 25 years (1979-2003) Wind Turbine Output Power. 150

6.1 Thematic Connection Across the Four Studies 157

Acknowledgements

I would like to express my sincere gratitude to my supervisor, Prof. Jin Yang, whose invaluable guidance, encouragement, and continuous support have inspired me to explore the academic world and gain precious experience throughout my PhD journey.

I am deeply grateful to Dr. Chengwei Lou for his insightful guidance on mathematical optimisation and modelling techniques. My sincere thanks also go to all my research group members for their companionship, collaboration, and generous help. I also acknowledge the use of AI-assisted language tools for proofreading and language refinement during the preparation of this thesis.

I would like to extend my appreciation to all the members of the James Watt School of Engineering for providing a supportive and stimulating academic environment. My thanks also go to Scottish Power Energy Networks for their support.

Finally, my heartfelt thanks go to my parents for their unconditional love, care, and unwavering support, both financially and emotionally. Their constant companionship, understanding, and encouragement have enabled me to complete this journey.

Declaration

The author hereby declares that this thesis is a record of work carried out in the James Watt School of Engineering at the University of Glasgow during the period from October 2022 to October 2025. With the exception of the chapters that contain introductory material, all work in this thesis was carried out by the author unless otherwise explicitly stated.

Chapter 1

Introduction

1.1 Background and Motivation

The twenty-first century has witnessed an accelerating and unprecedented transformation of the global energy landscape, driven by mounting concerns over climate change, energy security, and the depletion of fossil fuel reserves. The increasing frequency and severity of extreme weather events, rising sea levels, and the growing geopolitical instability associated with fossil fuel dependence have further underscored the urgency of transitioning towards a sustainable, low-carbon energy future. International agreements such as the Paris Agreement and the United Nations Sustainable Development Goals (SDGs) have established ambitious decarbonisation targets, urging countries to achieve net-zero greenhouse gas emissions by the middle of this century. According to the International Renewable Energy Agency (IRENA), renewable energy sources (RESs) must supply at least two-thirds of global primary energy demand by 2050 to limit the temperature rise to below 2°C [1, 2].

Recent global energy outlooks published by IRENA further quantify this transition through a set of key performance indicators (KPIs) that track progress in renewable energy deployment and energy efficiency improvements as shown is Fig. 1.1 [3]. Under the Planned Energy Scenario (PES), renewable electricity generation is expected to more than double from 8,440 TWh in 2022 to 16,504 TWh by 2030, while the 1.5°C Scenario projects an almost fivefold increase to over 82,000 TWh by 2050. Correspondingly, the share of renewables in global electricity generation is forecast to rise from 29% in 2022 to 73% by 2030 and exceed 90% by 2050, alongside a nearly tenfold expansion of installed renewable capacity.

Beyond the power sector, renewables are also expected to play a growing role in direct energy uses. The renewable share in the total final energy consumption (TFEC) is projected to be more than doubled by 2030 and to reach nearly 80% by 2050, supported by tripled modern

GLOBAL PERSPECTIVE	Historical		Planned Energy Scenario(PES)		1.5°C Scenario	
	2021	2022	2030	2050	2030	2050
KPI.01 REWEABLES (POWER)						
Renewable energy electricity generation (TWh/yr)	7873	8440	16504	38118	27358	82148
Renewable energy share in electricity generation (%)	28	29	46	73	68	91
Renewable energy installed capacity (GW)	3083	3391	6773	15835	11174	33216
Renewable energy share in installed capacity (%)	38	40	58	80	77	94

Figure 1.1: Global energy transition indicators under the 1.5°C scenario (adapted from IRENA, 2024).

use of bioenergy. Simultaneously, global energy intensity improvements must accelerate significantly—requiring an urgent doubling of the annual efficiency improvement rate by 2030—to align with a 1.5°C-compatible pathway. These indicators collectively illustrate the scale of systemic transformation required across all segments of the energy sector, encompassing electricity generation, direct fuel use, and energy efficiency, to meet mid-century decarbonisation goals.

Building upon this global transition trajectory, recent technological breakthroughs have played a pivotal role in accelerating the deployment of renewable energy systems and reshaping the economics of power generation. Over the past decade, rapid technological advances in renewable power generation and storage—particularly in wind, solar, biofuel, and battery technologies—have dramatically altered the global energy mix. As illustrated in Fig. 1.2, the total installed costs and levelised cost of electricity (LCOE) for major renewable technologies have declined sharply since 2010. Specifically, onshore and offshore wind technologies have seen cost reductions of around 70% and 63%, respectively, while solar photovoltaic (PV) systems have experienced a remarkable 90% decrease in LCOE. Concentrated solar power (CSP), another form of solar generation depicted in Fig. 1.2, has also achieved moderate cost reductions, benefiting from improved thermal storage integration and more efficient heliostat designs. CSP differs from conventional solar PV in that it uses mirrors or lenses to concentrate sunlight onto a small area, generating heat that drives a steam turbine for electricity production, which enables both high-temperature operation and dispatchable power supply, particularly valuable for smoothing daily solar variability.

These cost reductions, combined with moderate improvements in capacity factors, have made renewables cost-competitive sources of new generation in many regions. Countries such as China, Denmark, Germany, and the United Kingdom have emerged as global frontrunners, driven by forward-looking policies, large-scale demonstration projects, and growing public investment in renewable integration [4–6]. Among these, offshore wind energy stands out as a particularly promising technology. Offshore sites provide access to stronger and more persistent wind resources, minimal visual or land-use conflicts, and vast potential for utility-scale development close to coastal demand centres [7]. The deployment of offshore wind has consequently accelerated, with global installed capacity surpassing 65 GW by 2023 and projections indicating tenfold growth by 2050. These trends position offshore wind as a cornerstone technology for achieving national decarbonisation goals, supporting energy security, and ensuring a stable, renewable-dominated power supply.

Nevertheless, the rapid expansion of renewable energy has revealed the structural limitations of existing power systems, which were primarily designed around centralised, dispatchable fossil-fuel power generation. The intermittent and uncertain nature of renewable power generation poses operational challenges for maintaining real-time balance between supply and demand. Rapid fluctuations in output may cause renewable curtailment, necessitate increased reserves, and elevate

	Total installed costs (2023 USD/kW)			Capacity factor (%)			Levelised cost of electricity (2023 USO/kWh)		
	2010	2030	Percent change	2010	2030	Percent change	2010	2030	Percent change
Bioenergy	3 010	2 730	-9%	72	72	0%	0.084	0.072	-14%
Geothermal	3 011	4 589	52%	87	82	-6%	0.054	0.071	31%
Hydropower	1459	2 806	92%	44	53	20%	0.043	0.057	33%
Solar PV	5 310	758	-86%	14	16	14%	0.460	0.044	-90%
CSP	10 453	6 589	-37%	30	55	83%	0.393	0.117	-70%
Onshore wind	2 272	1 160	-49%	27	36	33%	0.111	0.033	-70%
Offshore wind	5409	2 800	-48%	38	41	8%	0.203	0.075	-63%

Figure 1.2: Total installed cost, capacity factor and LCOE trends by technology, 2010 and 2023.

balancing costs [8–10]. Simultaneously, the ongoing electrification of transport, heating, and industrial processes — exemplified by the rising penetration of electric vehicles (EVs) and heat pumps — has profoundly transformed demand profiles, increasing both the amplitude and volatility of load curves [11]. As these dynamics evolve, traditional grid operation paradigms are proving insufficient, necessitating more flexible, intelligent, and coordinated energy management strategies capable of operating under uncertainty while preserving economic efficiency and carbon reduction objectives.

In response to these challenges, the concept of multi-energy systems (MESs) has emerged as a powerful approach to enhance overall energy system flexibility and efficiency [12–14]. By integrating multiple energy carriers—electricity, gas, heat, hydrogen, and cooling—within a unified optimisation framework, MESs enable sector coupling, allowing energy to be converted, stored, and exchanged across domains. This holistic perspective improves resilience by exploiting complementarities between technologies; for instance, excess electricity from renewables can be transformed into heat or hydrogen, mitigating curtailment while strengthening system reliability. The energy hub concept provides a mathematical foundation for such coupling, allowing the modelling of energy conversion, demand response, and cross-vector storage with coordinated control [15]. As global energy systems become increasingly decentralised, MESs play a vital role in supporting the flexible and integrated operation of local, regional, and national grids.

However, as system complexity and interdependence grow, so too does the exposure to multi-dimensional uncertainty. The stochastic behaviour of renewable sources, fluctuating demands,

and varying market conditions all introduce significant operational and economic risks. Classical robust optimisation (RO) frameworks, while ensuring reliability under worst-case scenarios, often lead to overly conservative and suboptimal solutions, sacrificing economic performance [16]. On the other hand, stochastic optimisation (SO) depends heavily on precise probabilistic models, which may fail to capture rare or extreme conditions that are increasingly prevalent in a changing climate. To overcome these limitations, distributionally robust optimisation (DRO) has gained traction as a hybrid paradigm that balances robustness and flexibility by optimising decisions under an ambiguous probability distribution [17]. Recent applications of DRO in multi-energy microgrid (MMG) scheduling have shown its capacity to achieve a superior balance between cost, reliability, and emissions reduction—making it a key methodological innovation for next-generation energy systems.

Beyond local microgrids, the rapid growth of distributed renewables is fundamentally reshaping the interaction between transmission system operators (TSOs) and distribution system operators (DSOs). Increasing decentralisation means that actions taken at the distribution level—such as battery charging, hydrogen production, or demand-side management—can strongly influence system-wide stability at the transmission level [18, 19]. This growing interdependence calls for coordinated TSO–DSO optimisation frameworks, where multi-level decision-making ensures consistent and secure operation. Within this context, hydrogen energy storage has emerged as a particularly promising enabler of long-term system flexibility. Unlike batteries, hydrogen allows seasonal-scale energy storage, cross-sector coupling through power-to-gas (P2G) and power-to-hydrogen (P2H) technologies, and the potential to decarbonise industrial, transport, and heating sectors simultaneously [20]. The integration of P2H systems within MESs and network coordination frameworks thus represents a crucial step toward achieving a deeply decarbonised energy system.

In parallel, attention of larger-scale energy systems is turning to the offshore renewable energy domain, where the deployment of floating offshore wind turbines (FOWTs) is expanding access to deep-water resources previously beyond the reach of fixed-bottom installations [21]. However, this expansion introduces new engineering, environmental, and economic challenges, including greater exposure to extreme marine conditions, increased material intensity, and more complex maintenance logistics [22]. To ensure the long-term sustainability of these systems, life cycle assessment (LCA) approaches are essential. LCA-based evaluation allows for a holistic understanding of environmental and structural performance, accounting for energy use, emissions, and fatigue degradation across design, fabrication, operation, and decommissioning stages [23–25]. Incorporating such perspectives is particularly important as offshore infrastructure lifetimes extend and climate risks intensify.

The offshore energy island concept represents the next evolutionary step in the transition tra-

jectory. By integrating large-scale offshore wind generation with hydrogen production, energy storage, and interconnection capabilities, these islands serve as multi-energy offshore hubs that enable electricity-to-hydrogen conversion, cross-border energy trade, and enhanced grid flexibility. In addition to improving operational efficiency and resilience, offshore energy islands can facilitate the export of clean energy and hydrogen to continental markets, contributing to regional energy security and decarbonisation goals. Evaluating their techno-economic feasibility, structural reliability, and long-term sustainability is therefore essential for informing future offshore planning and investment strategies.

In summary, despite the significant progress made in renewable integration, key challenges remain unresolved—ranging from the short-term operational uncertainty of multi-energy microgrids, to the multi-level coordination required between transmission and distribution systems, and finally to the long-term techno-economic and structural optimisation of offshore energy infrastructures. Each of these challenges embodies distinct temporal and spatial characteristics, yet they share a common goal: to enhance the resilience, efficiency, and sustainability of future energy systems. This thesis is motivated by the multi-layered challenges and opportunities presented by the global energy transition—from managing renewable energy uncertainties in multi-energy off-grid systems, to enabling coordinated grid transmission–distribution optimisation through hydrogen integration, and finally to designing and assessing offshore hybrid energy islands that can withstand extreme environmental conditions.

Accordingly, the thesis is structured to address these interrelated problems in a systematic and hierarchical manner. It begins with the optimisation of low-carbon microgrid operations under uncertainty, extends the analysis to the coordination of multi-energy systems across network levels with hydrogen integration, and culminates in the design and evaluation of offshore hybrid energy islands that combine renewable power generation with hydrogen production and storage. The following section presents the research objectives and major contributions of this work, outlining how each chapter collectively contributes to advancing the state-of-the-art in renewable energy modelling, optimisation, and sustainable offshore energy system development.

1.2 Research Objectives and Major Contributions

From the above research background and motivation detailed, the overarching aim of this thesis is to develop comprehensive modelling and optimisation frameworks for MESs that operate under a high penetration of RESs, while explicitly accounting for the influence of weather conditions and environmental uncertainties. The global transition to low-carbon energy has introduced significant operational challenges—chiefly due to the variable nature of renewable power generation—which

requires the development of sophisticated models capable of accurately representing systems with balanced efficiency, reliability, and sustainability.

At the heart of this research lies the recognition that renewable energy integration fundamentally changes how modern power systems are planned and operated. The increasing coupling between electricity, hydrogen, and thermal networks introduces multiple temporal and spatial layers of interdependence. In such systems, weather condition variability—ranging from mild fluctuations in wind and solar irradiance to extreme meteorological events—can profoundly affect energy dispatch, storage dynamics, and even the structural safety of offshore infrastructures. Addressing these emerging complexities requires not only advanced optimisation and control algorithms but also novel methodological frameworks that combine physical realism, economic rationality, and computational tractability.

Against this backdrop, two key scientific questions form the foundation of the thesis:

1. How can optimal scheduling of multi-energy systems be achieved at both the transmission and distribution levels under conditions of deep renewable uncertainty and system-level interdependence?

2. How do extreme weather events influence the power output, structural integrity, and long-term fatigue performance of offshore wind turbines, and how can these effects be modelled to ensure operational resilience and device reliability?

To address these questions, the thesis consolidates and extends the principal outcomes of this doctoral research into a unified body of work, as structurally illustrated in Fig. 1.3. The figure outlines the thematic progression from multi-energy microgrid optimisation to coordinated transmission–distribution scheduling and, finally, to offshore energy island assessment—each layer contributing to the overarching goal of developing resilient and low-carbon energy systems. Detailed contributions of each chapter are presented in the following subsections.

1.2.1 Chapter 3: Data-Driven Decarbonising Scheduling of Multi-Energy Microgrids

The first strand of research, presented in Chapter 3, proposes a novel decarbonising data-driven robust optimal scheduling framework for MMGs. The system under study comprises wind turbines (WTs), photovoltaic (PV) cells, controllable generators (CGs), battery storage systems, and energy hubs. The objective of the proposed framework is to minimise the daily total cost over a 24-hour horizon, which includes the cost of power and gas transactions, CG operational costs, battery storage charging and discharging costs, as well as carbon costs. Unlike existing works that typically emphasise individual components, this framework integrates all major elements of an MMG with

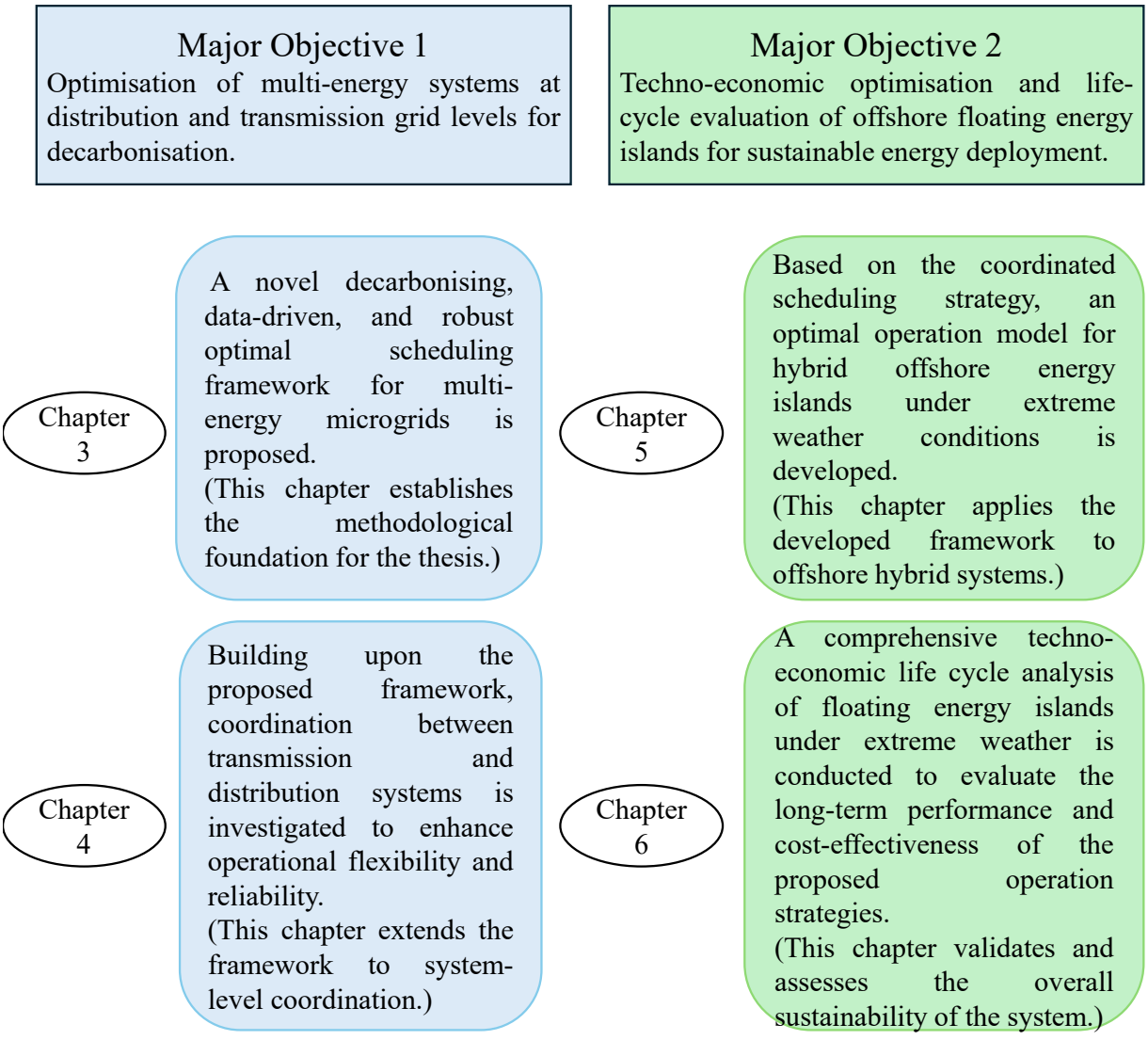

Figure 1.3: Major Objectives and Contributions of Chapters.

explicit treatment of uncertainty, thereby capturing the complexity of real-world operations while highlighting the importance of carbon reduction requirements. Table 2.4 provides a comparison with existing studies, demonstrating the comprehensive consideration of this approach.

The framework is based on a two-step methodology, as illustrated in Fig. 3.1. First, the day-ahead scheduling is formulated as a distributionally robust optimisation (DRO) problem and solved using the column-and-constraint generation (C&CG) algorithm. This step generates hourly dispatch plans while accounting for uncertainty distributions derived from clustered historical data of renewable energy sources and load demand. Subsequently, in the intra-day scheduling phase, model predictive control (MPC) is employed to adjust decisions every 15 minutes in order to align with the day-ahead schedule. This dual-stage structure reduces discrepancies between planned and actual operations, thereby minimising scheduling losses and improving the reliability of system operation. Overall, this approach establishes an innovative scheduling paradigm that integrates advanced algorithms into a multi-temporal, multi-energy MMG framework, with specific attention to uncertainty modelling and decarbonisation.

The major contributions of Chapter 3 can be summarised as follows:

- MMG with operational uncertainty fully considered:

  To enhance the cost-effectiveness of grid dispatch operations and minimize energy waste, this chapter focuses on a novel approach that rigorously addresses uncertainties inherent in both day-ahead and real-time grid dynamics. Specifically, our model incorporates factors such as RES outputs and load fluctuations and aligns the MMG more closely with complex real-world scenarios, which not only contributes to a more reliable MMG but also significantly improves its practical applicability.

- Carbon penalty (CP) proposed in combination of considering the above uncertainty:

  Considering the uncertainties of the MMG, the concept of CP is proposed. This CP is calculated based on carbon factors associated with different energy sources and is optimized as part of the objective function. Additionally, the carbon emissions and costs under different carbon prices are analysed to achieve an optimal solution for reducing total costs and carbon emissions.

- Proposed multi-temporal method with adapted algorithms:

  To implement the model put forth in this chapter, the advanced and efficient DRO method is employed. Additionally, the C&CG algorithm is leveraged to derive the optimal solution for hourly day-ahead power grid dispatching. In a bid to validate its real-time applicability, the intra-day dispatch results in 15-minute intervals are calculated through the utilization of the MPC algorithm, achieving optimal intra-day scheduling.

1.2.2 Chapter 4: Coordinated Scheduling of Transmission and Distribution Networks

Building on the microgrid-level insights from Chapter 3, Chapter 4 extends the analysis to the system level by introducing a coordinated transmission–distribution optimisation framework. The motivation for this work stems from the growing interdependence between system layers as distributed resources become increasingly active in balancing and ancillary services. Without coordination, local optimisation at one level (e.g., distribution) can conflict with global system objectives at another (e.g., transmission). The contributions of Chapter 4 can be summarised:

- Enhanced operational flexibility by bi-directional energy exchange: To resolve this tension, Chapter 4 introduces a novel power-to-hydrogen (P2H) integrated scheduling framework that introduces hydrogen storage capabilities at both transmission and distribution levels. The inclusion of hydrogen as a multi-functional energy carrier enhances operational flexibility by providing seasonal-scale storage, absorbing surplus renewable generation, and coupling the power system with the emerging hydrogen economy.
- Yield higher revenue after coordination between different network level: The proposed framework is formulated as a multi-objective optimisation problem, balancing the maximisation of annual revenue from both electricity and hydrogen sales against the minimisation of grid electricity purchase costs. Through comparative analysis, the study demonstrates that situating electrolyser and hydrogen storage units at both the production and consumption ends yields higher economic efficiency and smoother power flows across the network. This work thus contributes an important step towards multi-level system coordination and offers valuable insights into the design of integrated low-carbon power systems.

1.2.3 Chapter 5: Application and Techno-Economic Framework for Offshore Energy Island Design Considering Wind-Wave Conditions

The final research strand, presented in Chapter 5, further advances this line of research by developing a novel techno-economic framework for offshore energy island design and site selection. Unlike conventional methods that treat economic and structural aspects in isolation, this framework integrates wind-wave environmental conditions to jointly assess economic viability and structural resilience. By explicitly incorporating environmental forces into the analysis, the framework provides a more robust evaluation of site-specific conditions. Furthermore, the chapter introduces a

detailed scenario centred on P2H conversion with hydrogen storage, supported by advanced electrolyser modelling to optimise energy transformation and transportation. To address computational challenges, Kriging surrogate models validated against OpenFAST simulations are employed, enabling accurate predictions of turbine power output and fatigue damage with significantly reduced computational effort. The contributions of Chapter 5 are threefold:

- Development of a Techno-Economic Framework for Optimal Energy Island Location:

  This chapter presents an innovative techno-economic framework for selecting the optimal location of offshore energy islands. Unlike conventional methods, the proposed framework integrates wind-wave environmental conditions with economic considerations and structural damage risks to support multi-dimensional decision-making. A comprehensive assessment model has been developed to incorporate site-specific wind speed, wave height, whilst predicting fatigue damage to quantify their combined impact on energy island performance, lifespan, and maintenance costs. By employing advanced optimisation algorithms, this framework significantly enhances the computational efficiency of location evaluation under complex environmental conditions with a large volume of datasets. The approach addresses critical gaps in existing studies by coupling environmental, economic, and structural parameters, providing a robust foundation for the design and planning of future offshore energy islands.

- Application of Kriging Surrogate Models Validated by OpenFAST for Dual-Assessment:

  To address the challenges of predicting fatigue damage and power output under diverse environmental conditions, this study employs Kriging surrogate models, which have been validated against high-fidelity OpenFAST simulations. Unlike conventional approaches, our method leverages real historical environmental datasets, ensuring a high degree of practical relevance and accuracy. The Kriging models have been trained and tested using these datasets, enabling rapid and precise predictions of turbine performance and structural fatigue. By significantly reducing the computational effort required for direct simulation, while maintaining high accuracy, the proposed method facilitates the analysis of long-term fatigue damage and power generation even with limited computational resources. This chapter demonstrates a practical and scalable approach to enhance the design and operational reliability of offshore wind turbines, showcasing the advantages of integrating validated surrogate models with real-world data in offshore renewable energy research.

- Establishment of a Comprehensive Evaluation Case with Real Historical Environmental Data for Benchmark Simulations:

This chapter also establishes a detailed modelling and simulation benchmark that leverages real historical wind and wave datasets derived from multiple floating offshore wind platforms in the North Sea. Unlike previous studies that rely primarily on synthetic or simplified environmental inputs, our work integrates site-specific meteorological and oceanographic conditions to model the performance of proposed energy island scenarios with high fidelity. By incorporating authentic operational data and referencing actual floating wind farm configurations, this benchmark enables realistic simulations of power outputs and fatigue damages over the full life cycle of the energy island infrastructure. The simulation results are used to conduct a dual assessment of economic performance and fatigue-related structural degradation, providing actionable insights into long-term operational costs, maintenance planning, and system reliability. This contribution delivers a valuable reference framework for future research and industrial applications seeking to evaluate offshore energy islands under real-world conditions.

Overall, this chapter demonstrates how advanced optimisation methods, integrated modelling frameworks, and surrogate-based prediction tools can jointly address the dual challenges of renewable uncertainty and extreme environmental conditions. The overarching objective of this thesis is to mitigate the negative impacts of renewable energy uncertainty on multi-energy microgrids and offshore renewable systems, particularly those related to energy waste and carbon emissions. By systematically addressing uncertainty across microgrid, network, and offshore contexts, the research contributes to building resilient, efficient, and low-carbon energy systems of the future.

By outlining the progression from methodological development to practical application, this section contextualises the contributions of each chapter and highlights the interconnected nature of the research presented herein. Building on these research objectives and key contributions, a clear roadmap of the thesis is provided. The following section details the structure of the thesis, describing the logical flow of each chapter and how they collectively address the challenges of renewable integration, system optimisation, and offshore energy island design.

1.3 Structure of the Thesis

The thesis is organised as follows.

Chapter 2: Literature Review

A comprehensive review of existing literature is provided in Chapter 2, focusing on the state-of-the-art research related to robust scheduling of multi-energy microgrids, coordinated scheduling of integrated energy systems, and the techno-economic operation of offshore energy islands.

First, the review discusses deterministic and stochastic optimisation approaches for multi-energy microgrids. While early studies primarily emphasise cost minimisation and energy efficiency, recent works have started to incorporate environmental objectives, such as carbon emission reduction. However, these studies often neglect the high degree of uncertainty associated with renewable energy generation, which significantly limits their applicability in real-world scenarios.

Second, the review highlights research on the coordination of transmission and distribution networks under increasing renewable penetration. Particular attention is given to the role of hydrogen as a long-term energy storage option and as a flexible ancillary service. Although hydrogen integration has shown strong potential in enhancing operational flexibility, most studies remain limited to distribution-level optimisation and lack system-wide coordination mechanisms between TSOs and DSOs.

Third, the review examines the emerging research on offshore energy islands, which combine offshore wind generation with energy conversion and storage technologies, particularly power-to-hydrogen systems. Offshore environments introduce unique challenges, including extreme weather conditions, harsh marine environments, and high operational costs. While several techno-economic assessments have been carried out, only a few studies incorporate dynamic modelling tools, such as OpenFAST, to capture the structural and economic impacts of wind-wave interactions.

Across these domains, a consistent research gap is identified: the lack of integrated, low-carbon scheduling frameworks that simultaneously consider multi-temporal resolution, renewable uncertainties, system-level coordination, and offshore environmental challenges. This gap underscores the motivation of this dissertation, which aims to develop advanced optimisation models and frameworks that enhance both economic efficiency and environmental sustainability in future low-carbon energy systems.

This chapter is organised as follows. Section 2.1 reviews the related works on robust scheduling approaches for multi-energy microgrids. Section 2.2 discusses existing studies on the coordinated scheduling of integrated energy systems. Section 2.3 examines previous research concerning the operation of offshore energy islands under extreme weather conditions. Section 2.4 presents a review of the techno-economic optimisation of offshore wind energy systems.

Chapter 3: Robust Scheduling for Multi-Energy Microgrids

This chapter presents the modelling framework of a multi-energy system that integrates diverse energy carriers, including electricity, hydrogen, natural gas, and heat. To address operational uncertainties while ensuring both economic efficiency and system reliability, a DRO approach is employed. The DRO method combines the cost-effectiveness of stochastic optimisation with the conservativeness of robust optimisation, thereby enabling optimal energy dispatch even under adverse conditions. Furthermore, a multi-temporal scheduling framework with adapted algorithms is developed, explicitly accounting for carbon emission reduction targets as well as uncertainties in

renewable generation and load demand. The overall aim of this chapter is to mitigate the adverse impacts of renewable energy uncertainty on multi-energy microgrids, such as excessive energy curtailment and increased carbon emissions.

This chapter is organised as follows. Section 3.1 introduces the modelling of the multi-energy microgrid (MMG). Section 3.2 discusses the characterisation of uncertainties and presents the DRO formulations. Section 3.3 develops the mathematical models for day-ahead and intra-day scheduling. Section 3.4 details the case study setup and analyses the corresponding simulation results. Section 3.5 discusses the key findings and limitations. Finally, Section 3.6 summarises the main findings of the chapter.

Chapter 4: Coordinated Scheduling of Integrated Electricity and Green Hydrogen Systems

This chapter presents a new economic-oriented optimisation for the coordinated scheduling of power transmission and distribution systems, with a particular focus on integrating green hydrogen storage with offshore wind energy. The designed objective is to maximize annual revenue by considering both electricity and hydrogen revenues while reducing electricity purchase costs. With a case study, the optimal results of the coordinated system are obtained and analysed. This is compared with results for a system that employs a single storage system located only at the production side. This comparison highlights the economic advantages of situating electrolyzers and hydrogen storage systems at both the production and consumption ends, and improved coordination between the transmission and distribution of electricity.

This chapter is organised as follows. Section 4.1 introduces modelling of hydrogen components and power network coordination. Section 4.2 presents the optimisation framework and case studies. Section 4.3 discusses the numerical results of the case study. Section 4.4 discusses the key findings and limitations. Finally, section 4.5 concludes this chapter.

Chapter 5: Application and Techno-Economic Evaluation of Offshore Energy Systems under Environmental Factors

This chapter introduces a novel framework for optimising wind power dispatch in offshore energy islands, integrating wind energy conversion into hydrogen through electrolysis, followed by storage and transportation. Using OPENFAST simulations, the framework captures the dynamic behavior of floating wind turbines, accounting for wind-wave interactions and extreme offshore conditions. The “power-to-hydrogen" approach addresses wind power intermittency and enables long-term energy storage, transforming offshore energy islands into regional energy hubs. Key contributions include the optimisation of power dispatch under extreme weather conditions and the use of high-fidelity wind power simulations to enhance decision-making precision and reliability, ensuring resilient and efficient renewable energy systems.

Additionally, the application section of the long-term evaluation of a floating energy island pro-

poses a comprehensive techno-economic assessment framework for optimal offshore energy island site selection, emphasising both economic efficiency and structural resilience. By integrating the dynamic interaction of wind and wave conditions, the framework improves decision-making accuracy to ensure that selected locations are both cost-effective and environmentally robust. Additionally, a novel multi-energy island scenario is introduced, featuring detailed hydrogen production and storage modelling to enable efficient electricity-to-hydrogen conversion and flexible energy transport. To evaluate operational performance and life cycle sustainability, the study employs Kriging surrogate models, validated using OpenFAST simulations. These models predict turbine power output and fatigue damage across varying environmental conditions, including wind speed, wave height, and wave period. This integration significantly advances the optimisation process by allowing long-term behavior prediction while minimizing computational costs. Furthermore, real historical environmental datasets and multiple floating offshore wind platforms are utilized for simulation benchmarks, enhancing the framework's practical relevance. The results demonstrate substantial improvements in life cycle profit and structural reliability through optimal site selection. Ultimately, the framework provides a practical and scalable reference for planning offshore renewable energy systems, supporting the development of sustainable, resilient, and economically viable offshore energy islands in dynamic marine environments.

This chapter is organised as follows. Section 5.1.1 introduces a modelling framework under extreme conditions. Section 5.1.2 presents the engineering insights and case studies. Section 5.1.3 discusses the numerical results of the case study. Section 5.1.4 discusses the key findings and future research. For the long-term evaluation of energy islands under extreme weather conditions, Section 5.2.1 introduces the modelling framework for fatigue damage assessment under coupled wind–wave conditions. Section 5.2.2 presents the economic assessment of the proposed energy island configuration. Section 5.2.3 develops the techno-economic evaluation methodology. Section 5.2.4 describes the case study setup and analyses the corresponding simulation results. Section 5.2.5 discusses the key findings and limitations. Finally, Section 5.2.6 summarises the key findings of the chapter.

Chapter 6: Conclusion and Future Work

The final chapter synthesises the main findings and contributions of the thesis, drawing together insights from the four core studies to provide a coherent understanding of uncertainty management, system coordination, and offshore infrastructure planning. It highlights how the proposed frameworks collectively advance both methodological and practical aspects of low-carbon energy system optimisation, ranging from microgrid operations to large-scale offshore energy islands. In addition to summarising the principal contributions, this chapter critically reflects on the limitations of the research, such as modelling simplifications, data dependency, and the scope of hydrogen value chain assumptions. Finally, it outlines several promising avenues for future research, including

advanced uncertainty modelling, real-time coordination strategies, integrated hydrogen economy analysis, and resilience under extreme events. In doing so, the chapter positions the thesis not only as a contribution to current knowledge, but also as a foundation for further investigations into sustainable and resilient energy systems.

1.4 List of Publications

The publications produced from this PhD research work are listed in this section as follows:

1. Miaorui Ma, Chengwei Lou, Xiangmin Xu, Jin Yang, Jake Cunningham, and Lu Zhang. Distributionally robust decarbonising scheduling considering data-driven ambiguity sets for multi-temporal multi-energy microgrid operation. Sustainable Energy, Grids and Networks, 38:101323, 2024.

2. Miaorui Ma, Chengwei Lou, Lingte Chen, and Jin Yang. A Framework for Life-Cycle Profit-Damage Assessment of Floating Multi-Energy Islands with Wind-Wave Dynamics Integration. Renewable Energy, 262:125412, 2026.

3. Miaorui Ma, Yue Qi, Jin Yang, and James Yu. Protection insights from optimal operation of offshore energy islands under extreme weather conditions. IET Conference Proceedings CP916, pages 240–245, 2025.

4. Miaorui Ma, Jin Yang, and Chengwei Lou. Scheduling optimisation of integrated electricity and green hydrogen storage system for power transmission-distribution coordination. In 2024 IEEE PES Innovative Smart Grid Technologies Europe (ISGT EUROPE), 2024.

5. Miaorui Ma, Chengwei Lou, Lingte Chen, and Jin Yang. Operational scheduling of offshore wind-to-hydrogen energy islands under physical dynamic constraints validated via EMT co-simulation (under preparation).

Chapter 2

Literature Review

2.1 Robust Scheduling for Multi-Energy Microgrids

2.1.1 Multi-Energy Systems

Multi-energy systems are increasingly recognised as a key pathway of the global transition towards low-carbon energy infrastructures. Broadly defined, MES integrates multiple energy carriers—such as electricity, heat, gas, and hydrogen—within a coordinated framework to enhance overall energy efficiency, system flexibility, and reliability [12, 13, 26]. The conceptualisation and deployment of MES have been strongly influenced by national and international policy targets, particularly those aimed at reducing greenhouse gas emissions and achieving climate neutrality [27–29].

At the international level, the European Union's *Clean Energy Package* and the EU Hydrogen Strategy emphasise the integration of renewable energy with sector coupling, including electricity, heating, and transport, to achieve the 2030 and 2050 climate goals [30, 31]. These policies explicitly encourage the deployment of MES as a tool to enhance flexibility in electricity networks while supporting the broader adoption of hydrogen as an energy vector. Similarly, the International Energy Agency (IEA) defines MES as systems that enable the simultaneous management and optimisation of multiple energy carriers to meet demand, reduce emissions, and improve energy security [13, 32].

In Asia, China has also recognised the strategic importance of MES in its *13th and 14th Five-Year Plans*, promoting the development of integrated energy networks that combine renewable generation, energy storage, and flexible loads to decarbonise urban and industrial sectors [33]. These plans emphasise distributed energy resources, microgrid technologies, and the integration of hydrogen to enhance regional energy security and resilience. Denmark, as a global leader in

renewable integration, has developed national strategies for combined heat and power (CHP) and district heating networks, which are increasingly coordinated with large-scale offshore wind and hydrogen projects to facilitate sector coupling [34, 35].

In the United Kingdom, government strategies such as the *Net Zero by 2050* plan and the *UK Hydrogen Strategy* highlight MES as a means to optimise the interaction between electricity, heating, and transport sectors, while enabling large-scale integration of intermittent renewable sources [36]. These strategies promote research and demonstration projects that integrate multi-energy storage and flexible generation, including the use of hydrogen as a seasonal storage medium.

Overall, the policy landscape across Europe, Asia, and the UK consistently positions MES as a critical pathway to achieving decarbonisation and energy security targets. By integrating multiple energy vectors, MES are expected to play a central role in facilitating sector coupling, enabling renewable energy penetration, and supporting the development of a low-carbon energy economy.

2.1.2 Mathematical Optimisation and Decomposition Methods

The optimisation of multi-energy microgrids and hybrid energy systems requires the simultaneous coordination of heterogeneous energy carriers—typically electricity, heat, hydrogen, and natural gas—under a diverse set of technical, economic, and operational constraints. These systems are inherently large-scale, highly coupled, and often involve both continuous and discrete decision variables. As a result, their mathematical representation frequently leads to Mixed-Integer Linear Programming (MILP) or Mixed-Integer Nonlinear Programming (MINLP) formulations, which become computationally intractable when solved directly, especially in the presence of temporal coupling, stochastic uncertainty, and distributed system architectures. To overcome these challenges, a range of mathematical decomposition and coordination techniques has been developed, enabling scalable solution methods that retain solution optimality or near-optimality while significantly reducing computational burden.

Benders Decomposition and Its Extensions

Benders decomposition, originally developed for large-scale linear programming problems, has been widely adopted in energy system scheduling and planning due to its ability to exploit separable problem structures [37]. In multi-energy microgrids, this method partitions the original optimisation problem into a master problem—typically governing investment or commitment decisions—and one or more subproblems that address operational dispatch under different scenarios [38]. This decomposition allows subproblems to be solved in parallel, substantially enhancing

computational efficiency. Extensions of classical Benders decomposition integrate stochastic or robust formulations, leading to methods such as Stochastic Dual Dynamic Programming (SDDP) and Benders-like decomposition for multi-stage decision-making [39]. These approaches are particularly effective for robust scheduling, as they enable scenario-based representation of uncertainties without exponentially increasing problem size.

Column-and-Constraint Generation (C&CG)

The Column-and-Constraint Generation (C&CG) algorithm is a decomposition-based method specifically designed for solving robust optimisation problems characterised by a bi-level min–max structure [40]. In such formulations, the outer minimisation determines the first-stage decisions, while the inner maximisation identifies the worst-case realisation of uncertain parameters within a defined uncertainty set. The C&CG method alternates between solving a *master problem*—which includes only a subset of uncertainty scenarios—and an *adversarial subproblem*, which seeks the most critical (worst-case) scenario given the current decision. If this scenario violates feasibility or deteriorates the objective value, it is added to the master problem as a new "column" and "constraint." This iterative process continues until convergence is achieved, typically within a limited number of iterations [41]. Conceptually, C&CG can be interpreted as a robust counterpart to Benders decomposition, where the subproblem generates worst-case uncertainties rather than deterministic subproblems. Owing to its strong convergence properties and ability to handle mixed-integer structures, C&CG has become a cornerstone technique for solving two-stage robust optimisation problems in energy systems—particularly for capacity planning, security-constrained unit commitment.

Lagrangian Relaxation and Dual Decomposition

Lagrangian relaxation (LR) is another widely used technique for managing large-scale optimisation problems involving coupling constraints across subsystems. By relaxing coupling constraints—such as power balance or inter-system energy exchanges—into the objective function with associated Lagrange multipliers, the global problem can be decomposed into smaller, independent subproblems corresponding to distinct energy carriers or network layers [42]. In multi-energy microgrids, LR facilitates distributed optimisation, allowing local controllers (e.g., electricity, heat, or hydrogen subsystems) to optimise operations autonomously while exchanging minimal information through price signals or dual variables. This structure is particularly compatible with distributed control architectures, improving both scalability and data privacy. However, convergence of LR-based methods is highly sensitive to step-size rules and penalty parameters, prompting research into advanced update strategies and convex relaxation techniques to enhance

stability [43]. However, the convergence performance of LR-based methods is highly sensitive to parameter selection.

Alternating Direction Method of Multipliers (ADMM)

The Alternating Direction Method of Multipliers (ADMM) has gained significant traction for distributed optimisation in multi-energy systems, owing to its strong convergence properties and ease of parallelisation. ADMM combines the decomposability of dual methods with the stability of augmented Lagrangian techniques, enabling each subsystem to iteratively optimise its local decision variables while achieving global consensus through coordination terms [44]. For instance, in hybrid electricity–hydrogen networks, ADMM allows coordinated scheduling of electrolyzers, fuel cells, and battery systems without the need for centralised control. Its applicability to convex and certain non-convex problems further enables real-time implementation, especially when coupled with model predictive control or rolling horizon frameworks [45]. Despite these advantages, ADMM can experience slow convergence under tight coupling or highly non-convex settings, motivating hybrid approaches that combine ADMM with Benders decomposition or heuristic acceleration schemes.

Hybrid Decomposition–Coordination Frameworks

Despite their computational efficiency, decomposition methods may suffer from coordination complexity in highly coupled systems. Beyond classical decomposition techniques, hybrid decomposition–coordination frameworks have emerged as powerful tools for large-scale, multi-layer energy optimisation. These frameworks integrate complementary methods—such as Benders decomposition for intertemporal coupling, C&CG for robust uncertainty resolution, and ADMM for spatial coordination—allowing efficient treatment of both temporal and spatial complexity. For example, a hierarchical two-layer architecture may employ Benders decomposition to coordinate long-term scheduling between transmission and distribution systems, while an inner ADMM loop manages real-time coordination among distributed microgrids. Such architectures align naturally with the decentralised nature of modern power systems and are increasingly employed in robust optimisation settings, where uncertainty propagation and multi-timescale decision coupling are critical.

Relevance to Robust Scheduling

Overall, these decomposition and coordination methods form the mathematical backbone for robust and distributed scheduling of multi-energy microgrids. They provide scalable solution strategies capable of accommodating uncertainty, multi-carrier interactions, and decentralised control

structures. In this thesis, these methodologies underpin the proposed robust optimisation framework, enabling tractable high-resolution simulation–optimisation coupling and supporting real-time decision-making without compromising model fidelity. Leveraging these advanced decomposition principles can achieve both computational efficiency and operational realism, thereby facilitating the practical application of complex hybrid energy systems.

Comparison of Mathematical Optimisation Methods

To provide a clear overview of the discussed methods, Table 2.1 summarises their key characteristics, advantages, limitations, and typical applications in multi-energy system optimisation.

Table 2.1: Comparison of Mathematical Optimisation and Decomposition Methods for Multi-Energy Systems

Method	**Description**	**Examples / Applications**
Benders Decomposition	Divides problem into master (investment/commitment) and subproblems (operational dispatch); exploits separable problem structures; extensible to stochastic and robust formulations.	Long-term system planning; multi-stage investment optimisation; robust microgrid scheduling; unit commitment with mixed-integer structure.
C&CG	Iteratively alternates between master decisions and adversarial subproblems to identify worst-case scenarios; tailored for min–max robust optimisation.	Two-stage robust scheduling under renewable uncertainty; security-constrained unit commitment.
LR	Relaxes coupling constraints using Lagrange multipliers; decomposes global problem into independent subsystem subproblems; supports distributed optimisation.	Multi-carrier microgrid dispatch; inter-energy exchange optimisation; distributed market clearing; energy hub coordination.
ADMM	Alternating optimisation of local variables with global consensus updates; suitable for distributed and parallel environments; handles convex and certain non-convex problems.	Distributed scheduling of electricity–hydrogen networks; coordinated operation of battery and electrolyser systems; real-time–oriented distributed energy management.
Hybrid Decomposition–Coordination	Combines multiple decomposition schemes (e.g., Benders + ADMM + C&CG); designed for systems with both temporal and spatial coupling.	Hierarchical TSO–DSO coordination; multi-timescale microgrid scheduling; integrated RO/SO/DRO hybrid energy system optimisation.

Relationship Between Decomposition and Uncertainty-Handling Methods

To clarify the interplay between decomposition-based and uncertainty-handling frameworks, Table 2.2 outlines how each algorithmic family aligns with stochastic, robust, and distributionally robust optimisation paradigms.

Table 2.2: Relationship Between Decomposition Algorithms and Uncertainty Modelling Paradigms

Algorithm Type	**Typical Problem Domain**	**Uncertainty Handling**	**Solution Nature**
Benders Decomposition	Deterministic MILP and convex MINLP; multi-stage planning	Deterministic (extensions support SO/RO)	Centralised; exact for convex problems
C&CG	Robust optimisation with min–max structure	Worst-case uncertainty sets	Iterative; converges to robust-optimal solution
ADMM / LR	Distributed multi-energy optimisation; coupling constraint relaxation	Indirect handling via dual pricing or relaxed coupling	Decentralised; exact for convex problems, heuristic for non-convex
Hybrid Decomposition–Coordination	Multi-layer and multi-timescale systems	Potentially combine SO/RO/DRO within a hierarchical structure	Multi-level coordination with temporal and spatial decomposition

Concluding Remarks

While decomposition methods such as Benders decomposition, C&CG, Lagrangian relaxation, and ADMM primarily address the computational challenges of large-scale multi-energy optimisation, they often assume that uncertain parameters—such as renewable generation, demand, and price signals—are either fixed or represented through simplified scenario sets. In reality, these parameters exhibit complex temporal and probabilistic dynamics that require explicit uncertainty modelling. Consequently, optimisation paradigms such as Stochastic Optimisation (SO), Robust Optimisation (RO), and Distributionally Robust Optimisation (DRO) extend the decomposition-based frameworks by embedding uncertainty sets, probability distributions, or ambiguity representations directly within the optimisation process. The next section systematically compares these paradigms, highlighting their theoretical foundations, modelling assumptions, and implications for real-world scheduling of integrated electricity–hydrogen systems subject to uncertainty factors.

2.1.3 Comparison of Optimisation Problems with Uncertainties

The increasing penetration of RESs and distributed energy resources (DERs) has introduced significant uncertainties into modern power systems. Variability in wind and solar generation, coupled with fluctuating demand, necessitates optimisation frameworks that can ensure reliable, efficient, and low-carbon operation under uncertainty. Three primary approaches have emerged in the literature to address this challenge: SO, RO, and DRO, as detailed below.

Stochastic Optimisation (SO)

Stochastic optimisation explicitly incorporates uncertainty by modelling uncertain parameters as random variables with known or assumed probability distributions [46–48]. SO aims to minimise expected costs or maximise expected benefits across a set of scenarios representing possible future outcomes. In energy system applications, SO has been widely applied to unit commitment, renewable generation scheduling, and energy storage management. For instance, [49] developed a stochastic unit commitment model incorporating wind power forecasts, demonstrating improved cost-efficiency and reliability over deterministic approaches. However, the effectiveness of SO depends heavily on the accuracy of the probability distributions assumed for uncertain parameters, which can be challenging in practice due to limited historical data or rapidly changing operating conditions.

Robust Optimisation (RO)

Robust optimisation, in contrast, does not rely on precise probabilistic information but instead considers uncertainty sets, typically defined as bounded intervals or polyhedra, within which the uncertain parameters are assumed to lie [50–52]. RO seeks solutions that remain feasible and near-optimal for all realizations within these sets, thereby providing worst-case performance guarantees. Applications in energy systems include robust scheduling of microgrids [53–55], resilient planning of transmission networks [56–58], and hydrogen storage operation [59–61]. RO is particularly valued for its conservatism and reliability, but it can be overly cautious, potentially leading to higher operational costs compared to stochastic approaches [52].

Distributionally Robust Optimisation (DRO)

Distributionally robust optimisation combines the advantages of SO and RO by optimising against the worst-case probability distribution within an ambiguity set, which represents a family of plausible distributions consistent with known statistical properties (e.g., moments, support, or historical

data) [62–64]. DRO thus mitigates the risks of misspecified probability distributions while avoiding the excessive conservatism of classical RO [62]. In recent years, DRO has been increasingly adopted in energy systems, particularly in contexts with limited or uncertain historical data [65]. For example, [66] proposed a data-driven DRO framework for day-ahead microgrid scheduling, demonstrating superior balance between cost-efficiency and system reliability under uncertain renewable generation. Similarly, [67, 68] employed DRO for hydrogen-integrated multi-energy systems, achieving robust operation across various scenarios of wind and load uncertainties.

Comparative Insights and Applications

While SO, RO, and DRO share the common objective of addressing uncertainty, they differ in their assumptions, conservatism, and data requirements. SO is optimal when accurate probability distributions are available but is sensitive to distributional errors. RO ensures worst-case feasibility with minimal data requirements but may yield conservative solutions. DRO strikes a balance by considering an ambiguity set of distributions, combining robustness with a data-driven perspective. Consequently, DRO has emerged as a particularly suitable approach for modern multi-energy systems, microgrids, and hydrogen-integrated power networks, where uncertainty is both significant and partially characterised.

Overall, these optimisation paradigms form a continuum of strategies for managing uncertainty, as summarised in Table 2.3, each offering distinct advantages and limitations. The choice of approach should be guided by the specific system context, data availability, and the desired balance between reliability and cost efficiency. The present thesis leverages DRO to optimise multi-energy systems under renewable integration, combining the strengths of RO and SO while addressing the practical challenges of data uncertainty and system variability.

2.1.4 Deterministic Operations of Microgrid Systems

At a microgrid level, the majority of existing research primarily concentrates on the functionality of individual energy microgrids [69–71], without discussing the incorporation of multiple energy sources. To increase the system operating efficiency and dispatch flexibility, [72] proposes a comprehensive system-wide optimal coordinated dispatch method for the MMG in both grid-connected and islanding modes. The objectives are to optimize the net operational cost of the microgrid in both modes while adhering to the system's operational constraints. In [73], a general modelling approach for the steady-state energy balance equation of multi-energy systems is presented. This approach includes the incorporation of energy converters, energy storage, and renewable energy devices. [74] constructs a multi-scenario operation optimisation model for a park integrated energy

Table 2.3: Comparison of Optimisation Approaches for Uncertainty Modelling

Aspect	**Stochastic Optimisation (SO)**	**Robust Optimisation (RO)**	**Distributionally Robust Optimisation (DRO)**
Uncertainty representation	Explicit probability distributions of uncertain parameters	Bounded uncertainty sets without probabilistic information	Ambiguity sets over probability distributions (e.g., moment- or distance-based)
Data requirement	Requires accurate and sufficient historical data to estimate probability distributions	Requires only bounds or support information of uncertainties	Requires partial statistical information or historical data (e.g., moments, empirical samples)
Risk attitude	Risk-neutral; optimises expected performance	Highly risk-averse; optimises worst-case performance	Adjustable risk aversion; balances conservatism and performance
Feasibility guarantee	Probabilistic feasibility; constraint violations may occur with small probability	Deterministic feasibility for all realisations within uncertainty sets	Probabilistic robustness against worst-case distributions within ambiguity sets
Conservatism level	Low to moderate, depending on distribution accuracy	Typically high; may lead to overly conservative solutions	Moderate; less conservative than RO but more robust than SO
Computational complexity	High for large-scale or multi-stage problems	Moderate; often tractable with reformulation or decomposition	Higher than RO; depends on ambiguity set structure and solution method

system based on multi-energy demand response (DR), of which the energy utilization efficiency and net system profit show improvements of 2.30% and 2,652.775$ respectively, compared to the conventional scenario. A multi-period dispatch model using improved particle swarm optimisation (IPSO) is proposed in [75], which takes into account the potential profit from energy storage systems, the results of which demonstrate that the dispatch strategy successfully lowers the overall operational costs and provides improved scheduling of distributed generation units in grid-connected MMGs.

To consider environmental factors, the objective of [76] is to investigate the environmental economic dispatch for large-scale integrated energy systems (IESs), specifically in the integrated regional energy systems with coal, gas, combined heat and power (CHP), and renewable energy source (RES) systems, taking into account the influence of air pollutant control technologies and DR programs on the system. [77] proposes a low-carbon operation method for microgrids with the consideration of carbon emission quota trading. [78] presents an optimized energy management strategy to minimize an MMG network's operational expenses. The strategy takes into account operational constraints and carbon emissions in the decision-making process. Additionally, [79] proposes a framework aimed at assisting aggregators in the real-time provision of network-secure and multi-energy services. This framework takes into account the integration of green hydrogen and measures for carbon reduction. Collectively, these studies demonstrate a growing trend of incorporating environmental and carbon factors into microgrid scheduling, but their applicability under uncertainty remains limited.

2.1.5 Multi-Energy Operations Considering Uncertainties

In the above-mentioned literature [72] to [79], the multi-energy coordination is based on the deterministic day-ahead operation. However, they neglect uncertainties related to RES outputs, power loads, and transaction prices, which limits practicality for real-world applications. Guan et al. [80] put forward an alternate method to tackle these uncertainties. The SO techniques are used to minimize the power and natural gas expenses at the building level while considering the uncertain outputs of RES and power loads. This methodology takes into account the uncertainties, rendering it more feasible for real-world implementations. Experimental outcomes demonstrate substantial cost reductions attained in energy expenses by employing integrated scheduling and control of diverse building energy supply sources. [81] utilises the Latin Hypercube Sampling method to manage uncertainties in energy carriers, including power, heat, and hydrogen. The study introduces a decentralized bi-level SO method using the progressive hedging algorithm for multi-agent systems in MMGs, aiming to enhance network flexibility and improve the system's overall perfor-

mance. A temporally-coordinated optimal operation method for microgrids is solved by MILP and a multi-stage stochastic operation method is proposed to handle the uncertainties [82]. Similarly, MILP is also applied in [83] to solve the optimal scheduling problem for microgrids. A hybrid robust/stochastic framework is also proposed to address high-level uncertainty. These studies highlight the dominance of MILP in dealing with microgrid scheduling, but also reveal its limitations when uncertainty grows more complex. Column-and-constraint generation (C&CG) algorithm is applied in [84] to solve a DRO model considering the uncertainties of renewable energy sources.

2.1.6 Low-Carbon Performance with Uncertainties Considered

From the perspective of low-carbon performance in power systems with uncertainties considered, authors in [85] propose a dynamic economic dispatch model with the assistance of the particle swarm optimisation (PSO) algorithm to solve the power dispatching problem with a dual consideration of wind power uncertainty and carbon emission rights in a low-carbon setting. [86] focuses on the integrated energy system and develops a day-ahead low-carbon two-stage dispatch model applied to a regionally integrated energy system. Different from those at the microgrid level, this research considers purchasing electricity from the main grid and does not involve bi-directional transactions. This research also quantifies the impacts of wind/PV penetration, carbon price, and scenario numbers.

2.1.7 Research Gap

Despite the extensive research in microgrid scheduling and management, there is a noticeable research gap concerning the development of comprehensive strategies for low-carbon MMGs. Existing approaches lack in accurately emulating the operations of real power distribution systems and responding promptly to dynamic changes in energy supply and demand, limiting their practicality. Additionally, the uncertainty associated with renewable energies poses a significant challenge to achieving robust carbon reduction goals, requiring precise control at shorter intervals for seamless integration. The optimisation problem for multi-temporal scheduling in low-carbon MMG, considering uncertainties in renewable energies, is insufficiently explored.

Closing this gap is pivotal for the development of robust and decarbonising scheduling strategies for MMGs. To effectively tackle this research gap, it is imperative to advance energy management strategies and technologies. These advancements should possess the capability to seamlessly integrate and harness the full potential of renewable resources, ensuring both system reliability and environmental sustainability. Hence, there exists a critical need to formulate an advanced and

efficient framework for a comprehensive low-carbon scheduling approach with multi-temporal resolution. Therefore, this study aims to contribute by addressing this research limitation. The proposed framework will play a pivotal role in optimising MMG operations and aligning economic efficiency with environmental objectives in the context of the microgrid.

In Table 2.4, a thorough comparison of different reported pieces of research work on the management strategies of microgrids is presented, from the aspects of 1) allowed forms of energy carriers, 2) considered types of RES, 3) uncertainty modelling, 4) timescales, 5) enabled carbon trading, and 6) solving algorithms. It can be found that so far there is little literature published to fully consider key factors such as 1)-5). Thus, while previous studies provide valuable insights into deterministic and uncertain operations of MMGs, none fully address the challenge of low-carbon scheduling at multi-temporal resolution under uncertainty, which is precisely the focus of this PhD thesis.

Table 2.4: Comparison among Different Research Works on Management Strategies of MMGs

References	Energy Carriers				RES		Uncertainty Modelling	Problem or Algorithm	Timescale	Carbon Trade
	Power	Gas	Heat	Hydro	PV	WT				
[72]	✔	✔	✔	✖	✖	✔	✖	MILP	hourly	✖
[73]	✔	✔	✔	✔	✔	✔	✖	MINLP	hourly	✖
[74]	✔	✔	✔	✖	✔	✔	✖	MILP	hourly	✔
[75]	✔	✔	✔	✖	✔	✔	✖	IPSO	hourly	✖
[76]	✔	✔	✔	✖	✖	✔	✖	MILP	hourly	✔
[77]	✔	✖	✖	✖	✔	✔	✖	MILP	hourly	✔
[78]	✔	✔	✔	✖	✖	✔	✖	MILP and MIQP	hourly	✔
[79]	✔	✔	✔	✔	✔	✖	✖	MPC	hourly & 20s	✔
[80]	✔	✔	✔	✔	✔	✔	Stochastic	MILP	hourly	✖
[81]	✔	✔	✔	✔	✔	✔	Latin Hypercube Sampling	Bi-Level Stochastic	hourly	✖
[82]	✔	✔	✔	✖	✔	✔	Stochastic	MILP	hourly & 5-min	✖
[83]	✔	✔	✔	✖	✖	✔	Hybrid Robust/Stochastic	MILP	hourly	✖
[84]	✔	✖	✖	✖	✔	✔	Data-Driven Set Based RO	C&CG	hourly	✖
[85]	✔	✖	✖	✖	✖	✔	Random Sampling	PSO	hourly	✔
Proposed Model	✔	✔	✔	✔	✔	✔	Data-Driven Set Based RO	C&CG and MPC	hourly & 15-min	✔

2.2 Coordinated Scheduling of Integrated Energy Systems

Global efforts to decarbonise energy systems, as emphasised by the Paris Agreement, necessitate that renewable energy sources supply a substantial share of electricity demand—projected to be around two-thirds by 2050—to limit global warming to below 2°C [1] [87] [88]. Over the past decade, significant progress has been made in renewable energy technologies, with widespread adoption in countries such as China, Denmark, and the United Kingdom [4]. Among renewable energy sources, wind and solar power are widely recognised as the most abundant and scalable options for large-scale clean energy generation. While both resources play a critical role in achiev-

ing decarbonisation targets, wind energy — particularly offshore wind — has attracted growing attention in recent years due to its higher potential capacity, more stable resource availability, and reduced land-use, visual, and acoustic impacts compared with onshore installations. [7]. Recent studies also highlight the economic competitiveness and technological maturity of floating offshore wind platforms, which offer new opportunities for large-scale decarbonisation and energy security [89].

Despite these advances, the inherent intermittency and unpredictability of wind and solar generation pose substantial challenges to power system reliability, often resulting in renewable curtailment and under-utilisation of available resources [90] [8]. Energy storage has emerged as a critical solution to mitigate these issues. While battery storage systems are widely deployed, they are typically constrained by limited duration, high capital costs, and environmental concerns related to material extraction and disposal [91]. Hydrogen energy storage provides a complementary solution, with advantages including high gravimetric energy density, versatility, and suitability for seasonal storage [92]. Through electrolysis, excess electricity can be converted into hydrogen, which may then be stored and reconverted for electricity generation, heating, or transport applications [20]. As such, hydrogen is increasingly recognised as a key component of integrated renewable energy systems.

The growing penetration of renewable energy and storage systems necessitates enhanced operational flexibility across both transmission and distribution networks. Coordination between transmission system operators (TSOs) and distribution system operators (DSOs) is critical, as actions taken at one level may inadvertently violate constraints at the other [18] [93]. Consequently, effective cross-layer operational strategies are essential to ensure reliability, maximise renewable utilisation, and minimise curtailment.

2.2.1 Transmission and Distribution System Operators (TSOs and DSOs)

TSOs and DSOs are fundamental core entities in modern power systems, each managing distinct network layers while ensuring a secure and reliable electricity supply [94] [95] [96]. TSOs operate high-voltage transmission networks, transporting bulk electricity from large-scale generation units to regional distribution networks [97] [98] [99]. Their primary responsibilities include maintaining system stability, balancing supply and demand in real time, managing congestion, and ensuring frequency and voltage standards across the transmission grid [100] [101] [102].

DSOs, by contrast, manage medium- and low-voltage networks, delivering electricity directly to end-users [103]. Their responsibilities encompass local reliability management, voltage regulation, fault detection and repair, and the integration of DERs, such as rooftop photovoltaic

systems, small-scale wind turbines, and local energy storage [104] [103] [105]. DSOs operate closer to the consumer, facing more variable load profiles and distributed generation patterns than TSOs [106] [107].

The increasing integration of renewable energy sources (RESs) and distributed generation has highlighted the necessity for enhanced TSO-DSO coordination [108] [19] [109]. Traditionally, TSOs and DSOs operated largely independently; however, high levels of intermittent renewable generation and active demand-side participation can create operational conflicts [102]. For example, TSO-initiated activation of distributed resources for system balancing may violate local network constraints, such as voltage limits or feeder capacity, thus posing reliability risks [18].

Effective coordination between TSOs and DSOs is essential to enhance overall system flexibility, reduce renewable energy curtailment, and support the deployment of emerging technologies such as hydrogen storage and electric mobility [106, 107, 110]. Coordination enables efficient joint utilisation of transmission and distribution assets, facilitates participation in wholesale and ancillary service markets, and allows sector coupling between electricity, hydrogen, and heating systems [100, 111, 112]. Recent research has explored hierarchical control strategies, real-time data-driven dispatch, and integrated optimisation frameworks to address TSO-DSO interactions under high renewable penetration [110, 113, 114]. Additionally, regulatory initiatives in the European Union and other regions increasingly promote collaboration between TSOs and DSOs to support reliable, low-carbon energy transitions [115, 116].

In summary, TSOs and DSOs have complementary yet interdependent roles. Their comparison is presented in Table 2.5. Understanding their responsibilities, operational challenges, and coordination mechanisms provides a critical foundation for developing integrated optimisation frameworks, which are central to the multi-energy and hydrogen-integrated systems explored in this thesis.

2.2.2 Renewable Integration in Transmission Networks

Renewable energy integration at the transmission level has attracted significant attention due to the increasing deployment of large-scale wind and solar power plants located far from load centres. Existing studies on transmission network optimisation primarily address power flow management, congestion mitigation, operational security, and system flexibility under renewable uncertainty [117]. With the increasing penetration of distributed energy resources and multi-energy systems, however, greater attention has been directed toward enhancing coordination between transmission and distribution networks.

Furthermore, previous studies have demonstrated that renewable energy localisation and trans-

Table 2.5: Comparison of Transmission and Distribution System Operators (TSOs and DSOs)

Aspect	**TSO (Transmission System Operator)**	**DSO (Distribution System Operator)**
Network Level	High-voltage transmission network	Medium- and low-voltage distribution network
Primary Responsibilities	System stability and reliability, real-time balancing of supply and demand, congestion management, frequency and voltage control	Local network reliability, voltage regulation, fault detection and repair, integration of distributed energy resources
Interaction with RES	Coordinates large-scale generation (e.g., offshore wind, utility PV) for system-level balancing	Manages distributed generation (e.g., rooftop PV, local wind, storage) while ensuring local network security
Operational Challenges	Integrating intermittent renewable generation, maintaining grid stability under variable flows	Handling variability and bidirectional flows, avoiding voltage violations and overloads, coordinating DERs
Coordination Needs	Requires real-time data from DSOs to prevent local constraint violations; optimises system-wide flexibility	Needs TSO instructions for system-level balancing while maintaining local reliability; participates in market and flexibility services
Benefits of Coordination	Enhanced overall system flexibility, reduced renewable curtailment, improved market participation, support for sector coupling	Efficient utilisation of distributed resources, increased reliability, reduced local curtailment, enabling multi-energy integration

mission network characteristics can significantly affect grid reinforcement requirements and investment costs [118], highlighting the importance of transmission-level optimisation under high renewable penetration.

2.2.3 Multi-Energy Optimisation of Distribution Networks

Recent research has explored optimisation strategies within distribution networks, often incorporating multi-energy storage solutions. Studies have demonstrated that integrating power-to-gas systems with distributed photovoltaic installations can significantly enhance operational flexibility, reduce power imports, and decrease marginal emissions [119]. Optimal planning of distributed hydrogen resources has also been investigated to minimise investment and operational costs from the perspective of DSOs [120]. Moreover, robust stochastic models have been proposed for integrated electricity–hydrogen systems, accounting for both production and seasonal storage [121].

Economic analyses suggest that distributed hydrogen production often offers a more competitive solution than centralised onshore or offshore alternatives [122]. Additionally, integrated renewable–hydrogen systems can enhance profitability for green hydrogen operators while supporting direct gas-based applications [123]. Collectively, these studies establish the technical and economic feasibility of hydrogen as a flexible storage and grid-support solution at the power distribution level.

2.2.4 Research Gap

Despite these advances, the majority of existing literature remains focused on distribution-level optimisation, with limited attention to the system-wide implications of transmission–distribution interactions. Such a narrow focus may constrain overall system flexibility and exacerbate renewable curtailment. Furthermore, interactions between TSOs and DSOs under coupled electricity–hydrogen frameworks are underexplored, particularly when multi-energy storage and sector coupling are involved.

Emerging research directions suggest the importance of incorporating multi-scale, multi-energy optimisation that considers both spatial and temporal correlations of renewable resources and demand. Techniques such as data-driven distributionally robust optimisation (DRO), clustering-based scenario generation, and surrogate modelling (e.g., Kriging) offer potential to overcome computational challenges while providing realistic operational guidance. In addition, integrating hydrogen into system-wide coordination strategies could enhance flexibility, support seasonal energy balancing, and contribute to the decarbonisation of both electricity and gas sectors.

This thesis addresses these gaps by proposing a novel framework for coordinated scheduling of integrated systems, which jointly optimises transmission and distribution networks with integrated power-to-hydrogen storage. The framework aims to improve operational flexibility, minimise curtailment, and provide a scalable solution for low-carbon energy systems, thereby bridging the gap between distribution-focused studies and system-wide optimisation.

2.3 Operation of Offshore Energy Islands under Extreme Weather Conditions

Wind energy has become a key element in the global shift toward renewable energy, providing a significant opportunity for clean and sustainable power generation [124]. Among the different forms of wind energy, offshore wind has gained increasing attention due to its higher and more stable wind speeds compared to onshore sites [125]. This advantage makes offshore wind a crucial contributor to meeting the growing global energy demand while helping to reduce greenhouse gas emissions [126].

One of the most promising applications of wind energy is the integration of P2H systems [127]. These systems use wind-generated electricity to produce green hydrogen through water electrolysis, making hydrogen a versatile energy carrier [128]. Hydrogen produced from offshore wind energy not only provides a solution for decarbonizing hard-to-electrify sectors, such as heavy industry and transportation, but also offers a means of storing surplus wind power. This helps improve grid stability and enhances energy resilience [129].

However, the economic viability of offshore wind energy and its application in hydrogen production face challenges, especially under extreme weather conditions [130]. Harsh marine environments, such as strong winds, high waves, and severe storms, can negatively impact the operational efficiency, maintenance costs, and structural integrity of offshore wind turbines [131]. These conditions often result in increased downtime and higher repair costs, which in turn reduce the overall economic feasibility of offshore wind-to-hydrogen projects [132].

2.3.1 Offshore Wind Systems and Floating Offshore Energy Islands

Offshore Wind Systems

Offshore wind energy has become a cornerstone of the global transition towards low-carbon power generation. Compared to onshore wind farms, offshore installations offer several advantages, in-

cluding higher and more consistent wind speeds, lower turbulence, and minimal land-use conflicts [7,21,133,134]. These characteristics allow for greater capacity factors and more predictable energy output, making offshore wind particularly suitable for large-scale renewable integration in coastal regions [135–137].

Offshore wind energy systems typically consist of turbines mounted on fixed or floating foundations. Fixed-bottom turbines are suitable for relatively shallow waters (generally up to 60 metres depth), using monopile, jacket, or gravity-based structures [138–140]. These foundations provide mechanical stability but are constrained by seabed depth and geotechnical conditions [141, 142]. In contrast, floating wind turbines, supported by platforms such as spar-buoy, semi-submersible, or tension-leg platforms (TLPs), enable deployment in deeper waters where fixed structures are infeasible [143–145]. Floating systems are increasingly attractive as offshore wind expansion moves farther from shore, offering access to stronger and more consistent wind resources [21, 146, 147].

Floating Offshore Energy Islands

The concept of floating offshore energy islands extends the conventional offshore wind paradigm by integrating multiple energy technologies on a single platform [21, 148, 149]. A floating energy island typically combines offshore wind turbines with complementary renewable generation, such as solar photovoltaics, wave energy converters, and energy storage systems, including batteries and hydrogen production units [150]. By consolidating multiple energy sources, these islands can provide a stable, dispatchable power supply and serve as hubs for sector coupling, including electricity, hydrogen, and heat networks [151].

Floating offshore energy islands also offer strategic advantages in terms of spatial planning and environmental impact. By situating energy generation in deeper waters, conflicts with shipping lanes, coastal communities, and protected areas can be minimised [152]. Furthermore, the integration of energy storage and power-to-X technologies enhances operational flexibility, allowing the islands to respond to varying demand patterns and market conditions [153]. Life-cycle assessments of such systems have demonstrated that optimal siting and technology integration can substantially improve economic returns while maintaining long-term structural integrity [21, 154].

Technological and Operational Challenges

Key challenges in offshore wind and floating energy islands include the structural design of floating platforms, dynamic load management under coupled wind-wave conditions, and the integration of multi-energy storage systems [155]. High-fidelity numerical simulations and surrogate modelling techniques, such as Kriging, are increasingly employed to predict turbine power output, fatigue damage, and system reliability under variable environmental conditions [156, 157]. These models

are critical for optimising both operational performance and long-term investment decisions.

In summary, offshore wind systems, particularly floating platforms, represent a pivotal technology for large-scale renewable deployment. Floating offshore energy islands provide a flexible, multi-energy approach that enhances grid integration, improves economic viability, and supports the global transition towards a sustainable, low-carbon energy system. The comparison of offshore wind systems and floating offshore energy islands is shown in Table 2.6.

Table 2.6: Comparison of Offshore Wind Systems and Floating Offshore Energy Islands

Aspect	**Offshore Wind Systems**	**Floating Offshore Energy Islands**
Definition	Wind turbines installed offshore to harness wind energy, either on fixed-bottom or floating foundations.	Multi-energy platforms combining offshore wind, other renewables (solar, wave), and energy storage (battery, hydrogen).
Foundation Type	Fixed-bottom (monopile, jacket, gravity-based) for shallow waters; floating for deeper waters.	Floating platforms (spar-buoy, semi-submersible, tension-leg platforms).
Energy Sources	Primarily wind energy.	Wind, solar, wave, and integrated storage/hydrogen production.
Advantages	Higher and more consistent wind speeds than onshore, minimal land use, large capacity factor.	Flexible deployment in deep waters, integrated multi-energy generation, enhanced operational flexibility, supports sector coupling.
Challenges	Structural design, dynamic load under wind and waves, grid connection.	Complex platform design, multi-energy integration, energy storage management, operational coordination under variable environmental conditions.
Applications	Large-scale renewable electricity generation for coastal grids.	Multi-energy hubs for electricity and hydrogen supply, offshore low-carbon energy integration, energy storage and dispatchable power.

2.3.2 Economic Optimisation of Offshore Wind System

To explore the economic optimisation of offshore wind hybrid power plants, the authors in [158] created a model for the power-to-hydrogen system. The main components of the model include the offshore wind farm, an electrolyser, a hydrogen storage system, and a fuel cell. They focused on optimizing ancillary service revenues for hydrogen production. The researchers developed MILP models, which provide significant benefits, including increased revenues and reduced costs [159]. The thesis in [160] aims to explore and develop optimal operational strategies for hybrid offshore wind power plants, with an emphasis on balancing hydrogen production and electricity market sales. The study examines various electrolyzer operational strategies—ON/OFF, ON/Standby, and ON/OFF/Standby—and evaluates how these strategies affect system flexibility, operational efficiency, and overall profitability. The objective is to identify a dynamic control strategy that maximizes both hydrogen output and economic returns.

2.3.3 OpenFAST Framework and Applications

Introduction to Aero-Hydro-Servo-Elastic Modelling

The accurate prediction of offshore wind turbine (OWT) performance requires a fully coupled simulation framework capable of representing the interactions among aerodynamic loading, hydrodynamic excitation, structural flexibility, and control systems [161]. Early simulation tools often focused on isolated subsystems—for instance, aeroelastic solvers such as FAST and BHawC concentrated on rotor–tower dynamics, while hydrodynamic solvers like WAMIT and OrcaFlex modelled wave-induced platform motion [162]. However, as offshore wind technologies evolved toward floating and hybrid configurations, these simplified models became insufficient to capture the nonlinear, multi-physics interactions that govern system behaviour under realistic environmental conditions.

In response to this need, the U.S. National Renewable Energy Laboratory (NREL) developed the **OpenFAST** code—an open-source, modular, and physics-based simulator for the aero-hydro-servo-elastic dynamics of wind turbines [163]. Built upon the legacy FAST framework, OpenFAST integrates a suite of physics modules that collectively solve the coupled nonlinear equations of motion for both land-based and offshore configurations. Its open-source nature, rigorous validation, and extensibility have made it a cornerstone tool for research, design, and operational optimisation of modern wind turbines and offshore energy systems [161].

In the context of this research, OpenFAST is not only a simulation engine but also a high-

fidelity data generator that enables the construction of realistic datasets for subsequent optimisation and surrogate modelling. To situate its role, this section first reviews the theoretical foundation and structure of OpenFAST, followed by a discussion of its validation, extensions, and relevance to scheduling optimisation studies.

Modular Structure and Theoretical Foundation

OpenFAST follows a modular architecture that allows each physical process to be represented by an independent submodule while maintaining a consistent interface for data exchange. The core modules include [164]:

- **ElastoDyn**, which solves the nonlinear structural dynamics of the tower, blades, and drivetrain through a modal-based representation;
- **AeroDyn**, responsible for aerodynamic load computation using the blade element momentum (BEM) theory, optionally enhanced with dynamic stall and tower shadow models;
- **HydroDyn**, which models hydrodynamic loads using linear potential flow theory combined with Morison's equation for viscous drag and inertia; And it is applicable to both fixed-bottom and floating offshore substructures;
- **ServoDyn**, which simulates control and electrical drive systems, including generator torque, pitch control, and yaw mechanisms;
- **MoorDyn**, providing a quasi-static or dynamic representation of mooring line dynamics for floating platforms;
- **SubDyn**, which accounts for the structural response of fixed-bottom substructures such as monopiles or jackets using a finite-element approach.

The modules are time-integrated through a central coupling driver that ensures dynamic consistency between aerodynamic, hydrodynamic, and structural responses at every time step. This coupling enables OpenFAST to capture complex feedback effects—such as the impact of platform motion on rotor aerodynamics or the influence of control actions on tower vibrations—which are essential for realistic offshore simulations [165].

Model Validation and Benchmarking

OpenFAST has undergone extensive validation through international collaborative projects such as OC3, OC4, and OC5, coordinated by the International Energy Agency (IEA) Wind Task 30

[166]. These benchmarks compare simulated responses against experimental data and high-fidelity computational fluid dynamics (CFD) results.

For example, the OC3–OC4 studies validated fixed-bottom and floating configurations under combined wind and wave loading, demonstrating good agreement in tower-top displacement, mooring tension, and power performance. Subsequent campaigns, such as OC5, included fully coupled CFD–OpenFAST comparisons to assess wave–structure interactions under nonlinear sea states. These benchmarks have established OpenFAST as an industry-accepted standard for coupled aero-hydro-servo-elastic simulation.

Integration with Data Generation and Surrogate Modelling

While OpenFAST is primarily designed for dynamic analysis and load assessment, its ability to simulate high-resolution responses under diverse environmental conditions makes it an invaluable tool for data-driven optimisation. In particular, the time-domain outputs—including wind inflow, rotor speed, generator torque, blade root moments, and tower base loads—can be used to construct surrogate models that approximate system behaviour without requiring repeated high-fidelity simulations.

In the present thesis, OpenFAST serves as a data generation engine to produce realistic wind turbine operational datasets across varying wind speeds, wave heights, and turbulence intensities. Each simulation provides second-level resolution data for power output and structural load indicators, which are subsequently aggregated and processed into hourly-scale datasets compatible with optimisation models. This enables the development of Kriging-based surrogate models that replicate the nonlinear mapping between environmental inputs and turbine performance with minimal computational cost.

Such data-driven integration allows for efficient exploration of scheduling, dispatch, and control strategies for offshore hybrid energy systems. The approach bridges high-fidelity physical simulation and system-level optimisation, providing both accuracy and tractability that are often seen as conflicting in traditional modelling frameworks.

Relevance to the Present Study

Within the scope of this thesis, OpenFAST is employed to generate a physically consistent dataset that supports the scheduling optimisation of offshore wind–hydrogen systems. By simulating the aero-hydro-servo-elastic dynamics of floating wind turbines, it provides high-fidelity time series of turbine power output, aerodynamic thrust, and structural loads, thereby capturing the quantitative relationships between wind–wave conditions and energy conversion performance. These simulation results form the foundation for developing and validating surrogate models, such as Kriging

and Gaussian Process Regression, which enable efficient optimisation under complex and variable environmental scenarios.

This data-centric use of OpenFAST ensures that the optimisation framework developed later in the thesis retains physical interpretability and generalisability across different environmental regimes. By grounding the scheduling optimisation problem in high-fidelity physics-based data, the study bridges the gap between turbine-level dynamics and system-level planning—laying the foundation for scalable, resilient, and data-informed energy island operation strategies.

In summary, OpenFAST provides a validated, modular, and extensible platform for aero-hydro-servo-elastic simulation of offshore wind turbines. The OpenFAST modules and applications are shown in Table. 2.7. Its capacity to model nonlinear coupled dynamics under realistic wind–wave conditions makes it indispensable for both design and operational research. In this thesis, OpenFAST is employed not merely as a simulation tool but as a scientific instrument for generating structured datasets that feed into surrogate-assisted optimisation. This integration of physics-based modelling and data-driven optimisation represents a methodological advancement that enables more efficient and reliable scheduling of offshore hybrid energy systems under uncertainty.

While OpenFAST provides a high-fidelity simulation platform capable of capturing the coupled aero-hydro-servo-elastic dynamics of offshore wind turbines, most existing studies have primarily focused on design validation, load assessment, or surrogate model development under typical operational conditions. Although these analyses offer valuable insights into turbine-level performance, they often do not extend to system-level economic optimisation, particularly under extreme environmental scenarios. Given that wind power generation is highly sensitive to variations in wind speed, wave height, and storm events, integrating OpenFAST-derived data into optimisation frameworks is essential to evaluate not only the structural and aerodynamic performance but also the economic resilience of floating offshore wind farms. This observation highlights a clear research gap: while OpenFAST can generate detailed operational datasets, few studies have leveraged these datasets to inform cost-effective, weather-resilient operational strategies. Bridging this gap motivates the present thesis, which combines high-fidelity simulation with optimisation techniques to assess and enhance the economic and operational performance of offshore energy islands under extreme weather conditions.

2.3.4 Research Gap

OpenFAST is an open-source aero-hydro-servo-elastic software [163]. To determine the most cost-effective hull shape and mooring configuration among various design concepts, the paper [167] proposes an evaluation methodology based on long-term dynamic optimisation verified by Open-

Table 2.7: Summary of OpenFAST Modules and Key Applications

Module	Function / Description	Typical Applications
ElastoDyn	Nonlinear structural dynamics of tower, blades, and drivetrain using modal representation	Tower and blade deflection analysis, drivetrain load assessment, fatigue evaluation
AeroDyn	Aerodynamic load computation using BEM, dynamic stall, and tower shadow models	Rotor aerodynamics, power prediction, wake and tip-loss effects
HydroDyn	Hydrodynamic load modelling using linear potential flow + Morison's equation for viscous effects	Floating platform motion, wave-structure interactions, mooring line forces
ServoDyn	Control and electrical drive system simulation, including generator torque, pitch, and yaw	Generator performance, control strategy testing, dynamic response under wind/wave inputs
MoorDyn	Quasi-static or dynamic mooring line modelling for floating platforms	Mooring tension evaluation, platform stability analysis
SubDyn	Finite-element modelling of fixed-bottom substructure structural response	Monopile and jacket structural analysis, stress and fatigue estimation
Coupling Driver	Ensures dynamic consistency between aero, hydro, and structural responses at each time step	Integrated aero-hydro-servo-elastic simulations for offshore turbines
Data Generation	Time-domain outputs for turbine power, loads, and environmental inputs for surrogate model construction	Surrogate-assisted optimisation, Kriging model training, scheduling studies for hybrid energy systems

FAST. This methodology provides Pareto designs that offer the best trade-off between dynamic performance and manufacturing cost. However, wind power generation can be influenced by environmental factors, such as wind speed and wave height [168]. To the best of our knowledge, few studies have used OpenFAST to assess the economic optimisation of floating offshore wind farms under extreme weather conditions. Understanding and mitigating the impacts of extreme weather on offshore wind energy systems is essential for realising their full potential and ensuring their long-term sustainability. Extreme weather events, such as strong winds, high waves, and severe storms, can significantly affect the performance, maintenance, and economic viability of offshore wind farms. Given these challenges, it is crucial to develop operational strategies that enhance system resilience and economic efficiency under adverse conditions. Accordingly, this thesis proposes a novel optimisation framework for the operation of offshore energy islands under extreme weather conditions, as detailed in Chapter 5.

2.4 Techno-Economic Optimisation of Offshore Wind Systems

2.4.1 Offshore Energy Islands - State-of-the-Art

The potential of offshore wind power is explored in supporting the EU Green Deal's goals of green transition and renewable energy generation, with a particular focus on EU islands [169]. It addresses the high electricity costs in Mediterranean islands caused by heavy reliance on imported fossil fuels by optimizing offshore wind farm layouts for four selected sites near Mediterranean islands. The study finds that using higher-rated wind turbines can reduce the minimum levelized cost of energy (LCOE) of wind farms by approximately 10% and 25%, respectively.

Likewise, [170] explores the practical challenges of promoting floating offshore wind power in island power systems through a case study in the Canary Islands, revealing that the curtailment rate of offshore wind exceeds 35%. Due to curtailment and system limitations, the LCOE increases by up to 17%. It also suggests that government policy intervention is the key to neutralizing the increase in LCOE, such as through subsidies, improving the power system infrastructure, or developing energy storage technologies. Moreover, successful offshore wind projects like Denmark's offshore wind development showcase how community involvement and inclusive strategies can drive economic growth, create jobs, and gain social acceptance [171].

The global transition toward renewable energy has established offshore wind power as a critical component of sustainable energy systems [124]. With access to abundant and untapped wind resources over oceans, offshore wind turbines can achieve higher energy yields due to stronger and more consistent wind conditions compared to their onshore counterparts [172]. Thus, it is

important to raise attention to offshore wind energy due to its immense potential [173]. However, its widespread adoption faces significant economic and operational challenges [174]. For instance, the construction costs for floating platforms are substantially higher than those of onshore wind turbines [175]. Additionally, harsh marine environments — characterized by high waves and strong winds — can lead to damage of turbine components, increasing maintenance demands and associated costs [176]. The remote location of offshore installations further exacerbates these challenges, as greater distances from shore result in elevated transportation expenses for maintenance crews and specialized equipment [177].

In addition to economic concerns, the complex and highly dynamic offshore environment also introduces significant uncertainty in power stability and system reliability. Understanding the interplay between environmental loads and turbine response is therefore crucial for both structural resilience and economic planning. Recent research conducted by our group has highlighted the sensitivity of FOWTs to wind-wave interactions, especially during power ramp events, where platform-induced low-frequency dynamics significantly affect power stability and output reliability [178]. These findings highlight the need for integrated dynamic modelling approaches that reflect the complex multi-physical interactions in offshore floating systems. Therefore, a holistic framework is needed for the economic assessment of the life cycle and the evaluation of structural damage on the floating energy island under a complicated offshore environment. This framework also integrates power-to-hydrogen conversion and storage strategies to maximize the utilization of offshore wind resources, reduce reliance on grid connections, and enhance the resilience of the energy system. Additionally, it should serve as a valuable reference for identifying optimal locations of energy islands, offering insights into site selection that balance long-term sustainability and cost efficiency.

2.4.2 Offshore Wind Turbines

Offshore wind turbines (OWTs) are a key technology for large-scale renewable energy deployment, particularly in coastal and deep-water regions [148, 179, 180]. Compared to onshore turbines, OWTs benefit from higher and more consistent wind speeds, reduced turbulence, and minimal land-use conflicts, leading to higher capacity factors and more predictable energy output [21, 181]. Offshore wind turbines can generally be categorised based on their foundation type into fixed-bottom and floating turbines [182, 183].

Fixed-Bottom Offshore Wind Turbines

Fixed-bottom turbines are anchored directly to the seabed and are the most mature and widely deployed offshore wind technology. They are generally suitable for shallow waters, typically up to 60 metres in depth [184]. Common foundation types include:

- **Monopile:** A single large-diameter steel tube driven into the seabed, used extensively in shallow European waters due to simplicity and cost-effectiveness [185].
- **Jacket:** A lattice framework with multiple legs, anchored by piles, suitable for medium-depth waters and offering higher structural stability [186].
- **Gravity-based:** Heavy concrete or steel structures that rely on their weight for stability, generally employed where seabed conditions are favourable [187].
- **Tripod or Tripile:** Three-legged structures providing stiffness and load distribution, typically used in intermediate water depths [188].

Fixed-bottom turbines are preferred for their proven reliability and relatively straightforward installation. However, they are limited by seabed depth and geotechnical conditions, and their deployment in deeper waters becomes economically and technically challenging [189].

Floating Offshore Wind Turbines

Floating wind turbines overcome the depth limitations of fixed-bottom foundations and enable energy extraction in deeper waters (typically over 60 metres) [190]. These turbines are mounted on buoyant platforms, moored to the seabed using tension lines or catenary anchors. The main types of floating platforms include:

- **Spar-buoy:** A tall, cylindrical structure partially submerged, offering stability through ballast at the bottom, with low motion in deep waters [191].
- **Semi-submersible:** Multiple columns connected by pontoons, providing stability through buoyancy and suitable for a wide range of water depths [192].
- **Tension-leg platforms (TLPs):** Platforms anchored with taut vertical tendons, minimising vertical motion and offering high stability for deep-water deployment [193].

Floating turbines allow access to stronger, more consistent wind resources, and reduce environmental impacts on the seabed and coastal areas [21]. They also enable integration with multi-energy platforms and offshore energy islands, where wind energy can be coupled with solar, wave, and energy storage technologies [155].

Technological and Operational Challenges

Regardless of the foundation type, offshore wind turbines face a range of complex technological and operational challenges that significantly influence their performance and longevity. These challenges encompass the dynamic management of loads under coupled wind–wave interactions, the continuous assessment of structural fatigue and reliability over extended operational lifetimes, the effective integration of offshore generation into power grids—particularly within hybrid multi-energy systems—and the implementation of efficient maintenance and monitoring strategies in harsh and unpredictable marine environments. To address these issues, high-fidelity numerical simulations and surrogate modelling techniques, such as Kriging, are widely employed to predict turbine performance, evaluate fatigue damage, and inform long-term design and investment decisions [194]. These advanced computational tools are especially critical for floating wind turbines, where platform motion introduces additional degrees of complexity compared with fixed-bottom configurations.

In summary, offshore wind turbines, encompassing both fixed-bottom and floating types, form a fundamental component of global renewable energy strategies. Fixed-bottom turbines dominate shallow-water installations due to proven technology and cost advantages, whereas floating turbines enable exploitation of deep-water sites with superior wind resources. The continued development of floating platforms and hybrid energy integration is expected to play a pivotal role in achieving scalable, low-carbon energy systems.

2.4.3 Related Research on Offshore Wind Energy Life Cycle Economics and Fatigue Assessment

To explore the economic life cycle analysis (LCA) of offshore wind farms, [195] conducted a multi-objective optimisation study addressing both economic performance and social acceptability. The study emphasizes the importance of selecting optimal locations and turbine arrangements to maximize energy production while minimizing costs and mitigating potential social and environmental impacts. [196] proposed an integrated, automated, and optimized framework for the layout and electrical infrastructure design of offshore wind farms. The framework is designed to simultaneously optimize multiple objectives, such as annual energy delivered and investment cost, providing a holistic approach to wind farm planning. Considering the coordination of power and hydrogen, [158] explored the cost competitiveness of offshore wind-based hydrogen production through participation in ancillary services markets. The findings reveal that for offshore wind-based hydrogen production to achieve cost competitiveness under current wind power generation levels, participation in ancillary services markets is essential. It also highlighted that allowing hy-

Table 2.8: Comparison of Fixed-bottom and Floating Offshore Wind Turbines

Aspect	Fixed-bottom Turbines	Floating Turbines
Definition	Turbines anchored directly to the seabed, suitable for shallow waters.	Turbines mounted on buoyant platforms, anchored via mooring systems, suitable for deep waters.
Foundation Types	Monopile, jacket, gravity-based, tripod/tripile.	Spar-buoy, semi-submersible, tension-leg platform (TLP).
Water Depth	Typically up to 60 metres.	Typically 60–1000+ metres.
Advantages	Proven technology, high stability, simpler installation.	Access to deeper waters and stronger winds, reduced seabed impact, integration with multi-energy platforms.
Challenges	Limited by depth and seabed conditions, installation weather-sensitive.	Higher costs, complex dynamic stability, sensitive to coupled wind–wave loads.
Applications	Most existing offshore wind farms, e.g., UK North Sea, Denmark.	Emerging deep-water projects, e.g., Hywind Scotland, WindFloat Atlantic.

drogen producers to benefit from the same subsidy policies as offshore wind farms dedicated solely to electricity generation could significantly reduce costs, further supporting the economic viability of green hydrogen production.

Studies on the LCA of the environmental performance of floating offshore wind systems remain limited, though some key studies offer valuable insights. Weinzettel et al. were pioneers in conducting LCA for offshore wind turbines in 2009 [197], while Jesuina et al. expanded the scope by analyzing both onshore and offshore wind farms in 2018 [198]. Pujol et al. assessed a pilot floating offshore wind farm using a detailed inventory of primary data and a geo-located electricity estimation model, identifying steel as a major contributor to the production of floating platforms and turbines [199]. [200] further integrated floating technology into LCA, evaluating the effects of locational factors such as water depth and distance from shore. This analysis of 20 fixed and floating offshore wind farms in the Great Lakes region of Michigan demonstrated competitive environmental performance compared to other wind platform technologies. Additionally, [201] introduced a holistic tool grounded in systematic and comprehensive methodologies to evaluate the economic and environmental impacts of floating offshore wind farms over their life cycles. This tool provides an integrated perspective, supporting the optimisation of wind farm design and operation.

Collectively, these studies highlight the dual economic and environmental impacts of floating

offshore wind systems, addressing indicators such as abiotic resource depletion, global warming, human ecotoxicity, freshwater ecotoxicity, and terrestrial ecotoxicity. However, they notably overlook the influence of environmental conditions on the performance and durability of power plant equipment.

Given the stronger wind and wave loads encountered by offshore turbines, certain critical components of the turbine may experience severe fatigue damage, potentially leading to catastrophic failures. To assess the life cycle fatigue damage on floating wind turbines, [202] proposed a stochastic deterioration model and fatigue damage assessment method for composite wind turbine blades in offshore environments. It can reliably estimate stress states, assess fatigue damage, analyse lifetime fatigue failure probability, and optimize the maintenance timing of composite wind turbine blades. [203] evaluated the fatigue damage of floating offshore wind turbine blades with three different hull configurations. The fatigue life of the blades is predicted by accumulating damage under various wind-wave conditions, based on a long-term Weibull distribution.

However, fatigue assessment requires extensive dynamic analyses across various environmental scenarios, resulting in high computational demand and complex numerical simulations. To tackle this issue, the study [204] proposed a probabilistic long-term fatigue damage assessment approach that combines the C-vine copula model with surrogate models such as the Kriging model and artificial neural networks (ANN). This approach is suitable for evaluating the long-term fatigue damage of structures in real-world environments and helps reduce computational costs. Likewise, the authors of [205] proposed a methodology to assess the energy production and fatigue mechanical loads of FOWT over a 30-year operational period. It employs cluster analysis to reduce the data to a computationally manageable number of simulation cases for evaluating energy production and mechanical fatigue loads. This approach can not only be used to predict the lifespan of offshore wind turbines but also to select potential optimal wind farm locations based on climatic patterns and the evolution of meteorological data. Moreover, to improve the efficiency of utilising limited datasets, the study in [206] explored fatigue damage prediction for offshore wind turbines by incorporating in-situ environmental conditions to assess the stresses at the base of offshore wind turbine towers and analysing the cumulative fatigue damage of the structure.

2.4.4 Research Gap

Despite the significant advancements in offshore energy systems, several critical research gaps persist that hinder the holistic development of sustainable energy island solutions. To the best of our knowledge, there is limited literature that comprehensively considered the dual impact of wind-wave conditions on both the economic feasibility and structural integrity of offshore infrastructure.

Existing studies often addressed these factors in isolation, neglecting the interdependence between environmental forces and their combined effects on energy system performance, durability, and life cycle costs. This lack of integrated analysis may lead to suboptimal site selection and insufficient planning for long-term operational resilience.

Another critical gap lies in fatigue damage prediction methodologies. Current approaches heavily rely on computationally expensive numerical models, such as those used in simulations of offshore wind turbines. While these models provide detailed insights, they are often unsuitable for long-term environmental assessments due to the typically short duration of available datasets and the computational burden of running simulations over extended periods. This limitation restricts the ability to conduct robust evaluations of structural reliability and operational performance under diverse environmental conditions, particularly in scenarios requiring large-scale or multi-site analyses.

2.5 Summary

This chapter has presented a comprehensive review of the existing literature relevant to robust scheduling of multi-energy microgrids, coordinated operation of integrated transmission–distribution systems, and the techno-economic optimisation of offshore energy islands under complex environmental conditions.

Firstly, the literature on MMGs has been reviewed, with particular emphasis on optimisation frameworks under uncertainty. Deterministic scheduling approaches, while widely adopted, are shown to be insufficient for real-world applications due to their inability to capture the variability of renewable energy sources and loads. Stochastic optimisation, robust optimisation, and DRO have been systematically compared. Among these, DRO has emerged as a particularly promising paradigm, offering a balanced trade-off between conservatism and economic performance by accounting for ambiguity in probability distributions. However, existing studies predominantly focus on single microgrids or short-term scheduling horizons, with limited consideration of low-carbon objectives and multi-temporal coordination under uncertainty.

Secondly, the chapter has examined coordinated scheduling of integrated energy systems, particularly the interaction between TSOs and DSOs. While substantial progress has been made in distribution-level optimisation and hydrogen-integrated energy systems, most existing works remain confined to a single network layer. The increasing penetration of renewable energy sources and multi-energy storage highlights the necessity for system-wide coordination between transmission and distribution networks. Nevertheless, the literature reveals a lack of comprehensive optimisation frameworks that jointly consider TSO–DSO coordination, electricity–hydrogen coupling,

and uncertainty-aware scheduling, especially from a low-carbon operational perspective.

Thirdly, the state of the art in offshore wind systems and floating offshore energy islands has been reviewed, with particular attention to their operational, economic, and structural challenges. Offshore wind, especially floating offshore wind, offers significant potential for large-scale decarbonisation and deep-water deployment. The integration of power-to-hydrogen technologies further enhances system flexibility and energy resilience. However, existing research largely addresses economic optimisation, structural design, or energy production in isolation. The impacts of extreme wind-wave conditions on both economic performance and structural integrity are rarely considered in a unified framework, despite their critical importance for long-term viability.

Finally, the chapter has reviewed techno-economic life-cycle analysis and fatigue assessment methodologies for offshore wind systems. Although high-fidelity simulation tools such as OpenFAST provide detailed insights into turbine dynamics and fatigue behaviour, their high computational cost limits their applicability for long-term and large-scale assessments. Recent studies employing surrogate models, such as Kriging, and clustering-based scenario reduction demonstrate potential for alleviating these computational challenges. Nonetheless, an integrated approach that combines environmental uncertainty modelling, fatigue assessment, and economic optimisation for offshore energy islands remains underexplored.

In summary, the literature reveals several key research gaps the lack of low-carbon, multi-temporal scheduling frameworks for multi-energy microgrids under uncertainty; insufficient coordination between transmission and distribution systems in hydrogen-integrated energy networks; and the absence of holistic techno-economic frameworks for offshore energy islands that jointly account for extreme environmental conditions, structural fatigue, and long-term economic performance.

These gaps motivate the research presented in this thesis, which aims to develop advanced, data-driven optimisation frameworks for integrated energy systems and offshore energy islands. By leveraging distributionally robust optimisation, coordinated system-level scheduling, and surrogate modelling techniques, this thesis seeks to bridge the divide between high-fidelity physical modelling and system-level operational optimisation, thereby contributing to the development of resilient and low-carbon energy infrastructures.

Chapter 3

Robust Scheduling for Multi-Energy Microgrids

Growing global concerns over environmental sustainability have intensified the need for low-carbon energy production and consumption. While multi-energy microgrids has emerged as a promising approach to achieving both decarbonisation and operational resilience, by coupling various energy carriers—such as electricity, heat, and gas—within a coordinated framework. This chapter presents a novel MMG optimisation framework designed to enhance both economic efficiency and carbon performance under uncertain operational conditions, as illustrated in Fig. 3.1.

In the first step, a day-ahead scheduling problem is formulated as a DRO model and solved using a C&CG algorithm. The day-ahead model determines hourly energy dispatch decisions by explicitly accounting for uncertainties in RES and load demand. In the second step, an intra-day scheduling scheme is implemented using MPC. The intra-day optimisation is performed at a 15-minute resolution to adjust operational decisions in response to updated system conditions, while remaining consistent with the day-ahead schedule.

To address the inherent uncertainties in renewable generation and demand variability, a data-driven distributionally robust optimisation approach is developed. The proposed two-stage, three-level structure employs the C&CG algorithm for day-ahead scheduling, supported by a K-means-based uncertainty modelling technique derived from historical datasets. This integration allows the MMG to anticipate and adapt to probabilistic variations in system inputs, thus improving reliability and cost-effectiveness in real-world applications.

Furthermore, the robustness of the day-ahead scheduling framework is complemented by a real-time operational layer based on model predictive control. This enables adaptive day–intra-hour optimisation, dynamically adjusting to updated system conditions and forecasts. The overall methodology is validated through empirical studies using an MMG model based on the IEEE 33-

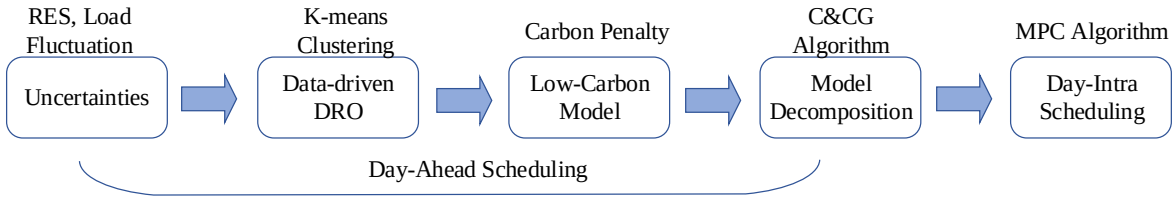

Figure 3.1: Framework of the 2-Step Approach and Research Methodology.

bus test system, demonstrating the practical feasibility of the proposed coordinated optimisation under realistic operational uncertainty.

Overall, the chapter provides an integrated modelling and optimisation framework for the flexible and low-carbon operation of MMGs, offering a robust and adaptive solution for future distributed energy systems facing the challenges of renewable variability and market volatility.

3.1 System Description and Modelling

3.1.1 Configuration of the MMG

As a microgrid with multi-energy capabilities, the system represented in Fig. 3.2 should be able to self-sustain in islanding mode or draw electricity from the main grid. The heart of this system lies in its energy hubs (EH), which contain dual energy forms of electricity and gas. The electricity network caters to hydrogen, electric-heating, and electrical loads, while the gas network attends to the hydrogen and gas-heating requirements. Hydrogen loads can be included through a power-to-gas (P2G) process. Heat loads, on the other hand, are fulfilled by an energy turbine (ET), CHP systems, and a gas turbine (GT). Electrical loads are satisfied through a controllable/dispatchable generator (CG), transactions with the main grid, battery storage (BS), and RES systems. The system's carbon footprint stems principally from three sources: the primary grid, gas network, and CGs.

3.1.2 Component modelling

As this study focuses on the operation of the multi-energy microgrid, the corresponding cost functions and constraints that each component needs to satisfy during the operation of the microgrid will be introduced and modeled separately in this section.

(1) Battery Storage

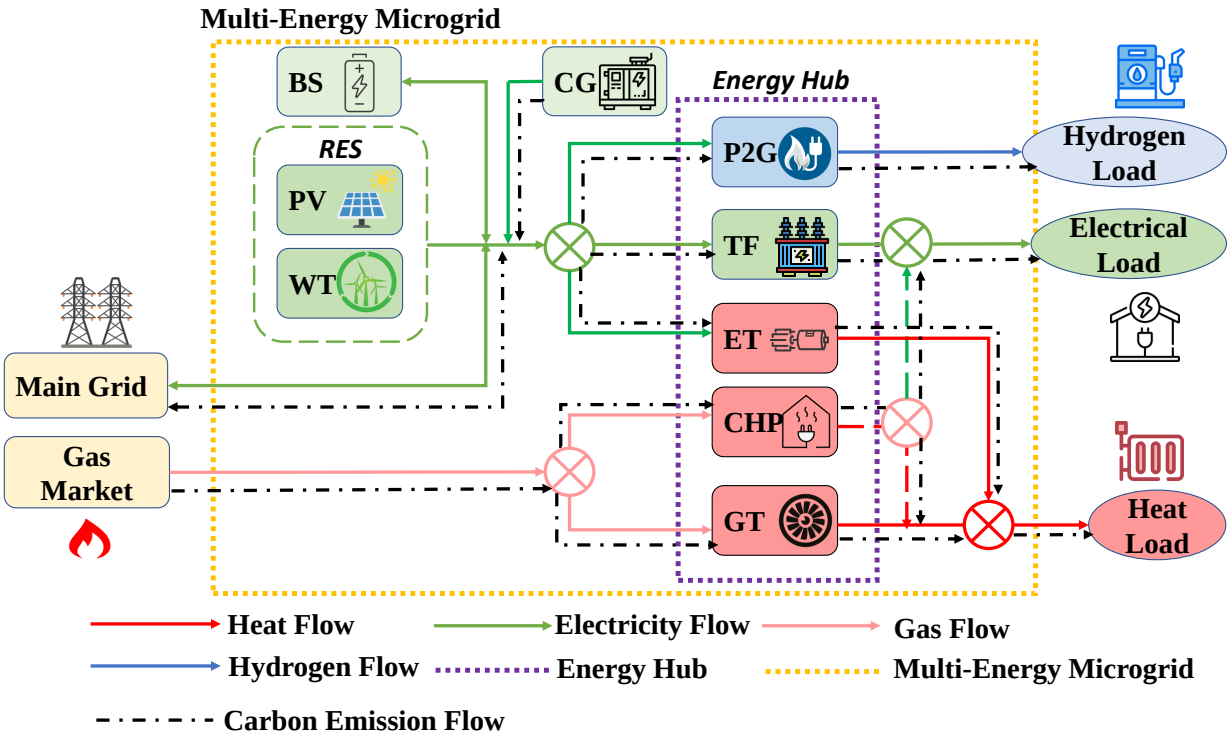

Figure 3.2: A Representative MMG Configuration.

i. Cost Function

The average charging and discharging cost of battery storage is:

$$C_{\mathrm{BS,t}} = \sum_{B \in B_e^{\mathrm{BS}}} \{K_{\mathrm{BS}} \left[\frac{1}{\eta_{B,\mathrm{dis}}} P_{B,t}^{\mathrm{sum,dis}} + \eta_{B,\mathrm{ch}} P_{B,t}^{\mathrm{sum,ch}} \right] \} \Delta t \tag{3.1}$$

where K_{BS} denotes the charging and discharging cost factor of the battery storage system; $\eta_{B,\mathrm{dis}}$ and $\eta_{B,\mathrm{ch}}$ represent the discharging and charging efficiency coefficients of the battery storage, respectively; B_e^{BS} refers to the set of battery storage systems; $P_{B,t}^{\mathrm{sum,dis}}$ and $P_{B,t}^{\mathrm{sum,ch}}$ denote the discharging and charging power of the battery at time t; and Δt is the scheduling time step.

ii. Constraints

The charging and discharging power of energy storage need to satisfy the maximum and minimum limit constraints:

$$u_{B,t}^{\mathrm{ch}} P_{B,\mathrm{BS}}^{\mathrm{min,ch}} \leq P_{B,t}^{\mathrm{sum,ch}} \leq u_{B,t}^{\mathrm{ch}} P_{B,\mathrm{BS}}^{\mathrm{max,ch}} \tag{3.2}$$

$$u_{B,t}^{\mathrm{dis}} P_{B,\mathrm{BS}}^{\mathrm{min,dis}} \leq P_{B,t}^{\mathrm{sum,dis}} \leq u_{B,t}^{\mathrm{dis}} P_{B,\mathrm{BS}}^{\mathrm{max,dis}} \tag{3.3}$$

where $P_{B,\mathrm{BS}}^{\max,\mathrm{ch}}$ and $P_{B,\mathrm{BS}}^{\min,\mathrm{ch}}$ denote the upper and lower limits of charging power; $P_{B,\mathrm{BS}}^{\max,\mathrm{dis}}$ and $P_{B,\mathrm{BS}}^{\min,\mathrm{dis}}$ denote the upper and lower limits of discharging power; and $u_{B,t}^{\mathrm{dis}}$ and $u_{B,t}^{\mathrm{ch}}$ represent the discharging and charging status of the energy storage system, respectively.

Logically, energy storage can only work in one of the states of charging or discharging. Therefore, the binary variables indicating the status of charging $u_{B,t}^{\mathrm{ch}}$ and discharging $u_{B,t}^{\mathrm{dis}}$ cannot both be 1 at the same time:

$$u_{B,t}^{\mathrm{ch}} + u_{B,t}^{\mathrm{dis}} \leq 1 \tag{3.4}$$

The number of transitions between charge and discharge states should be less than the maximum transition numbers.

$$\sum_{t} \left| u_{B,t}^{\mathrm{dis}} - u_{B,t-1}^{\mathrm{dis}} \right| \leq N_{B,\mathrm{BS}}^{lim} \tag{3.5}$$

where $N_{B,\mathrm{BS}}^{lim}$ denotes the maximum charge and discharge state transition times of energy storage.

The State-of-Charge (SOC) of battery storage at time t can be represented as below:

$$E_{B,t}^{SOC} = E_{B,t-1}^{SOC} - \frac{1}{\eta_{B,\mathrm{dis}}} P_{B,t}^{\mathrm{sum,dis}} \Delta \mathrm{t} + \eta_{B,\mathrm{ch}} P_{B,t}^{\mathrm{sum,ch}} \Delta \mathrm{t} \tag{3.6}$$

$$E_{B}^{SOC,\min} \leq E_{B,t}^{SOC} \leq E_{B}^{SOC,\max}, \forall t \in T \tag{3.7}$$

where $E_{B,t}^{SOC}$ denotes the energy stored in the energy storage device connected to node B at time t; $E_{B}^{SOC,\max}$ and $E_{B}^{SOC,\min}$ denote the upper and lower limits of the energy that the storage device can store, respectively.

(2) Controllable Generation

i. Cost Function

The start-up and shut-down cost of CG can be written as:

$$C_{ud} = [\max\{0, u_{G,t} - u_{G,t-1}\} S_{G,t}] \Delta t \tag{3.8}$$

where C_{ud} denotes the start-stop cost of the controllable generator (CG); $u_{G,t}$ and $u_{G,t-1}$ represent the start-stop status of the CG at time t and $t-1$, respectively; and $S_{G,t}$ denotes the start-stop cost factor.

The operation cost of a controllable generator is:

$$C_{\mathrm{CG},t} = A P_{\mathrm{CG},t} \Delta \mathrm{t} \tag{3.9}$$

where A is the operation cost factor of the CG; $P_{\mathrm{CG},t}, P_{\mathrm{CG},t-1}$ are Active power output of controllable generators at time t and t-1; A is the price of CG operation, £/kWh.

ii. Constraints

The maximum and minimum output of controllable generators can be restricted as:

$$u_{G,t} P_{\mathrm{CG}}^{\min} \leq P_{\mathrm{CG},t} \leq u_{G,t} P_{\mathrm{CG}}^{\max} \tag{3.10}$$

where $P_{\mathrm{CG}}^{\max}$ and $P_{\mathrm{CG}}^{\min}$ denote the maximum and minimum active power outputs of the CG.

Additionally, the controllable generators should meet the ramping constraints:

$$P_{\mathrm{CG},t} - P_{\mathrm{CG},t-1} \leq R^{up} \Delta \mathrm{t} \tag{3.11}$$

$$P_{\mathrm{CG},t-1} - P_{\mathrm{CG},t} \leq R^{down} \Delta \mathrm{t} \tag{3.12}$$

where R^{up} and R^{down} denote the upper and lower bounds of the ramping rate.

(3) Mutual Transactions

i. Cost Function

Power transaction cost between the micro-grid and distribution grid can be described as:

$$P_{\mathrm{SUB},t} = P_{\mathrm{SUB},t}^{buy} - P_{\mathrm{SUB},t}^{sell} \tag{3.13}$$

$$C_{M,t} = [\lambda_{M,t} P_{\mathrm{SUB},t}] \Delta \mathrm{t} \tag{3.14}$$

where $P_{\mathrm{SUB},t}$ denotes the transmission power between the main grid and the MMG; $P_{\mathrm{SUB},t}^{buy}$ and $P_{\mathrm{SUB},t}^{sell}$ denote the purchased and sold electricity between the microgrid and the distribution network, respectively; $\lambda_{M,t}$ denotes the time-varying price of power transaction, £/kWh.

And the gas purchase can be expressed as:

$$C_{G,t} = [\lambda_{G,t} Q_{buy,t}] \Delta \mathrm{t} \tag{3.15}$$

where $G_{buy,t}$ denotes gas purchase; $\lambda_{G,t}$ is gas price; $\lambda_{G,t}$ denotes the time-varying price of gas purchase, £/kWh.

ii. Constraints

The maximum purchase and selling of electricity at time t should also be restrained:

$$0 \leq P_{\mathrm{SUB},t}^{buy} \leq v_{M,t} u_{\mathrm{SUB},t} P_{\mathrm{SUB}}^{\max} \tag{3.16}$$

$$0 \leq P_{\mathrm{SUB},t}^{sell} \leq v_{M,t} [1 - u_{\mathrm{SUB},t}] P_{\mathrm{SUB}}^{\max} \tag{3.17}$$

where $P_{\mathrm{SUB}}^{\max}$ and $G_g^{\max}$ denote the maximum limits of power and gas transactions; $v_{M,t}$ denotes the operation mode of the microgrid, either island mode or grid-connected mode; $u_{\mathrm{SUB},t}$ denotes the status of power transaction from the microgrid to the distribution network in grid-connected operation mode.

The maximum purchase and selling of gas at time t should be restricted in (3.18):

$$0 \leq G_{g,t}^{buy} \leq G_g^{\max} \tag{3.18}$$

(4) Renewable Energy Generation

i. Cost Function

Wind and solar energy curtailment penalties at time t can be expressed as:

$$C_{\mathrm{WT},t} = \sum_{w \in U_w} \{c_{w,t}^{WTP} [P_{\mathrm{WT},t}^{*} - P_{\mathrm{WT},t}]\} \Delta \mathrm{t} \tag{3.19}$$

$$C_{\mathrm{PV},t} = \sum_{p \in U_p} \{c_{p,t}^{PVP} [P_{\mathrm{PV},t}^{*} - P_{\mathrm{PV},t}]\} \Delta \mathrm{t} \tag{3.20}$$

where $C_{\mathrm{WT},t}$ and $C_{\mathrm{PV},t}$ denote the cost of wind and solar curtailment at time t; $P_{\mathrm{WT},t}^{*}$ and $P_{\mathrm{WT},t}$ denote the predicted and actual output power of wind at time t; $c_{w,t}^{WTP}$ and $c_{p,t}^{PVP}$ denote the penalty cost factors for wind and solar curtailment; U_w and U_p denote the uncertainty sets of wind and solar energy; $P_{\mathrm{PV},t}^{*}$ and $P_{\mathrm{PV},t}$ denote the predicted and actual output power of solar at time t.

(5) Energy Hub

i. Cost Function

Assuming the EH is an integrated system, the start-stop cost is constant and included in $S_{G,t}$. The operation cost of EH can be expressed as a linear function:

$$C_{\mathrm{EH},t} = B P_{\mathrm{EH},t} \Delta \mathrm{t} \tag{3.21}$$

where $P_{\mathrm{EH},t}$ denotes the power output of the energy hub; B denotes the operational cost factor of EH equipment.

ii. Constraints

The maximum and minimum limits of EH facilities, which include CHP, GT, P2G, TF, and ET are defined by equation (3.22) to (3.26):

$$G_{\mathrm{CHP}}^{\min} \leq G_{\mathrm{CHP},t} \leq G_{\mathrm{CHP}}^{\max} \tag{3.22}$$

$$G_{\mathrm{GT}}^{\min} \leq G_{\mathrm{GT},t} \leq G_{\mathrm{GT}}^{\max} \tag{3.23}$$

$$P_{\mathrm{P2G}}^{\min} \leq P_{\mathrm{P2G},t} \leq P_{\mathrm{P2G}}^{\max} \tag{3.24}$$

$$P_{\mathrm{TF}}^{\min} \leq P_{\mathrm{TF},t} \leq P_{\mathrm{TF}}^{\max} \tag{3.25}$$

$$P_{\mathrm{ET}}^{\min} \leq P_{\mathrm{ET},t} \leq P_{\mathrm{ET}}^{\max} \tag{3.26}$$

where $G_{\mathrm{CHP}}^{\max}$ and $G_{\mathrm{CHP}}^{\min}$ denote the maximum and minimum outputs of the CHP; $G_{\mathrm{GT}}^{\max}$ and $G_{\mathrm{GT}}^{\min}$ denote the maximum and minimum outputs of the GT; $P_{\mathrm{P2G}}^{\max}$ and $P_{\mathrm{P2G}}^{\min}$ denote the maximum and minimum outputs of the P2G; $P_{\mathrm{TF}}^{\max}$ and $P_{\mathrm{TF}}^{\min}$ denote the maximum and minimum outputs of the TF; $P_{\mathrm{ET}}^{\max}$ and $P_{\mathrm{ET}}^{\min}$ denote the maximum and minimum outputs of the ET.

The corresponding ramping constraints of these facilities are also defined by equation (3.27) to (3.36):

$$G_{\mathrm{CHP},t} - G_{\mathrm{CHP},t-1} \leq R^{up}\Delta\mathrm{t} \tag{3.27}$$

$$G_{\mathrm{GT},t} - G_{\mathrm{GT},t-1} \leq R^{up}\Delta\mathrm{t} \tag{3.28}$$

$$P_{\mathrm{P2G},t} - P_{\mathrm{P2G},t-1} \leq R^{up}\Delta\mathrm{t} \tag{3.29}$$

$$P_{\mathrm{TF},t} - P_{\mathrm{TF},t-1} \leq R^{up}\Delta\mathrm{t} \tag{3.30}$$

$$P_{\mathrm{ET},t} - P_{\mathrm{ET},t-1} \leq R^{up}\Delta\mathrm{t} \tag{3.31}$$

$$G_{\mathrm{CHP},t-1} - G_{\mathrm{CHP},t} \leq R^{down}\Delta\mathrm{t} \tag{3.32}$$

$$G_{\mathrm{GT},t-1} - G_{\mathrm{GT},t} \leq R^{down}\Delta\mathrm{t} \tag{3.33}$$

$$P_{\mathrm{P2G},t-1} - P_{\mathrm{P2G},t} \leq R^{down}\Delta\mathrm{t} \tag{3.34}$$

$$P_{\mathrm{TF},t-1} - P_{\mathrm{TF},t} \leq R^{down}\Delta\mathrm{t} \tag{3.35}$$

$$P_{\mathrm{ET},t-1} - P_{\mathrm{ET},t} \leq R^{down}\Delta\mathrm{t} \tag{3.36}$$

where $G_{\mathrm{CHP},t}$ and $G_{\mathrm{CHP},t-1}$ denote the outputs of the CHP at times t and $t-1$; $G_{\mathrm{GT},t}$ and $G_{\mathrm{GT},t-1}$ denote the outputs of the GT at times t and $t-1$; $P_{\mathrm{P2G},t}$ and $P_{\mathrm{P2G},t-1}$ denote the outputs of the P2G at times t and $t-1$; $P_{\mathrm{TF},t}$ and $P_{\mathrm{TF},t-1}$ denote the outputs of the TF at times t and $t-1$; $P_{\mathrm{ET},t}$ and $P_{\mathrm{ET},t-1}$ denote the outputs of the ET at times t and $t-1$.

(6) Carbon Penalty

i. Cost Function

The carbon emission is mainly embedded in three parts: the power purchase, the gas purchase, and the CG output. The carbon emissions of EH are encompassed in the gas transactions. Therefore, the CP cost can be expressed as:

$$C_{\mathrm{CO2},t} = [\lambda^{P}_{\mathrm{CO2},t}(P^{buy}_{\mathrm{SUB},t} + P_{\mathrm{CG},t}) + \lambda^{G}_{\mathrm{CO2},t} G^{buy}_{g,t}]\Delta \mathrm{t} \tag{3.37}$$

where $\lambda^{P}_{\mathrm{CO2},t}$ denotes the cost factor for carbon emissions generated by power purchase and CG generation; $\lambda^{G}_{\mathrm{CO2},t}$ denotes the cost factor for carbon emissions generated by gas purchase.

(7) Power Balance

From Figure 3.2, the power balance can be expressed in general as below:

$$\begin{aligned} P_{\mathrm{CG},t} + P_{\mathrm{PV},t} + P_{\mathrm{WT},t} + P^{\mathrm{dis,sum}}_{B,t} + P_{\mathrm{SUB},t} = \\ P_{\mathrm{P2G},t} + P_{\mathrm{TF},t} + P_{\mathrm{ET},t} + P^{\mathrm{ch,sum}}_{B,t} \end{aligned} \tag{3.38}$$

$$G_{buy,t} = G_{\mathrm{CHP},t} + G_{\mathrm{GT},t} \tag{3.39}$$

$$P_{\mathrm{LG},t} = \eta_{\mathrm{P2G}} P_{\mathrm{P2G},t} \tag{3.40}$$

$$P_{\mathrm{LE},t} = \eta_{\mathrm{TF}} P_{\mathrm{TF},t} + \eta_{ce} G_{\mathrm{CHP},t} \tag{3.41}$$

$$P_{\mathrm{LH},t} = \eta_{\mathrm{ET}} P_{\mathrm{ET},t} + \eta_{\mathrm{ch}} G_{\mathrm{CHP},t} + \eta_{\mathrm{GT}} G_{\mathrm{GT},t} \tag{3.42}$$

where η_{P2G} denotes the energy conversion coefficient of P2G; η_{TF} denotes the energy conversion coefficient of TF; η_{ET} denotes the energy conversion coefficient of ET; η_{GT} denotes the energy conversion coefficient of GT; η_{ce} denotes the power conversion coefficient of CHP; η_{ch} denotes the heat conversion coefficient of CHP.

3.2 Uncertainty Characterisation and DRO Formulation

3.2.1 Mathematical Model of Day-Ahead Scheduling Problem

In this study, a data-driven DRO approach is employed for day-ahead scheduling to characterize the uncertainty associated with load demand and the RES system, specifically accounting for wind and solar power uncertainties. Utilizing empirical data, the K-means clustering algorithm is leveraged to generate K scenarios with initial probabilities.

Given that the actual distribution often deviates from the aforementioned distribution, a nuanced approach is adopted. Instead of solely relying on either the norm-1 or norm-inf separately to constrain the probability distribution, both norms are simultaneously considered. This approach culminates in the formation of an uncertain probability confidence set, guided by the constraints imposed by the comprehensive norm [207].

The overall structure of the data-driven distributionally robust day-ahead optimal scheduling model can be succinctly formulated in a two-stage matrix representation, as articulated in [208]. This study takes the start-stop status as the first-stage decision variable to instruct the dispatch scheduling, which cannot be adjusted after the uncertainties are revealed [207]. The second-stage variables stand for the operation decisions. The primary objective, as represented by the equation below, entails the minimization of start-up and shut-down costs, operational expenditures, and capacity payment costs, while simultaneously ensuring adherence to all equality and inequality constraints, where $a^T x$ is the start-up and shunt-down cost, and $b^T y_k$ represents the operational cost and CP.

$$\min_{x\in X}[a_T x+\max_{p_k\in\Omega}\sum_{k=1}^{K}p_k\min_{y_{k\in Y(x,\xi_k)}}b^T y_k] \tag{3.43}$$

$$s.t.\ Ax\le d \tag{3.44}$$

$$Bx=e \tag{3.45}$$

$$Cy_k\le D\xi_k,\forall\, k=0,\ \ldots,K \tag{3.46}$$

$$Gx+Hy_k\le g,\forall\, k=0,\ \ldots,K \tag{3.47}$$

$$Jx+Ky_k=h,\ \forall\, k=0,\ \ldots,K \tag{3.48}$$

3.2.2 Confidence Set of Day-Ahead Scheduling Model

In the DRO day-ahead scheduling model, there is uncertainty in the probabilities of various discrete scenarios. To ensure that the probability distribution of scenarios fluctuates within a reasonable range, the probability distributions of forecast errors in the output of renewable energy sources and load demand, are defined as sets of uncertainties. The confidence set is constructed as follows [207]:

$$\Omega = \left\{ \{p_k\} \left| \begin{array}{c} p_k \geq 0,\ k = 1,\ldots,K \\ \sum_{k=1}^{K} p_k = 1 \\ \sum_{k=1}^{K} \left| p_k - p_k^0 \right| \leq \theta_1 \\ \max_{1\leq k\leq K} \left| p_k - p_k^0 \right| \leq \theta_\infty \end{array} \right. \right\} \tag{3.49}$$

where p_k^0 stands for the initial probability of the scenario k. The norm-1 and norm-inf are used to constrain the confidence set of probability distributions.

Taking both types of norm constraints into account avoids extreme situations. Norm-1 limits the upper bound of the sum of the allowable deviations of all scenario probability distributions, while the norm-inf limits each scenario probability distribution. Assuming there are K scenarios from M historical samples, to construct confidence constraints under different values θ according to the historical data and confidence level [208]:

$$Pr\left\{ \sum_{k=1}^{K} \left| p_k - p_k^0 \right| \leq \theta_1 \right\} \geq 1 - 2Ke^{-2M\theta_1/K} \tag{3.50}$$

$$Pr\left\{ \max_{1\leq k\leq K} \left| p_k - p_k^0 \right| \leq \theta_\infty \right\} \geq 1 - 2Ke^{-2M\theta_\infty} \tag{3.51}$$

Let the right-hand side of the above formula be the confidence degree of uncertainty probability α_1 and α_∞ respectively, the tolerance values of norm-1 and norm-inf for the DRO model can be obtained as:

$$\theta_1 = \frac{K}{2M} \ln \frac{2K}{1-\alpha_1} \tag{3.52}$$

$$\theta_\infty = \frac{1}{2M} \ln \frac{2K}{1-\alpha_\infty} \tag{3.53}$$

To linearise the absolute value constraint, a binary auxiliary variable z_s^+,z_s^- is introduced in the norm-1 constraints [208]:

$$\begin{cases} \sum_{k=1}^{K} (p_k^+ - p_k^-) \leq \theta_1 \\ p_k = p_k^0 + p_k^+ - p_k^- \\ z_k^+ + z_k^- \leq 1 \\ 0 \leq p_k^+ \leq z_k^+ \theta_1 \\ 0 \leq p_k^- \leq z_k^- \theta_1 \end{cases} \tag{3.54}$$

Also, introducing y_s^+,y_s^- in the norm-inf constraints:

$$\begin{cases} p_k^+ - p_k^- \leq \infty \\ p_k = p_k^0 + p_k^+ - p_k^- \\ y_k^+ + y_k^- \leq 1 \\ 0 \leq p_k^+ \leq y_k^+ \theta_\infty \\ 0 \leq p_k^- \leq y_k^- \theta_\infty \end{cases} \tag{3.55}$$

3.3 Mathematical Model of 2-Step Scheduling

3.3.1 First Step: C&CG Method for Day-Ahead Scheduling

The C&CG method is a relatively efficient algorithm [209]. The C&CG algorithm is applied to decompose the original problem into the main problem (MP) and sub-problem (SP). Iterative calculations are performed until the difference in the optimisation results between MP and SP meets the set tolerance to solve the two-stage DRO problem.

(1) Master Problem

The MP is to minimize the optimal scheduling and CP cost under the condition that the worst-case scenario is known. It is a two-stage three-level optimisation problem, solved by the C&CG algorithm in this study. The results of the MP provide the lower bound (LB) to the C&CG algorithm [209]. Then the first-stage decision variables can be passed to the SP for iteration calculations.

$$\min_{x \in X, y_k^m \in Y(x,\xi_k), L} a^T x + L \tag{3.56}$$

$$L \geq \sum_{k=1}^{K} p_k^m b^T y_k^m, \forall m = 1,2,\ldots,n \tag{3.57}$$

where n is the iteration number.

(2) Sub-Problem

Under the condition that the first-stage decision variables are known, SP results provide the upper bound (UB) for the C&CG algorithm.

$$L(x^*) = \max_{p_k \in \Omega} p_k^m \min_{y_k^m \in Y(x^*,\xi_k)} b^T y_k^m, \forall m = 1,2,\ldots,n \tag{3.58}$$

The inner level can be reformulated into:

$$L(x^*) = \max_{p_k \in \Omega} \sum_{k=1}^{K} p_k^m \eta_k \tag{3.59}$$

$$s.t.\ \eta_k = argmin(b^T y_k^m) \tag{3.60}$$

The inner level represents the optimal scheduling result under scenario k, while the outer level represents the worst expectation of each scenario. The inner model should be solved first, and the outer model is subsequently handled [209]. Meanwhile, the probability of each scenario under the worst expectation can be obtained after clustering.

3.3.2 Second Step: MPC Method for Intra-Day Scheduling

Based on the results of optimal 24-hour day-ahead scheduling, the MPC is applied to obtain intra-day scheduling. MPC includes model prediction, rolling optimisation, and feedback correction, which has excellent tracking performance and anti-interference ability [210]. The scheduling step time interval for predicting the operation decision variables should be done in a 15-minute interval in the 2-hour ahead rolling horizon [211]. Only the first 15-minute decisions are adopted.

The start-up and shut-down status of CG should follow the day-ahead scheduling results. Therefore, the cost of CG start-stop should stay the same with the day-ahead scheduling results. The operational cost is:

$$C_{\mathrm{CG},t}^{intra} = A P_{\mathrm{CG},t}^{intra} \Delta t \tag{3.61}$$

where $C_{\mathrm{CG},t}$ and $C_{\mathrm{CG},t}^{intra}$ denote the day-ahead and intra-day costs of CG operation; $P_{\mathrm{CG},t}^{intra}$ denotes the intra-day CG generation.

Additionally, the charging and discharging power of battery storage during intra-day scheduling should try to follow day-ahead scheduling as well. The intra-day cost of the battery storage system is:

$$C_{\mathrm{BS},t}^{intra} = \sum_{B \in B_e^{\mathrm{BS}}} \{K_{\mathrm{BS},i} \left[\frac{1}{\eta_{B,\mathrm{dis}}} P_{B,t}^{\mathrm{sum,dis}} + \eta_{B,\mathrm{ch}} P_{B,t}^{\mathrm{sum,ch}} \right] + \lambda_{\mathrm{BS}}^{intra} \Delta E_{\mathrm{BS},t}\} \Delta t \tag{3.62}$$

where $C_{\mathrm{BS},t}$ and $C_{\mathrm{BS},t}^{intra}$ denote the day-ahead and intra-day costs of the battery storage system; $E_{\mathrm{BS},t}^{intra}$ and $E_{\mathrm{BS},t}^{ahead}$ denote the intra-day and day-ahead battery storage energies at time t; $\lambda_{\mathrm{BS},t}^{intra}$ denotes the cost coefficient for the difference between day-ahead and intra-day costs of the battery storage system.

$$s.t.\Delta E_{\mathrm{BS},t} \geq E^{intra}_{\mathrm{BS},t} - E^{ahead}_{\mathrm{BS},t} \tag{3.63}$$

$$\Delta E_{\mathrm{BS},t} \geq -(E^{intra}_{\mathrm{BS},t} - E^{ahead}_{\mathrm{BS},t}) \tag{3.64}$$

where $\lambda^{intra}_{\mathrm{BS}}$ is the cost coefficient for the difference between day-ahead and intra-day cost of battery storage.

Similar to battery storage, the intra-day power transactions can be written as:

$$C^{intra}_{M,t} = [\lambda_{M,t} P_{\mathrm{SUB},t} + \lambda^{intra}_{M,t} \Delta E_{M,t}]\Delta t \tag{3.65}$$

$$s.t.\Delta E_{M,t} \geq E^{intra}_{M,t} - E^{ahead}_{M,t} \tag{3.66}$$

$$\Delta E_{M,t} \geq -(E^{intra}_{M,t} - E^{ahead}_{M,t}) \tag{3.67}$$

where $C_{M,t}$ and $C^{intra}_{M,t}$ denote the day-ahead and intra-day costs of power transactions; $\Delta E_{M,t}$ and $\Delta E_{\mathrm{BS},t}$ denote the differences between day-ahead and intra-day power transactions and battery storage at time t; $E^{intra}_{M,t}$ and $E^{ahead}_{M,t}$ denote the intra-day and day-ahead power transactions at time t; $\lambda^{intra}_{M,t}$ denotes the cost coefficient for the difference between day-ahead and intra-day costs of power transactions.

The flow chart for day-ahead and intra-day scheduling problems is shown in Figure 3.3. The objective function of intra-day scheduling is:

$$min \sum_{t=1}^{T} (C^{intra}_{\mathrm{CG},t} + C^{intra}_{\mathrm{EH},t} + C^{intra}_{M,t} + C^{intra}_{\mathrm{BS},t} + C^{intra}_{G,t} + C^{intra}_{\mathrm{CO2},t} + C^{intra}_{\mathrm{WT},t} + C^{intra}_{\mathrm{PV},t}) \tag{3.68}$$

where $C^{intra}_{\mathrm{WT},t}$ and $C^{intra}_{\mathrm{PV},t}$ stand for the curtailment penalty of wind and solar energy.
where $C_{\mathrm{EH},t}$ and $C^{intra}_{\mathrm{EH},t}$ denote the day-ahead and intra-day operation costs of the energy hub; $C_{G,t}$ and $C^{intra}_{G,t}$ denote the day-ahead and intra-day costs of gas purchase; $C_{\mathrm{CO2},t}$ and $C^{intra}_{\mathrm{CO2},t}$ denote the day-ahead and intra-day carbon costs; $C_{\mathrm{WT},t}$ and $C^{intra}_{\mathrm{WT},t}$ denote the day-ahead and intra-day costs of wind curtailment; $C_{\mathrm{PV},t}$ and $C^{intra}_{\mathrm{PV},t}$ denote the day-ahead and intra-day costs of solar curtailment.

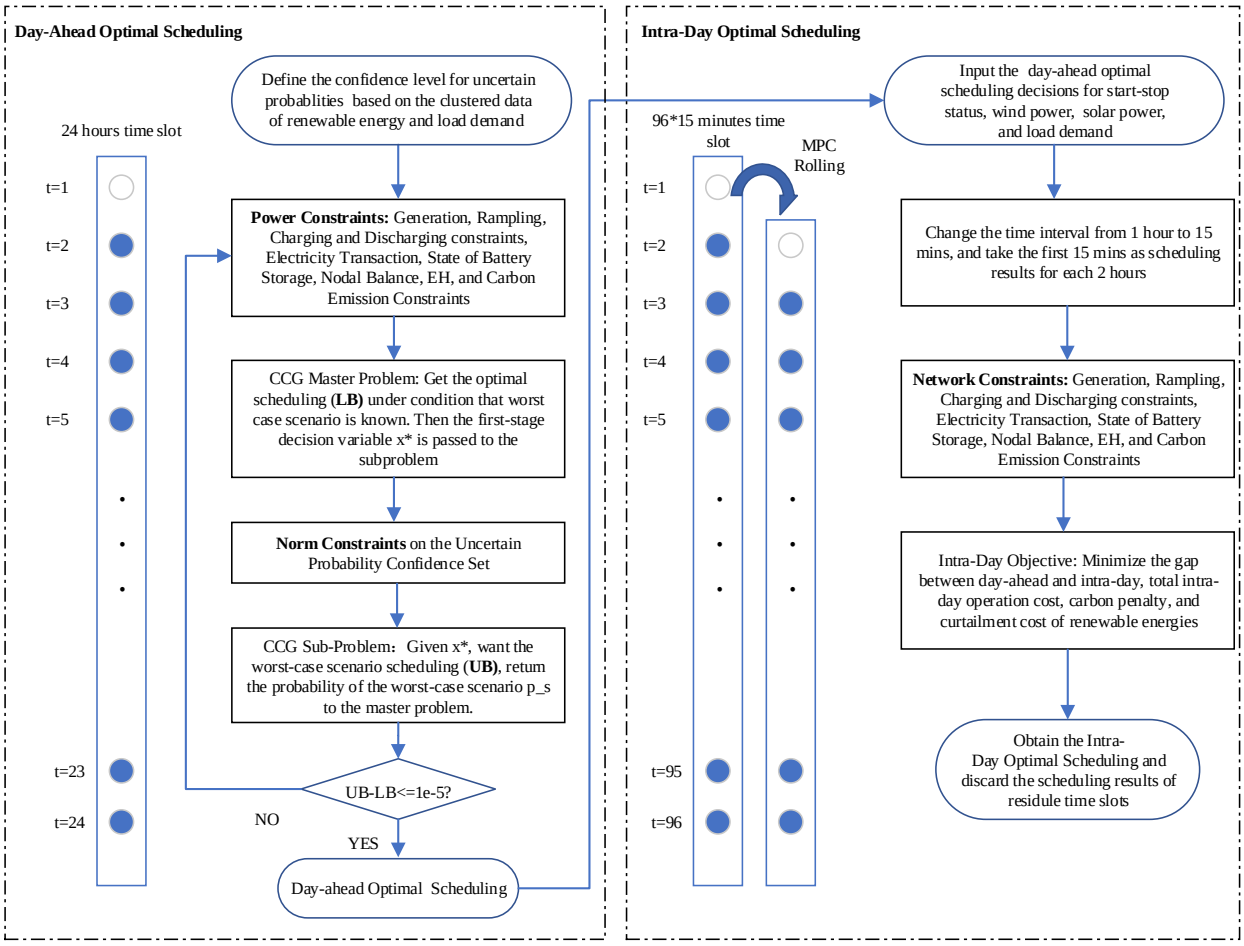

Figure 3.3: Flow Chart of Day-ahead and Intra-day Scheduling.

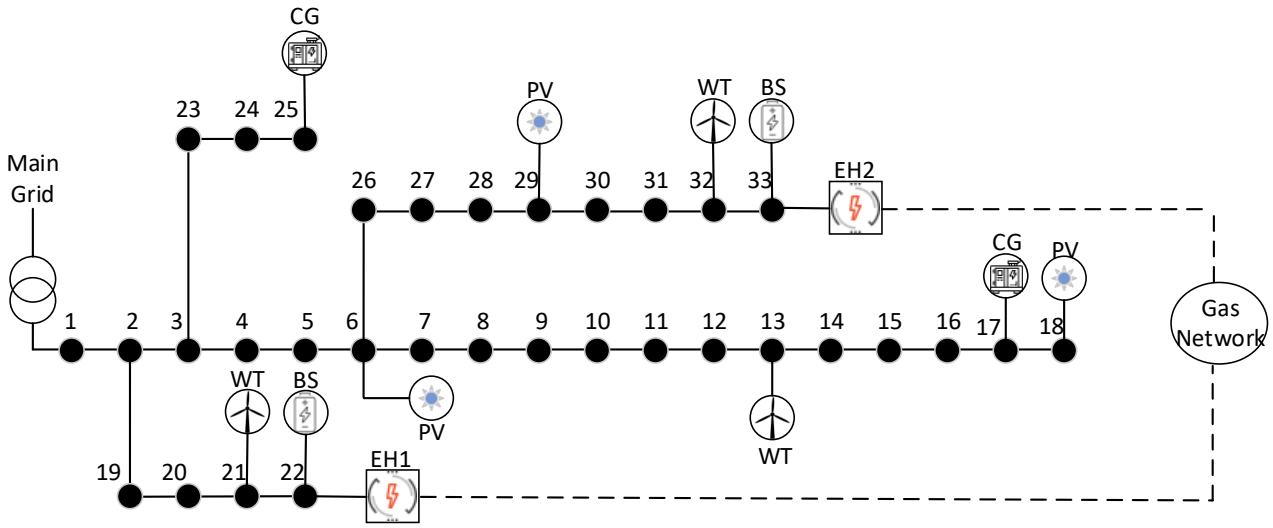

Figure 3.4: 33-Bus MMG System.

3.4 Case Study Setup and Simulation Results

The proposed method is tested on an MMG, which is structured based on the IEEE 33-bus radial distribution system [212]. Fig. 3.4 consists of 33 load buses, 2 battery storage systems, 2 controllable generators, 3 wind turbines, 3 photovoltaic generators, and 2 energy hubs, connected to the main grid and the gas network for power and gas transactions. The inner structure of the energy hub is shown in Fig. 3.5.

The power ratings of CG, WT, and PV are 0.5 MW, 0.8 MW, and 0.8 MW respectively, while the system load-rated active power is 3.715 MW [213]. The electricity (Elect), hydrogen (Hydro), and heat load (Heat) of EH are 0.1 MW, 0.05 MW, and 0.05 MW at node 22 and node 33. The ramp-up and down rates are set in Table 3.3 and the power ratings of generation and load can be seen in Table 3.1.

Given the pronounced time delays and substantial thermal losses inherent in long-distance thermal transmission [214], [215], this study adopts a strategy of localized thermal energy supply ignoring the losses. The substation voltage is 12.66 kV and voltage limits $\Delta V_{\text{max BUS}}$ are set to be $\pm 5\%$ of the nominal level [212], [216].

To exemplify the feasibility of our proposed model. A linearized DistFlow model [217] is employed to attain the optimal voltage profile for the reconstructed IEEE 33-bus MMG by minimizing generation cost while adhering to network constraints Eq. (3.70) to (3.73). The resulting optimal voltage profile is visually depicted in Figs. 3.6, providing a comprehensive illustration

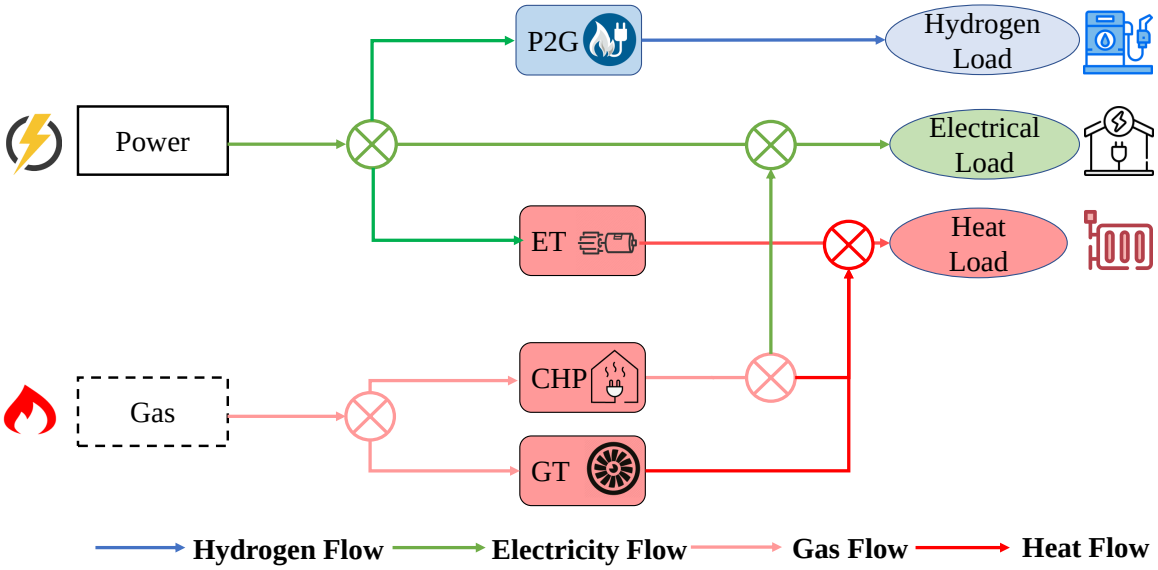

Figure 3.5: Internal Configuration of an EH.

of the feasibility and practical application of our devised approach in the realm of electric power systems.

$$\min \sum_{t \in T} C_t \tag{3.69}$$

$$P_{\mathrm{CG}}^{i,t} + P_{\mathrm{PV}}^{i,t} + P_{\mathrm{WT}}^{i,t} + P_{B,i,t}^{\mathrm{dis,sum}} + P_{\mathrm{SUB}^{i,t}} = P_{\mathrm{P2G}}^{i,t} + P_{\mathrm{TF}}^{i,t} + P_{\mathrm{ET}}^{i,t} + P_{B,i,t}^{\mathrm{ch,sum}} \tag{3.70}$$

$$V_{i+1,t} = V_{i,t} - (r_{ij}^{\mathrm{line}} P_{ij,t}^{\mathrm{line}} + x_{ij}^{\mathrm{line}} Q_{ij,t}^{\mathrm{line}})/V_0 \tag{3.71}$$

$$\underline{V}_i \le V_{i,t} \le \overline{V}_i \quad \forall i \in N \tag{3.72}$$

$$\underline{P}_{ij}^{\mathrm{line}} \le P_{ij,t}^{\mathrm{line}} \le \overline{P}_{ij}^{\mathrm{line}} \quad \forall (i,j) \in E \tag{3.73}$$

Among these, C_t represents the generation cost at time t, while Eq. (3.70) defines the power balance at node i during time t. The parameters r_{ij}^{line} and x_{ij}^{line} signify the resistance and reactance of branch $i-j$. The variables $\underline{V}_i$ and $\overline{V}_i$ denote the lower and upper limits of the voltage magnitude at node i, respectively. Here, V_0 represents the reference voltage. The terms $P_{ij,t}^{\mathrm{line}}$ and $Q_{ij,t}^{\mathrm{line}}$ correspond to the active power and reactive power of branch $i-j$. The quantities $\underline{P}_{ij}^{\mathrm{line}}$ and $\overline{P}_{ij}^{\mathrm{line}}$ indicate

the lower and upper limits of the active power flow on edge $i-j$, respectively. Additionally, T represents the set of hours. N denotes the set of all nodes in the power system, and E represents the set of all edges in the power system.

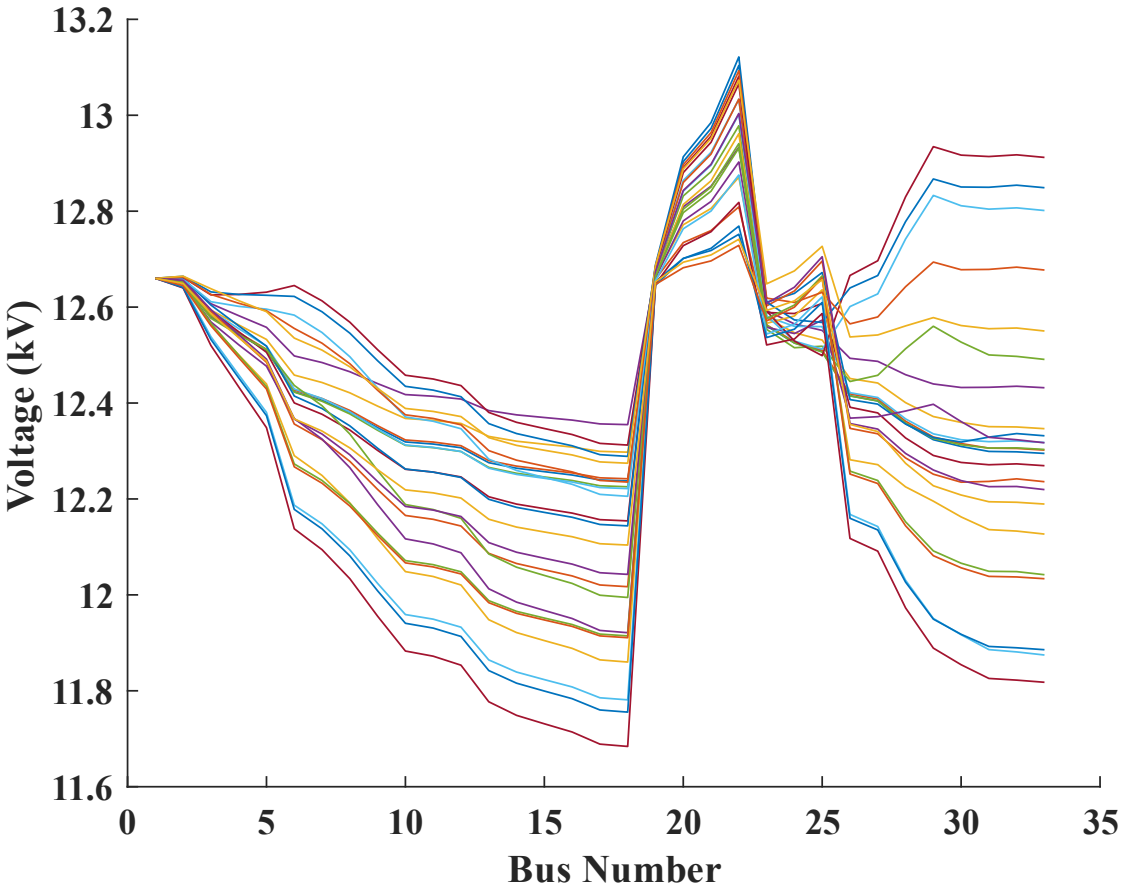

Figure 3.6: Bus Voltage Variation Over 24 Hours.

Table 3.1: Generation and Load Power Ratings

Unit	WT	PV	CG	Elect	Hydro	Heat
Power (MW)	0.8	0.8	0.5	0.1	0.05	0.05

3.4.1 DRO Uncertainty Modelling and Settings

At the day-ahead scheduling stage, 24-hour data of 365 scenarios of wind speed and solar intensity are collected, as well as load demand. The K-means method is subsequently employed to cluster

10 representative scenarios. The selection of the clustering center number K is assessed using the silhouette coefficient, thereby reinforcing the robustness of our approach. The silhouette coefficient for a given sample is calculated as (b - a)/max(a, b), where 'a' represents the average distance from the sample to other points within the same cluster, and 'b' denotes the average distance to points in the nearest neighboring cluster [218]. A silhouette coefficient nearing 1 indicates precise sample clustering, whereas proximity to -1 suggests a higher likelihood of samples being inaccurately assigned to the wrong cluster. A silhouette coefficient close to 0 signifies that samples are positioned on the boundary of clusters. For our model with $K = 10$, the computed average silhouette coefficient is 0.82267, which reflects the effectiveness of our approach. Figs. 3.7 (a) and (b) show the wind and solar power of the 10 clustering scenarios. The initial possibility of each scenario is generated as shown in Table 3.2. The confidence levels for uncertain probabilities are defined as $\alpha_1 = 0.5$ and $\alpha_\infty = 0.99$.

Table 3.2: Probabilities of Scenarios

K	1	2	3	4	5	6	7	8	9	10
p_k	0.139	0.073	0.030	0.080	0.022	0.054	0.095	0.098	0.295	0.113

The power price for bilateral transactions between the main grid and the MMG in the test system, denoted as P, are shown in Fig 3.8. The prices of carbon emissions embedded in the generation of power and gas are defaulted as 0.35 and 0.21 times the power transaction price separately. The gas price is 0.8 times the power price [219]. Moreover, the operation price of a controllable generator is 0.1£/kWh, while the charging and discharging price of battery storage is 0.005£/kWh. The operation cost of the EH is 0.1£/kWh and the start-stop cost is £1000. Details of these parameter settings are shown in Table 3.3.

Table 3.3: Setting of Case Study Parameters

Variable	**Value**	**Variable**	**Value**	**Variable**	**Value**
$C_{WT,t}^{intra}$	£0.1/kWh	$P_{B,\mathrm{BS}}^{\min/\max}$	0 / 80 kW	$S_{G,t}$	£1000
$C_{PV,t}^{intra}$	£0.1/kWh	R^{up}/R^{down}	80 / 80	η_{P2G}	0.6
K_{BS}	£0.005/kWh	$P_{\mathrm{CG}}^{\min/\max}$	0 / 300 kW	η_{TF}	0.95
A	0.1	$P_{\mathrm{P2G}}^{\min/\max}$	0 / 300 kW	η_{ET}	0.7
B	0.1	$P_{\mathrm{TF,ET}}^{\min/\max}$	0 / 200 kW	η_{GB}	0.7
λ_{BS}^{intra}	£0.1/kWh	$G_{\mathrm{CHP,GB}}^{\min/\max}$	0 / 200	η_{ce}	0.4
$\lambda_{M,t}^{intra}$	£0.1/kWh	$E_B^{SOC,\min/\max}$	200 / 1000 kWh	η_{ch}	0.45

The predicted total renewable energy output can be seen in Fig. 3.9 (a). At 11-14h, the output power of the PV keeps increasing and reaches the peak value of about 1600 kW at around 14h.

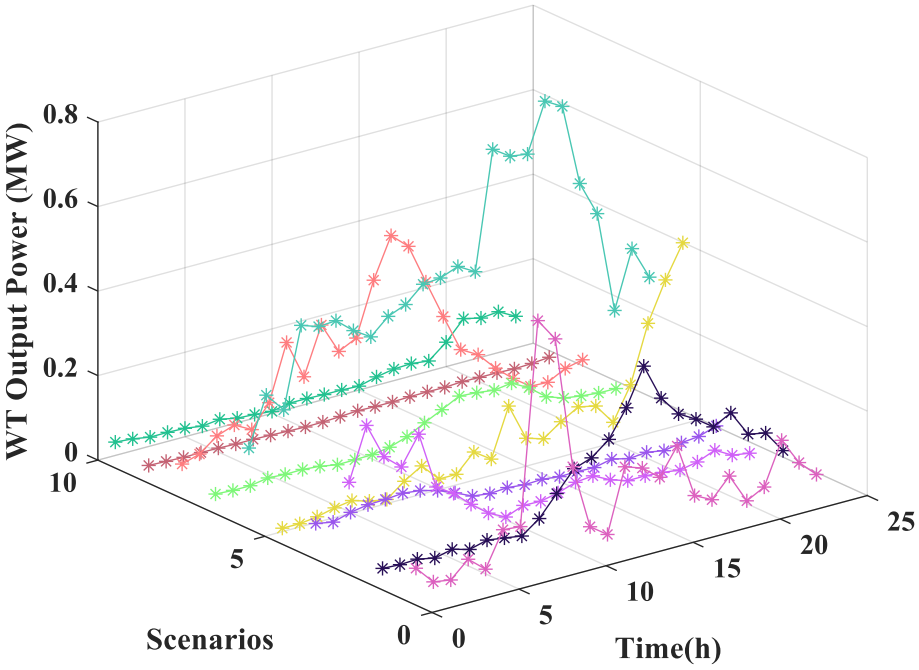

(a) Wind Power Scenarios with Possibility

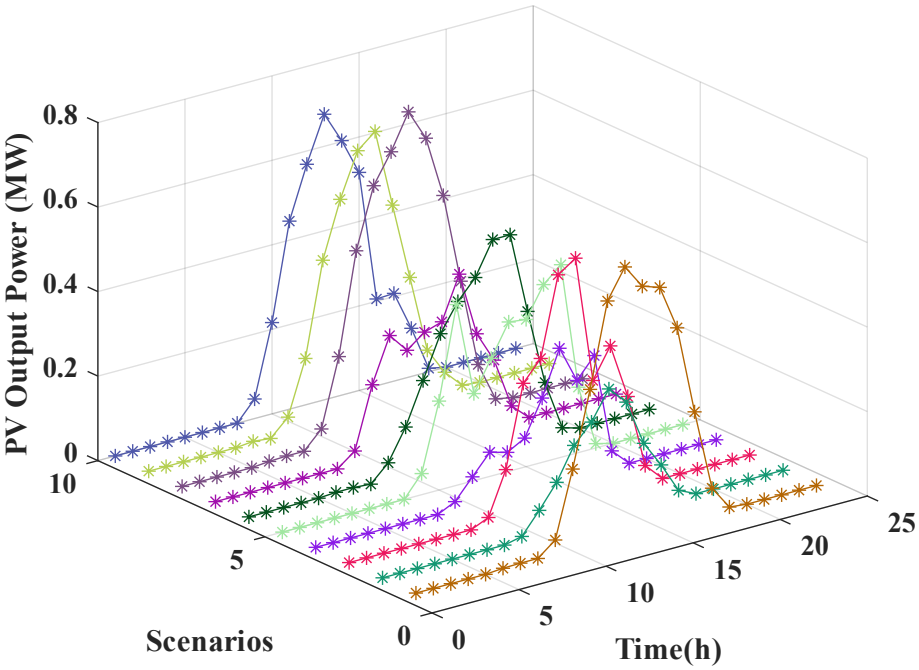

(b) Solar Power Scenarios with Possibility

Figure 3.7: 10 Clustered Scenarios of RES.

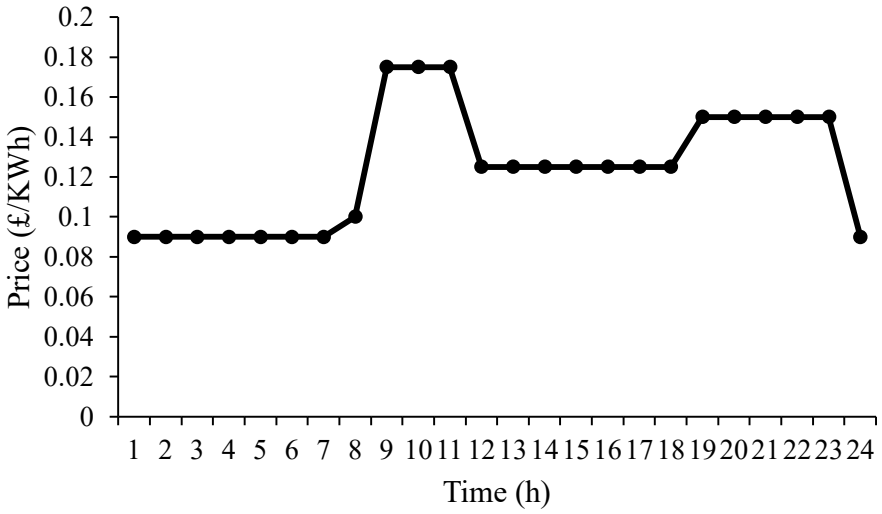

Figure 3.8: Electricity Price Setting (P).

However, wind power output stays about 200-400 kW all day and reaches peak values at around 8h and 16h. The hydrogen, heat, and electricity loads of the energy hub are shown in Fig. 3.9 (b). The load of the energy hub keeps rising from 6h and reaches its peak value of about 800 kW at around 17h, then decreases steadily to 250-300 kW. The total nodal load in the test system is depicted in Fig. 3.9 (c). It is obvious that there are two peaks at around 11h and 21h, which are both about 2250kW.

3.4.2 Day-Ahead Results and Discussion

In the day-ahead operation, initial worst-case expectations are predicated on ten representative scenarios with corresponding probabilities, thereby setting the groundwork for the first iterative application of C&CG to day-ahead optimisation. The optimal scheduling, depicted in Fig. 3.10, demonstrates strategic energy management across different hours of the day. During peak load periods, around 9h and 21h, controllable generators exhibit maximum output, nearly 900kW, ensuring sufficient power supply. Concurrently, the microgrid draws electricity from the primary grid during off-peak hours, namely between 1-10h and 15-24h, correlating with a relatively high level of carbon emissions.

As Fig. 3.10 shows, around 9h and 21h, the total output of controllable generators reaches the peak value of about 900kW, providing enough power during the period when the load reaches its peak value. Also, during 1-10h and 15-24h, the microgrid draws electricity from the main grid. At the same time, the amount of carbon emitted is relatively high during the day accordingly. Conversely, the microgrid sells electricity to the main grid over 11-15h corresponding to the period

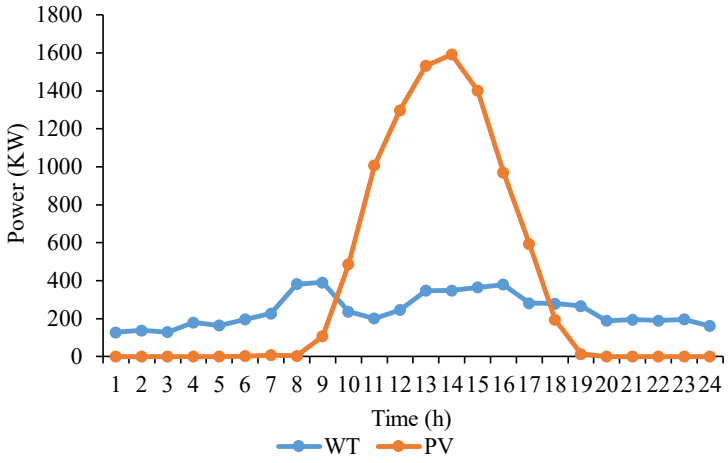

(a) RES Power Day-ahead Prediction

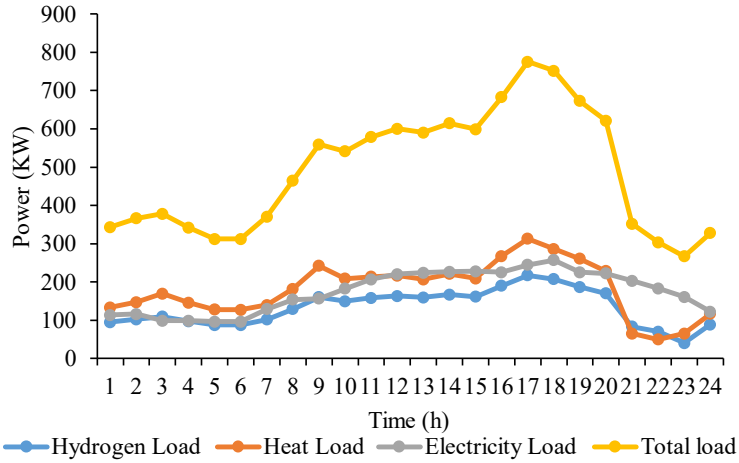

(b) EH Load Day-ahead Prediction

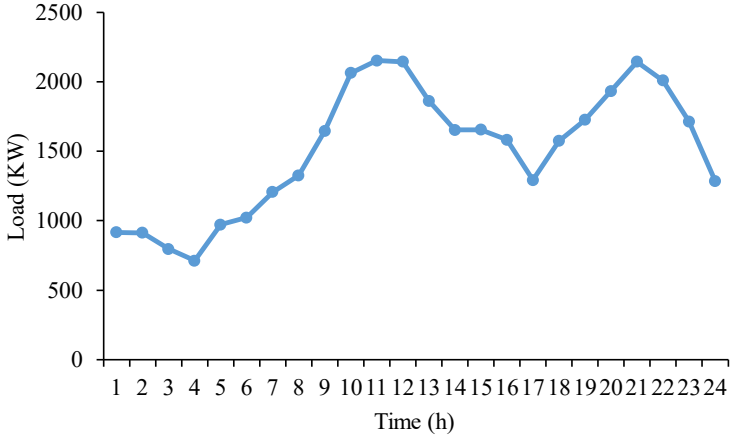

(c) Total Nodal Load Day-ahead Prediction

Figure 3.9: Day-Ahead Prediction Results.

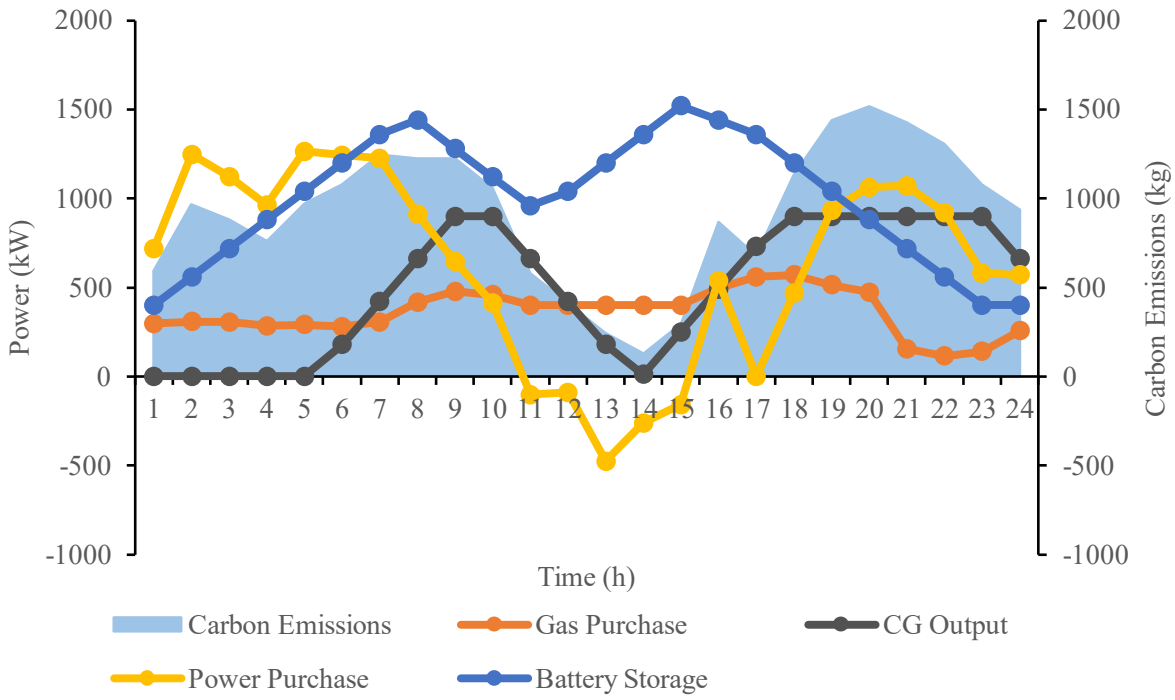

Figure 3.10: Day-Ahead DRO Scheduling Results.

that the RES generates the maximum power. Consequently, the overall carbon emissions reach the valley value because of the high output of the RES.

Conversely, the microgrid exports power back to the main grid from 11-15h, which is the period of peak RES production. This results in a significant dip in carbon emissions due to the substantial RES output. Meanwhile, the battery storage system displays two significant charging peaks at around 8h and 20h, which are associated with the times when the CG is operating at its highest capacity and the microgrid purchases a considerable amount of electricity from the main grid. However, the battery discharges during 8-11h and 15-24h, in line with the periods of decreased RES output. This behavior demonstrates the critical role of the battery system in supplementing the CG during high load demands, ensuring a well-balanced and efficient microgrid operation.

3.4.3 Result Comparison with RO/SO Methods

To showcase the advantages of the DRO approach, it is essential to draw comparisons with both RO and SO methods. In this context, the worst-case scenario outcome is considered as the optimal scheduling result for RO, while for SO, the optimal scheduling is obtained by approximating a normal distribution for the probability distribution in the clustered 10 typical scenarios. This comparative analysis serves as a means to highlight the advantages of the DRO approach in effectively

addressing uncertainties inherent in optimisation problems.

In Fig. 3.11 (a) and (b), the optimal scheduling results for RO and SO are presented. The trends among the three methods are observed to be similar, yet notable differences persist. Specifically, the overall CG output under RO is the lowest, amounting to 11820 KWh, while its power purchase is the highest at 14864.71 KWh. In contrast, the overall CG output under SO is the highest at 12185.49 KWh, and the corresponding power purchase is the lowest at 14499.25 KWh.

This indicates that the MMG produces less electricity and relies more on power purchases from the main grid under RO, whereas it produces more and purchases less under SO. As DRO results lie between RO and SO, it implies that DRO achieves greater savings than RO while adopting a more conservative approach than SO. To enhance the clarity of the advantages of DRO, a quantified cost and carbon emissions comparison is conducted of RO and SO in Table 3.4. The results show that RO yields the highest cost, while SO incurs the lowest expenses. Meanwhile, DRO falls between RO and SO in terms of cost implications, further signifying that DRO strikes a balance between the conservative attributes of RO and the economic efficiency associated with SO.

Table 3.4: Result Comparison of Solving Methods

Methods	**Cost with CP (£)**	**Carbon Emissions (kg)**
RO	6405.97	21981.73
DRO	6279.81	22053.65
SO	6023.19	22221.65

3.4.4 Effects of Employing EH

To illustrate the advantages of employing EH, generation is bifurcated to cater to distinct loads, as highlighted in [220]. In this case, the CHP unit is partitioned into two segments. Electricity and heat loads are independently provided by gas-fired power plants and boilers with higher energy conversion efficiencies, which are 0.53 and 0.8 as mentioned in [220]. The internal configuration of the EH system is modified, as depicted in Fig. 3.12. It is assumed that the operational costs of the CHP unit are equivalent to those of the power plant and boiler, with the gas price set at 0.8 times the power transaction price.

The presented findings, as delineated in Table 3.5, distinctly manifest a consequential increase in both total cost and carbon emissions when the CHP system is omitted from the energy framework. Specifically, the absence of CHP leads to a significant rise of £62 in total costs and an increase of 950 kg in carbon emissions, notwithstanding the fact that the power plant and boiler exhibit higher energy conversion efficiencies compared to the CHP. This observed phenomenon

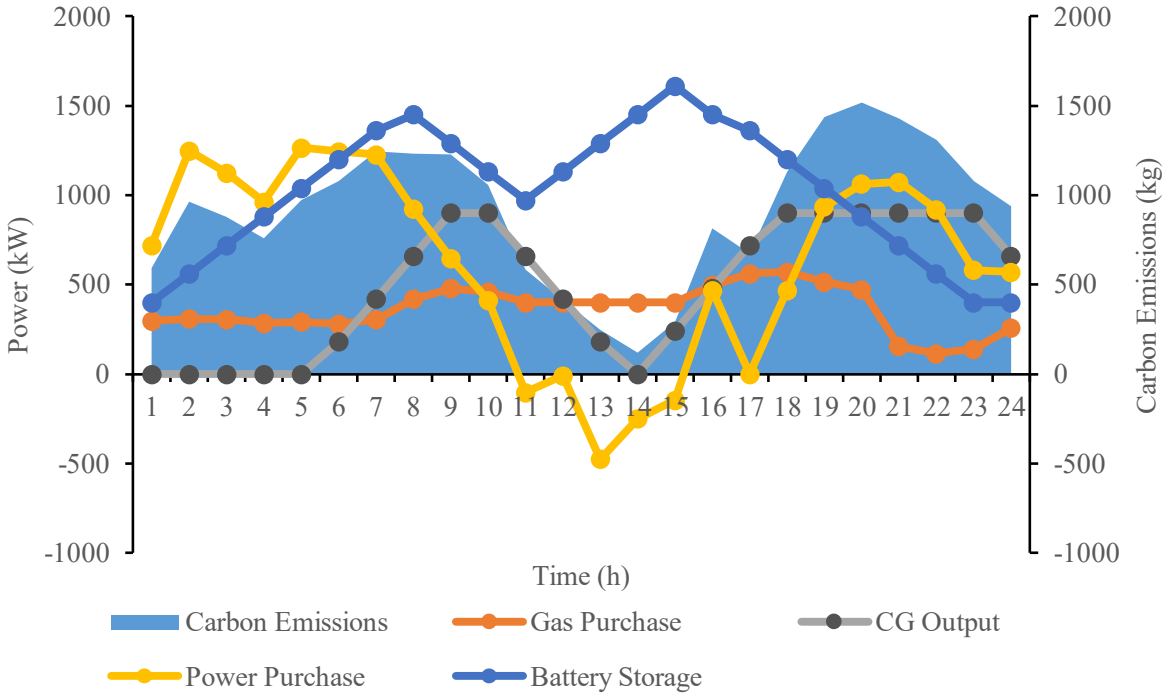

(a) Robust Optimal Scheduling Results

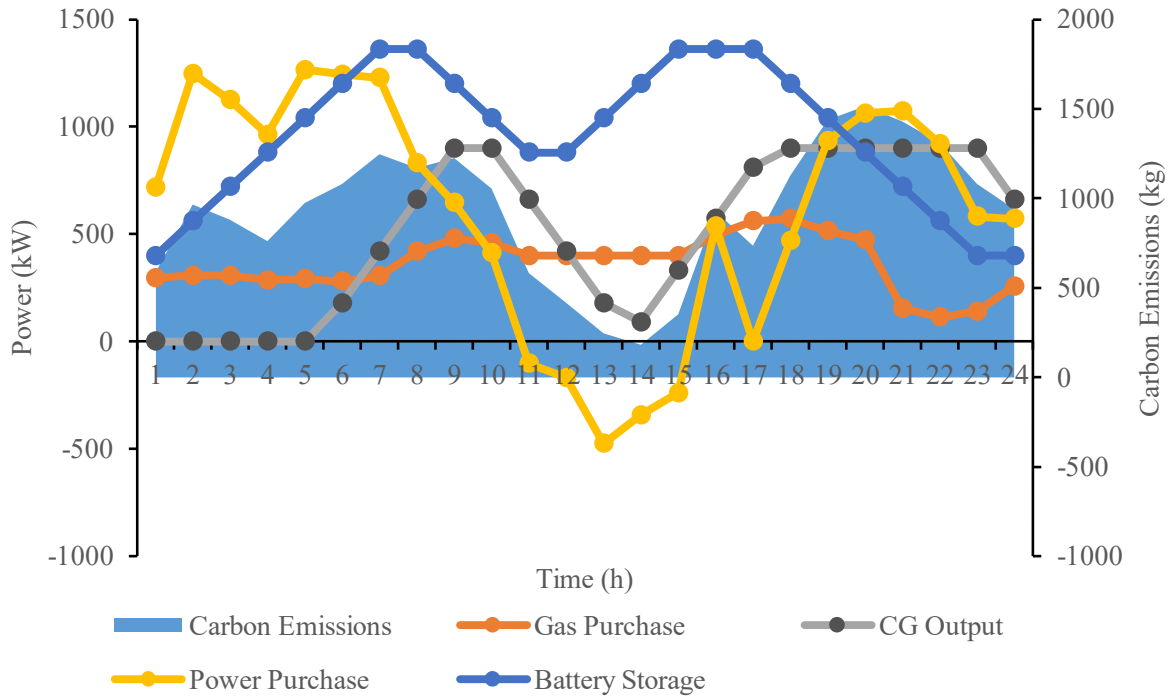

(b) Stochastic Optimal Scheduling Results

Figure 3.11: Robust and Stochastic Scheduling Results.

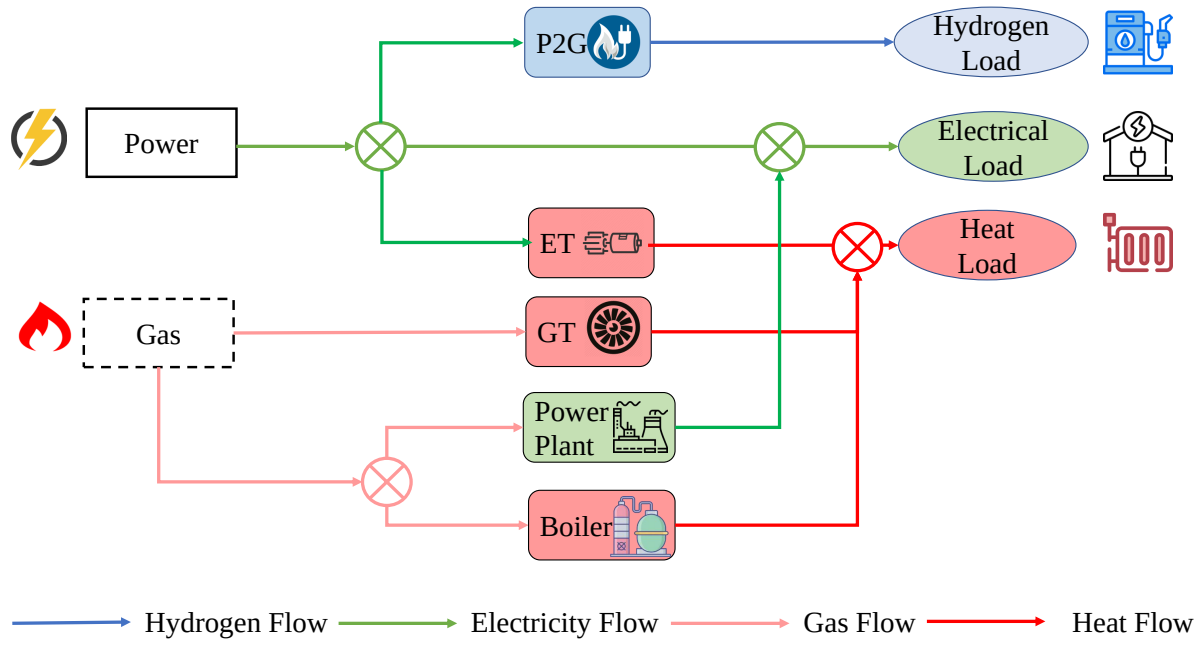

Figure 3.12: Internal Configuration of EH without CHP.

underscores the capacity of CHP to capitalize on residual energy, converting it into a usable form, thereby substantially enhancing overall energy utilization within the power system [221]. In a broader context, the incorporation of CHP emerges as a potent driver for expediting the critical endeavor of decarbonization.

Table 3.5: Cost and Carbon Impacts of CHP

Impacts of CHP	**No CHP**	**With CHP**
Cost (£)	6341.58	6279.80
Carbon Emissions (kg)	23002.60	22053.65

3.4.5 Impacts of Carbon Penalty

From Fig. 3.13 (a), the carbon emissions decrease significantly when considering the CP between 10-18h (hours 10 to 18), a period characterized by relatively high load demand for EH in Fig. 3.9 (b). That is because the operator prefers to use cleaner energy sources like wind and solar power, which can be stored in a battery, rather than using energy sources that produce more carbon emissions to meet the electricity and heat demands. Therefore, the battery in Fig. 3.13 (c) would

store the excess power instead of selling it to the main grid, which can be seen in Fig. 3.13 (d). Accordingly, the gas purchase in Fig. 3.13 (b) goes down slightly because the EH prefers cleaner energies to supply the electricity and heat loads. Meanwhile, the output of controllable generators in Fig. 3.13 (e) decreases greatly even though the demand is high during that time.

To represent the effects of CP, Table 3.6 is shown, where with CP, the total carbon emissions of one day are reduced by 2.6t while the day cost increases by £1560. Overall, it underscores the significant potential of CP in facilitating substantial reductions in carbon emissions.

Table 3.6: Cost and Carbon Impacts of CP

Day-Ahead Results	**Cost (£)**	**Carbon Emissions (kg)**
No CP	4719.24	24676.63
With CP	6279.80	22053.65

In addition, it is discernible that alterations in carbon pricing have contrasting effects on both the total cost and carbon emissions. To investigate the effects of carbon pricing, variations in carbon prices are introduced based on multiples of P, leading to distinct outcomes. Table 3.7 shows the embedded carbon prices for both power and gas generation, alongside the ensuing optimal scheduling costs. This analysis contributes to a more comprehensive understanding of the dynamics associated with carbon pricing within the context of our study, by employing the random sampling methodology [222].

Table 3.7: Carbon Penalty of Power and Gas under Different Cases

Parameter	**Case 1**	**Case 2**	**Case 3**	**Case 4**	**Case 5**
P_{cp}	0.21	0.28	0.35	0.42	0.49
P_{cg}	0.07	0.14	0.21	0.28	0.35
Cost (£)	5615.96	5952.15	6279.80	6603.41	6911.46

where P, P_{cp}, and P_{cg} denote the real-time power price, the carbon penalty price of power, and the carbon penalty price of gas, respectively.

The results among five cases clearly show that the total cost rises with increasing carbon price in Table 3.7. In order to comprehensively assess the effects of varying carbon prices on additional cost factors, a broader spectrum of data comparisons is required. Fig. 3.14 provides an illustrative representation of the trends in total carbon emissions, power transactions, CG output, gas purchases, and battery storage across multiple scenarios over a full day. This analysis contributes to a more comprehensive understanding of the dynamics associated with carbon pricing within the context of this study.

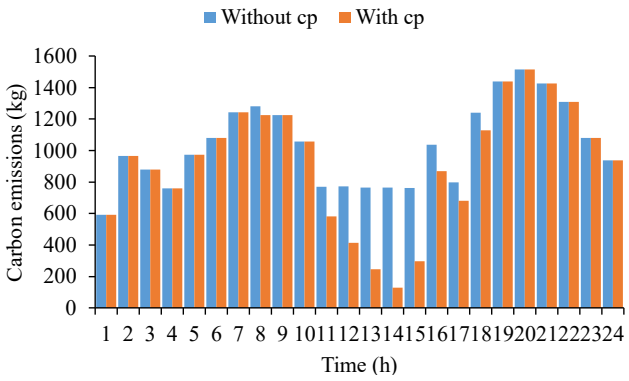

(a) Day-Ahead Carbon Emissions

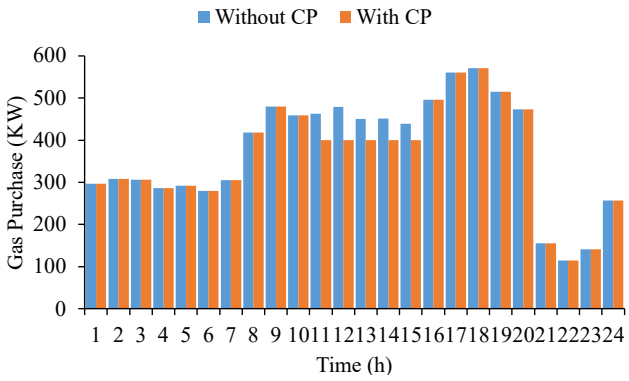

(b) Day-Ahead Gas Purchase

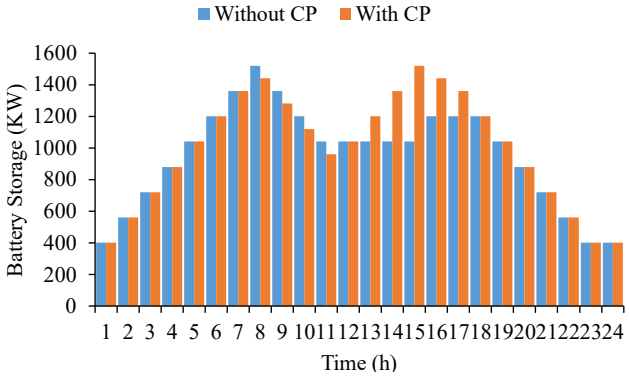

(c) Day-Ahead Battery Storage

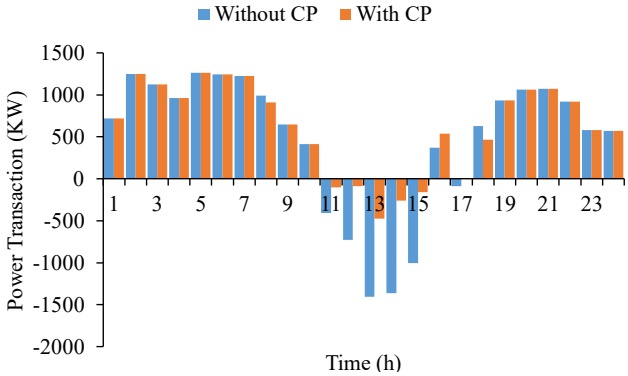

(d) Day-Ahead Power Transaction

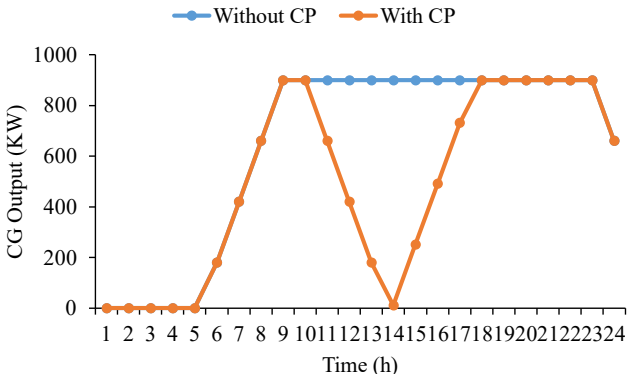

(e) Day-Ahead CG Output

Figure 3.13: Day-Ahead Scheduling Results Comparison Under Conditions With And Without Carbon Penalty.

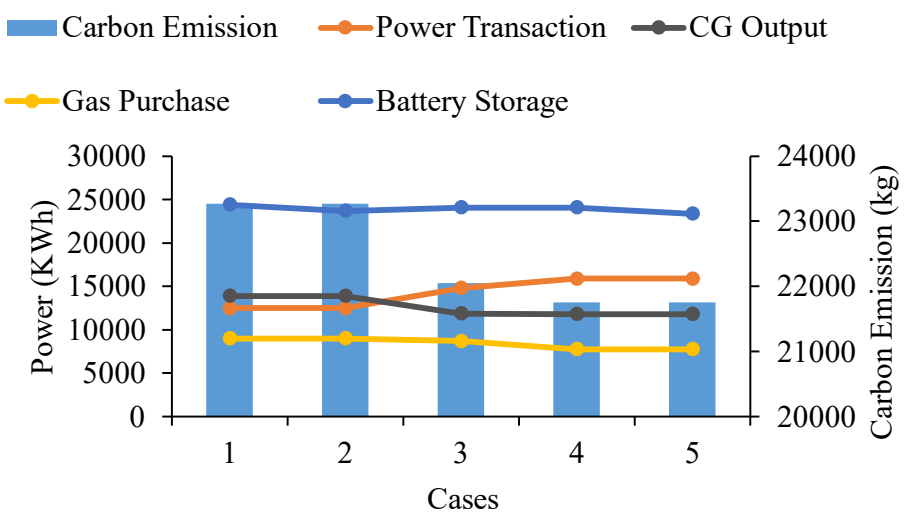

Figure 3.14: Carbon Penalty Impacts over 5 Cases.

In Fig. 3.14, the observed slight increase in power transactions is not indicative of the microgrid procuring more electricity from the main grid; rather, it results from a reduction in power sold by the microgrid to the main grid, enabling more energy storage for self-consumption. Consequently, the overall volume of power transactions slightly increases. Conversely, there is a general decline in carbon emissions, gas purchases, and CG output. Additionally, the SOC of the battery diminishes, as it needs to discharge energy to meet the prevailing load demands.

Interestingly, the carbon emission stays the same in Cases 1 and 2 as well as Cases 4 and 5 even though the total costs of Cases 2 and 5 are higher than those of Cases 1 and 4. And the same phenomenon happens with power transactions, gas purchases, and CG output. The reason is that the total load demand is unchanged among these cases. Moreover, the CP cost may account for less weight than other costs. It can be concluded that Case 4 is the overall optimal carbon price setting that achieves the lowest carbon emission with less cost than Case 5.

In [86], the carbon price stays the same over the whole day. To analyse the impact of time-varying versus constant carbon pricing, a comparison is made using the results from Case 4, as previously discussed, where the CP price for power and gas stands at 0.42 and 0.28 times of the transaction price, respectively. The average daily prices for power and gas, which amount to £0.0520 and £0.0347, respectively, are considered. Table 3.8 reveals that the application of time-varying carbon pricing yields lower carbon emissions at the expense of higher costs compared to a constant carbon price in this case study. This analysis offers valuable insights that can aid utility companies in devising strategies tailored to specific requirements and objectives.

Table 3.8: Comparison between Time-Varying and Constant Carbon Prices

Carbon Price	**Cost (£)**	**Carbon Emissions (kg)**
Time-Varying	6603.41	21751.75
Constant	6551.68	21766.15

3.4.6 Intra-Day Results and Discussions

To illustrate the feasibility of real-time intra-day scheduling, the intra-day predictions and results are discussed in this section. The comparison of day-ahead and intra-day predictions for solar and wind energy as well as the total load can be seen in Fig. 3.15. (a) and (b) represent the forecasts for PV and WT output, respectively, while (c) indicate the load predictions. It is evident that there are observable minor differences between intra-day and day-ahead predictions. The intra-day outputs of renewable energies are slightly higher than day-ahead predictions at around 9h and 18h, while intra-day load predictions generally show a slightly lower magnitude compared to day-ahead predictions around 8h and 21h. This reflects the robustness of the day-ahead scheduling.

The optimal intra-day scheduling is shown in Fig. 3.16. The intra-day results should ideally closely follow the day-ahead decision. As seen in the figure, the overall trends of intra-day and day-ahead scheduling are generally consistent. However, there are some moments where slight differences exist due to variations in day-ahead and intra-day renewable energy and load forecasts. During the low RES and high load demand period around 9h and 21h mentioned in Section 5.2, the utility procures more gas to accommodate the elevated heat load. Given that the CP price is lower than the power transaction price, the utility's inclination is to sell surplus power to the main grid for higher overall revenue, despite the associated increase in carbon emissions. In general, the intra-day scheduling effectively aligns with the preceding scheduling decisions. With a shorter time scale and swift response, it can adeptly accommodate dynamic changes in natural and human-induced uncertainties.

When considering the CP for intra-day scheduling, the total cost of intra-day scheduling is £6964.36, while the intra-day cost without CP is £5359.72. Additionally, the carbon emissions have been reduced by over 1100 kg. Both cost and carbon emissions data for intra-day scheduling are presented in Table 3.9. This observation underscores the pronounced impact of decarbonizing strategies once again. From the results of both day-ahead and intraday scheduling, this multi-timescale scheduling method provides a decarbonizing and robust optimized scheduling solution for MMGs.

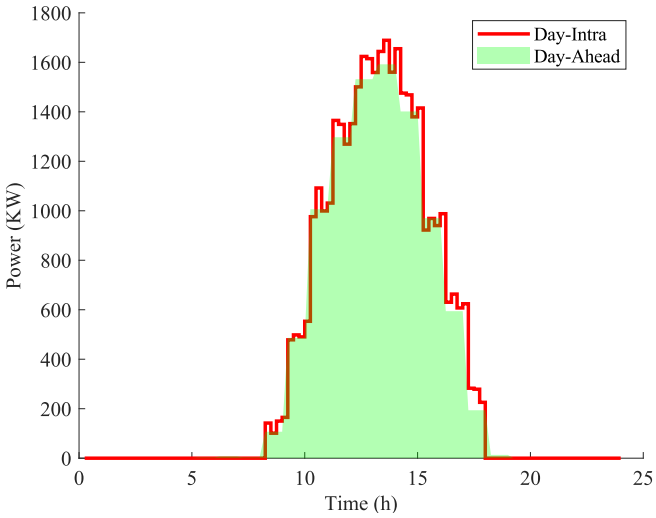

(a) PV Output Prediction

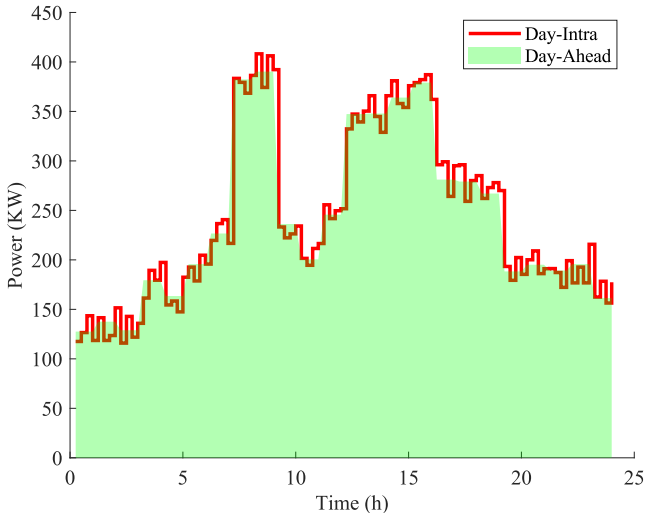

(b) WT Output Prediction

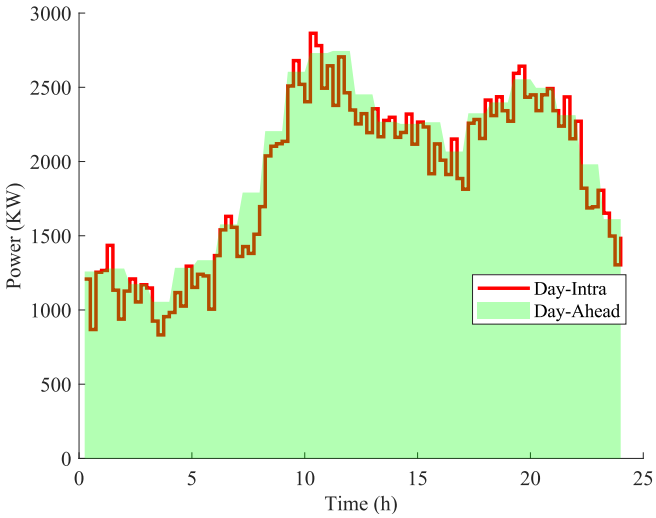

(c) Total Load Prediction

Figure 3.15: Comparison between Day-ahead and Intra-day Power and Load Prediction.

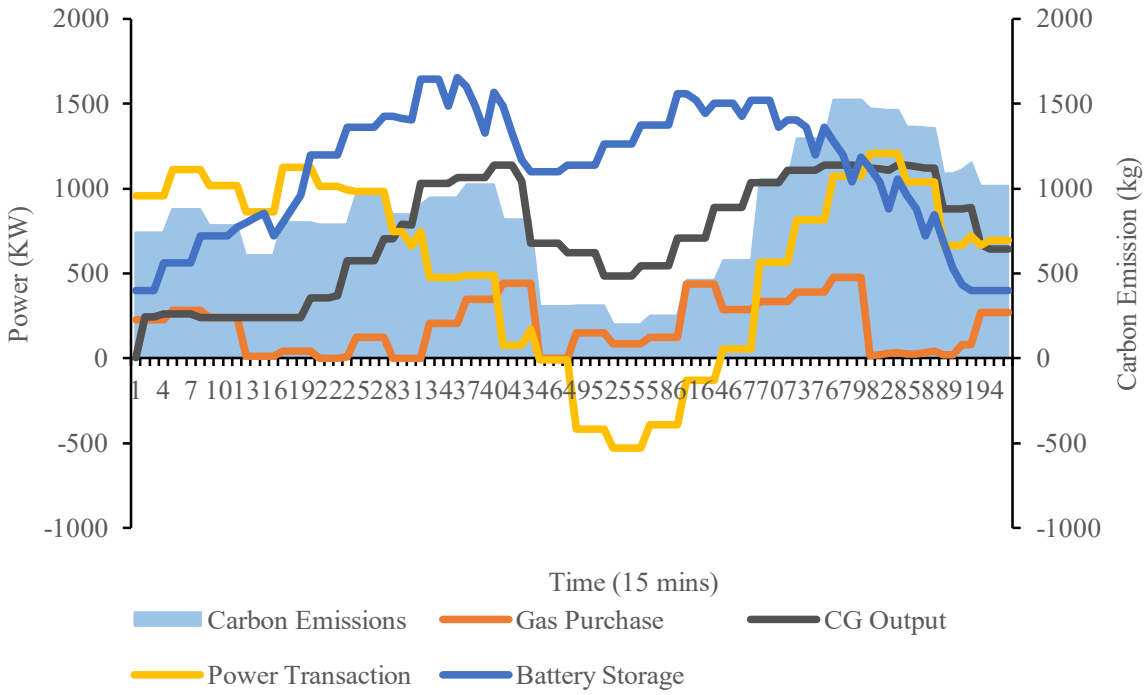

Figure 3.16: Intra-day Optimal Scheduling Results.

Table 3.9: Intra-day Carbon Penalty Impact

Intra-day Results	**Cost (£)**	**Carbon Emissions (kg)**
No Carbon Penalty	5359.72	22033.13
With Carbon Penalty	6964.36	20136.56

3.5 Discussions

3.5.1 Interpretation of Key Findings

It can be seen that the proposed low-carbon operational framework for MMGs provides a systematic and data-driven solution to address both economic efficiency and carbon reduction under renewable energy uncertainty. The implementation of a multi-temporal optimisation approach, combining day-ahead and intra-day scheduling, allows the system to dynamically adapt to fluctuations in solar and wind generation. The strong alignment between the hourly and 15-minute optimisation outcomes validates the robustness of the framework, ensuring consistent operational decisions even under varying renewable profiles.

The incorporation of carbon penalty pricing further enhances the framework's ability to support low-carbon operation. The model demonstrates that integrating environmental costs into dispatch

decisions can effectively reduce emissions while maintaining cost competitiveness. A reduction of approximately 10.6% in total carbon emissions under the carbon-pricing condition underscores the impact of carbon penalties as a regulatory mechanism. This finding supports the conception that economic instruments can meaningfully drive decarbonisation in microgrid operations without compromising reliability or flexibility.

3.5.2 Methodological Reflection

From a methodological standpoint, the study contributes to the broader field of robust optimisation for energy systems. The combination of clustering-based scenario generation and DRO provides a novel way to model uncertainty. Unlike conventional stochastic programming, which assumes a known probability distribution, the DRO formulation accounts for distributional ambiguity, ensuring resilience against imperfect or limited raw datasets. The inclusion of empirical data clustering further improves computational tractability, enabling the model to handle realistic variability in renewable and load data while retaining robustness.

Another notable contribution is the multi-temporal structure of the model, which bridges strategic day-ahead planning with real-time intra-day adaptation. This dual timescale approach enhances the operational flexibility of MMGs, ensuring both long-term scheduling efficiency and short-term adaptability. Such design is particularly valuable in systems with high shares of variable renewables, where short-term fluctuations can compromise energy balance and reliability.

3.5.3 Practical Implications for Low-Carbon Operation

The results provide actionable insights for DNOs and microgrid managers pursuing carbon-neutral operation. The proposed framework serves as a decision-support tool that co-optimises economic and environmental objectives, aligning operational planning with national decarbonisation targets. In practical applications, the ability to integrate carbon penalties within scheduling decisions allows operators to explicitly quantify the trade-offs between cost and emissions. This transparency can support more informed regulatory policies, tariff structures, and investment strategies for distributed energy systems.

Furthermore, the demonstrated reduction in energy curtailment and emissions implies that the framework can support renewable integration without excessive reliance on energy storage facilities. This is particularly relevant for regions where large-scale storage deployment remains economically constrained. The results thus highlight the potential of optimisation-based scheduling as a near-term measure to enhance renewable utilisation and grid efficiency.

3.5.4 Limitations and Future Outlook

While the framework performs effectively under the tested IEEE 33-bus case, certain limitations must be acknowledged. The accuracy and robustness of the DRO-based approach depend on the representativeness of the historical data used in clustering. In data-sparse contexts or regions with rapidly evolving renewable profiles, the framework may require adaptive re-clustering or online learning mechanisms. Additionally, the MILP formulation, while computationally tractable, inevitably simplifies certain nonlinearities inherent in power and heat systems.

Future extensions could focus on scaling the framework to larger or interconnected systems, exploring decentralised or distributed optimisation strategies to improve computational efficiency. Another promising direction involves integrating energy storage devices and demand-side flexibility schemes within the same multi-temporal structure, enabling more holistic management of multi-energy resources. Finally, coupling this framework with predictive control or reinforcement learning could facilitate real-time adaptation under highly uncertain operational environments.

3.6 Conclusions

This chapter introduces a novel operational framework for MMG that emphasises low-carbon sustainability and addresses uncertainties in generation, e.g. solar and wind energy sources, along with demand fluctuations. The framework's primary objective is to optimise decarbonisation by concurrently minimising operational costs and mitigating carbon penalty expenses. To address this optimisation challenge, a unique multi-temporal approach grounded in data-driven DRO is proposed. Here the key aim is to create an hourly day-ahead optimal scheduling framework that seamlessly integrates considerations of economic efficiency and robustness within the context of decarbonisation. Furthermore, the practicality of real-time dispatch in 15-minute intervals by presenting intra-day operations is demonstrated within our case study. To effectively confront the challenges posed by significant uncertainties, a comprehensive approach is adopted. This includes the utilisation of clustering techniques to derive representative scenarios from empirical data of renewable energies and load demand altogether, while accounting for the ambiguity set within the probability distribution.

Validation of this model and the framework was conducted through testing on the IEEE 33-bus distribution network, from which several key findings have emerged: 1) Within the framework of the multi-energy microgrid featuring CHP technology, a commendable reduction of 9.5t in carbon emissions is observed, coupled with a lower cost saving amounting to £61.78. 2) Notably, un-

der the CP condition, a significant reduction in carbon emissions, amounting to 10.6%, has been attained. 3) The alignment between intra-day 15-minute scheduling and day-ahead hourly scheduling is demonstrated, addressing the stochastic nature of renewable energy sources at various stages through multi-temporal scheduling approaches which enhances the integration of renewable energy and leads to carbon reduction.

In conclusion, the study in this chapter uses advanced methods to address uncertainties in the MMG, with a focus on reducing carbon emissions and energy consumption. Key contributions include the effective use of data-driven DRO for improved energy utilisation in microgrids. The optimisation framework highlights the efficacy of carbon penalty pricing mechanisms, and the proposed approach considers multi-temporal uncertainties, reducing operational costs and enhancing MMG reliability. Overall, this study provides a practical framework for achieving low-carbon and energy-saving outcomes in microgrid management. In future research endeavors, it is essential to explore improvements that address the dynamic challenges inherent in integrating renewable energy and managing power grids. This involves a thorough consideration of intricate details within the power grid infrastructure to enhance overall system efficiency and reliability.

Chapter 4

Coordinated Scheduling of Integrated Electricity and Green Hydrogen Systems

Building on the multi-energy microgrid optimisation framework for distribution networks developed in Chapter 3, this chapter extends the analysis to the coordinated operation of interconnected transmission and distribution systems. To enhance transmission–distribution coordination from an economic perspective, an optimisation framework is proposed in this chapter for the joint scheduling of power transmission and distribution networks, with a particular focus on the integration of offshore wind generation and green hydrogen storage. As renewable penetration increases, system operators face growing challenges in maintaining economic efficiency and operational reliability. In this context, hydrogen offers a promising solution for large-scale, long-duration energy storage, capable of enhancing grid flexibility and enabling a more resilient low-carbon energy system.

The proposed optimisation framework aims to maximise the annual net revenue of the integrated energy system by jointly accounting for both electricity and hydrogen markets. This objective involves not only increasing the revenues from power generation and hydrogen production but also minimising the costs associated with electricity purchases from the main grid. By capturing these coupled interactions, the model provides a comprehensive representation of multi-energy coordination across transmission and distribution levels, reflecting the real-world complexity of offshore energy systems.

A comparative case study is undertaken to assess the performance of the proposed approach. The coordinated scheduling results are benchmarked against a reference configuration in which hydrogen production and storage are installed solely on the generation side. The findings reveal clear economic advantages of deploying hydrogen storage and electrolysers at both the production and consumption ends, thereby enhancing the overall operational flexibility and financial performance of the integrated system. Furthermore, the results demonstrate that closer coordination between

transmission and distribution networks can significantly improve resource utilisation and energy balance, particularly under variable offshore wind generation conditions.

4.1 Modelling of Hydrogen Components and Power Network Coordination

In this chapter, the main grid refers to the bulk power system operating at the transmission level, which is responsible for large-scale power generation and long-distance electricity transfer. The transmission network connects generation sources and regional substations through high-voltage infrastructure managed by the TSO. In contrast, the distribution network operates at lower voltage levels and delivers electricity to end users and distributed energy resources under the management of DSOs. The proposed framework focuses on the coordinated optimisation of transmission and distribution systems to enhance operational flexibility and renewable energy utilisation.

A highly integrated energy scenario is investigated, in which both transmission–distribution coordination and the conversion between electrical power and hydrogen are explicitly considered. The integrated configuration, schematically illustrated in Fig. 4.1, is designed to capture the complex interactions among different system layers and energy carriers. At its core, the framework consists of two interconnected stages, namely the transmission stage and the distribution stage, each playing a distinct yet complementary role in ensuring efficient and flexible resource utilisation.

The overall power input to the system originates from two principal sources: offshore wind generation and electricity purchased directly from the main grid. Within the transmission stage, a proportion of the incoming electricity is channelled into electrolysers, where it is converted into hydrogen. This hydrogen can either be stored for later use or distributed to downstream systems, while the remaining electricity is transmitted directly to the distribution network. The stored hydrogen offers additional flexibility, as it can be reconverted into electricity through fuel cells when required, thereby providing a valuable buffer against variability in renewable generation or fluctuations in demand.

Similarly, in the distribution stage, the electricity supplied from the transmission network can follow multiple pathways. It may be dispatched directly to meet local demand, or alternatively, it can be converted into hydrogen via electrolysers. The hydrogen produced at this stage can be stored in dedicated tanks, delivered directly to end-users, or converted back into electricity through fuel cells to supplement supply when necessary. In this way, the distribution system not only delivers electricity but also functions as a hub for hydrogen production, storage, and utilisation,

thus enhancing operational flexibility and resilience.

The optimal scheduling and coordination of these processes are formulated within an MILP framework. This model explicitly represents the physical and operational constraints of both electricity and hydrogen subsystems while enabling coordinated decision-making across transmission and distribution levels. The central objective of the optimisation problem is to maximise the total profit of the integrated network, which is shown in equation (4.1). This is achieved by simultaneously considering revenue from electricity and hydrogen sales, the costs associated with grid purchases and system operations, and the benefits of minimising energy curtailment through efficient sector coupling. In doing so, the proposed framework not only improves economic performance but also supports the strategic integration of renewable energy within multi-energy networks.

$$\max \sum_{t \in \mathcal{T}} P_{L,t} C_{p,t} + H_{L,t} C_h - P_{buy,t} C_{p,t}^{buy} \tag{4.1}$$

where $P_{L,t}$ and $H_{L,t}$ denotes the power and hydrogen load respectively, $C_{p,t}$ represents the day-ahead selling electricity price, while $C_{p,t}^{buy}$ denotes the electricity purchase price, calculated as the sum of $C_{p,t}$ and an assumed electricity tariff of 20.05 €/MWh. Additionally, C_h represents the hydrogen price, set at 2.3 €/kg [223].

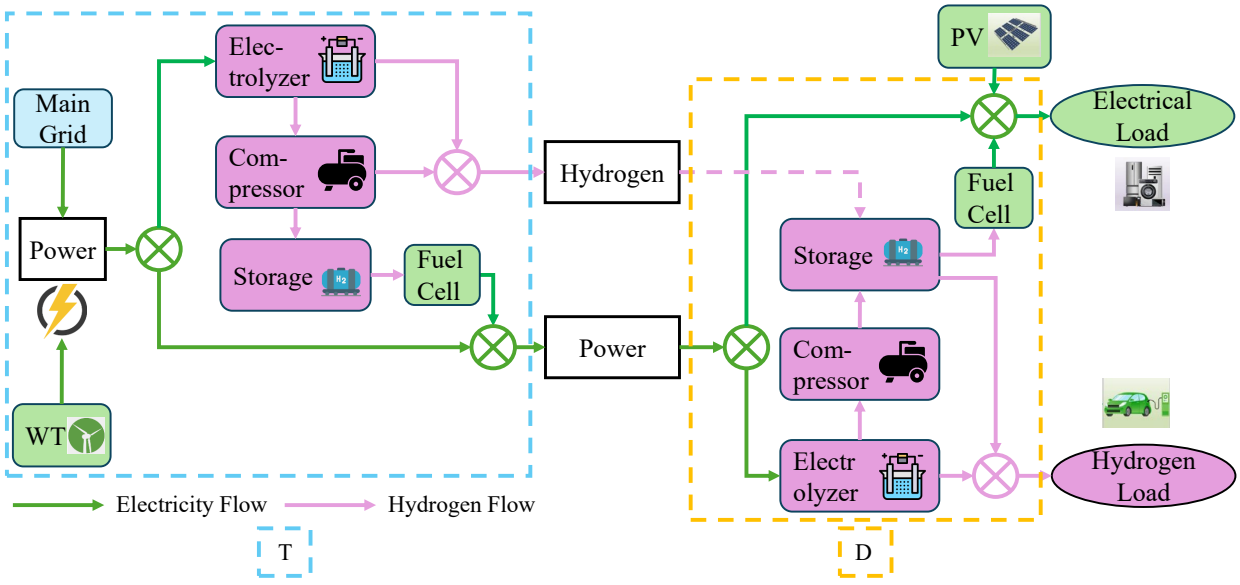

Figure 4.1: Internal Configuration of Transmission and Distribution of Integrated Power and Hydrogen System

4.1.1 Transmission Network Modelling

The transmission network in the proposed framework encompasses several key processes, including offshore wind power generation, electricity transactions with the external grid, hydrogen production through electrolysers, hydrogen storage in dedicated facilities, and the subsequent regeneration of electricity via fuel cells. Together, these elements form an integrated multi-energy system that enables both flexibility and reliability in balancing supply and demand at the transmission level. To facilitate clear representation within the mathematical model, all variables associated with the transmission network are denoted by the superscript 'M'.

In order to accurately capture the operational behaviour of this power–hydrogen system, a set of constraints is formulated. These constraints define the relationships between electricity generation, grid exchanges, hydrogen conversion, storage dynamics, and fuel cell operation. Specifically, they ensure that energy balances are satisfied at each stage, that physical limitations of equipment such as electrolysers, storage tanks, and fuel cells are respected, and that the coupling between the electricity and hydrogen subsystems is consistently represented. Collectively, these constraints provide the foundation for the MILP optimisation model, allowing for coordinated scheduling and profit maximisation across the integrated transmission and distribution network.

The set of constraints outlined below plays a crucial role in ensuring the physical feasibility and economic consistency of the proposed coordinated transmission and distribution network model. Equations (4.2) and (4.3) establish the active power flow balance within the transmission system, thereby guaranteeing that the supply and demand of electricity are matched at all times. Similarly, the hydrogen balance is maintained through Equations (4.4) and (4.5), which regulate both the production and consumption of hydrogen across the system.

$$P_{buy,t} + P_{WT,t} = P^{M}_{e,t} + P^{M}_{c,t} + P^{M}_{d,t} \quad \forall t \in T \tag{4.2}$$

$$P_{DB,t} = P^{M}_{d,t} + P^{M}_{fc,t} \quad \forall t \in T \tag{4.3}$$

where $P_{buy,t}$ represents the power purchased from the main grid, while $P_{WT,t}$ denotes wind power generation. $P^{M}_{e,t}$ indicates the consumption of electrolyzers in the transmission network, $P^{M}_{c,t}$ represents the consumption of compressors in the transmission network, and $P^{M}_{d,t}$ denotes electricity directly supplied to demand. $P_{DB,t}$ indicates electricity sent to the distribution grid, and $P^{M}_{fc,t}$ represents the power output from the transmission fuel cell.

$$H^{M}_{e,t} = H^{M}_{d,t} + S^{M}_{in,t} \quad \forall t \in T \tag{4.4}$$

$$H_{DB,t} = H^M_{d,t} + S^M_{hout,t} \quad \forall t \in T \tag{4.5}$$

where $H^M_{e,t}$ represents hydrogen production in the transmission network, while $H^M_{d,t}$ denotes hydrogen directly delivered to demand in the transmission network. $S^M_{in,t}$ indicates hydrogen injection into storage from the electrolyzer. $H_{DB,t}$ represents hydrogen delivered from transmission to distribution grid storage, and $H^M_{d,t}$ signifies hydrogen directly supplied to demand in the transmission network. Finally, $S^M_{hout,t}$ represents the output of the storage.

To avoid unrealistic system behaviours, additional restrictions are introduced. For instance, Equation (4.6) prevents the simultaneous purchase of electricity from the main grid during hydrogen production, thereby reflecting practical operational strategies. Equations (4.7) and (4.8) impose upper and lower bounds on the power consumption of the electrolyser, ensuring that hydrogen generation remains within its technical limits. The dynamics of hydrogen storage are represented by Equations (4.9) to (4.11), which govern both charging and discharging processes, while Equations (4.12) and (4.13) specify the maximum permissible state-of-charge and output capacity of the storage units.

$$P_{buy,t} \leq P^M_{sb}(1 - u_{os,t}) \quad \forall t \in T \tag{4.6}$$

where P^M_{sb} represents the standby power consumption of the electrolyzer, while $u_{os,t}$ is a binary variable indicating whether the electrolyzer is operational (on) or on standby at time t.

$$P^M_{e,t} \leq C_e u^M_{os,t} + P^M_{sb}(1 - u^M_{os,t}) \quad \forall t \in T \tag{4.7}$$

$$P^M_{e,t} \geq P^{min} u^M_{os,t} + P^M_{sb}(1 - u^M_{os,t}) \quad \forall t \in T \tag{4.8}$$

C_e is the electrolyzer capacity. P^{min} is the minimum power consumption limit of the electrolyzer.

$$S^M_{t=1} = S^M_{ini} + S^M_{in,t=1} - S^M_{out,t=1} \quad \forall t \in T \tag{4.9}$$

$$S^M_t = S^M_{t-1} + S^M_{in,t} - S^M_{out,t} \quad \forall t \in T \tag{4.10}$$

$$S^M_{out,t} = S^M_{hout,t} + S^M_{pout,t} \quad \forall t \in T \tag{4.11}$$

$$S^M_t \leq C^s \quad \forall t \in T \tag{4.12}$$

$$S^{M}_{out,t} \leq S^{max}_{out} \quad \forall t \in T \tag{4.13}$$

where $S^{M}_{t=1}$ represents the state-of-charge of the transmission storage at time $t = 1$. S^{M}_{ini} denotes the initial hydrogen stored in the storage at the beginning of the time horizon. $S^{M}_{in,t=1}$ is the storage input at time $t = 1$, while $S^{M}_{out,t=1}$ represents the storage output at time $t = 1$. S^{M}_{t} indicates the state-of-charge of the storage at time t. $S^{M}_{hout,t}$ denotes the hydrogen delivered to the hydrogen demand from the storage, while $S^{M}_{pout,t}$ represents the hydrogen delivered to the power demand from the storage. C^{s} denotes the storage capacity, and S^{max}_{out} is the maximum output of the storage.

In order to capture the non-linear characteristics of hydrogen production, Equations (4.14) to (4.16) employ a piecewise linear approximation for the electrolyser's output. Finally, Equations (4.17) to (4.18) define the operational constraints for electricity generation from the fuel cell, as well as the associated compressor process. Collectively, these constraints provide a rigorous mathematical foundation for the MILP formulation, ensuring that the optimisation results are not only cost-effective but also technically viable and consistent with the physical behaviour of the integrated power–hydrogen system.

$$P^{M}_{e,t} = \sum_{s \in S} P^{s,M}_{e,t} + P^{M}_{sb}(1 - u^{M}_{os,t}) \quad \forall t \in T \tag{4.14}$$

$$H^{M}_{e,t} = \sum_{s \in S} (A_s P^{s,M}_{e,t} + B_s u^{s,M}_{hp,t}) \quad \forall t \in T \tag{4.15}$$

$$u^{M}_{os,t} = \sum_{s \in S} u^{s,M}_{hp,t} \quad \forall t \in T \tag{4.16}$$

where $\sum_{s \in S} P^{s,M}_{e,t}$ represents the sum of power consumption of electrolyzers across all segments. A_s denotes the slope of the hydrogen production function for segment s, while $P^{s,M}_{e,t}$ indicates the power consumption of the electrolyzer in segment s. B_s represents the intercept of the hydrogen production function for segment s, and $u^{s,M}_{hp,t}$ is a binary variable indicating whether the hydrogen production segment s is active at time t.

$$P^{M}_{fc,t} = \alpha S^{M}_{pout,t} \quad \forall t \in T \tag{4.17}$$

$$P^{M}_{c,t} = K^{c} S^{M}_{in,t} \quad \forall t \in T \tag{4.18}$$

where α is the energy conversion rate of the fuel cell. K^{c} is the compressor efficiency.

4.1.2 Distribution Network Modelling

The distribution network encompasses several critical components, including hydrogen production facilities, dedicated hydrogen storage units, and electricity generation systems based on fuel cells. In order to distinguish the operational variables associated with the distribution level from those of other subsystems, all distribution network variables are denoted by the superscript 'D'. Within the broader framework of power–hydrogen network modelling, the operational behaviour of the distribution network must adhere to a series of physical and operational restrictions. These restrictions, expressed mathematically in the form of constraints, are formulated as follows:

Equations (4.19) and (4.20) establish the active power flow balance within the distribution system, ensuring that electricity demand is reliably satisfied. In this configuration, the load is met not only through electricity delivered from the transmission network but also by photovoltaic units installed in close proximity to end-users, thereby capturing the role of distributed renewable generation in enhancing local supply security.

$$P_{DB,t} = P^D_{e,t} + P^D_{c,t} + P^D_{d,t} \quad \forall t \in T \tag{4.19}$$

$$P_{L,t} = P_{PV,t} + P^D_{d,t} + P^D_{fc,t} \quad \forall t \in T \tag{4.20}$$

where $P^D_{e,t}$ denotes the electricity consumption of electrolyser units within the distribution network, while $P^D_{c,t}$ refers to the electricity consumed by compressors in the same network. The variable $P^D_{d,t}$ represents the portion of electricity that is directly delivered to meet consumer demand. In addition, $P_{DB,t}$ corresponds to the electricity imported from the transmission grid, whereas $P^D_{fc,t}$ signifies the power generated by the distribution-level fuel cell. The consumer load is denoted by $P_{L,t}$, and the electricity produced by photovoltaic (PV) units is represented by $P_{PV,t}$.

Equations (4.21) to (4.23) govern the hydrogen balance within the distribution network. Specifically, they ensure that the total input of hydrogen storage is equal to the sum of the hydrogen delivered from the transmission system and the fraction of hydrogen produced locally via electrolysers. In this way, the equations enforce consistency between inter-network hydrogen transfer and local hydrogen generation, while reflecting the operational flexibility of the distribution system.

$$H^D_{e,t} = H^D_{d,t} + S^D_{in,t} \quad \forall t \in T \tag{4.21}$$

$$H^D_{L,t} = H^D_{d,t} + S^D_{hout,t} \quad \forall t \in T \tag{4.22}$$

$$H_{DB,t} + S^D_{in,t} = S_{intot,t} \quad \forall t \in T \tag{4.23}$$

where $H^D_{e,t}$ represents hydrogen production in the distribution network, while $H^D_{d,t}$ denotes hy-

drogen directly delivered to demand in the distribution network. $S^D_{in,t}$ indicates hydrogen injection into storage from the electrolyzer in the distribution network. $H_{DB,t}$ represents hydrogen delivered from transmission to distribution grid storage, and $H^D_{d,t}$ signifies hydrogen directly supplied to demand in the distribution network. Finally, $S^D_{hout,t}$ represents the output of the storage in the distribution network.

The dynamics of hydrogen storage at the distribution level are described by Equations (4.24) to (4.28), which define the charging, discharging, and state-of-charge limits. These constraints play a crucial role in maintaining technical feasibility and preventing infeasible storage behaviours. In addition, Equations (4.29) and (4.30) impose minimum thresholds on both power and hydrogen loads, ensuring that essential demand is always satisfied even under adverse operational conditions.

$$S^D_{t=1} = S^D_{ini} + S_{intot,t=1} - S^D_{out,t=1} \quad \forall t \in T \tag{4.24}$$

$$S^D_t = S^D_{t-1} + S_{intot,t} - S^D_{out,t} \quad \forall t \in T \tag{4.25}$$

$$S^D_{out,t} = S^D_{hout,t} + S^D_{pout,t} \quad \forall t \in T \tag{4.26}$$

$$S^D_t \leq C^s \quad \forall t \in T \tag{4.27}$$

$$S^D_{out,t} \leq S^{max}_{out} \quad \forall t \in T \tag{4.28}$$

where the variable $S^D_{t=1}$ represents the state of charge of the distribution-level hydrogen storage at the initial time step, $t = 1$. The parameter S^D_{ini} specifies the initial amount of hydrogen stored in the distribution storage at the commencement of the scheduling horizon. The variable $S^D_{in,t=1}$ denotes the hydrogen inflow into the distribution storage at time $t = 1$, whereas $S^D_{out,t=1}$ captures the hydrogen outflow from the storage at the same time. More generally, S^D_t expresses the state of charge of the storage unit at any time t. Furthermore, $S^D_{hout,t}$ refers to the quantity of hydrogen discharged from the distribution storage to directly meet hydrogen demand, while $S^D_{pout,t}$ represents the quantity of hydrogen discharged to supply power demand, for instance via fuel cells. The parameter C^s designates the rated storage capacity, and S^{max}_{out} defines the maximum permissible output of the storage system.

$$P_{L,t} \geq P^{\min}_d \quad \forall t \in T \tag{4.29}$$

$$\sum_{t \in \mathscr{H}_n} H_{L,t} \geq H^{\min}_d \quad \forall t \in T \tag{4.30}$$

where $P^{\min}_d$ denotes the minimum power demand, $H^{\min}_d$ denots the minimum hydrogen demand.

Finally, it is important to note that the constraints relating to the power consumption limits of electrolysers, the hydrogen production process, fuel cell operation, and compressor requirements

are structurally identical to those applied at the transmission stage. To avoid redundancy, they are therefore not explicitly restated in this section. Collectively, these constraints provide a coherent mathematical representation of the distribution network, enabling its seamless coordination with the transmission stage in the proposed integrated power–hydrogen system.

4.1.3 Model Coupling and Coordination Strategy

The increasing penetration of distributed generation (DG), energy storage systems (ESS), and flexible demand resources has blurred the traditional boundary between transmission and distribution networks. Historically, transmission systems were modelled and optimised independently from distribution systems, under the assumption that the latter behaved as passive loads. However, with the emergence of distributed energy resources (DERs), active distribution grids can significantly affect the operational conditions of the upper-level transmission system. Therefore, a coordinated transmission–distribution (T–D) optimisation framework becomes necessary to ensure efficient, secure, and economically optimal operation of the integrated system.

Energy Coupling

From the energy perspective, the coupling between transmission and distribution systems is established through the power exchanged at the points of common coupling (PCCs). The total power injected from the transmission grid into each distribution network directly influences voltage profiles, power losses, and congestion patterns in both domains. Conversely, the flexibility offered by distributed resources—such as local generation, storage, and demand response—can actively support the transmission grid by providing balancing capacity, reactive power support, and congestion relief.

In an uncoordinated setting, such local actions might even counteract the global optimum; for instance, local voltage regulation may lead to undesired reverse power flows or violate transmission constraints. Hence, energy coupling requires a consistent operational framework that simultaneously considers both T-level and D-level constraints to guarantee system-wide feasibility.

Information Coupling

At the informational level, T–D coordination relies on the timely and accurate exchange of system states, operational limits, and control signals. Transmission operators (TSOs) typically manage

wide-area data, such as line flows, bus voltages, and system frequency, while distribution operators (DSOs) handle high-resolution local data, including DER outputs and load forecasts. The bidirectional information exchange forms the foundation of coordinated decision-making.

Information coupling is particularly crucial for implementing advanced optimisation and control strategies, such as distributed optimal power flow (D-OPF) or hierarchical model predictive control (MPC). In such frameworks, the transmission and distribution operators iteratively exchange boundary variables—either power setpoints or price signals—until convergence is achieved. This distributed computation paradigm not only enhances scalability but also preserves the data privacy and autonomy of each subsystem, which is essential for future decentralised energy systems.

Economic Coupling

From the economic perspective, transmission and distribution systems are linked through energy prices and market signals. Locational marginal prices (LMPs) determined by the transmission-level market influence the operation of distributed resources, while local price adjustments at the distribution level can modify the aggregate power exchange with the transmission grid. However, traditional market structures are primarily designed for transmission-level participants, often neglecting the value of local flexibility and the associated network constraints within distribution grids.

The development of coordinated T–D markets or two-layer pricing mechanisms represents an active area of research. Such schemes enable DERs to participate in ancillary services and balancing markets through distribution aggregators, creating a more efficient allocation of flexibility. The coupling of economic signals thus provides a mechanism to internalise local network effects within system-wide optimisation.

Need for Coordination and Innovation

The necessity of T–D coordination arises from the increasing interdependence of operational decisions across network layers. Without a coordinated mechanism, independent optimisation may lead to conflicting actions, suboptimal resource utilisation, or even violations of network constraints. Coordinated optimisation, by contrast, enables a holistic view of the power system where both global efficiency and local flexibility are respected.

The proposed T–D coupling strategy in this work introduces an integrated optimisation structure that links transmission-level optimal power flow with distribution-level optimisation models via an iterative exchange of boundary variables. Unlike conventional top-down approaches that treat the distribution system as a passive load, the proposed framework recognises its active role in

contributing to system balancing and ancillary services. This methodological innovation ensures that the integrated optimisation not only minimises system-wide costs but also enhances resilience and adaptability under renewable generation uncertainties.

Furthermore, the coupling framework facilitates a decentralised computational architecture, where both TSO and DSO maintain operational autonomy while achieving a globally coordinated solution through iterative consensus. This design aligns with the future trend of distributed energy management and supports the transition towards flexible, interoperable, and low-carbon energy systems.

4.2 Case Study

4.2.1 Description of Datasets and Simulation Settings

A comprehensive model is developed for the integrated power and hydrogen energy management through the coordinated operation of both distribution and transmission networks, as illustrated in Fig. 4.2. The proposed framework integrates the reconstructed IEEE 3-node transmission system with two 13-node distribution feeder test networks, thereby providing a multi-layered representation of energy flow from generation to end-use. In this setup, electricity and hydrogen are first produced at the generation units and subsequently injected into the 3-node transmission network, which acts as the backbone for energy transport across the system. From there, energy is dispatched to the two 13-node distribution networks, where a variety of loads are connected and supplied according to demand patterns.

For clarity, the detailed internal configurations of generation units and load structures have been omitted in this depiction. Instead, Fig. 4.1 provides a schematic overview of the transmission (“T") and distribution (“D1" and “D2") processes, highlighting the sequential stages of power generation, hydrogen production, and storage at both transmission and distribution levels. This representation enables a clear understanding of the interactions between different network layers and the role of hydrogen as a flexible energy carrier. Additionally, photovoltaic (PV) systems are installed at the load nodes to capture the increasing penetration of distributed energy resources, reflecting their contribution to local energy supply and further enhancing the overall sustainability and resilience of the integrated system.

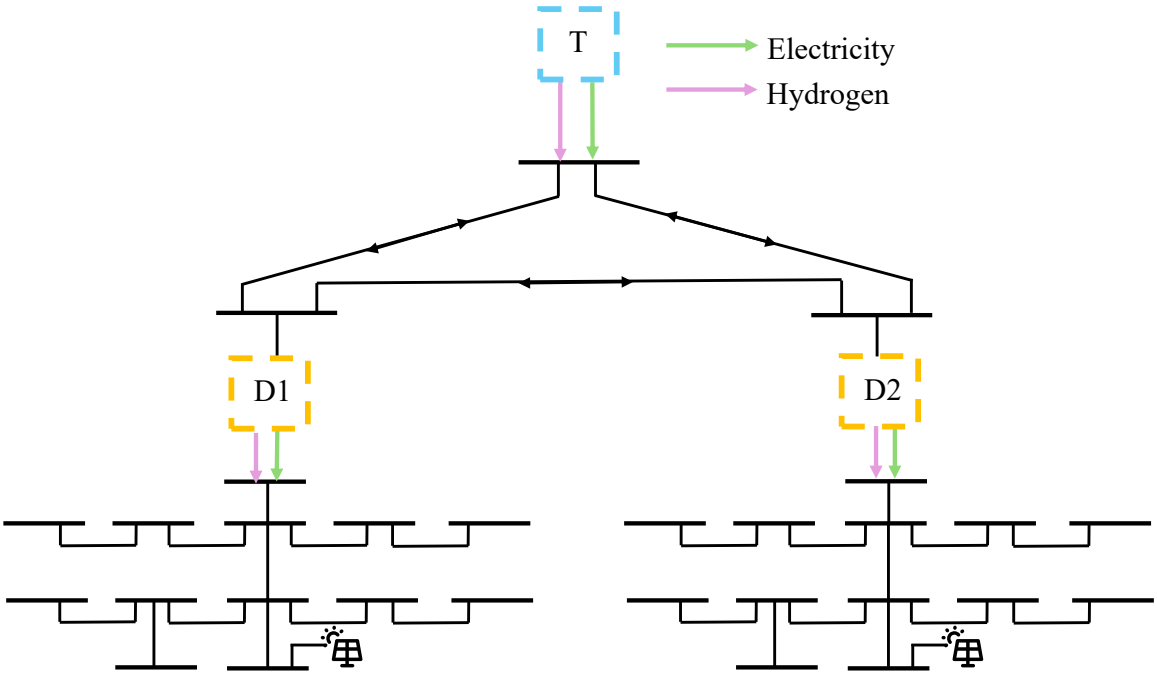

Figure 4.2: Reconstructed Transmission and Distribution Network Case

4.2.2 Parameter Setting

To ensure the representativeness and robustness of the proposed optimisation framework, this study employs a set of well-defined and realistic parameters reflecting the operational characteristics of a hybrid offshore energy system. The offshore wind farm considered in this case study is integrated into the transmission network and possesses a maximum installed capacity of 110.5 MW. The day-ahead electricity prices for the East Denmark market zone (DK2) are obtained from the ENTSO-E Transparency Platform [224], which provides authentic market data essential for modelling energy trading and revenue optimisation. Hourly historical wind capacity factors for the year 2019, corresponding to the same geographical region, are sourced from the Renewable.ninja platform [225]. These data series jointly serve as the fundamental inputs for accurately characterising the wind generation profile and its temporal correlation with market price volatility. Incorporating both meteorological and market datasets enables a high-fidelity representation of real-world dynamics, bridging the gap between technical performance and economic evaluation.

The main operational and design specifications of the electrolyser are summarised in Table 4.1. The electrolyser is modelled with a nominal capacity of 55.25 MW, which represents approximately half of the total installed wind generation capacity. This configuration is selected to ensure a balanced power-to-hydrogen conversion ratio, facilitating flexible operation under fluctuating

wind conditions. The standby power consumption of the electrolyser is 0.55 MW, while the minimum stable load is maintained at 8.29 MW, preventing operational inefficiencies at low load levels. The system operates under standard high-efficiency conditions, with an operating temperature of 90°C and a pressure of 30 bar, and a maximum current density of 5000 A/m^2 [225].

The corresponding hydrogen storage system is designed to complement the electrolyser operation, with a total storage capacity of 23,267 kg and a maximum discharge rate of 969.47 kg/h. This enables the system to buffer short-term fluctuations in hydrogen production and demand, enhancing operational flexibility and reliability. In this study, the hydrogen selling price is assumed to remain constant at 2.3 €/kg, a representative market value for industrial hydrogen under current European conditions. To ensure consistent energy service delivery, the minimum daily hydrogen demand is fixed at 3,878 kg, reflecting a realistic lower bound for continuous hydrogen supply in island-scale applications.

The energy content of hydrogen is taken as 0.033 MWh/kg, consistent with its lower heating value [226]. Considering that the efficiency of commercial fuel cells typically ranges between 50% and 70% [227], a conservative conversion efficiency of 60% is adopted in this work. This corresponds to an effective energy conversion rate of 0.0198 MWh/kg when hydrogen is reconverted into electricity. Such an assumption provides a realistic estimate of round-trip efficiency in power-to-hydrogen-to-power systems and facilitates accurate assessment of overall system profitability.

Table 4.1: Case Study Parameters

Component	**Parameter**	**Symbol**	**Value**	**Unit**
Electrolyzer	Capacity	C_e	55.25	MW
	Standby Load	P^{sb}	0.55	MW
	Minimum Load	P^{min}	8.29	MW
Storage	Capacity	C^s	23267	kg
	Maximum Output	S^{max}_{out}	969.47	kg/h
Compressor	Consumption coefficient	K^c	0.0012	MWh/kg
Hydrogen	Price	C_h	2.3	€/kg
	Minimum demand	H^{min}_d	3878	kg/day
Power	Minimum demand	P^{min}_d	0.02	MW
Fuel Cell	Conversion Rate	α	0.0198	MWh/kg

4.3 Numerical Results

This section presents a comprehensive analysis of the numerical results obtained from the optimisation model of the integrated power and hydrogen plant. The results demonstrate how the coordinated operation of electricity and hydrogen subsystems at both transmission and distribution levels enhances overall system flexibility, reliability, and profitability. The discussion is structured into three main subsections: (1) *Power Network Performance*, which examines the temporal operation of the electricity subsystem and storage dynamics; (2) *Hydrogen System Dynamics*, which elaborates on the production, flow, and storage behaviour of hydrogen as an energy carrier; and (3) *Economic Evaluation*, which quantifies the resulting cost and revenue structure, highlighting the comparative advantages of multi-storage coordination over a single-storage configuration.

Over the 8,760-hour operational horizon, the integrated system injected a total of 428.001 GWh of electricity into the combined transmission–distribution network. Among this, 39.831 GWh was directly supplied to the distribution-level consumers, while the remainder supported transmission-level exchange and electrolysis processes for hydrogen generation. Electricity sales accounted for a revenue of €6.103 million, whereas the plant incurred €0.192 million in costs for electricity procured from the main grid during periods of low renewable generation. These figures indicate that the system remains largely self-sufficient, relying on external grid imports only during unfavourable wind conditions or peak local demand hours.

As shown in Fig. 4.3, electricity exchange occurs frequently and dynamically among the transmission network and the two interconnected distribution networks. This dynamic bidirectional flow pattern reflects the continuous adjustment of power exchange pathways in response to local generation–demand imbalances. The coordinated management of power transfer across networks significantly enhances system flexibility by enabling spatial balancing of electricity, thus preventing local overloads, reducing curtailment of renewable power, and ensuring that supply consistently meets demand across all nodes of the system.

A closer examination of the temporal evolution of the state-of-charge (SOC) for the three electricity storage systems shown in Fig. 4.4 further reveals distinct operational characteristics shaped by their locations and roles. During the initial two months of the simulation, when wind generation exhibits high intermittency and overall demand is moderate, the storage system positioned near the production site (a) and the one located in the left distribution network (b) primarily engage in charging operations. This behaviour reflects the accumulation of surplus renewable electricity generated during high-wind periods. In contrast, from approximately the third month onward, as overall load increases and seasonal wind variability stabilises, storage systems (a) and (c) begin to discharge continuously to sustain downstream electricity demand. Meanwhile, the distribution-

side storage (b) demonstrates frequent cyclic charging and discharging behaviour, functioning as a local balancing asset that absorbs short-term fluctuations and supports voltage stability within the distribution grid.

This coordinated spatial–temporal interaction between transmission and distribution storage systems underscores the technical advantage of distributed energy storage deployment. The localised responsiveness of distribution-level storage mitigates the burden on upstream assets, while the transmission-side storage provides large-scale buffering capability that smooths the overall system operation. Such complementary functionality ensures more stable energy delivery, mitigates curtailment, and reduces dependence on grid imports.

When comparing configurations, the integrated three-storage system exhibits clear superiority over the single-storage configuration (located only at the production site). Under the single-storage scenario, the absence of distributed flexibility resources leads to greater mismatch between generation and demand, resulting in reduced overall energy utilisation. The multi-storage system achieves an annual revenue of €60.539 million, representing a 9.3% increase relative to the single-storage setup (€55.385 million). This improvement stems largely from enhanced operational flexibility, more efficient balancing of spatially distributed resources, and improved utilisation of renewable generation capacity.

4.3.1 Hydrogen System Dynamics

Hydrogen production, transport, and storage form a crucial part of the integrated system, serving as a buffer and energy vector that bridges temporal and spatial imbalances in renewable generation. Over the course of the simulated year, the plant produced a total of 7,017.157 t of hydrogen, with 9.440 t injected into the transmission network and 7,007.717 t distributed across the two local distribution networks. Hydrogen sales constitute the dominant revenue source, contributing €54.725 million to total annual earnings—nearly an order of magnitude greater than the electricity-related income.

The temporal profile of hydrogen generation closely mirrors the variability of renewable input and electricity exchange patterns. During hours of abundant wind generation, surplus electricity is channelled to the electrolyzers, enabling intensive hydrogen production and charging of storage units. Conversely, during low-wind or high-demand periods, hydrogen storage systems discharge to maintain a continuous hydrogen supply to industrial and mobility consumers within both distribution networks. This interplay between production and storage facilitates time-shifting of renewable energy utilisation, effectively converting temporal variability into a storable and transportable energy form.

The SOC evolution of the hydrogen storage systems highlights a clear spatial hierarchy in their operational behaviour. The storage unit located near the production site operates predominantly as a bulk energy reservoir, absorbing large-scale fluctuations in electrolysis output and providing base-load stability. In contrast, the hydrogen storage units situated within the distribution networks act as fast-response buffers that address demand-side variations, ensuring reliable supply to end users even under fluctuating renewable availability. This multi-layer coordination mechanism not only improves hydrogen availability but also alleviates transmission constraints and reduces the need for long-distance hydrogen transport.

Under the single-storage scenario, where only transmission-side hydrogen storage is available, the overall system performance deteriorates notably. Hydrogen production declines by approximately 33.76%, and the hydrogen-related revenue falls by 33.6%. This reduction arises because the single centralised storage facility cannot adequately accommodate spatial demand variations, resulting in higher hydrogen curtailment and lower overall utilisation. By contrast, when electrolyzers and hydrogen storage units are distributed across both production and consumption sites, the system achieves a more effective balance between generation and load, thereby increasing hydrogen throughput and improving economic outcomes.

This finding highlights hydrogen's pivotal role as an integrative medium between the power and gas domains. Its dual capability for long-term energy storage and flexible spatial distribution enables the overall system to operate with greater adaptability, supporting both electricity network stability and the decarbonisation of end-use sectors.

4.3.2 Economic Evaluation

From an economic standpoint, the joint optimisation of power and hydrogen systems produces substantial financial benefits, driven primarily by the synergistic operation of distributed storage and conversion assets. The total annual revenue of the integrated plant amounts to €60.539 million, comprising three major components: electricity sales (€6.103 million), hydrogen sales (€54.725 million), and minor costs associated with electricity imports (€0.192 million). This composition reveals that hydrogen not only complements electricity in operational terms but also dominates the economic performance of the hybrid energy hub.

A closer examination of the revenue breakdown illustrates that hydrogen contributes roughly 90.4% of total income, while electricity sales account for about 10.1%. The remaining 0.3% represents net grid import costs. This revenue distribution reflects the greater economic leverage provided by power-to-hydrogen conversion under optimised operation, particularly when hydrogen demand remains strong throughout the year.

Comparing the two storage configurations reveals the economic significance of distributed coordination. The single-storage configuration, though simpler, limits the plant's ability to respond to locational imbalances and results in suboptimal use of renewable generation. In contrast, the multi-storage configuration enhances the flexibility of both electricity and hydrogen systems, leading to more stable operation and higher energy utilisation efficiency. Consequently, the multi-storage scenario yields a 9.3% increase in the total revenue compared to the single-storage baseline.

Moreover, the distribution of revenue sources suggests an evolving operational strategy: while electricity sales remain a steady but smaller contributor, the hydrogen sector emerges as the principal revenue driver. This shift implies that future integrated systems may increasingly operate as hydrogen-oriented energy hubs, in which electricity acts primarily as a facilitator for hydrogen production, storage, and distribution.

In addition to revenue enhancement, the coordinated operation strategy contributes to system-level cost reduction. By leveraging storage flexibility to minimise grid purchases and reduce curtailment losses, the plant achieves a higher overall efficiency. The combination of spatial coordination, inter-network energy exchange, and sector coupling thus leads to improved economic resilience against fluctuating market prices and variable renewable availability.

Overall, the economic evaluation confirms that the proposed integrated framework—featuring joint electricity–hydrogen optimisation and distributed storage deployment—provides a robust, scalable, and economically viable pathway for multi-energy systems. It validates the hypothesis that coordination across transmission and distribution levels, complemented by hydrogen's long-term storage capacity, can significantly enhance both operational efficiency and financial performance of future decarbonised energy networks.

Table 4.2: Comparison between Two Hydrogen Storage Placements

Category	**Placement**	**Value**	**Unit**
Annual Revenue	Transmission and Distribution	60.539	€m
	Transmission Only	55.385	€m
Electricity Revenue	Transmission and Distribution	6.103	€m
	Transmission Only	14.466	€m
Hydrogen Revenue	Transmission and Distribution	54.725	€m
	Transmission Only	40.966	€m
Hydrogen Production	Transmission and Distribution	7017.157	t
	Transmission Only	5245.945	t

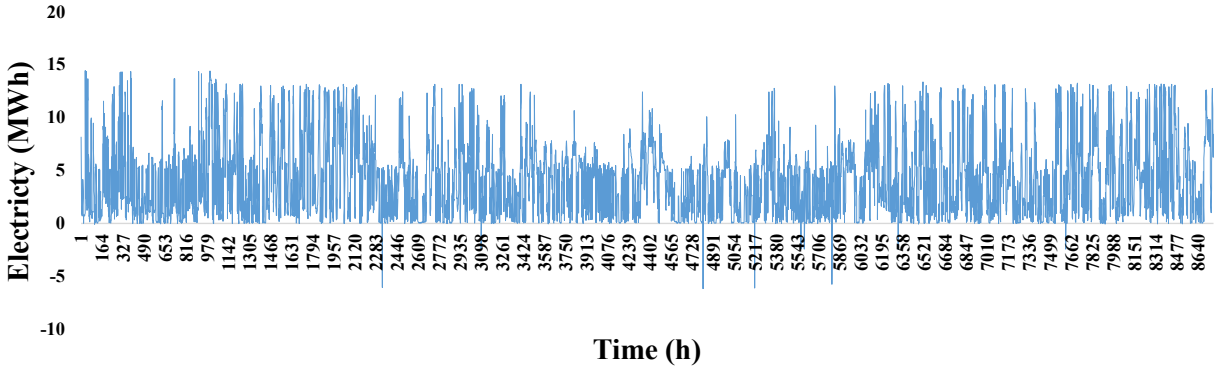

(a) Electricity Exchange between the Two Distribution Networks

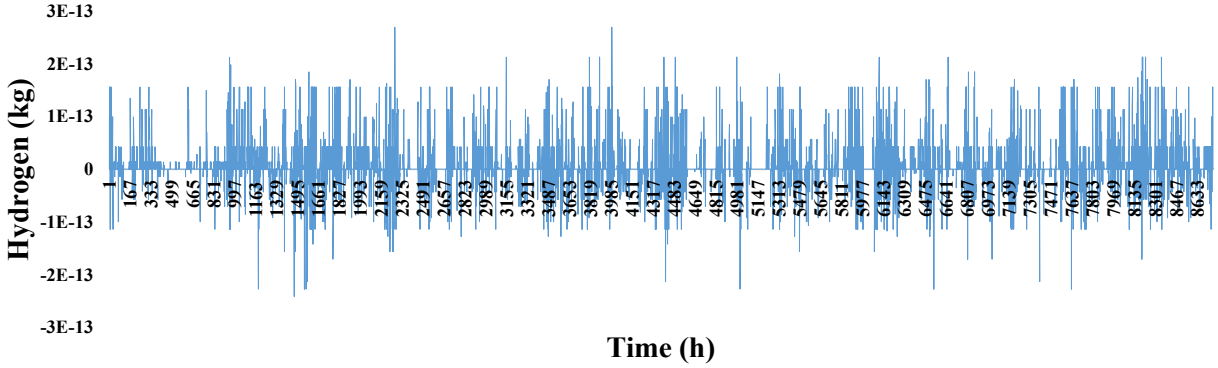

(b) Hydrogen Exchange between the Two Distribution Networks

Figure 4.3: Energy Exchange between Distribution Networks

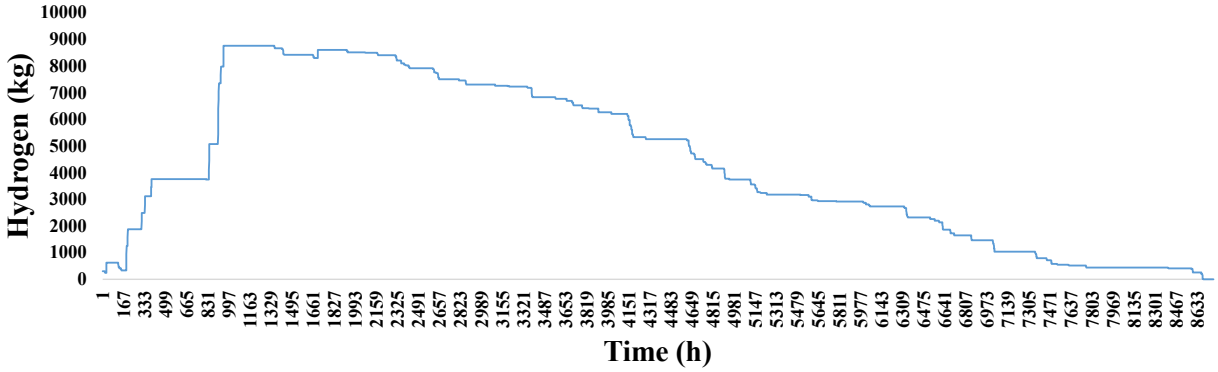

(a) State-of-Charge of Transmission Storage System (T)

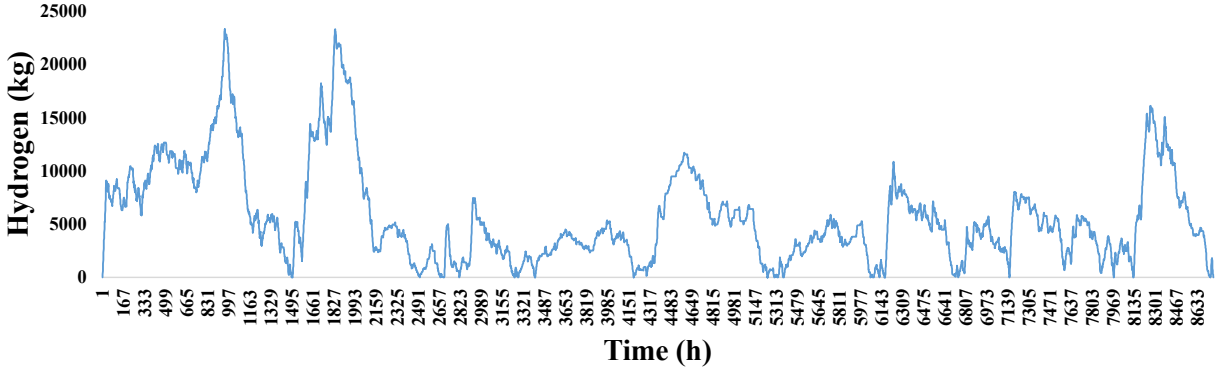

(b) State-of-Charge of Distribution Storage System (D1)

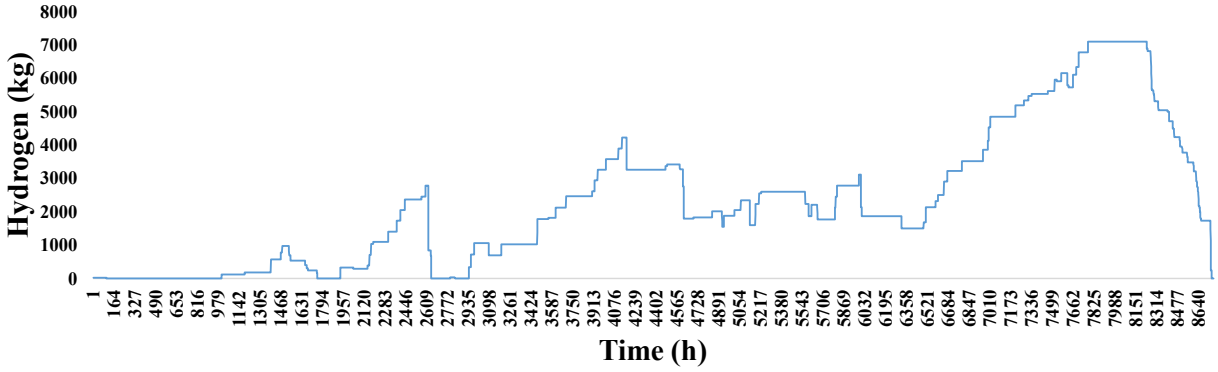

(c) State-of-Charge of Distribution Storage System (D2)

Figure 4.4: State-of-Charge of Three Hydrogen Storage Systems

4.4 Discussions

4.4.1 Practical Implications for Power-Hydrogen Integration

The proposed TSO–DSO coordination mechanism offers several practical insights into the evolving integration between the power and hydrogen sectors. The first and perhaps most significant implication lies in the necessity of multi-level coordination across system boundaries. As hydrogen technologies—particularly electrolysers and storage units—are increasingly deployed at both transmission and distribution levels, the absence of coordinated operation can lead to resource duplication, suboptimal capacity allocation, and underutilisation of renewable resources. The results of this study demonstrate that an integrated scheduling framework can mitigate these inefficiencies by jointly optimising electricity and hydrogen flows, thereby enabling a more efficient use of renewable generation and reducing system curtailment.

A second implication concerns the economic potential of hydrogen storage as a flexibility resource. Through coordinated dispatch, electrolysers can absorb excess renewable electricity during low-price periods, while stored hydrogen can later be converted back or sold during peak prices. This dual operational role not only supports system balancing but also enhances market value. Quantitatively, the coordinated framework achieved up to a 9.3% increase in annual revenue compared with uncoordinated operation, indicating that hydrogen technologies can deliver tangible economic and flexibility benefits to both TSOs and DSOs.

From a policy and regulatory perspective, the study highlights the importance of establishing clear coordination and information-sharing protocols between system operators. Without an appropriate institutional framework, even technically optimal solutions may face implementation barriers. A harmonised market mechanism that recognises the cross-sectoral value of hydrogen flexibility—such as joint pricing of ancillary services or shared balancing markets—would be instrumental in unlocking the full benefits of the proposed coordination scheme.

Finally, this research underscores the need for integrated system planning that aligns hydrogen infrastructure development with power system reinforcement. Strategic co-optimisation of electrolyzer siting, storage sizing, and grid expansion can significantly improve investment efficiency and ensure long-term energy security. As the energy transition accelerates, such joint planning approaches will become essential to achieving a cost-effective and resilient hydrogen-inclusive energy system.

4.4.2 Model Limitations and Future Extensions

While the proposed coordination model provides valuable insights, several limitations must be acknowledged to contextualise the findings and guide future research.

First, the optimisation framework relies on MILP formulations, which necessarily involve linear approximations of nonlinear relationships—such as power flow equations, electrolyser efficiency curves, and hydrogen storage dynamics. Although this approach ensures computational tractability and interpretability, it inevitably introduces simplifications that may affect the accuracy of system representations. Future work could explore mixed-integer nonlinear programming (MINLP) formulations or convex relaxation techniques to better capture the inherent nonlinearities of power–hydrogen interactions while maintaining manageable computational complexity.

Second, the study is subject to data-related limitations. The stochastic characterisation of renewable generation, electricity prices, and hydrogen demand was based on representative scenarios rather than real-time data. Consequently, the robustness of the results depends on the quality and representativeness of these datasets. Future research should consider data-driven or distributionally robust optimisation approaches that explicitly account for uncertainty distributions derived from large-scale historical datasets or high-resolution forecasts, thereby enhancing model generalisability and realism.

Third, the current framework primarily focuses on hydrogen production and short-term storage at the system operation level, without fully incorporating downstream components of the hydrogen value chain such as transportation, compression, and end-use applications in industrial or mobility sectors. Extending the model to encompass the entire hydrogen supply chain would enable a more holistic techno-economic assessment of hydrogen's role in multi-energy systems and its contribution to deep decarbonisation targets.

Another limitation relates to computational scalability. While the presented coordination problem is solvable for single-region configurations, large-scale multi-DSO or cross-border systems could lead to exponential growth in computational complexity. This issue may be addressed through decomposition-based algorithms (e.g., Benders or Dantzig–Wolfe decomposition) or distributed optimisation frameworks, which would allow more efficient computation and near-real-time coordination between TSOs and DSOs.

Lastly, existing transmission–distribution coordination studies have adopted decentralised optimisation methods, in which transmission and distribution operators solve their respective optimisation problems iteratively while exchanging limited information. Such approaches can improve scalability and preserve data privacy. In this thesis, however, an integrated optimisation framework is adopted to enable global coordination of multi-energy resources and to better evaluate overall system-level operational benefits under uncertainty.

4.5 Conclusion

This chapter has presented an innovative optimisation framework for the coordinated operation of coupled power transmission and distribution networks, strategically integrated with green hydrogen production and storage systems. The proposed framework bridges the gap between technical modelling and economic decision-making by jointly considering the physical characteristics, operational constraints, and economic interactions of multiple system layers. Through the independent yet interconnected modelling of the transmission and distribution networks, the study captures the hierarchical complexity of modern power systems while preserving computational tractability. The deterministic optimisation problem is formulated as a mixed-integer linear programming (MILP) model and solved using the Gurobi optimiser, ensuring both modelling precision and numerical efficiency. This formulation enables a rigorous quantification of system-level revenues while maintaining operational realism and physical consistency across the networked infrastructure.

In the case study, the framework is applied to a representative offshore–onshore hybrid energy system configuration. One electrolyser–hydrogen storage pair is situated at the production side, upstream of the transmission network, while two additional electrolyser–storage units are distributed within distinct downstream distribution systems. This spatial arrangement reflects a decentralised yet coordinated approach to hydrogen deployment, allowing each system layer to contribute to the overall flexibility. The results demonstrate that coordinated power and hydrogen exchanges between the transmission and distribution levels can significantly enhance the utilisation of renewable power generation and improve system economics. Specifically, the analysis reveals a clear distinction between the operational roles of storage assets located at different network levels—transmission-side storage supports large-scale balancing and system reliability, whereas distribution-level storage primarily facilitates local flexibility and demand-side management.

To evaluate the practical advantages of the proposed framework, a benchmark scenario with a single hydrogen storage system located solely at the production end is used for comparison. The coordinated configuration achieves an annual revenue increase of 9.3% relative to the benchmark case, providing clear quantitative evidence of the economic benefits derived from the spatial diversification of hydrogen and storage assets. Beyond financial gains, the results highlight the critical role of multi-level coordination in enabling higher renewable penetration, reducing curtailment, and mitigating the adverse impacts of intermittency. Such findings reinforce the importance of cross-layer optimisation frameworks in supporting the operational and economic stability of future integrated energy systems.

Nevertheless, the chapter also recognises that the economic advantages and operational effectiveness of the proposed configuration are inherently dependent on a variety of external factors,

including market price volatility, technology costs, and regulatory conditions. Sensitivity analyses suggest that while the proposed approach remains economically advantageous across a range of assumptions, its robustness under stochastic market environments warrants further investigation. Incorporating dynamic pricing schemes, hydrogen demand uncertainty, and potential grid congestion effects could provide valuable insights into the long-term feasibility and adaptability of such coordinated systems.

From a broader perspective, the outcomes of this study offer important implications for energy system planning and policy formulation. By demonstrating the synergies between hydrogen energy storage and transmission–distribution coordination, the proposed framework contributes to the growing body of research supporting integrated, multi-energy optimisation. The results highlight that hydrogen—when strategically deployed—not only serves as a clean energy carrier but also as a key enabler of flexibility, bridging spatial and temporal mismatches between renewable power generation and end-user demand.

Overall, this chapter provides both methodological and practical contributions to the coordinated optimisation of power and hydrogen networks. The developed framework offers a scalable and adaptable foundation for the analysis of future integrated energy systems, capable of balancing economic efficiency, operational resilience, and environmental sustainability. Future research could extend this framework to incorporate stochastic and multi-objective optimisation, explore real-time control strategies, or evaluate cross-sectoral interactions between electricity, hydrogen, and heat networks. Such extensions would further strengthen the applicability of the framework to the evolving challenges of the energy systems transition, supporting the development of resilient, carbon-neutral, and economically viable power–hydrogen ecosystems.

Chapter 5

Application and Techno-Economic Evaluation of Offshore Energy Systems under Environmental Factors

5.1 Optimal Operation of Offshore Energy Islands under Extreme Weather Conditions

This chapter investigates the operational behaviour and protection challenges of offshore hybrid energy systems under extreme weather conditions, with a particular focus on overcurrent phenomena arising during high wind events. As offshore wind farms are increasingly deployed in deeper waters and harsher environments, ensuring system reliability and electrical protection has become a critical research and engineering priority. The analysis presented herein builds upon the framework developed in the previous chapters, extending it to examine how extreme wind and wave conditions influence both the mechanical response of floating wind turbines and the optimal dispatch of power within an integrated offshore energy island.

To this end, a modelling framework is established that couples offshore wind generation with hydrogen production through electrolysis, incorporating both storage and transport considerations. This integrated configuration allows for a comprehensive examination of energy conversion and utilisation processes within a multi-vector offshore system. Through high-fidelity simulations conducted using the OpenFAST platform, the dynamic performance of the NREL 5 MW OC3 Spar floating wind turbine is evaluated under a spectrum of environmental conditions, ranging from normal operation to extreme wind speeds approaching the turbine's cut-out threshold.

The primary objective of this chapter is twofold. First, it seeks to optimise the power dispatch

strategy of the offshore energy island under extreme weather conditions, ensuring that energy generation and hydrogen production targets are maintained while avoiding electrical and structural overstress. Second, it aims to identify the mechanisms through which adverse environmental factors contribute to overcurrent occurrences and associated operational risks. By linking the results of detailed aero-hydro-servo-elastic simulations with economic optimisation outcomes, the chapter provides new insights into the interplay between system dynamics, energy management, and electrical protection.

In addition, the discussion is contextualised within the broader body of literature addressing offshore wind integration and protection coordination. The chapter concludes by presenting potential mitigation strategies proposed in prior studies, evaluating their applicability to the extreme scenarios considered herein, and highlighting directions for future research on resilient offshore hybrid energy systems.

5.1.1 Modelling Framework under Extreme Conditions

Advancements in offshore energy technologies indicate that floating offshore energy islands, which combine offshore wind with complementary renewable sources and energy storage, are likely to become both more economically viable and more widely implemented than earlier projections suggested [89]. This chapter examines a hybrid power plant, as illustrated in Figure 5.1. The plant integrates power-to-hydrogen systems, including electrolyzers, compressors, and hydrogen storage tanks. It is powered by offshore wind energy and the main power grid. Electricity generated can either be supplied directly to consumers or partially allocated to hydrogen production, converting it into hydrogen for subsequent use. Additionally, hydrogen stored in tanks can be reconverted into electricity via fuel cells to address power shortages.

The study presents a 10000-second simulation with a 5-minute time step to evaluate the environmental impacts of ocean conditions on economic performance. Specifically, it investigates how wind-wave interactions affect offshore wind power output and revenue generation. The primary objective is to maximise short-term revenue during the simulation period.

$$\max \sum_{t \in \mathscr{T}} P_{L,t} C_{p,t} + H_{L,t} C_h - P_{buy,t} C_{p,t}^{buy} \tag{5.1}$$

where $P_{L,t}$ and $H_{L,t}$ represent the power and hydrogen loads, respectively. The electricity selling price is denoted by $C_{p,t}$, while the electricity purchase price, $C_{p,t}^{buy}$, is determined by adding an assumed electricity tariff of 20.05 €/MWh to $C_{p,t}$. Furthermore, the hydrogen price, C_h, is fixed at 2.3 €/kg [223].

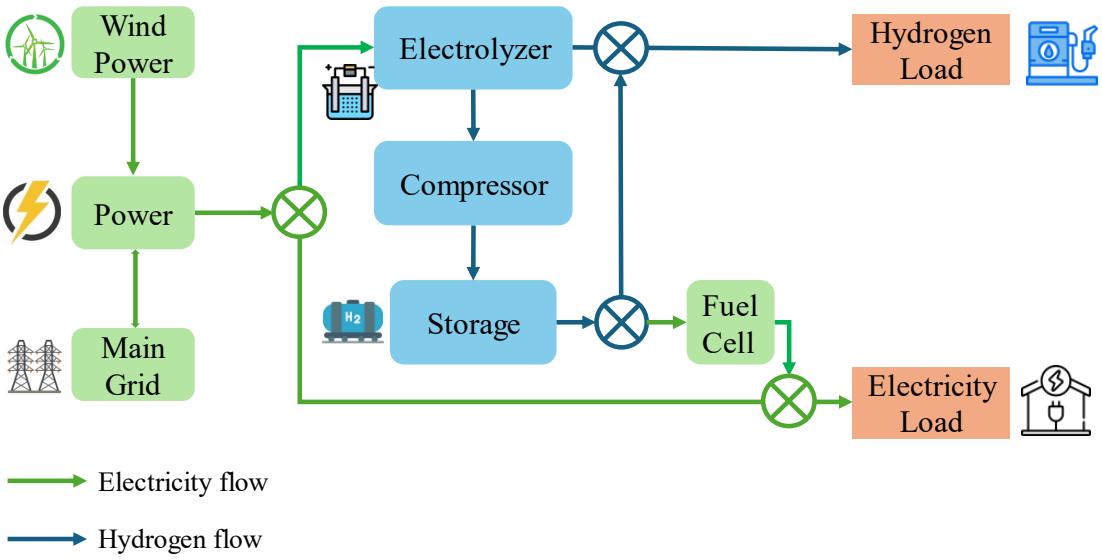

Figure 5.1: Internal Configuration of Distribution of Integrated Power and Hydrogen System

The mathematical model involves offshore wind generation, grid transactions, hydrogen production and storage, and electricity generation via fuel cells. The constraints for the power-hydrogen network are as follows:

$$P_{buy,t} + P_{WT,t} = P_{e,t} + P_{c,t} + P_{d,t} \quad \forall t \in T \tag{5.2}$$

$$P_{L,t} = P_{d,t} + P_{fc,t} \quad \forall t \in T \tag{5.3}$$

where $P_{buy,t}$ represents the power purchased from the main grid, while $P_{WT,t}$ denotes wind power generation. $P_{e,t}$ indicates the consumption of electrolyzers in the transmission network, $P_{c,t}$ represents the consumption of compressors, and $P_{d,t}$ denotes electricity directly supplied to demand. $P_{L,t}$ indicates electricity sent to the consumers, and $P_{fc,t}$ represents the power output from the fuel cell.

It is noteworthy that each constituent exhibits characteristic operational behaviour. The wind power output, $P_{WT,t}$, is inherently stochastic and highly susceptible to extreme weather events, such as elevated wind speeds or storm conditions. Electricity procurement, $P_{buy,t}$, may fluctuate in accordance with market conditions and grid availability, whilst the operation of electrolysers, $P_{e,t}$, is constrained by ramping rates and conversion efficiencies. Similarly, storage operations, $P_{c,t}$, are subject to limits imposed by capacity and charge/discharge rates. By explicitly defining

these variables and associated constraints, the framework provides a detailed operational map of the system under varying environmental conditions, without necessitating additional numerical results.

$$H_{e,t} = H_{d,t} + S_{in,t} \quad \forall t \in T \tag{5.4}$$

$$H_{L,t} = H_{d,t} + S_{hout,t} \quad \forall t \in T \tag{5.5}$$

$H_{e,t}$ represents hydrogen production, while $H_{d,t}$ denotes hydrogen directly delivered to demand. $S_{in,t}$ indicates hydrogen injection into storage from the electrolyzer. $H_{L,t}$ represents hydrogen delivered to consumers, and $H_{d,t}$ signifies hydrogen directly supplied to demand. Finally, $S_{hout,t}$ represents the output of the storage.

$$P_{e,t} \leq C_e u_{os,t} + P_{sb}(1 - u_{os,t}) \quad \forall t \in T \tag{5.6}$$

$$P_{e,t} \geq P^{min} u_{os,t} + P_{sb}(1 - u_{os,t}) \quad \forall t \in T \tag{5.7}$$

P_{sb} represents the standby power consumption of the electrolyzer, while $u_{os,t}$ is a binary variable indicating whether the electrolyzer is operational (on) or on standby at time t. C_e is the electrolyzer capacity. P^{min} is the minimum power consumption limit of the electrolyzer.

$$S_{t=1} = S_{ini} + S_{in,t=1} - S_{out,t=1}, \quad \forall t \in T \tag{5.8}$$

$$S_t = S_{t-1} + S_{in,t} - S_{out,t}, \quad \forall t \in T \tag{5.9}$$

$$S_{out,t} = S_{hout,t} + S_{pout,t}, \quad \forall t \in T \tag{5.10}$$

$$S_t \leq C^s, \quad \forall t \in T \tag{5.11}$$

$$S_{out,t} \leq S_{out}^{max}, \quad \forall t \in T \tag{5.12}$$

$S_{t=1}$ represents the state-of-charge of the storage at time $t = 1$. S_{ini} denotes the initial hydrogen stored in the storage at the beginning of the time horizon. $S_{in,t=1}$ is the storage input at time $t = 1$, while $S_{out,t=1}$ represents the storage output at time $t = 1$. S_t indicates the state-of-charge of the storage at time t. $S_{hout,t}$ denotes the hydrogen delivered to the hydrogen demand from the storage, while $S_{pout,t}$ represents the hydrogen delivered to the power demand from the storage. C^s denotes the storage capacity, and S_{out}^{max} is the maximum output of the storage.

$$P_{e,t} = \sum_{s \in S} P_{e,t}^{s,M} + P_{sb}^{M}(1 - u_{os,t}^{M}) \tag{5.13}$$

$$H_{e,t} = \sum_{s \in S} (A_s P_{e,t}^{s,M} + B_s u_{hp,t}^{s,M}) \tag{5.14}$$

$$u_{os,t} = \sum_{s \in S} u_{hp,t}^{s,M} \quad \forall t \in T \tag{5.15}$$

$\sum_{s \in S} P_{e,t}^{s,M}$ represents the sum of power consumption of electrolyzers across all segments. A_s denotes the slope of the hydrogen production function for segment s, while $P_{e,t}^{s,M}$ indicates the power consumption of the electrolyzer in segment s. B_s represents the intercept of the hydrogen production function for segment s, and $u_{hp,t}^{s,M}$ is a binary variable indicating whether the hydrogen production segment s is active at time t.

$$P_{fc,t} = \alpha S_{pout,t} \quad \forall t \in T \tag{5.16}$$

α is the energy conversion rate of the fuel cell.

$$P_{c,t} = K^c S_{in,t} \quad \forall t \in T \tag{5.17}$$

K^c is the compressor efficiency.

The constraints outlined above serve various purposes within the model. Equations (5.2) and (5.31) ensure the active power flow balance, while (5.32) and (5.33) govern the balance of hydrogen. Constraints (5.35) and (5.36) impose limits on the power consumption of the electrolyzer, and (5.37) to (5.39) manage the input and output of hydrogen storage. Additionally, (5.40) and (5.41) set maximum limits for the state-of-charge and output of the storage system, respectively. (5.42) to (5.44) represent piece-wise linearized hydrogen production of the electrolyzer, while (5.45) and (5.47) relate to electricity generation from the fuel cell and compressor process.

5.1.2 Case Study and Engineering Insights

Parameter Setting

This hybrid offshore energy island derives the majority of its electrical energy from an array of offshore wind turbines, which constitute the primary source of renewable power for the system. In the present study, the power generation characteristics of a representative wind turbine—the NREL 5 MW OC3 Spar platform—are rigorously examined under a range of environmental con-

ditions, encompassing variations in both wind and wave parameters. The numerical simulations are performed using the well-established aero-hydro-servo-elastic modelling framework OPENFAST, which enables a fully coupled analysis of turbine aerodynamics, hydrodynamics, structural dynamics, and control system interactions. By employing OPENFAST, the study captures the dynamic responses of the wind turbine under realistic operational conditions, thereby facilitating an accurate assessment of power output fluctuations and operational constraints in response to complex wind-wave interactions.

The OC3-Hywind spar platform, which serves as the reference turbine in this analysis, is characterised by a draft of 120 metres, reflecting the vertical extent of the substructure beneath the water surface. Its geometric configuration comprises a cylindrical upper section with a diameter of 6.5 metres, a cylindrical lower section with a diameter of 9.4 metres, and an intermediate conical segment that linearly tapers between these two regions, thereby ensuring smooth structural transition and hydrodynamic stability [228]. This particular structural design is intended to mitigate excessive platform motion under extreme environmental loading, while simultaneously optimising the distribution of buoyancy and mass along the vertical axis. A schematic representation of the OC3-Hywind spar platform is provided in Fig.5.2, illustrating the detailed configuration of the substructure, the tower, and the rotor assembly. Furthermore, a comprehensive summary of the platform's technical specifications, encompassing geometric dimensions, mass properties, and operational parameters, is presented in Table 5.1 [229].

It is noteworthy that the combination of the spar-type floating platform and the NREL 5 MW wind turbine has been widely adopted in both academic and industrial studies as a benchmark system for evaluating the dynamic performance of floating offshore wind turbines. The inclusion of wave-induced motions in the simulation enables the study to account for realistic sea states, which are known to influence not only the instantaneous power output but also the fatigue loading experienced by the turbine components. By providing both a visual schematic and detailed numerical specifications, this section establishes a clear foundation for subsequent case studies, allowing the reader to fully appreciate the interaction between environmental conditions, structural response, and power generation in the offshore setting.

The wind turbine has a rated capacity of 5 MW. Day-ahead electricity prices for the East Denmark region (DK2) are retrieved from the ENTSOe Transparency platform [224], while hourly wind capacity factors for 2019 at the specified location are derived from the Renewable.ninja web platform [225]. Table 5.2 provides the specifications of the electrolyzers, which have a capacity of 2.5 MW, with standby and minimum load requirements of 0.025 MW and 0.375 MW, respectively. The electrolyzers operate at 90°C and 30 bar, with a maximum current density of 5000 A/m^2 [225]. The hydrogen storage system is designed with a capacity of 1052.82 kg and a maximum output of 43.868 kg/h. Hydrogen is priced at a fixed rate of 2.3 €/kg, with a daily minimum demand of

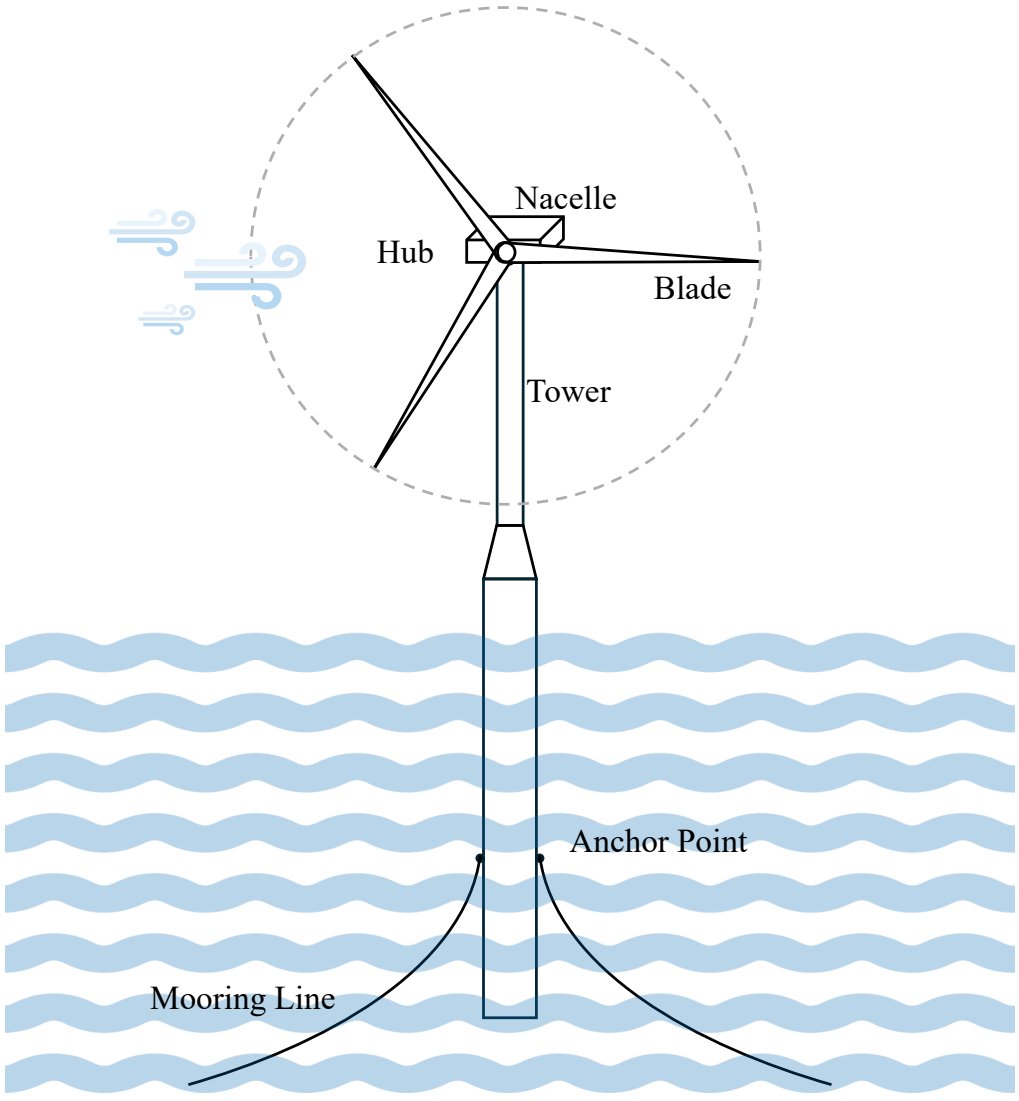

Figure 5.2: Construction of NREL 5MW OC3 Spar Hywind Model.

Table 5.1: NREL 5MW OC3-Spar Hywind Parameters.

Item	Value
Rating	5 MW
Rotor diameter	126 m
Hub diameter	3 m
Hub height	90 m
Cut-in wind speed	3 m/s
Rated wind speed	11.4 m/s
Cut-out wind speed	25 m/s
Water depth	320 m
Total draft	120 m

1.7539 kg. The energy density of hydrogen is 0.033 MWh/kg [226]. Assuming a fuel cell efficiency of 60%, which is within the typical range of 50–70% [227], the energy conversion rate for the fuel cell is estimated at 0.0198 MWh/kg.

Table 5.2: Case Study Parameters.

Component	Parameter	Symbol	Value	Unit
Electrolyser	Capacity	C_e	2.5	MW
	Standby Load	P^{sb}	0.025	MW
	Minimum Load	P^{min}	0.375	MW
Storage	Capacity	C^s	1052.82	kg
	Maximum Output	S_{out}^{max}	43.868	kg/h
Compressor	Consumption coefficient	K^c	0.0012	MWh/kg
Hydrogen	Price	C_h	2.3	€/kg
	Minimum demand	H_d^{min}	175.39	kg/day
Power	Minimum demand	P_d^{min}	0.0375	MW
Fuel Cell	Conversion Rate	α	0.0198	MWh/kg

Wind-Wave Condition Cases

In order to rigorously evaluate the optimal power dispatch strategy and the associated economic revenue of the offshore energy island under extreme environmental conditions, the present study systematically examines a series of operational scenarios corresponding to the cut-in, rated, and cut-out wind speeds of the NREL 5 MW OC3 Spar wind turbine, together with the associated characteristics of the surrounding wind-wave environment. The overarching objective of this analysis is to identify the specific environmental conditions under which the energy island can achieve maximal revenue generation, while simultaneously ensuring the reliable and continuous provision of electrical power and the guaranteed production of hydrogen for downstream consumers. Such

an assessment is particularly critical in the context of offshore hybrid energy systems, where the coupling between variable renewable generation and hydrogen production imposes stringent requirements on operational stability and system flexibility.

Specifically, as detailed in [230], the cut-in wind speed scenario is characterised by an average wind speed of 3 m/s, an average significant wave height of 0.409 m, and an average wave period of 5.548 s. These environmental parameters correspond to the lower threshold of the turbine's operational envelope and provide essential insights into the coupled dynamics of wind and wave interactions at minimal energy input conditions. Understanding the implications of such low-wind, low-wave environments is of particular importance, as the turbine's ability to initiate and sustain rotation is highly sensitive to the available aerodynamic energy. Moreover, the concomitant wave characteristics influence not only the stability and motion of the floating platform but also the hydrodynamic loading on the substructure, which in turn can affect the efficiency and reliability of the turbine's power conversion process.

By systematically analysing these cut-in conditions alongside the rated and cut-out wind speed scenarios, the study is able to construct a detailed and holistic characterisation of the energy island's operational performance across a broad spectrum of environmental states. This approach enables a thorough assessment of both the economic and technical resilience of the system, encompassing fluctuations in power output, potential revenue variations, and the continuity of hydrogen production under varying wind-wave conditions. In doing so, the analysis provides a robust framework for understanding the operational limits of offshore hybrid energy systems and for informing strategic decisions regarding energy dispatch, maintenance planning, and long-term economic optimisation.

Under the rated wind speed conditions, the average wind speed reaches 11.4 m/s, accompanied by an average wave height of 1.967 m and an average wave period of 6.269 s. These parameters reflect a more energetic and relatively stable marine environment, which is highly favourable for efficient power generation by offshore wind turbines. The elevated wind speeds and moderate wave conditions ensure that the turbines operate closer to their nominal capacity, thereby enhancing both electricity and hydrogen production. Furthermore, the consistent energy input under rated conditions reduces the reliance on supplemental electricity from the main grid, contributing to higher overall revenue for the energy island. By examining these operational characteristics, the study provides a clear understanding of how rated wind-wave conditions influence system performance and economic outcomes in offshore hybrid energy systems.

Under cut-out wind speed conditions, the average wind speed reaches 24 m/s, accompanied by an average wave height of 5.333 m and an average wave period of 8.268 s. These parameters characterise highly dynamic and extreme marine conditions, which present significant operational and structural challenges for offshore wind turbines and associated energy systems. At such elevated wind speeds, turbines must implement protective cut-out mechanisms to avoid mechanical damage,

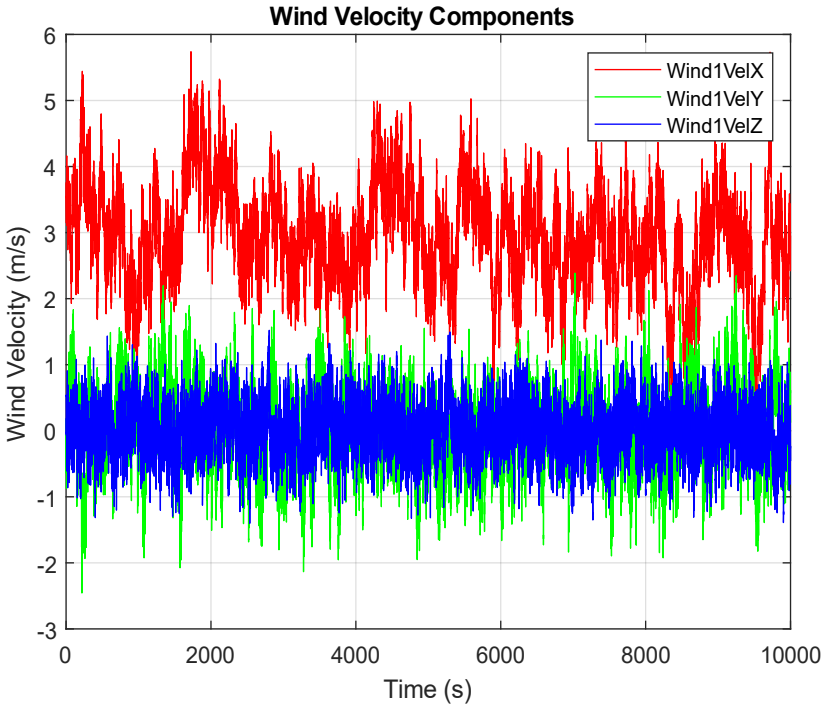

(a) Cut-in Wind Condition Time-Varying Turbulent Wind Speed.

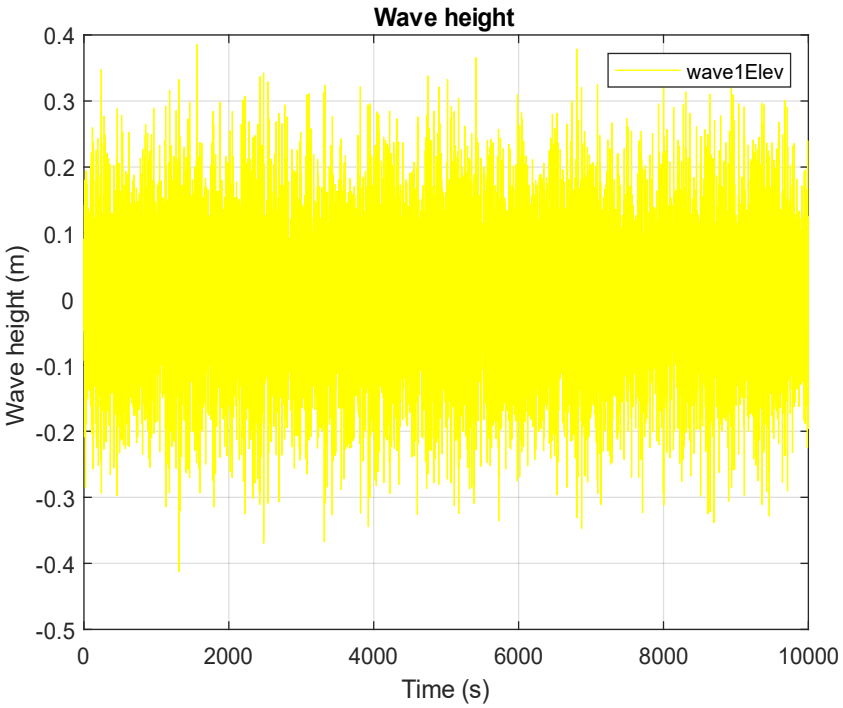

(b) Cut-in Wind Condition Time-Varying Wind Wave Height.

Figure 5.3: Cut-in Wind Condition: Time-Varying Parameters.

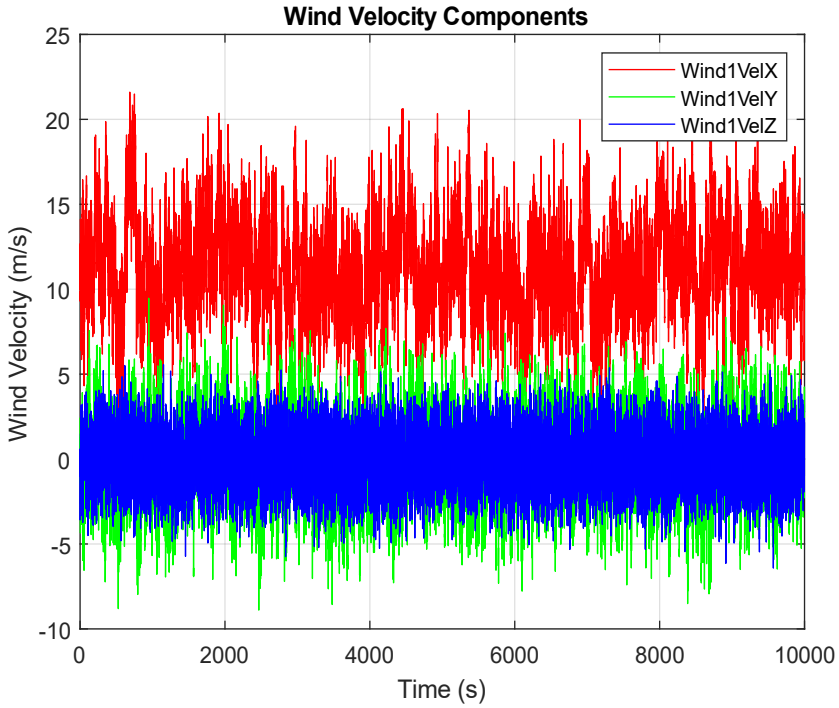

(a) Rated Wind Condition Time-Varying Turbulent Wind Speed.

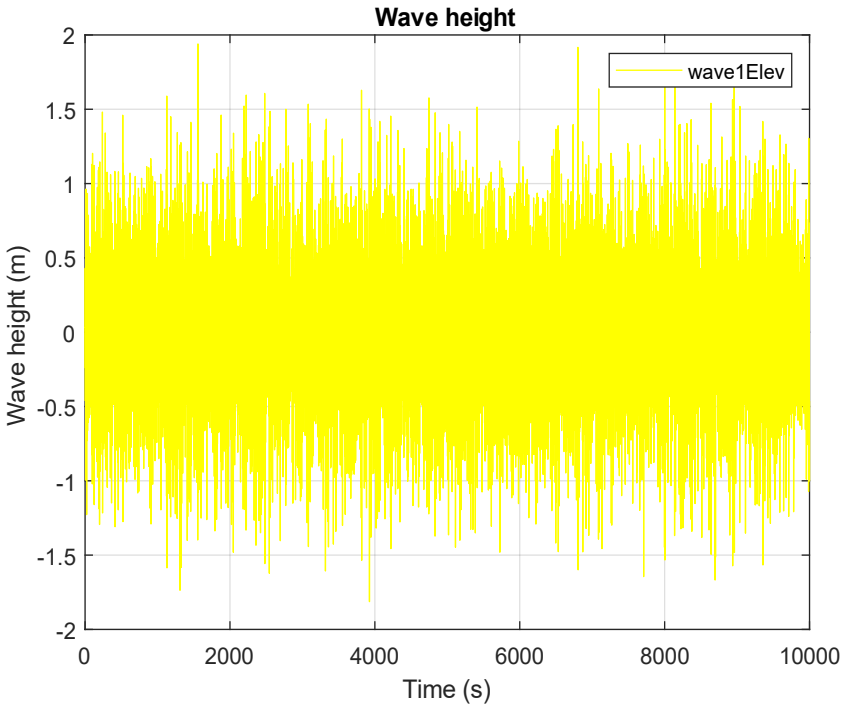

(b) Rated Wind Condition Time-Varying Wind Wave Height.

Figure 5.4: Rated Wind Condition: Time-Varying Parameters.

which can lead to temporary reductions in power generation and hydrogen production. Moreover, the large waves and increased turbulence impose additional loads on the platform structure, necessitating careful consideration of fatigue and stability in both design and operational planning. Analysing these extreme scenarios is therefore essential to assess the resilience of the energy island, optimise operational strategies, and ensure the safe and reliable integration of renewable energy into the broader system.

5.1.3 Result Analysis

The power output behaviour of the offshore hybrid energy system under the three distinct wind-wave input conditions—namely, cut-in, rated, and cut-out wind speeds—is illustrated in Fig. 5.6. A detailed examination of these scenarios offers valuable insights into the dynamic operational performance of the energy island, capturing the response of the system across the complete range of environmental conditions that are likely to be encountered in a North Sea offshore setting. Such an analysis is essential for understanding not only the variations in instantaneous power generation, but also the broader implications for system reliability, energy yield, and the effective integration of complementary hydrogen production units. By systematically comparing the system behaviour under low, moderate, and extreme wind conditions, it becomes possible to identify the thresholds at which the turbines operate sub-optimally, achieve nominal capacity, or require protective intervention. This, in turn, informs both the design of robust operational strategies and the assessment of the economic performance of the hybrid energy island under stochastic environmental influences, thereby providing a comprehensive foundation for subsequent revenue and optimisation analyses.

Under cut-in wind speed conditions, the overall average power output of the system is observed to be merely 0.041 MW. This output is markedly lower than the corresponding values recorded under the rated and cut-out scenarios, as visually highlighted in Fig. 5.6a. The relatively low power generation in this case is primarily attributable to the limited aerodynamic energy available at the turbine rotor, which lies near the lower operational threshold of the NREL 5 MW OC3 Spar turbine. Consequently, the generation of electrical energy is significantly constrained, and the capacity of the system to produce hydrogen is similarly restricted. From an operational perspective, these low-wind conditions underscore the importance of accurately modelling the cut-in behaviour, as even marginal variations in wind speed can exert disproportionate effects on both power output and the economic performance of the hybrid system.

By contrast, under rated wind speed conditions, the overall average power output increases markedly to approximately 3.844 MW, with instantaneous outputs fluctuating within a range of 1 MW to 6 MW, as depicted in Fig. 5.6b. This scenario represents a more stable and productive

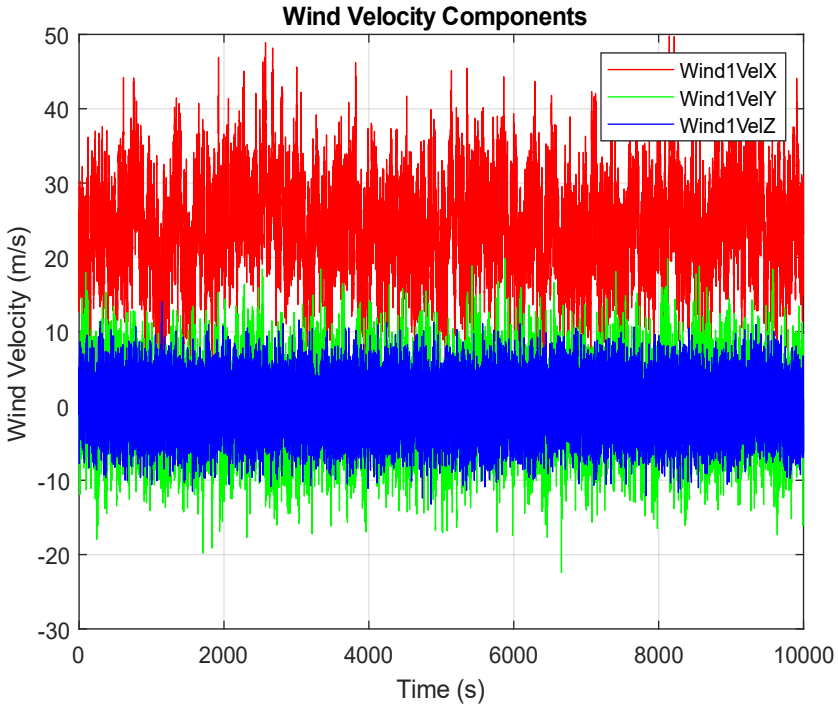

(a) Cut-out Wind Condition Time-Varying Turbulent Wind Speed.

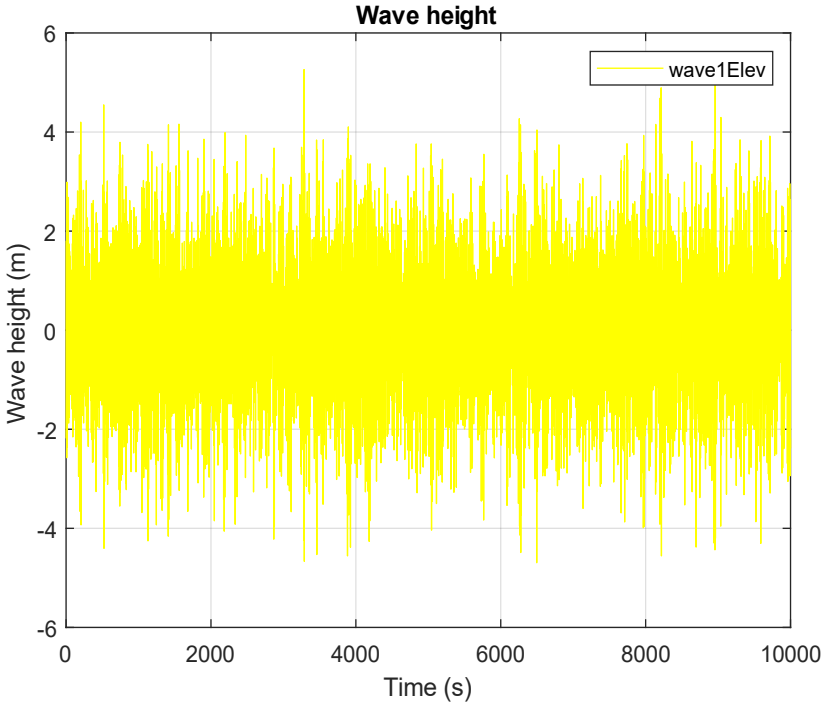

(b) Cut-out Wind Condition Time-Varying Wind Wave Height.

Figure 5.5: Cut-out Wind Condition: Time-Varying Parameters.

operational regime, wherein the wind turbines are functioning near their nominal capacity. The enhanced energy yield under these conditions contributes not only to improved system efficiency but also to a more predictable and reliable supply of hydrogen. Importantly, the fluctuations observed in instantaneous power highlight the inherent variability of wind resources, even at nominally rated conditions, emphasising the need for robust operational strategies that can accommodate short-term changes in environmental input while maintaining system stability.

Finally, under cut-out wind speed conditions, the system exhibits an overall average power output of approximately 5.007 MW, with instantaneous peaks reaching up to 7 MW, as shown in Fig. 5.6c. These elevated outputs, which exceed the rated capacity of the turbine, indicate the substantial energy potential associated with extreme wind events. Nevertheless, the operational regime under such conditions necessitates the implementation of protective mechanisms, including turbine shut-down and pitch control, in order to safeguard the structural integrity of the platform and prevent catastrophic damage. As a result, the instantaneous power output may be intermittently limited, highlighting a trade-off between maximising energy capture and ensuring long-term system reliability.

Taken together, the results across these three wind-wave scenarios underscore the profound influence of environmental variability on the performance of offshore hybrid energy systems. They reveal that both electrical power generation and hydrogen production are highly sensitive to wind-wave conditions, which must therefore be carefully accounted for in operational planning, revenue optimisation, and system design. Such a comprehensive understanding is essential for informing the development of resilient offshore energy islands capable of maintaining stable performance and economic viability under a wide range of environmental conditions.

The total revenue generated by the offshore hybrid power plant over the duration of the simulation period exhibits a clear dependence on the prevailing wind-wave conditions. Specifically, the cumulative revenue under the three considered scenarios—extreme low, rated, and extreme high wind speeds—amounts to €70,694.67, €73,115.47, and €73,494.84, respectively. The comparatively low revenue observed under extreme low wind speed conditions can be attributed to the limited availability of aerodynamic energy at the turbine rotor. In such conditions, the wind turbines alone are insufficient to sustain the minimum operational requirements for hydrogen production. Consequently, the plant must resort to procuring electricity from the main grid in order to satisfy the stipulated hydrogen production threshold. This additional expenditure on externally sourced electricity directly diminishes the overall revenue, highlighting the operational and economic vulnerability of the system under sub-optimal environmental conditions.

By contrast, under rated wind speed conditions, the wind and wave resources provide sufficient energy to meet both the electrical and hydrogen production demands autonomously, obviating the need for supplementary grid purchases. This scenario therefore results in a more favourable eco-

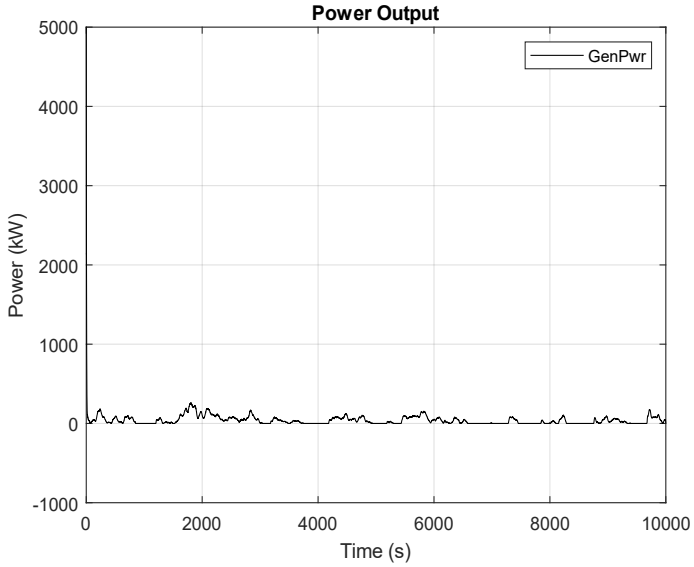

(a) Power Output under Cut-in Wind Speed.

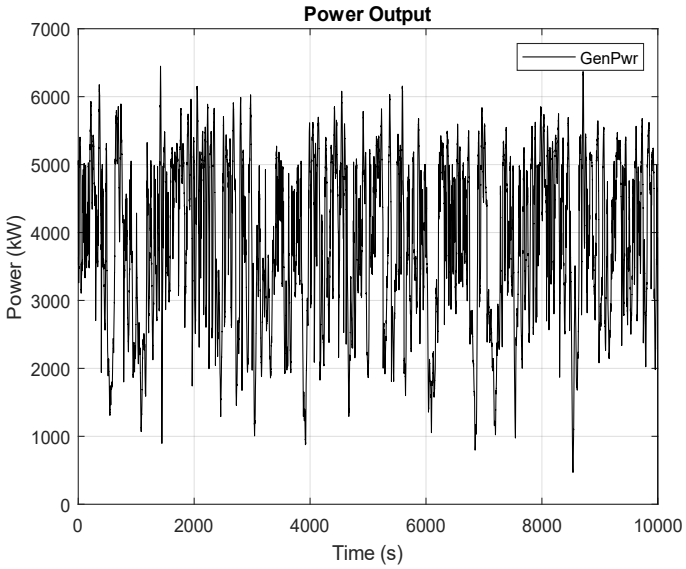

(b) Power Output under Rated Wind Speed.

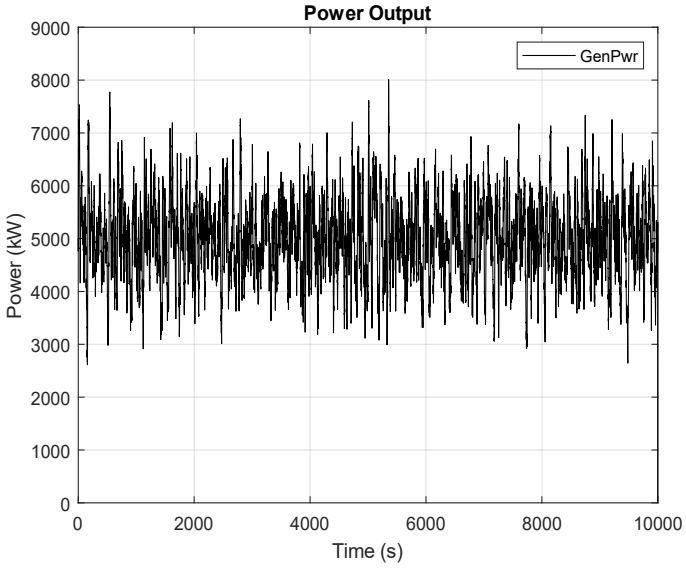

(c) Power Output under Cut-out Wind Speed.

nomic outcome, as reflected in the higher cumulative revenue of €73,115.47. Furthermore, under extreme high wind speed conditions, the abundance of kinetic and wave energy enables the system to operate near, or occasionally above, nominal turbine capacity, thereby slightly enhancing overall revenue. The observed cumulative revenue of €73,494.84 under these conditions represents a modest increase of approximately 0.52% relative to the rated wind speed scenario, demonstrating the marginal gains achievable when operating in extreme high-wind environments over the considered 10,000-second simulation period.

Quantitatively, the extreme low wind scenario results in the lowest economic performance, with revenue being 3.31% lower than that attained under rated wind conditions. This quantitative comparison underscores the sensitivity of the hybrid energy system's profitability to variations in environmental conditions. The findings collectively emphasise that the economic output of offshore hybrid energy islands is not solely determined by turbine capacity or hydrogen production efficiency, but is also profoundly influenced by the stochastic nature of wind and wave resources. Consequently, these observations highlight the critical importance of adaptive operational strategies that are capable of responding to fluctuating environmental inputs. By implementing such strategies, system operators can optimise revenue streams while simultaneously ensuring that minimum hydrogen production requirements are consistently satisfied, thereby maintaining both economic viability and operational reliability under a broad spectrum of environmental conditions, as summarised in Table 5.3.

Table 5.3: Comparison between Two Hydrogen Storage Placements.

Scenario	**Category**	**Value**	**Unit**
Extreme Low Wind Case	Total revenue	70694.67	€
	Sold Electricity revenue	71385.88	€
	Electricity Purchase Cost	691.21	€
Rated Wind Case	Total revenue	73115.47	€
	Sold Electricity revenue	71805.29	€
	Electricity Purchase Cost	0	€
Extreme High Wind Case	Total revenue	73494.84	€
	Sold Electricity revenue	72184.67	€
	Electricity Purchase Cost	0	€

5.1.4 Discussion of Key Findings and the Need for Long-term Evaluation

Interpretation of Key Findings

The analysis presented in this chapter underscores the critical influence of environmental variability—specifically wind–wave dynamics—on the operational and economic performance of offshore hybrid power plants. The integrated optimisation and simulation framework demonstrates how fluctuations in offshore meteorological and hydrodynamic conditions directly affect the plant's power generation capability, hydrogen production, and overall revenue. The comparative evaluation of the three representative wind–wave scenarios (cut-in, rated, and cut-out) reveals that the plant exhibits distinct performance regimes under varying environmental intensities.

At rated and extreme high wind speeds, the hybrid system achieves near-complete operational independence from the main grid. This finding has significant implications for offshore energy self-sufficiency, indicating that under favourable conditions, such systems can sustain hydrogen production and revenue generation autonomously. Conversely, the decline in revenue under low wind conditions (by approximately 3.31%) illustrates the vulnerability of renewable-dependent systems to meteorological intermittency. The operational need to import electricity during these periods not only reduces profitability but also introduces additional complexity in ensuring hydrogen supply continuity.

These findings highlight the fundamental trade-off between renewable variability and operational reliability, emphasising the necessity for flexible dispatch mechanisms, dynamic scheduling, and potentially complementary energy storage integration. The results confirm that a hybrid offshore configuration—combining renewable generation, hydrogen production, and grid interaction—can effectively balance self-sufficiency with reliability, provided that operational strategies are appropriately tuned to environmental dynamics.

Methodological and Technical Insights

From a methodological perspective, this study advances the modelling of offshore hybrid energy systems by combining high-fidelity physical simulations (via OPENFAST) with deterministic MILP-based optimisation. This dual-layer modelling approach bridges the gap between environmental physics and system-level decision-making. By computing time-averaged power outputs at five-minute intervals across 10,000-second simulations, the model captures transient aerodynamic and hydrodynamic interactions while maintaining computational tractability for optimisation.

The deterministic MILP formulation, while simplified relative to full stochastic treatment, enables clear quantification of the operational trade-offs between electricity exports, grid imports, and hydrogen production commitments. The approach demonstrates how deterministic optimisa-

tion can still yield operationally meaningful insights when informed by representative environmental regimes. This methodological integration of physical simulation and mathematical optimisation represents a valuable contribution to offshore system analysis, where capturing both mechanical realism and operational decision logic remains challenging.

Practical and Economic Implications

The results from this chapter offer several key practical insights for the planning, operation, and design of offshore hybrid power plants. First, the identified sensitivity of system performance to environmental conditions underscores the importance of site-specific resource characterisation. Accurate long-term assessment of wind and wave correlations is essential to ensure reliable hydrogen supply and financial stability. The relatively small (0.52%) revenue increase under high wind scenarios, compared to the rated case, highlights that marginal environmental improvements yield limited economic benefit once design limits are approached—pointing to the diminishing returns of oversizing generation capacity without adequate storage or grid coupling.

From an operational perspective, the findings reaffirm the role of hydrogen production as a strategic flexibility mechanism. By acting as an energy sink during periods of surplus renewable generation, hydrogen systems can mitigate curtailment and stabilise revenues. Conversely, the requirement to meet a guaranteed minimum hydrogen output introduces a constraint that drives optimal scheduling decisions. This tension between flexibility and obligation illustrates the complex balancing act required in hybrid offshore operations.

Economically, the integration of robust protection mechanisms and adaptive control strategies, although adding initial investment, is justified by the long-term benefits in system resilience and reduced downtime. These insights are directly relevant to policymakers and developers seeking to scale up offshore hybrid installations, as they highlight the intertwined relationship between technical design choices, economic performance, and regulatory compliance in safety and reliability.

Limitations and Future Research Directions

While the deterministic MILP model successfully captures key operational behaviours, several limitations remain. The reliance on representative wind–wave regimes simplifies the inherent stochastic variability of offshore environments. Future research should incorporate stochastic or distributionally robust formulations that explicitly model probabilistic uncertainties in environmental parameters and electricity prices. Such enhancements would enable more realistic assessments of risk and resilience in offshore operations.

The framework also assumes fixed hydrogen pricing and grid tariffs, which may not hold in liberalised market conditions subject to volatility. Integrating dynamic market participation mod-

els, including price-responsive hydrogen demand and grid service provision, would yield a more comprehensive understanding of hybrid plant economics. Moreover, incorporating energy storage technologies—such as battery or compressed hydrogen storage—could mitigate low-wind deficits and further stabilise operation.

From a technical perspective, the integration of digital twin systems presents a promising avenue for future work. By coupling real-time monitoring data with predictive analytics, digital twins could enable adaptive control, predictive maintenance, and real-time optimisation under variable environmental and market conditions. Finally, further exploration of fault-tolerant control strategies and advanced protection schemes could enhance the safety and reliability of offshore hybrid systems, bridging the gap between theoretical optimisation and practical deployment.

These findings underscore the importance of incorporating a detailed understanding of wind–wave variability when evaluating the operational and financial performance of offshore hybrid power plants. They further illustrate the critical role that minimum hydrogen production requirements play in shaping optimal operational strategies. In particular, the study demonstrates the need for flexible system design and operational planning to mitigate periods of low renewable generation, thus ensuring both economic efficiency and reliable supply of hydrogen.

Looking forward, future research can build upon this framework by introducing stochastic representations of wind and wave resources, allowing a more realistic assessment of uncertainty in renewable generation. Additionally, extending the model to consider long-term electricity market price fluctuations, grid constraints, and the integration of larger-scale energy storage systems could further enhance the resilience, reliability, and revenue stability of such plants. Furthermore, combining these improvements with advanced forecasting methods, real-time control strategies, and adaptive electrical protection could provide valuable insights into the practical implementation of offshore hybrid power plants, supporting their deployment as reliable, low-carbon, and economically viable energy solutions in a future sustainable energy system.

5.2 Life-Cycle Analysis: Techno-Economic Optimisation and Evaluation of Offshore Wind Systems

Building upon the multi-energy integration strategies established in earlier chapters, this study extends the concept of offshore hybrid systems to include detailed hydrogen production, storage, and transport modelling. This allows for a flexible and efficient electricity-to-hydrogen conversion pathway, supporting the wider ambition of sustainable offshore energy transition. Kriging surrogate modelling is adopted in this study due to its strong capability in approximating nonlinear

input–output relationships with relatively limited training samples. Compared with high-fidelity OPENFAST simulations, the surrogate model significantly reduces computational cost while maintaining satisfactory prediction accuracy. In addition, Kriging models have been widely applied in engineering optimisation and reliability analysis, making them suitable for the present offshore energy island assessment framework. To facilitate this analysis, Kriging surrogate models are employed and validated using high-fidelity OpenFAST simulations. These models are used to predict turbine performance and fatigue damage across a spectrum of realistic wind and wave conditions, thus capturing both operational variability and long-term structural effects.

This chapter develops a comprehensive techno-economic framework for the optimal site selection of offshore energy islands, integrating both economic efficiency and structural resilience as central decision criteria. Recognising the inherently dynamic nature of marine environments, the framework incorporates coupled wind–wave interactions to enhance the accuracy and reliability of location-based assessments. In doing so, it enables more informed decisions that ensure the selected sites are not only cost-effective but also capable of maintaining operational integrity under varying environmental conditions.

The proposed framework also draws upon historical environmental datasets and multiple floating platform configurations to benchmark performance under practical offshore conditions. The resulting analysis provides valuable insights into how optimal site selection can enhance life-cycle profitability, structural reliability, and system resilience. In summary, the chapter contributes a scalable and data-informed decision-making tool for future offshore renewable energy developments, with direct relevance to emerging concepts of floating energy islands and integrated hydrogen production systems.

5.2.1 Fatigue Damage Assessment under Coupled Wind-Wave Conditions

Numerical Model of Wind Turbine and Environment

The offshore Tension-Leg Platform (TLP) supporting the 5-MW baseline wind turbine developed by the National Renewable Energy Laboratory (NREL) [231] is adopted in this study as the representative floating wind platform. To accurately capture the dynamic and stochastic characteristics of the offshore environment, the coupled wind and wave conditions are simulated in the time domain using the spectral representation method [232], which allows for the realistic generation of wind-wave time series with proper statistical properties. These simulations are implemented using the open-source wind turbine analysis software OpenFAST [164], which facilitates fully coupled aero-hydro-servo-elastic modelling. Within OpenFAST, the AeroDyn module provides high-fidelity aerodynamic calculations, ensuring consistency and compatibility with the hydrodynamic

and structural dynamics modules. This integrated modelling approach enables a comprehensive assessment of turbine performance, structural loads, and power output under varying environmental conditions, forming a robust basis for subsequent optimisation and reliability analyses.

Short-term Fatigue Damage Estimation Method

The stress experienced at the base of the wind turbine foundation is a critical parameter for estimating the fatigue damage of offshore wind structures. In this study, the assessment follows the DNV GL standard [233], which provides established guidelines for evaluating fatigue in offshore high-strength steel structures. Initially, the time histories of forces and bending moments at the foundation base are obtained through detailed simulations conducted in OpenFAST. These simulations capture the coupled aero-hydro-servo-elastic response of the wind turbine under realistic wind and wave loading conditions. The resulting force and moment time series are subsequently converted into time histories of stress at the critical cross-section of the foundation. These stress time series form the fundamental input for fatigue analysis, which is performed using the methodology described by equations (5.18) to (5.20) [234], [235]. This approach enables a quantification of fatigue damage accumulation over the operational lifetime of the turbine, providing essential insights for the structural design, maintenance planning, and long-term reliability assessment of offshore wind installations.

$$\sigma_x = \frac{F_x}{A} - \frac{M_z}{2\pi r^2 \delta}\sin\theta \tag{5.18}$$

$$\sigma_y = \frac{F_y}{A} + \frac{M_z}{2\pi r^2 \delta} cos\theta \tag{5.19}$$

$$\sigma_z = \frac{F_z}{A} + \frac{M_x}{I_x} rsin\theta - \frac{M_y}{I_y} rcos\theta \tag{5.20}$$

where σ, F, M represent the stress, force, and bending moments at the wind turbine foundation base, respectively. σ_x, σ_y, and σ_z denote the streamwise, transverse, and vertical axial stresses at the foundation of the wind turbine; F_x, F_y, and F_z denote the streamwise shear, transverse shear, and vertical axial forces at the foundation; M_x, M_y, and M_z denote the streamwise, transverse, and vertical axial bending moments at the foundation; A denotes the area of the foundation base section; I_x and I_y denote the moments of inertia of the base section about the x and y axes; r and δ denote the outer radius and wall thickness of the foundation base section; θ denotes the orientation angle.

Fatigue damage analysis reveals that the axial stress at the base section of the wind turbine foundation causes significantly greater fatigue damage compared to shear stress, a phenomenon

widely documented in numerous studies [234], [235], [236]. To validate this observation, we conducted experimental measurements under operational conditions with a wind speed of $U = 9\,\mathrm{m/s}$, wave height of $H = 5\,\mathrm{m}$, and wave period of $T = 15\,\mathrm{s}$. The time history of stress at the foundation base was recorded, and the corresponding fatigue life curve is presented in Fig. 5.7. The experimental results demonstrate that the fatigue damage induced by axial stress is substantially higher than that caused by other stress components. Therefore, given the dominant role of axial stress in fatigue damage, this study focuses exclusively on axial stress for fatigue damage assessment, consistent with the approach adopted in previous research [234], [235].

The short-term damage d, as calculated in equation. (5.21), is determined from the simulated stress time histories over one hour using the rainflow counting method and the S-N curve for class C1 in a seawater environment with cathodic protection, according to the DNV GL standard [233], as shown in equation. (5.22).

$$d = \sum \frac{n}{N} \tag{5.21}$$

where d denotes the short-term fatigue damage; n denotes the cycle numbers estimated by the rainflow counting method with the stress range $\Delta\sigma$; N denotes the failure cycle numbers with the stress range $\Delta\sigma$.

$$logN = log\bar{a} - mlog\Delta\sigma \tag{5.22}$$

where $\Delta\sigma$ represents the stress range (in MPa), n is the number of cycles estimated by the rainflow counting method for the stress range $\Delta\sigma$, N denotes the failure cycles corresponding to the stress range $\Delta\sigma$, m is the negative inverse slope of the S-N curve, and $log\bar{a}$ is the intercept of the S-N curve on the log N axis. The S-N curve for class C1 from the DNV GL standard is used to estimate the fatigue damage of offshore wind turbines in a seawater environment with cathodic protection [233], and it is applied to evaluate the short-term fatigue damage of the tower base for the 5 MW OC4-Semi under conditions F110, F210, and F310 [237].

Long-term Fatigue Damage Estimation Method

The long-term fatigue damage D_i for a specific environmental condition is determined by multiplying the short-term damage d under that condition by its probability of occurrence and the total number of short-term conditions the wind turbine is expected to experience during its operational lifespan. The overall long-term fatigue damage, D_{total}, is then calculated by summing the individual long-term damages D_i across various environmental conditions, based on the principles of the Miner cumulative damage model.

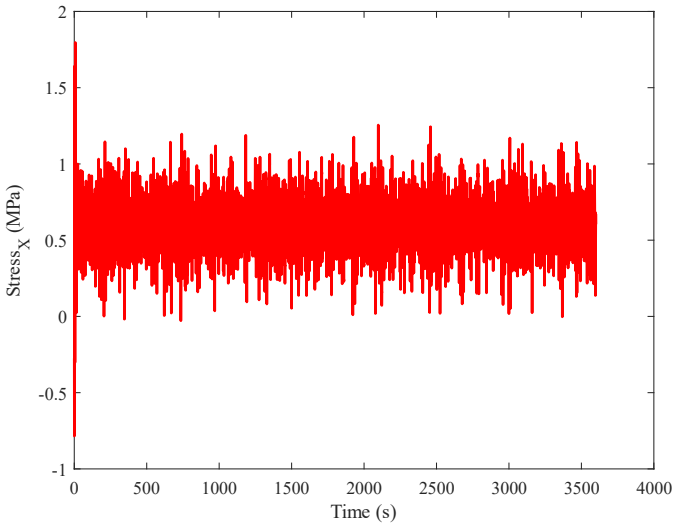

(a) Streamwise Shear Stress.

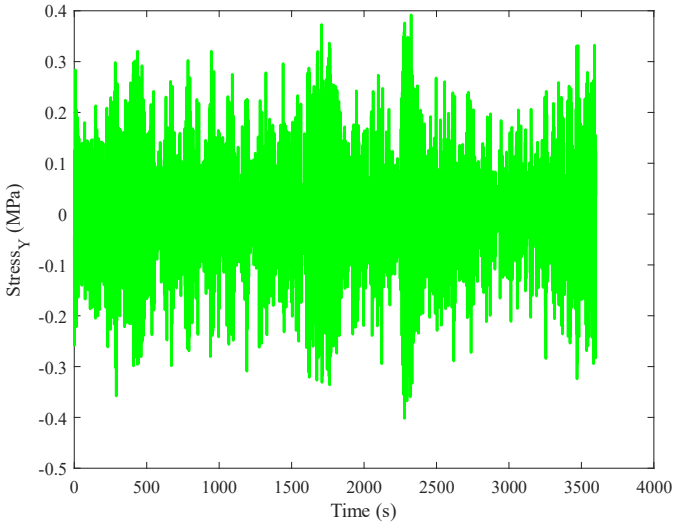

(b) Transverse Shear Stress.

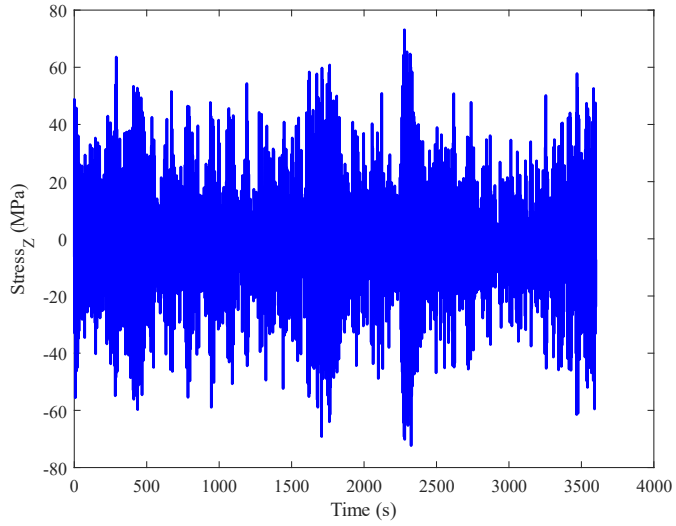

(c) Vertical Axial Stress.

Figure 5.7: Time history of streamwise shear, transverse shear, vertical axial stress.

$$D_i = d \times p \times T_{life} \tag{5.23}$$

where D denotes the long-term fatigue damage for a specific environmental condition; T_{life} denotes the number of one-hour short-term conditions that the wind turbine will experience during its service lifetime; p denotes the occurrence probability of the wind-wave environmental condition.

$$D_{total} = \sum D_i \tag{5.24}$$

$$T_{life} = N_{yr} \times 365 \times 24 \tag{5.25}$$

where D_{total} denotes the overall long-term fatigue damage. N_{yr} refers to the service years, set to 25 [238], [239], [240]. Since the fatigue life can be calculated as the reciprocal of the fatigue damage, evaluating the fatigue damage is equivalent to assessing the fatigue life. To avoid redundancy, the value of the fatigue life is not provided [235].

The occurrence probability p of wind-wave environmental condition (U,H,T) is calculated by the joint probability distribution of wind speed, wave height, and period as:

$$p(U,H,T) = f(U) \cdot f(H|U) \cdot f(T|U,H) \tag{5.26}$$

$$f(U) = \frac{\alpha_U}{\beta_U}\left(\frac{U}{\beta_U}\right)^{\alpha_U - 1} \cdot \exp\left[-\left(\frac{U}{\beta_U}\right)^{\alpha_U}\right] \tag{5.27}$$

$$f(H|U) = \frac{\alpha_H}{\beta_H}\left(\frac{H}{\beta_H}\right)^{\alpha_H - 1} \cdot \exp\left[-\left(\frac{H}{\beta_H}\right)^{\alpha_H}\right] \tag{5.28}$$

$$f(T|U,H) = \frac{1}{\sqrt{2\pi}\sigma_{ln(T)}t} \cdot \exp\left[-\frac{1}{2}\left(\frac{ln(T) - \mu_{ln(T)}}{\sigma_{ln(T)}}\right)^2\right] \tag{5.29}$$

where $p(U,H,T)$ denotes the occurrence probability of a certain wind-wave environmental condition (U,H,T); $f(U)$ denotes the probability density function of wind speed; $f(H|U)$ denotes the probability density function of wave height; $f(T|U,H)$ denotes the probability density function of wave period; α_U and β_U denote the shape and scale parameters of the Weibull distribution of wind speed; α_H and β_H denote the shape and scale parameters of the Weibull distribution of wave height; $\mu_{ln(T)}$ denotes the mean of the natural logarithm of wave period; $\sigma_{ln(T)}$ denotes the standard deviation of the natural logarithm of wave period.

Kriging Surrogate Model for Fatigue Damage and Power Output Prediction

As specified in IEC 61400–3-1 [241], a variety of wind-wave conditions must be considered to assess the fatigue damage of offshore wind turbines. These conditions should include wind speed intervals smaller than 2 m/s, wave height intervals smaller than 0.5 m, and wave period intervals less than 0.5 s. For the current wind-wave conditions, with wind speeds ranging from 3 to 25 m/s, wave heights from 1 to 6 m, and wave periods from 5 to 15 s, at least 2772 simulations of turbine responses under different environmental scenarios are required, which is highly time-consuming. To enhance the efficiency of fatigue damage estimation, surrogate models are employed, reducing the number of wind and wave conditions analysed and the total load cases to 432 [235]. These 432 simulation results are sampled using a hyper-Latin cube method, with part of the samples used as the training set and the remaining samples used for testing. The corresponding data points can be seen in Fig. 5.8.

To predict the fatigue damage and the power output of offshore wind turbines efficiently, we employ a Kriging surrogate model trained on the reduced dataset of 432 simulations. This dataset, representing a variety of environmental conditions, is used to build a probabilistic model that captures the complex relationships between the input environmental parameters and the turbine's fatigue damage. The Kriging model is particularly well-suited for this task due to its ability to handle sparse data and its inherent capability to provide not only predictions but also uncertainty estimates. Once trained, the Kriging model can be used to predict fatigue damage for unseen combinations of wind speed, wave height, and wave period. Its efficiency comes from significantly lowering the number of direct simulations needed while providing valuable uncertainty quantification that is crucial for assessing the reliability of offshore wind turbines in varying conditions.

The accuracy of the Kriging model is further validated through comparisons with direct OpenFAST simulations. By cross-referencing the predictions from the surrogate model with results from full-scale simulations of turbine responses, we ensure that the Kriging model accurately captures the underlying physical processes governing the fatigue damage under different wind-wave conditions. The OpenFAST simulations serve as a benchmark, providing a reliable reference for validating the surrogate model's predictions. This verification step ensures that the Kriging model not only reduces computational costs but also maintains a high degree of accuracy, making it a robust tool for efficiently estimating the fatigue damage of offshore wind turbines in various environmental scenarios.

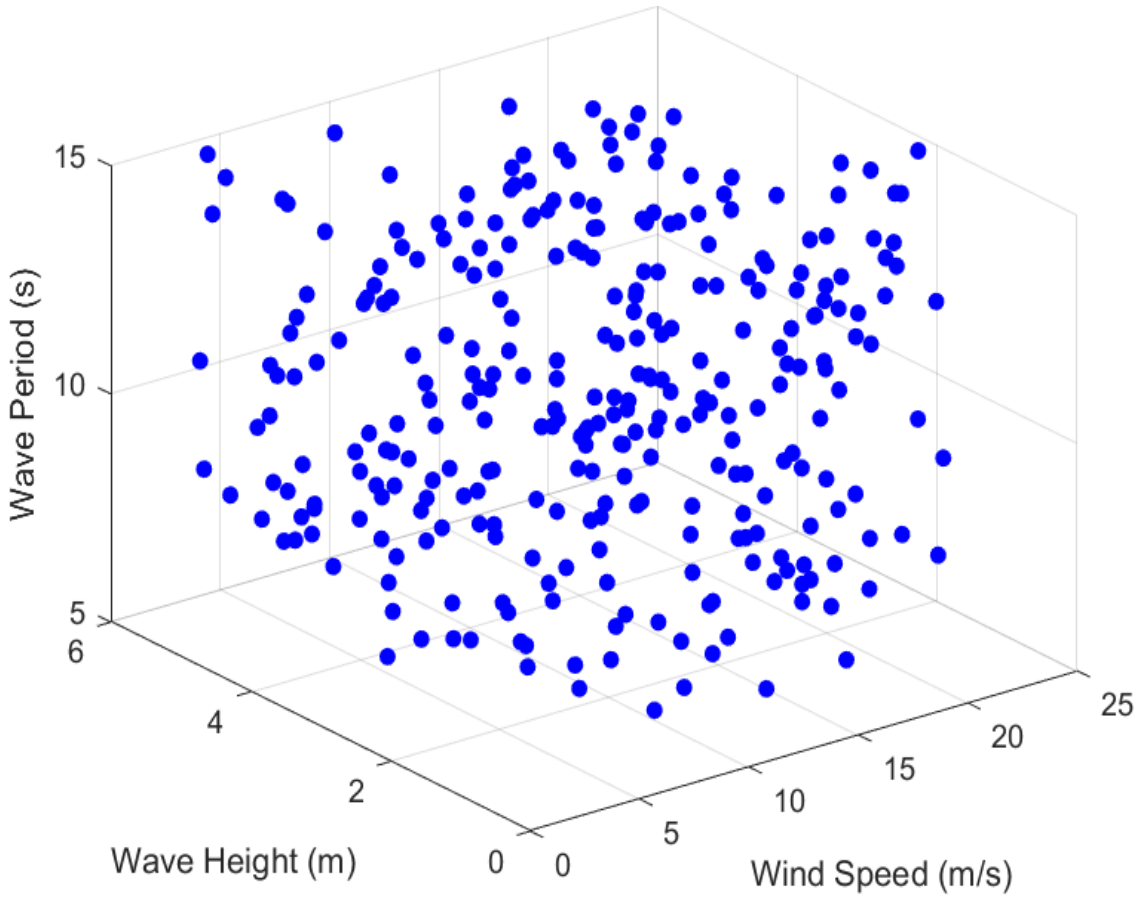

Figure 5.8: LHS data sets.

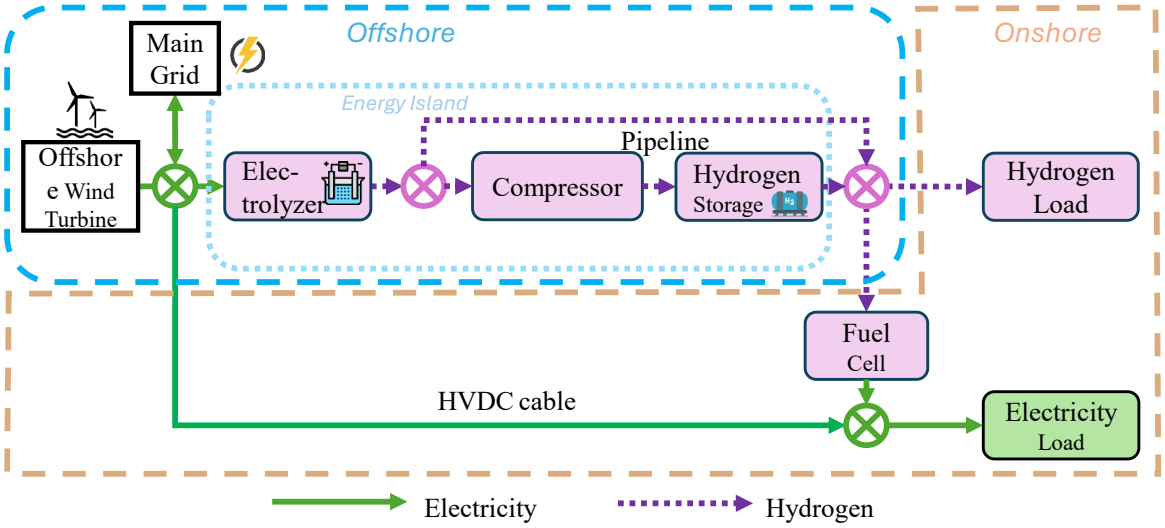

Figure 5.9: Energy island configuration.

5.2.2 Economic Assessment of Energy Islands

Structure and Component of the Energy Island

The operational structure of the proposed energy island is shown in Fig. 5.9, which includes both the electricity supply and hydrogen supply processes derived from offshore wind energy and the main grid. The electrolyzer and compressor work together to convert electricity into hydrogen. Simultaneously, the storage tank can store hydrogen for direct supply, or the hydrogen can be converted back into electricity by a fuel cell for electricity supply.

Economic-Oriented optimisation of Energy Islands

The overall objective of the hybrid energy island plant is to maximize the total life cycle net revenue, which includes the revenue from power and hydrogen sold to consumers and the main grid, minus the cost of purchasing power from the main grid.

$$OBJ = max \sum_{t=1}^{T} \left(C_{PL,t} + C_{HL,t} + C_{sell,t} - C_{buy,t} \right) \tag{5.30}$$

where $C_{PL,t}$ denotes the revenue of the power sold to the load at time t; $C_{HL,t}$ denotes the revenue of the hydrogen sold to the load at time t; $C_{sell,t}$ denotes the revenue of the power sold to the grid at time t; $C_{buy,t}$ denotes the cost of the power bought from the grid at time t.

Equations (5.31) and (5.32) represent the power flow balance, while the constraints for the

hydrogen flow balance are given by equations (5.33) and (5.34). These equations indicate the energy balance between the energy island and the main grid, as well as the relationship between the energy island and the consumers.

$$P_{buy,t} + P_{WT,t} = P_{e,t} + P_{c,t} + P_{d,t} + P_{sell,t}, \quad \forall t \in T \tag{5.31}$$

$$P_{L,t} = P_{d,t} + P_{fc,t}, \quad \forall t \in T \tag{5.32}$$

$$H_{e,t} = H_{d,t} + S_{in,t}, \quad \forall t \in T \tag{5.33}$$

$$H_{L,t} = H_{d,t} + S_{hout,t}, \quad \forall t \in T \tag{5.34}$$

where $P_{buy,t}$ denotes the power bought from the grid at time t; $P_{WT,t}$ denotes the electricity generated by the wind turbine at time t; $P_{e,t}$ and $P_{c,t}$ denote the power consumption of the electrolyzer and compressor at time t; $P_{d,t}$ denotes the power sold directly to the demand at time t; $P_{sell,t}$ denotes the power sold to the grid at time t; $P_{L,t}$ denotes the load demand of power at time t; $P_{fc,t}$ denotes the power output of the fuel cell at time t; $H_{e,t}$ denotes the hydrogen production by the electrolyzers at time t; $H_{d,t}$ denotes the hydrogen delivered directly to the load at time t; $S_{in,t}$ and $S_{out,t}$ denote the hydrogen input to and output from the hydrogen storage at time t; $H_{L,t}$ denotes the hydrogen load demand at time t.

The constraints for hydrogen storage are presented in equations (5.35) to (5.39). Specifically, the equality constraints in equations (5.35) to (5.37) represent the state-of-charge status of the storage, ensuring that the energy balance is maintained over time. Meanwhile, the inequality constraints in equations (5.38) and (5.39) define the storage capacity and the maximum output limit of the storage systems, which set the operational boundaries for these systems.

$$S_{t=1} = S_{ini} + S_{in,t=1} - S_{out,t=1}, \quad \forall t \in T \tag{5.35}$$

$$S_t = S_{t-1} + S_{in,t} - S_{out,t}, \quad \forall t \in T \tag{5.36}$$

$$S_{out,t} = S_{hout,t} + S_{pout,t}, \quad \forall t \in T \tag{5.37}$$

$$S_t \leq C^s, \quad \forall t \in T \tag{5.38}$$

$$S_{out,t} \leq S_{out}^{max}, \quad \forall t \in T \tag{5.39}$$

where S_t and $S_{t=1}$ denote the state-of-charge of the storage at time t and $t = 1$; S_{ini} denotes the initial hydrogen stored in the storage at the beginning of the time horizon; $S_{in,t}$ and $S_{in,t=1}$ denote the storage input at time t and $t = 1$; $S_{out,t}$ and $S_{out,t=1}$ denote the storage output at time t and $t = 1$; $S_{hout,t}$ and $S_{pout,t}$ denote the hydrogen delivered to the hydrogen demand and power demand from the storage; C^s and C_e denote the storage capacity and the electrolyzer capacity; S_{out}^{max} denotes the maximum output of the storage.

The constraints for the minimum limits of power and hydrogen load are provided in equations (5.40) and (5.41), which ensure that the required minimum levels of power and hydrogen are maintained to meet the operational and demand requirements of the system.

$$P_{sell,t} \geq P_{load}^{min}, \quad \forall t \in T \tag{5.40}$$

$$\sum_{t=1}^{T} H_{L,t} \geq H_{Load}^{min}, \quad \forall t \in T \tag{5.41}$$

where P_{load}^{min} denotes the minimum power load demand, H_{Load}^{min} denotes the minimum hydrogen load demand.

The constraints for electrolyzers are presented in equations (5.42) to (5.46). Specifically, equations (5.42) to (5.44) represent the piecewise linearized hydrogen production of the electrolyzer, while equations (5.45) and (5.46) ensure that the electricity consumption of the electrolyzer remains within its operational range, neither exceeding its maximum capacity nor falling below the minimum load limit.

$$P_{e,t} = \sum_{s \in S} P_{e,t}^s + P_{sb}(1 - u_{os,t}), \quad \forall t \in T \tag{5.42}$$

$$H_{e,t} = \sum_{s \in S} (A_s P_{e,t}^s + B_s u_{hp,t}^s), \quad \forall t \in T \tag{5.43}$$

$$u_{os,t} = \sum_{s \in S} u^s_{hp,t}, \quad \forall t \in T \tag{5.44}$$

$$P_{e,t} \leq C_e u_{os,t} + P_{sb}\left(1 - u_{os,t}\right), \quad \forall t \in T \tag{5.45}$$

$$P_{e,t} \geq P_e^{\min} u_{os,t} + P_{sb}\left(1 - u_{os,t}\right), \quad \forall t \in T \tag{5.46}$$

where $P^s_{e,t}$ denotes the power consumption of the electrolyzer of segment s at time t, P_{sb} denotes the power consumption of the electrolyzer of segment s at time t, A_s and B_s denote the slope and intercept of the hydrogen production function of segment s, $u^s_{hp,t}$ and $u_{os,t}$ are binary variables indicating whether the hydrogen production segment s is active and whether the electrolyzer is on or in standby at time t, and $P_e^{\min}$ denotes the minimum power consumption limit of the electrolyzer.

The constraints for fuel cells and compressors are provided in equations (5.47) to (5.49), which describe the electricity generation process of the fuel cell and the operation of the compressor.

$$P_{fc,t} = \alpha S_{\text{pout},t}, \quad \forall t \in T \tag{5.47}$$

$$R^{\text{down}}\,\Delta t \leq P_{fc,t} - P_{fc,t-1} \leq R^{up}\Delta t, \quad \forall t \in T \tag{5.48}$$

$$P_{c,t} = K^c S_{in,t}, \quad \forall t \in T \tag{5.49}$$

where α denotes the conversion efficiency of the fuel cell, R^{up} and R^{down} denote the upper and lower bounds on ramping rate limits of the fuel cell, and K^c denotes the compressor efficiency.

5.2.3 Techno-Economic Evaluation Methodology

The methodology is illustrated in Fig. 5.10.

- Training Dataset Generation by OpenFAST

  Power output, along with tower base forces and moments, are derived by simulating various environmental parameters such as wind speed, wave height, and wave period using OpenFAST. These simulation results serve as training and testing data for separate Kriging surrogate models developed to predict power output and tower forces and moments. The entire process is divided into two key components: the economic LCA and the damage LCA for the devices integrated within the energy island.

Table 5.4: TLP Parameters in OpenFAST Settings.

Parameter	Value
ElastoDyn	
Water depth	200 m
Blade length	63 m
Tower height	87.6 m
Platform mass	8,600,410 kg
Hub mass	56,780 kg
Nacelle mass	240,000 kg
Hub Inertia	115,926 kg·m^2
Nacelle Inertia	2,607,890 kg·m^2
Platform Inertia (Roll, Pitch, Yaw)	571,624,000 kg·m^2
MooringDyn	
Number of mooring lines	8 (4 pairs)
Unstretched line length	151.73 m
Line diameter	0.127 m
Line extensional stiffness	1,500,000,000 N
HydroDyn	
Floating body volume	7000 m^3
Floating body density	800 kg/m^3

- Train the Kriging Surrogate Model

  First, OpenFAST simulations are conducted using environmental input variables $\mathbf{x} = [v, H_s, T_p]$, where v, H_s, and T_p denote wind speed, significant wave height, and wave period, respectively. The corresponding outputs, including power generation and tower base loads, are then used to construct the Kriging surrogate model. The surrogate model approximates the nonlinear relationship between environmental conditions and system responses, enabling efficient prediction of power output and fatigue-related variables without repeatedly performing high-fidelity simulations.

- Dual Assessments of the Energy Island For the fatigue damage analysis, Dynamic stress responses obtained from OpenFAST simulations are processed through rainflow counting and S–N curve analysis to estimate cumulative fatigue damage D. This short-term damage, along with the corresponding environmental parameters, forms the training dataset for a Kriging model, which predicts the long-term fatigue damage of the floating wind turbine. Finally, the platform's total life cycle profit (LCP) and lifetime fatigue damage are assessed, providing an integrated evaluation of both economic and structural performance.

  For the economic optimisation, power output predictions from the Kriging surrogate model,

Costs (€)	FINO1	BORS0	CAB
Pipeline	1,204,875	990,765	1,499,400
Fuel Cell	4,325,354.96	4,395,355.31	4,741,357.04
Storage Tank	50,000	50,000	50,000
Alkaline Electrolyzers	3,500,000	3,500,000	3,500,000
Compressors	10,000	10,000	10,000
Floating TLP	9,600,396.099	10,377,992.2	10,685,108.91
Total Costs	18,690,626.059	19,324,112.51	20,485,865.95
Life Cycle Net Revenue	26,226,927.43	24,540,477.83	15,820,970.37
Life Cycle Profit	7,536,301.37	5,216,365.32	–4,664,895.58

Table 5.5: 25-year Costs and Profit of Energy Islands for Three Platforms.

based on a 25-year historical dataset, serve as inputs to an economic optimisation model designed to maximize life cycle net revenue. This optimisation is conducted using the energy flow diagram of the "energy island" shown in Fig. 5.10.

5.2.4 Case Study and Simulation Results

Environmental Settings

To investigate the environmental impacts on offshore energy islands, this study selects three offshore wind platforms with varying annual average wind speeds, wave heights, and wave periods. The life cycle profit and fatigue damage at the tower base are calculated to assess both the economic and structural effects of environmental conditions on offshore energy islands. The selected offshore sites are: FINO1, located in the North Sea off the coast of Germany at 54.015° N latitude and 6.587° E longitude [242]; BORS0, approximately situated in the Dutch North Sea with a latitude of 51.63° N and a longitude of 3.24° E [243]; and CAB, located inland in the Netherlands at 51.971° N latitude and 4.927° E longitude [244], as shown in Fig.5.11. These platforms are reconstructed as energy islands for the analysis. We utilise OpenFAST to simulate the power output of the NREL 5 MW TLP floating wind turbine under various wind-wave conditions.

Regarding the selection of the wind turbine, various new concepts for TLP FOWT systems have been proposed and studied over the past few decades. Wayman et al. [245] introduced the first-generation 5-MW MIT/NREL TLP FOWT concept in 2006. While this design demonstrated good stability and allowed for installation using the wet-tow method, it also had certain drawbacks,

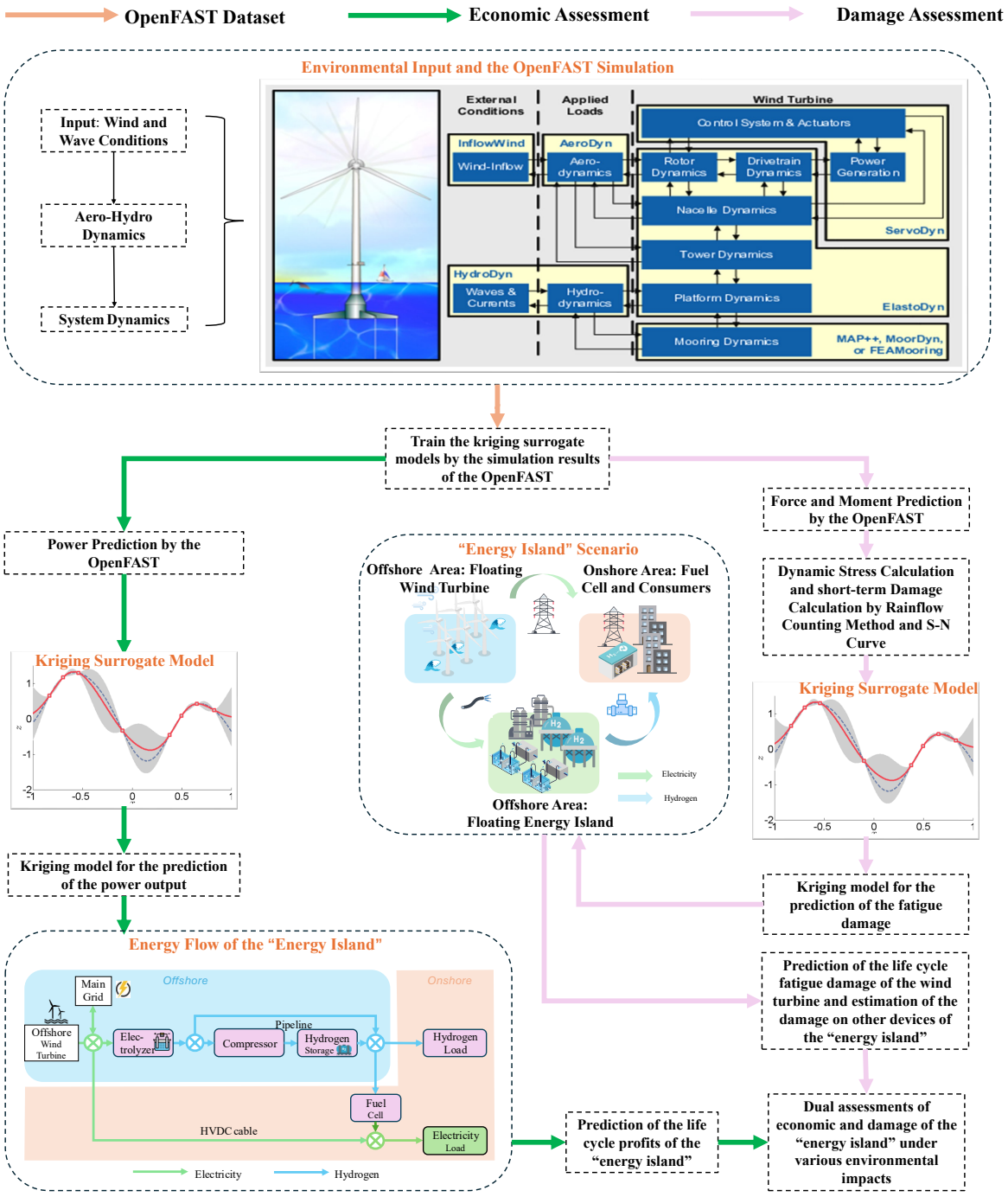

Figure 5.10: Framework of the Dual Economic and Damage Assessment and Research Methodology.

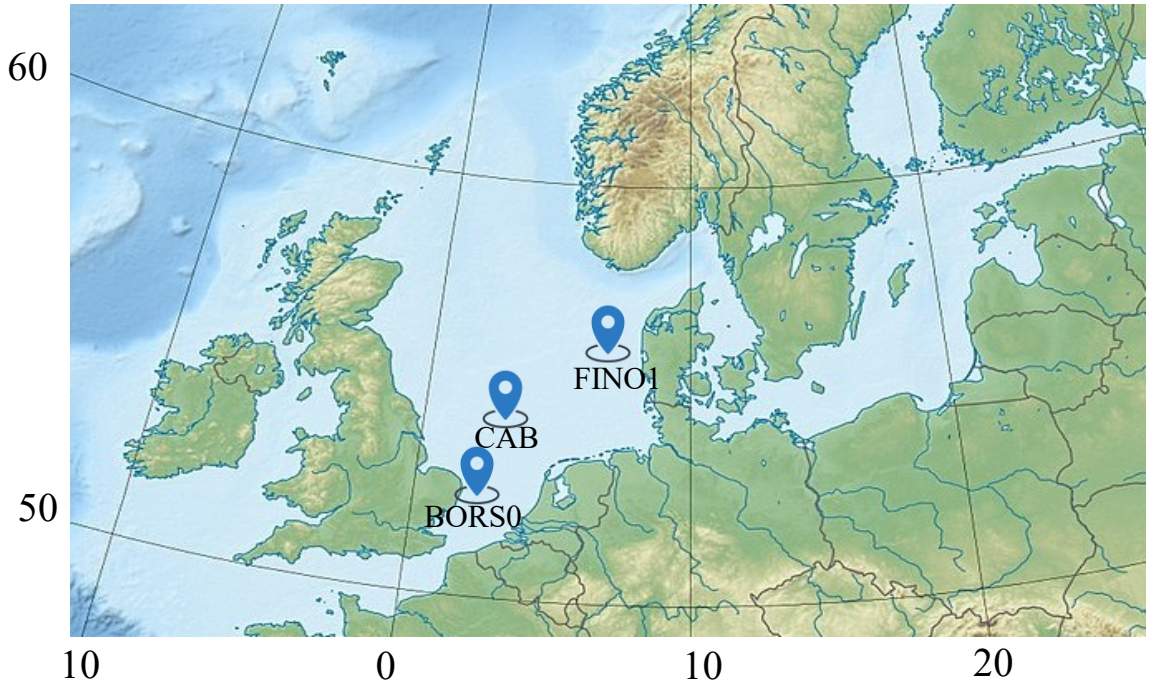

Figure 5.11: The Location of Three Platforms.

such as large displacement and high costs [246]. In this study, the life cycle economic performance and fatigue damage of a 5 MW floating TLP are evaluated using a hybrid approach that integrates simulation and surrogate modelling.

The physical characteristics of the TLP floating wind turbine model are described through detailed parameters across multiple modules. Firstly, the ElastoDyn module defines the mass and elasticity characteristics of the tower and blades. The maximum blade length is 63 metres, the tower top height is 87.6 metres. The platform mass is 8,600,410 kg, the hub mass is 56,780 kg, and the nacelle mass is 240,000 kg. The corresponding inertia parameters include a hub inertia of 115,926 $\mathrm{kg} \cdot \mathrm{m}^2$, a nacelle inertia of 2,607,890 $\mathrm{kg} \cdot \mathrm{m}^2$, and platform inertia values for roll, pitch, and yaw of 571,624,000 $\mathrm{kg} \cdot \mathrm{m}^2$ each. The platform's initial displacements in the surge, sway, heave, pitch, and roll directions are all set to 0. Next, the HydroDyn module describes the hydrodynamic response of the floating body, utilizing the JONSWAP/Pierson-Moskowitz irregular wave spectrum. The floating body has a volume of 7,000 m^3 and a density of 800 kg/m^3.

Following this, the MoorDyn module defines the mooring system, which consists of 8 main cables, each with a diameter of 0.127 metres, an axial stiffness of 1,500,000,000 N, and an unstretched length of 151.73 metres. Meanwhile, the ServoDyn module provides the turbine's control system parameters, with a maximum output power of 5 MW. Furthermore, the BeamDyn module details the blade rigidity and modal analysis, with the blade material's elastic modulus

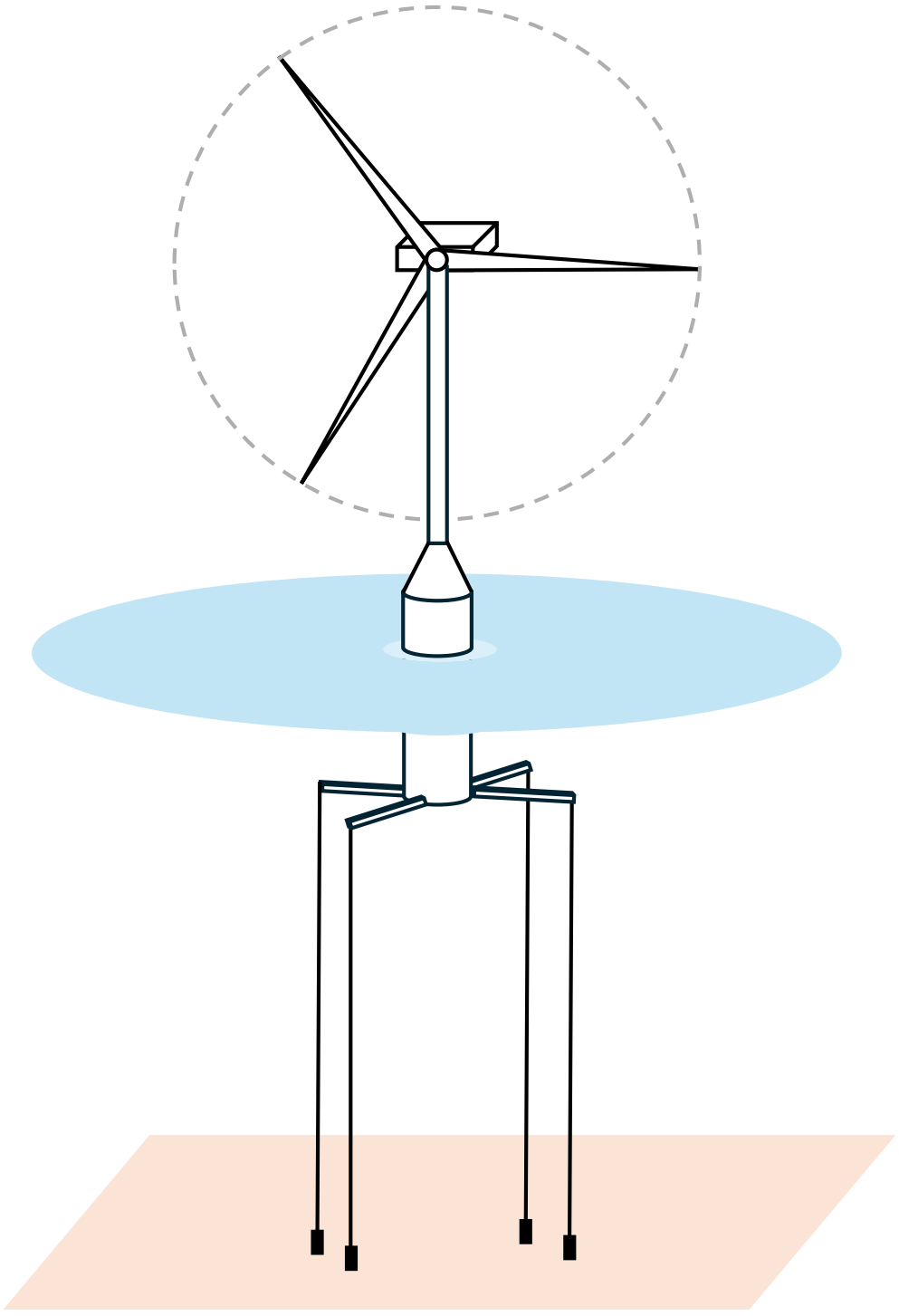

Figure 5.12: Configuration of NREL TLP.

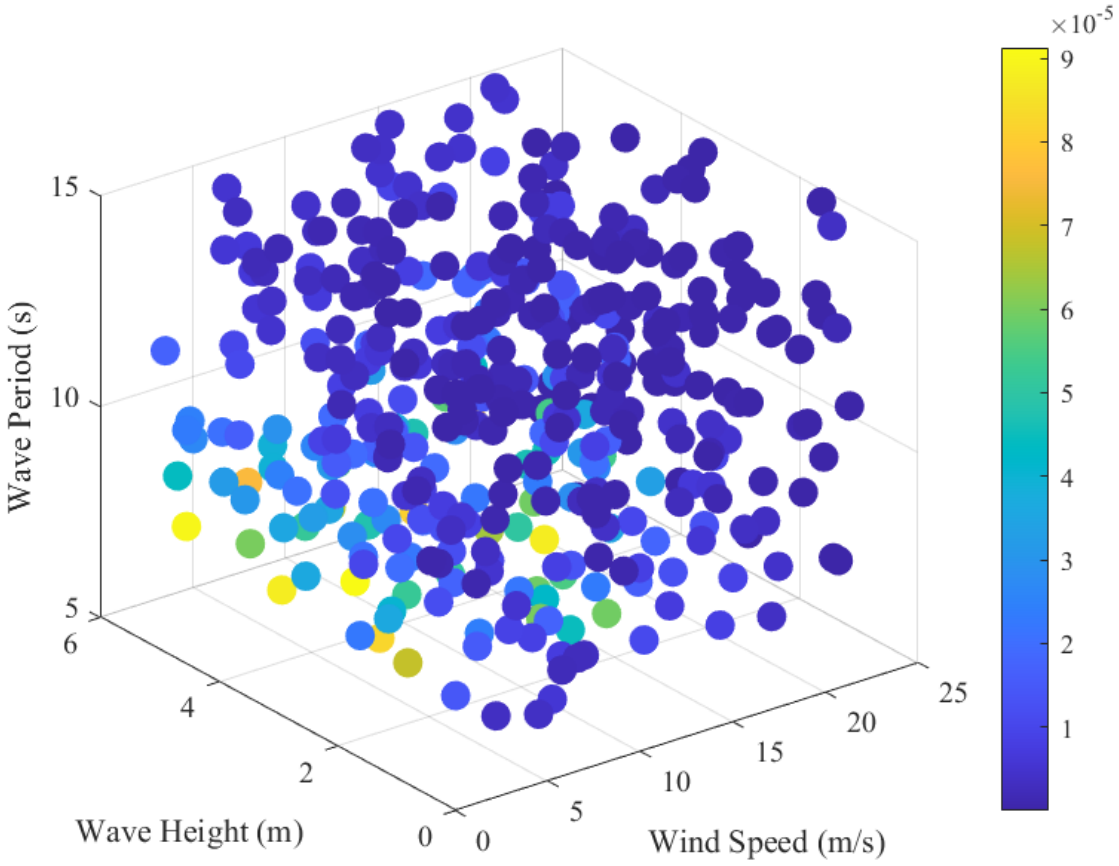

Figure 5.13: Short-term Damage of Environmental Data Sets.

being 30,000,000 $\mathrm{N/m^2}$. Finally, the InflowWind module defines the steady-state wind field. By integrating these modules, a comprehensive physical model of the TLP floating wind turbine is established, encompassing structural, control, aerodynamic, hydrodynamic, and mooring characteristics. A schematic of the TLP model is illustrated in Fig. 5.12, while its detailed specifications are presented in Table 5.4.

Life Cycle Damage Analysis-Calculation of Long-Term Fatigue Damage on the Tower Base of Wind Turbine

According to the calculation process described in Section 5.2.1, the short-term damage of the datasets is illustrated in Fig. 5.13. Subsequently, the Kriging surrogate model is trained in MATLAB to approximate the damage predictions. The model achieves a mean absolute error (MAE) of 1.6265×10^{-5} and a mean relative error (MRE) of 6.91%, indicating a high level of accuracy. A comparison between the predicted and true values is presented in Fig. 5.14.

To visualize the individual environmental impacts on fatigue damage at the tower base calcu-

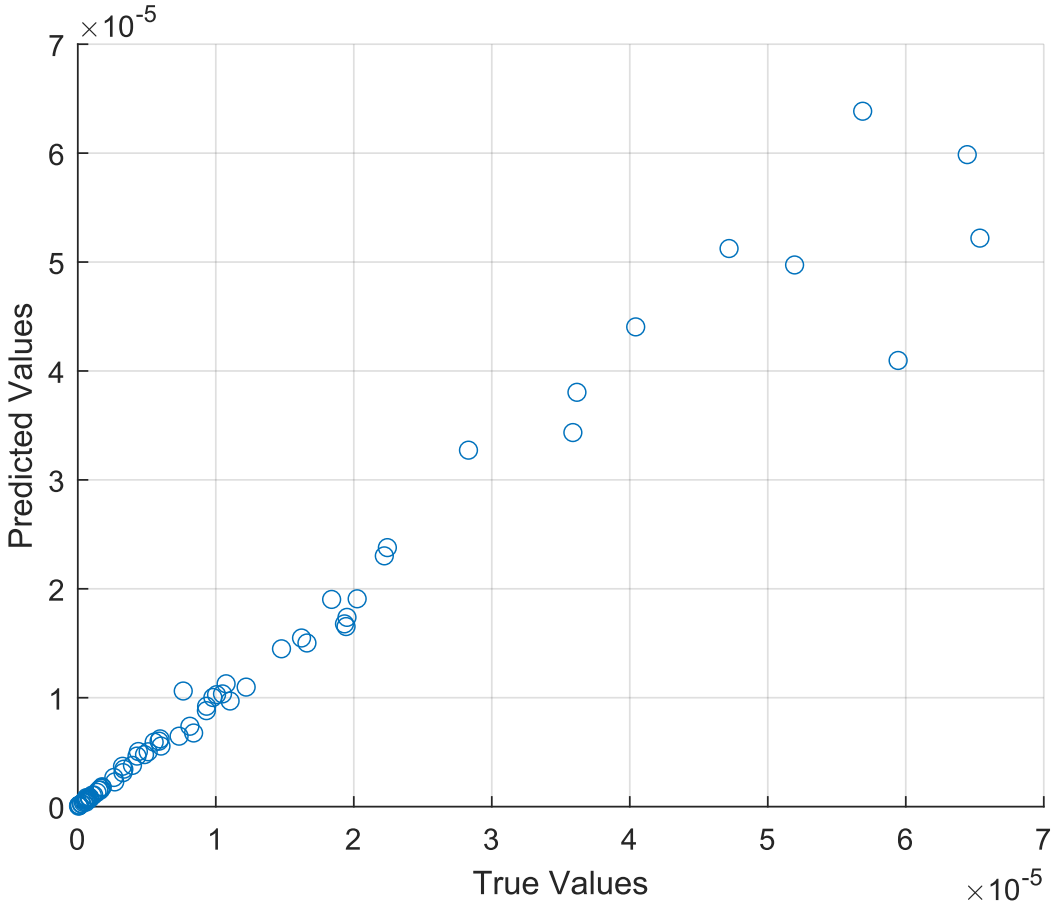

Figure 5.14: Fatigue Damage Kriging Model Performance.

lated by OpenFAST, the three-dimensional effects of wind speed, wave period, and wave height — including their interactions, such as wave height and wind speed, wave period and wave height, and wave period and wind speed—are illustrated in Fig. 5.15. As shown in Fig. 5.15a, fatigue damage peaks at a wind speed of 14 m/s and increases as wave height rises. Similarly, Fig. 5.15b and Fig. 5.15c indicate that fatigue damage decreases with increasing wave period. Additionally, fatigue damage is highest when the wave height is around 3.3 m, then slightly decreases at 4.3 m, before rising again as wave height continues to increase.

With the trained Kriging surrogate model, historical environmental data from the three offshore wind platforms previously mentioned were collected. The wind speed, wave height, and wave period distributions for FINO1, BORS0, and CAB from 1979 to 2003 were calculated and are presented in Fig. 5.17. The 25-year average values for each platform are as follows: for FINO1, the average wind speed is 9.99 m/s, the average wave height is 1.69 m, and the average wave period is 6.89 s. For BORS0, the corresponding averages are 9.52 m/s, 1.41 m, and 6.90 s, respectively. The CAB platform, on the other hand, has an average wind speed of 7.33 m/s, an average wave height of 1.87 m, and an average wave period of 7.11 s.

According to the calculations in Section 5.2.1, the joint probability is obtained using the Weibull distribution parameters for the wind speed and wave height probability functions, along with the logarithmic distribution parameters for the wave period probability density function. The joint probabilities for the three floating platforms are shown in Fig. 5.18. Utilizing equations (5.23) to (5.25), the life cycle fatigue damage can be calculated. The 25-year fatigue damage for FINO1, BORS0, and CAB are 0.60025, 0.648868, and 0.66807, respectively. Consequently, the estimated lifespans for FINO1, BORS0, and CAB are 41.649, 38.529, and 37.421 years, respectively.

Life Cycle Damage Analysis - Long-Term Damage on Peripheral Devices on Energy Islands

To evaluate the damage to the integrated island, the damage to other components, such as the pipeline, electrolyzer, hydrogen storage tank, fuel cell, and compressor, is also considered. The pipelines in underwater environments are exposed to hydrostatic pressure, water currents, and thermal gradients, and are typically designed to last up to 50 years [247]. The electrolyzers used in this study are alkaline electrolyzers, which generally have a lifespan between 20 and 30 years [248]. The lifespan of the hydrogen storage tank is assumed to be 10 years [249]. The hydrogen fuel cell, under normal operating conditions, has a lifespan ranging from 5 to 10 years [250], and we calculate the 25-year fuel cell costs per megawatt. The hydrogen compressor is expected to have a minimum lifespan of 20 years [251].

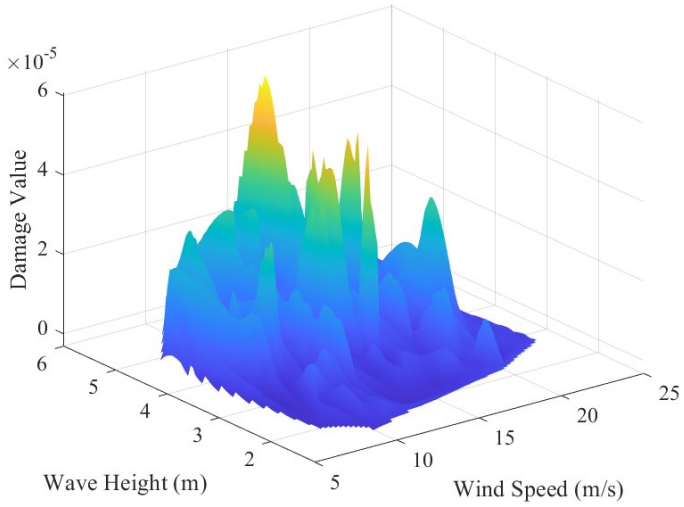

(a) Wave Height and Wind Speed vs. Damage

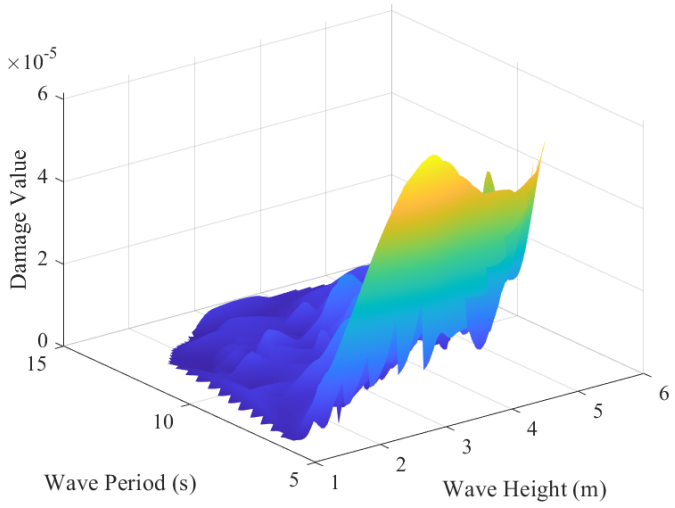

(b) Wave Period and Wave Height vs. Damage

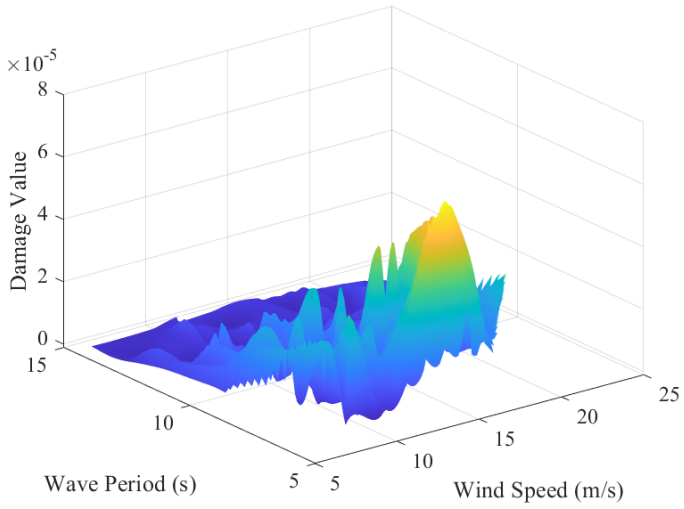

(c) Wave Period and Wind Speed vs. Damage

Figure 5.15: The Relationship between Wind, Wave, and Fatigue Damage.

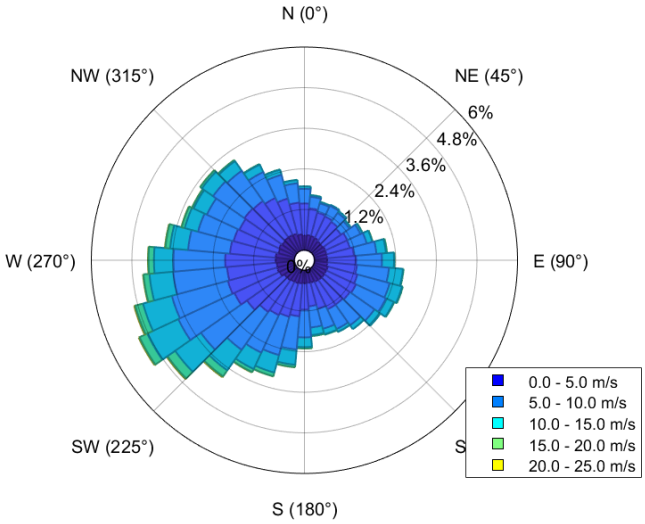

(a) FINO1 Wind Rose

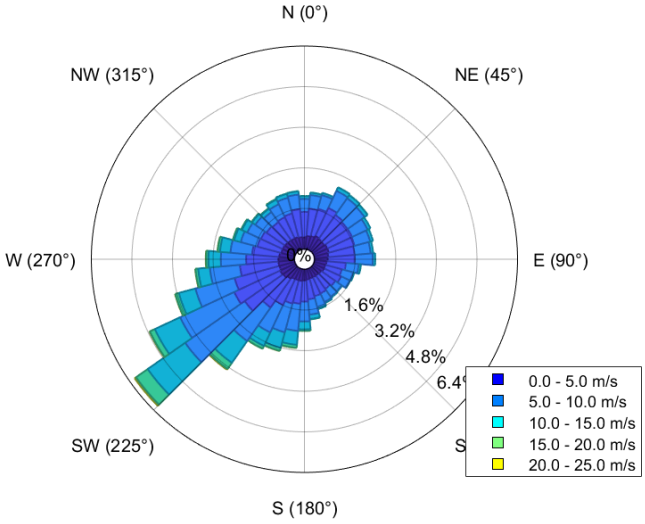

(b) BORS0 Wind Rose

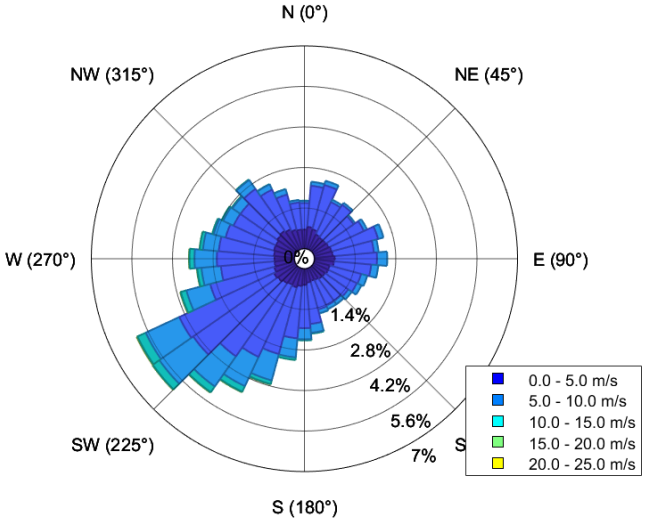

(c) CAB Wind Rose

Figure 5.16: 1979-2003 Wind Rose.

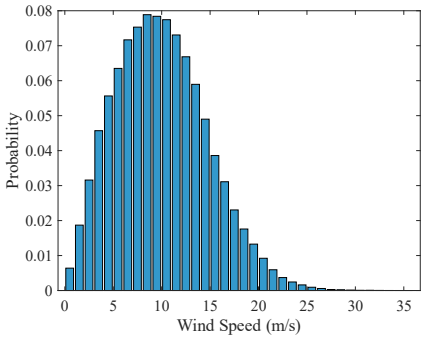

(a) FINO1 Wind Speed Distribution

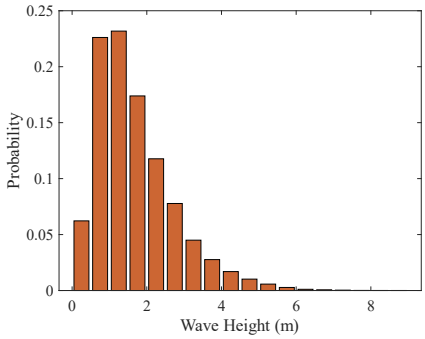

(b) FINO1 Wave Height Distribution

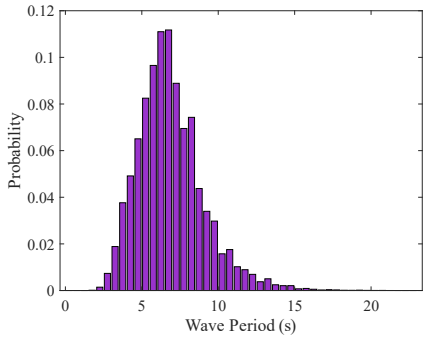

(c) FINO1 Wave Period Distribution

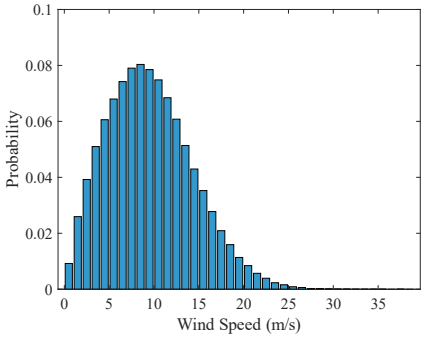

(d) BORS0 Wind Speed Distribution

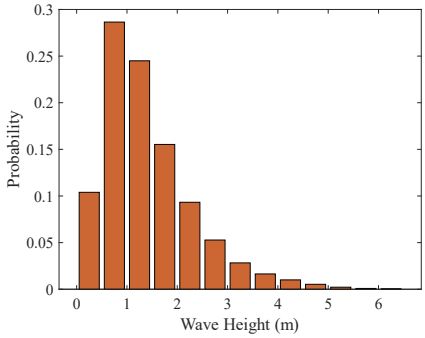

(e) BORS0 Wave Height Distribution

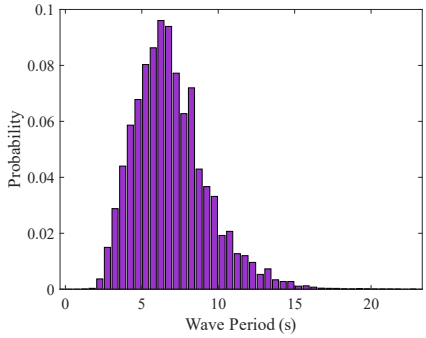

(f) BORS0 Wave Period Distribution

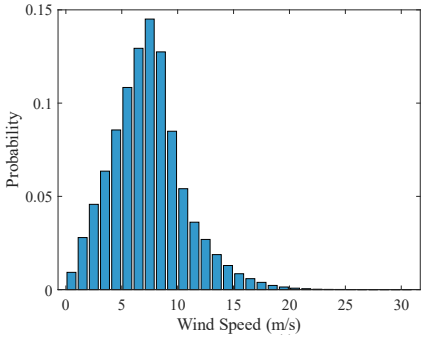

(g) CAB Wind Speed Distribution

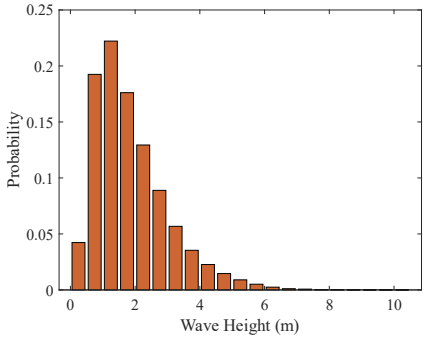

(h) CAB Wave Height Distribution

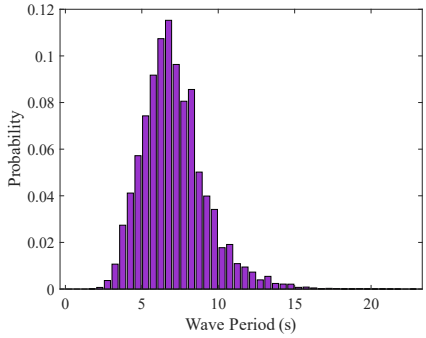

(i) CAB Wave Period Distribution

Figure 5.17: 1979-2003 Distribution of the Environmental Input Variables.

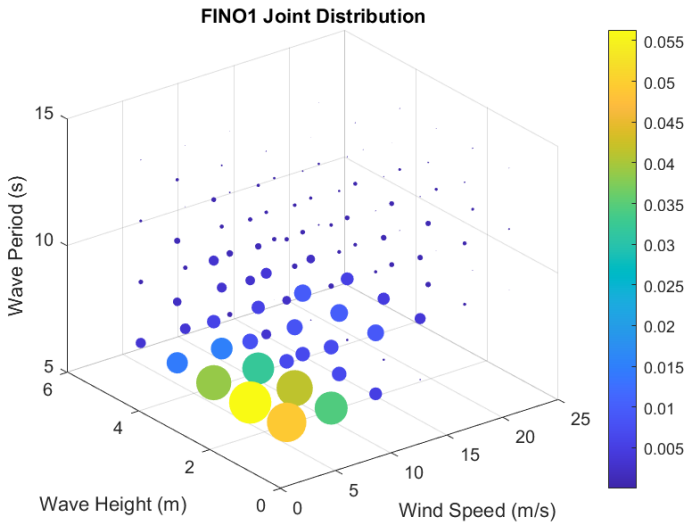

(a) FINO1 Joint Probability

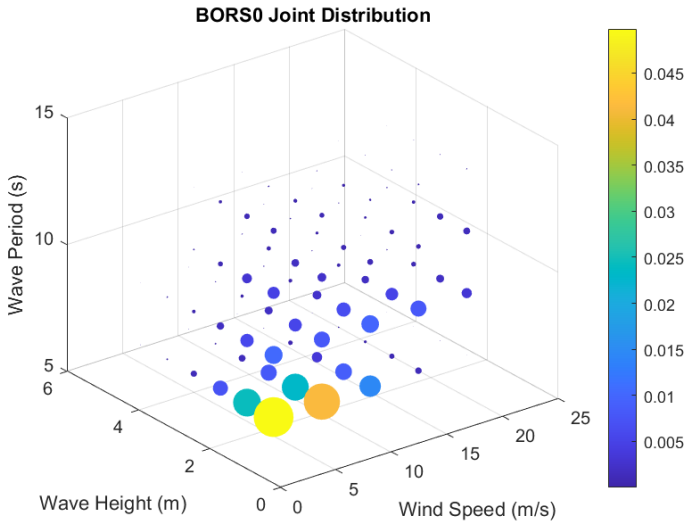

(b) BORS0 Joint Probability

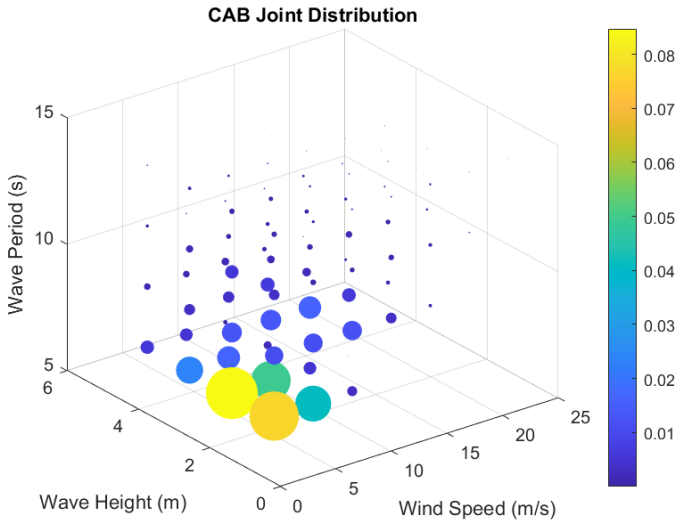

(c) CAB Joint Probability

Figure 5.18: Three Wind Platforms 1979-2003 Joint Probability.

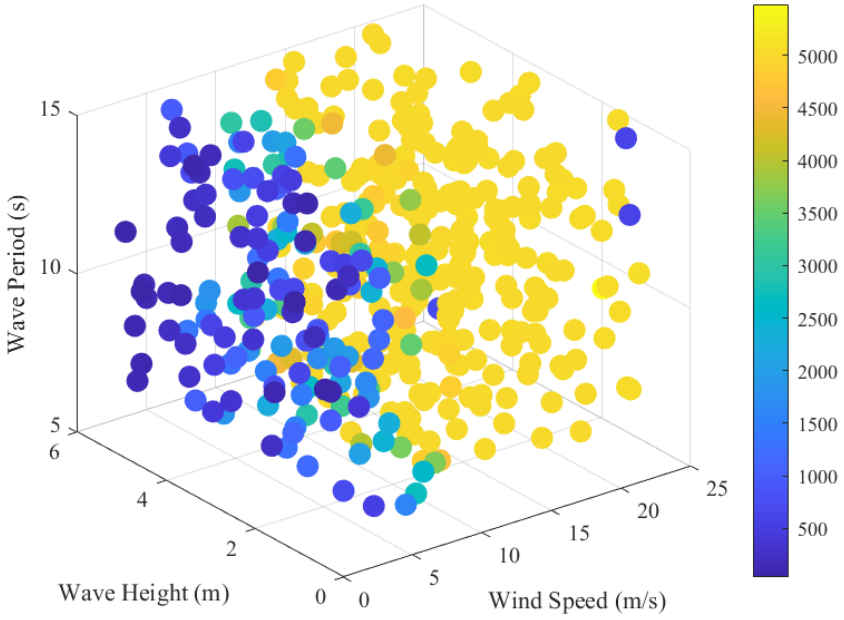

Figure 5.19: Wind Power Output of Environmental Data Sets.

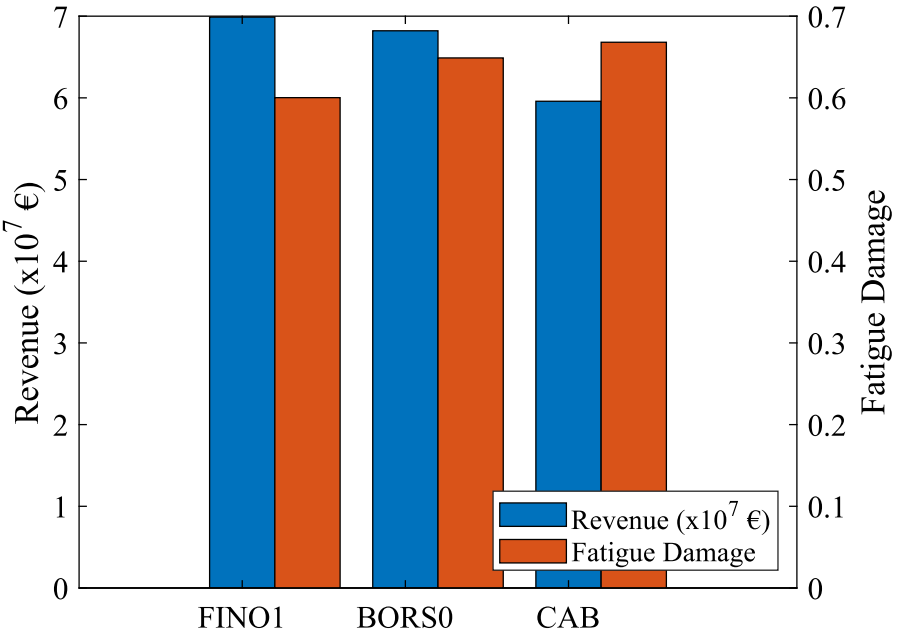

Figure 5.20: Wind Turbine Life Cycle Profit vs Life Cycle Damage.

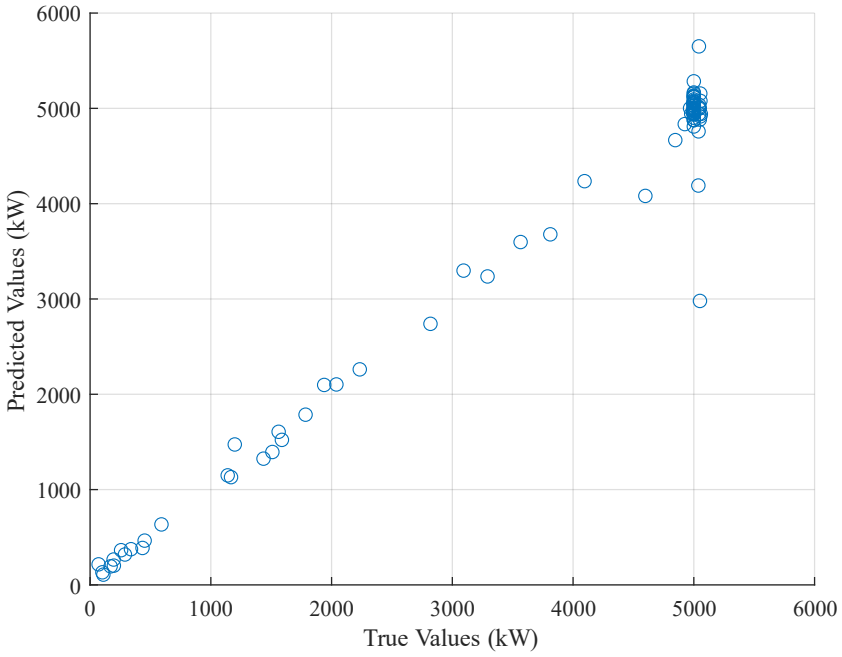

Figure 5.21: Wind Power Kriging Model Performance.

Life Cycle Economic Analysis of Energy Islands - Long-Term Wind Power Net Revenue of Energy Islands

To predict the long-term power output, a Kriging surrogate model is trained. The training set is generated using OpenFAST, with the input set consisting of 432 variables sampled via the hyper-Latin cube method. The results are presented in Fig. 5.19. As expected, the power output generally increases with wind speed. When the wind speed reaches the rated wind speed of 11.4 m/s, the power output reaches its rated value of approximately 5000 kW. As the wind speed increases further, up to 25 m/s, which is the cut-out wind speed, the power output sharply decreases to below 500 kW. The MAE of the trained model is 118.4985, and the normalized mean absolute error (NMAE) is 4.74%. The model performance can be visualized in Fig. 5.21.

Using the historical hourly wind and wave data, the trained Kriging surrogate model predicts the 25-year hourly wind power output for the 5 MW TLP floating wind turbine located at the three research platforms. To enhance readability, the yearly average output power for the FINO1, BORS0, and CAB platforms is presented in Fig. 5.22. Based on the economic-oriented optimisation model outlined in Section 5.2.2, the optimal life cycle net revenue can be calculated using the predicted 25-year wind turbine power output results. The electricity price is set according to the day-ahead electricity prices for the East Denmark area (DK2), as obtained from the ENTSOe Transparency platform [252]. The life cycle net revenues generated by the 5 MW TLP floating

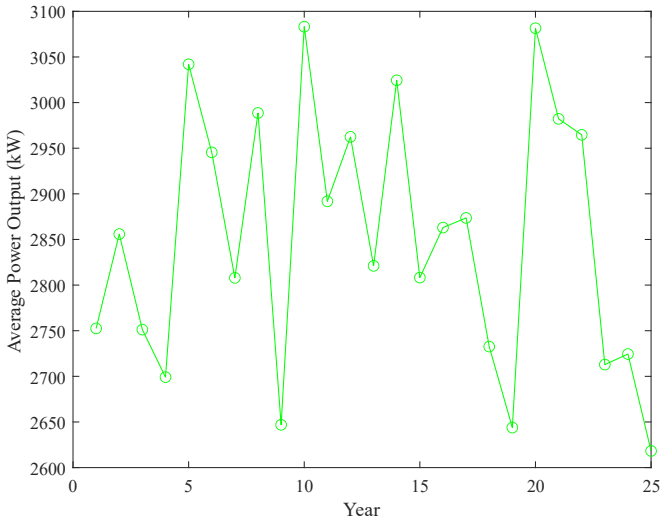

(a) FINO1 Power Output Prediction

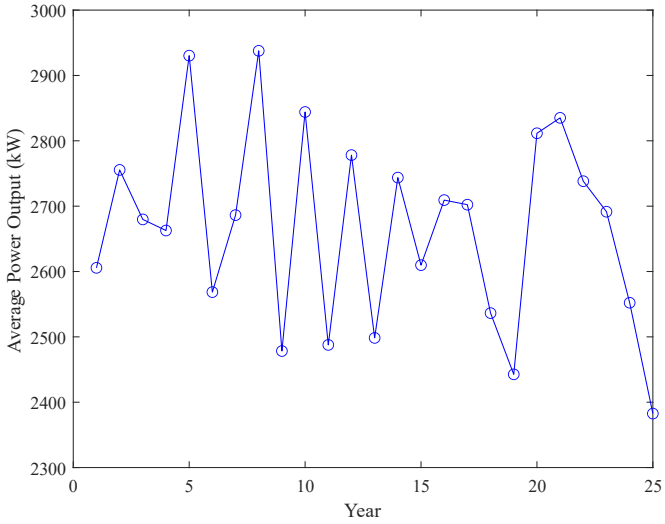

(b) BORS0 Output Prediction

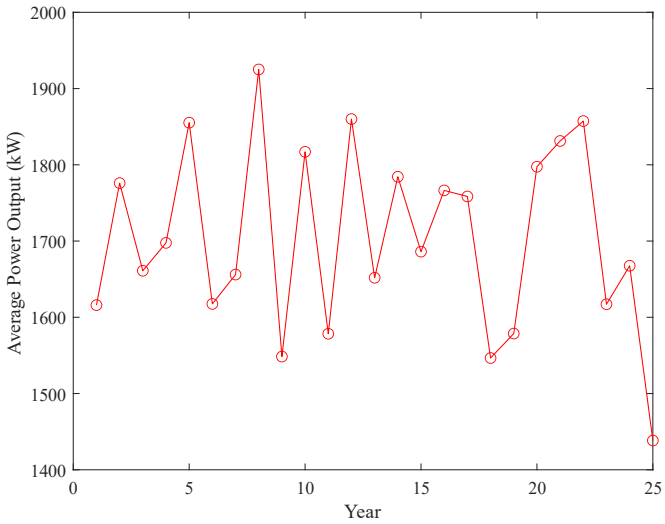

(c) CAB Output Prediction

Figure 5.22: Three Wind Platforms 25 years (1979-2003) Wind Turbine Output Power.

wind turbine at the FINO1, BORS0, and CAB platforms are €26,226,927.43, €24,540,477.83, and €15,820,970.37, respectively. The comparison of the TLP life cycle net revenue and fatigue damage on the tower base is shown in Fig. 5.20. It demonstrates that FINO1 generates the highest wind energy net revenue with the least fatigue damage.

Life Cycle Economic Analysis of Energy Islands - The Costs Evaluation of Energy Islands

The replacement costs for the pipeline and fuel cell are assumed to be €53,550 per kilometre and €66,667 per megawatt, respectively. Additionally, the replacement cost for the storage tank with a capacity of 1052.82 kg is €20,000, while the replacement cost for the compressor is €10,000. The cost of replacing a 2.5 MW electrolyzer is estimated at €3,500,000. Furthermore, the replacement cost for a floating offshore TLP, which includes installation, plant, and foundation costs, is assumed to be €15,993,996 [253].

Regarding the offshore distances, BORS0 is located 37 km from shore, while CAB is 56 km offshore. In comparison, the FINO1 Platform is situated 45 km from shore [254]. The total 25-year electricity generation of the fuel cell on FINO1, BORS0, and CAB is 64.88 MW, 65.93 MW, and 71.12 MW, respectively. As a result, the replacement costs of the pipeline for FINO1, BORS0, and CAB are €2,409,750, €1,981,350, and €2,998,800, respectively. Meanwhile, the costs of the fuel cells for FINO1, BORS0, and CAB amount to €4,325,354.96, €4,395,355.31, and €4,741,357.04, respectively.

Since the pipelines have a lifespan of 50 years, the replacement costs for the pipelines over a 25-year period are estimated at half of the total price. Thus, the pipeline replacement costs for FINO1, BORS0, and CAB are €1,204,875, €990,765, and €1,499,400, respectively. The storage tanks, which are used identically for these platforms, have a lifespan of 10 years, and the cost for 25 years is €50,000. The alkaline electrolyzer's lifespan is set at 25 years, meaning its replacement cost is €3,500,000. Similarly, the compressor has a lifespan of 25 years, and its cost is €10,000.

Finally, based on the calculated fatigue damage on the TLP at FINO1, BORS0, and CAB, which is 0.60025, 0.648868, and 0.66807, respectively, the costs of the TLP due to wind and wave damage are estimated to be €9,600,396.10, €10,377,992.20, and €10,685,108.91, respectively. The detailed breakdown of these costs is provided in Table 5.5. The final life cycle profit of FINO1 is 44.47% higher than that of BORS0, while CAB even incurs a loss due to not only higher transportation costs and increased device damage but also lower energy production. Therefore, we conclude that the FINO1 platform exhibits the best overall performance under the assessment framework proposed in this paper, achieving the highest profit and the lowest damage.

5.2.5 Discussions

Integrated Evaluation of Economic and Structural Dimensions

The findings of this study highlight the crucial interdependence between economic feasibility and structural resilience in the design and site selection of offshore energy islands. Unlike conventional techno-economic assessments that often treat environmental conditions as exogenous parameters, the present framework embeds wind–wave interactions directly into the decision-making process. This methodological advancement ensures that both the profitability and durability of offshore systems are assessed under a unified analytical structure. The observed 44.5% increase in life-cycle profit for optimally located sites underscores the significant economic gains achievable through spatially explicit modelling. Furthermore, the inclusion of structural resilience indicators in the optimisation framework allows for the identification of sites that balance cost efficiency with long-term survivability, thereby advancing the reliability and sustainability of future offshore developments.

The integration of environmental dynamics into techno-economic evaluation also provides critical insights into the trade-offs between investment cost, operational risk, and system performance. For example, locations exhibiting high energy potential may also be subject to elevated fatigue loads or extreme weather exposure. By capturing these nonlinear trade-offs through surrogate-based modelling, this research bridges the gap between economic optimisation and engineering resilience, contributing to more informed and risk-aware decision-making in offshore energy planning.

Surrogate Modelling and Computational Efficiency

A key methodological innovation in this chapter is the application of Kriging surrogate models to approximate the outcomes of computationally intensive simulations, such as those generated by OpenFAST. These surrogate models have proven capable of predicting turbine power output and fatigue damage across diverse environmental conditions with high fidelity, while reducing the computational burden associated with long-term offshore analyses. The validation of Kriging-based predictions demonstrates that such models can effectively capture complex nonlinear relationships between environmental drivers and structural responses, enabling rapid scenario evaluation and optimisation.

This surrogate-based approach is particularly valuable in the early design and site screening stages, where multiple configurations and locations must be compared within limited time and computational resources. By providing a scalable and flexible modelling framework, this methodology allows researchers and engineers to explore a wide range of design alternatives and environ-

mental conditions without sacrificing accuracy. However, it is important to acknowledge that the surrogate models remain dependent on the quality and representativeness of the training dataset. As such, future improvements should aim to integrate adaptive learning mechanisms and uncertainty quantification to ensure robust performance under previously unseen environmental regimes.

Broader Implications and Future Research Directions

Beyond methodological contributions, the study provides broader implications for the sustainable development of offshore hybrid systems. The inclusion of electricity-to-hydrogen conversion and storage not only enhances operational flexibility but also aligns with the global transition toward multi-energy integration and carbon neutrality. This feature enables offshore energy islands to act as autonomous energy hubs capable of balancing renewable intermittency and supporting both onshore and maritime energy demand. The demonstrated adaptability of the system to fluctuating wind–wave conditions reinforces its potential role within future offshore energy clusters and green hydrogen value chains.

Nevertheless, several avenues for further research remain open. Future studies could incorporate stochastic representations of extreme weather events, which are increasingly relevant under changing climatic conditions. Moreover, expanding the framework to include additional renewable sources, such as offshore solar or ocean current energy, could enhance the resilience and diversification of offshore islands. Finally, integrating the developed framework into real-time control and market participation strategies would provide deeper insights into its operational and economic scalability within large-scale offshore networks.

5.2.6 Conclusions

This chapter has presented a comprehensive techno-economic framework for the design and site selection of offshore energy islands, addressing key research gaps in both economic assessment and structural resilience. By explicitly integrating wind-wave environmental conditions into the decision-making process, the framework enables a dual evaluation of economic feasibility and structural integrity, ensuring that selected sites are both cost-effective and resilient to varying marine conditions. This integrated approach enhances the predictive accuracy of site assessments and supports the long-term sustainability of offshore energy systems.

A central contribution of this work is the evaluation of multiple floating wind platform designs under realistic historical environmental datasets, providing a robust benchmark for assessing site-specific performance. The results indicate that optimal site selection can lead to a substantial improvement in life-cycle profit—approximately 44.5% higher compared to non-optimised loca-

tions—highlighting the critical importance of location-specific analyses for offshore energy island planning. Moreover, the study demonstrates the effectiveness of validated Kriging surrogate models in addressing the computational challenges associated with high-fidelity simulations. These models enable rapid and accurate predictions of turbine power output and fatigue damage across diverse environmental conditions, thereby facilitating long-term operational planning without excessive computational cost.

In addition, the work has shown that incorporating integrated electricity-to-hydrogen conversion and storage strategies enhances the adaptability of offshore energy islands to fluctuating energy demands and environmental conditions. This flexibility not only supports operational efficiency but also contributes to the broader objectives of renewable energy integration and decarbonisation.

In summary, the framework developed in this chapter represents a significant advancement over existing methodologies for offshore energy island design and optimization. It provides a systematic and scalable approach for evaluating the techno-economic and structural performance of offshore systems under realistic environmental conditions. The findings reinforce the importance of combining detailed environmental modelling, surrogate-based simulation, and integrated energy system design to enable robust, efficient, and sustainable offshore energy infrastructures. Future research could extend this framework by incorporating additional environmental factors, such as extreme weather events, or by integrating other multi-energy systems to further enhance the operational versatility and applicability of offshore energy islands.

Chapter 6

Conclusions and Future Research

6.1 Cross-Chapter Synthesis and Discussion

6.1.1 Thematic Connection Across the Four Studies

The four studies from Chapters 3 to 6 presented in this thesis form an integrated research trajectory that collectively addresses the challenges of designing, optimising, and operating multi-energy systems under conditions of uncertainty, variability, and environmental influence. Instead of being treated as independent case studies, these works were intentionally structured as an onshore microgrid-level scheduling model under coordinated operation of large-scale energy networks, and ultimately to offshore hybrid energy systems that combine power and hydrogen production under complex environmental conditions.

Chapter 3 establishes the theoretical foundation by developing a distributionally robust optimisation framework for the day-ahead and intra-day scheduling of multi-energy microgrids. It simultaneously models energy and carbon flows, enabling the coordinated management of electricity, heat, and gas subsystems. This chapter demonstrates how uncertainty in renewable energy can be effectively managed through distributionally robust optimisation, resulting in reduced energy waste and carbon dioxide emissions. It provides a fundamental methodological baseline: the ability to achieve low-carbon, reliable operation through data-driven uncertainty sets and probabilistic constraints.

Chapter 4 expands the modelling scope from a single microgrid at the distribution level to the coordinated operation of transmission and distribution networks. It introduces a multi-layer optimisation architecture that captures inter-level energy exchanges and highlights the role of storage in enhancing system flexibility. This chapter builds on the first study by showing that the coordination between different voltage levels can yield significant operational and economic benefits. It

quantifies how transmission–distribution coupling allows for better utilisation of distributed generation and shared storage resources, establishing a scalable framework for integrated energy system operation.

Chapter 5 introduces a new dimension to the analysis: the impact of environmental variability and extreme weather on system performance. Using high-resolution environmental simulations, it investigates how fluctuating wind conditions, turbulence, and temperature variations affect renewable generation and microgrid operation. Additionally, it extends the research framework into the offshore domain, focusing on floating energy islands that integrate offshore wind power and hydrogen production. This final study couples environmental dynamics, including wind–wave interactions, with techno-economic optimisation, thereby connecting system design, operation, and economic assessment within a single analytical framework. It demonstrates how extreme marine conditions influence both energy production and equipment lifetime, highlighting the importance of including environmental and mechanical constraints in the design of offshore hybrid energy systems.

Collectively, these main chapters form a progressive and interconnected framework (Figure 6.1). The focus evolves from microgrid scheduling to network coordination, environmental integration, and offshore hybrid system evaluation, illustrating a consistent methodological deepening and spatial broadening of scope. Each study extends the previous one both conceptually and practically, leading to a unified framework that links robust optimisation, coordinated network control, environmental coupling, and economic evaluation under the shared objective of achieving low-carbon, resilient, and efficient multi-energy systems.

6.1.2 Methodological and Policy-Level Reflections

Methodological Integration

From a methodological perspective, this thesis contributes a layered and interconnected modelling framework that combines robust optimisation, coordinated system modelling, environmental simulation, and offshore energy island scenario application. The distributionally robust approach used in the first study establishes a mathematical foundation for managing uncertainty, while the coordinated network optimisation in the second study expands the methodology to larger system scales. The incorporation of environmental factors in the third study introduces a physical realism often absent in optimisation literature, enabling a more holistic representation of system operation under real-world conditions. Several methodological insights emerge from this integration:

Progressive Model Scaling: The research follows a bottom-up trajectory, evolving from microgrid-scale operation to regional transmission–distribution coordination, and ultimately to offshore en-

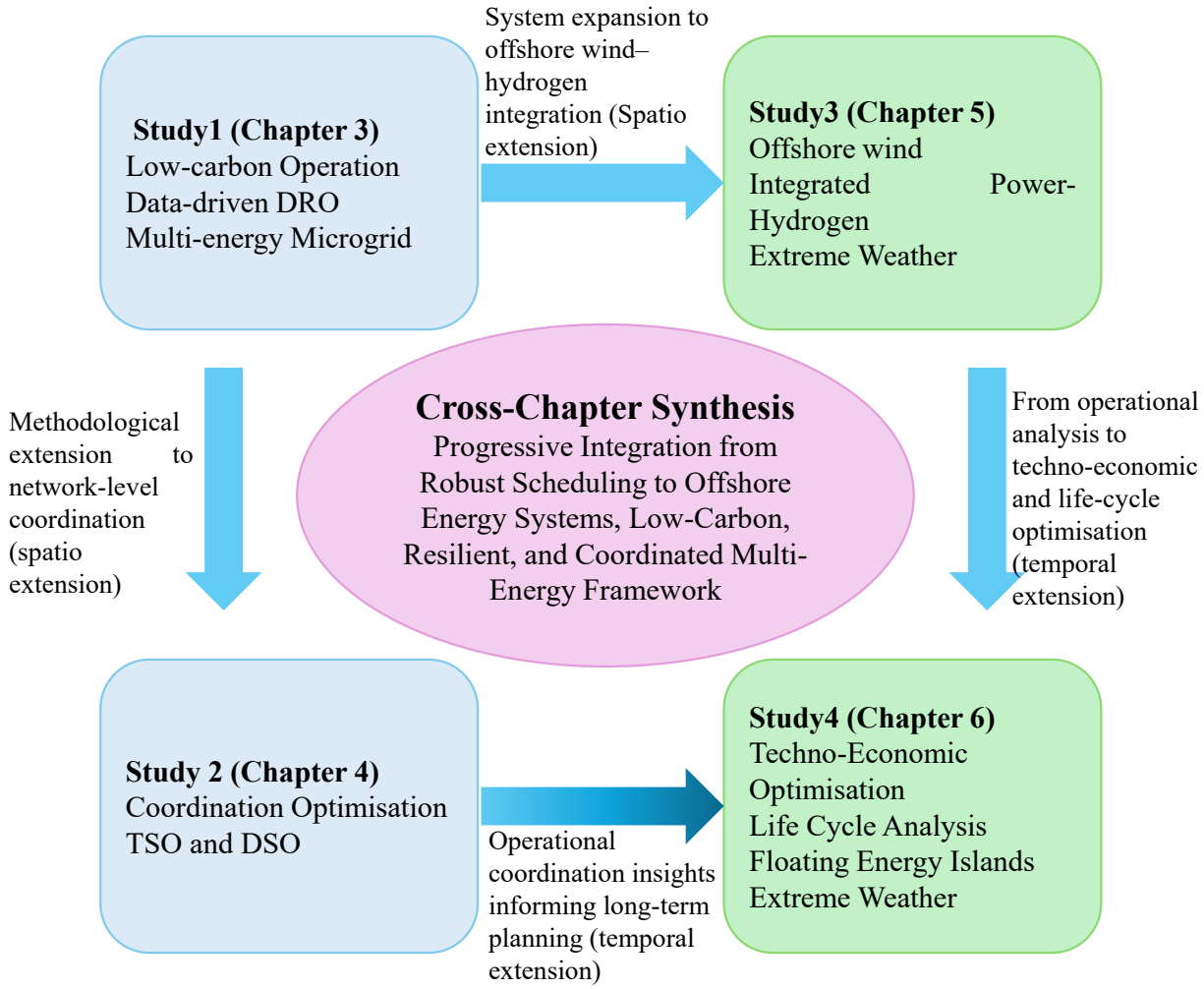

Figure 6.1: Thematic Connection Across the Four Studies

ergy island systems. This progressive scaling allows for cumulative insight building: results from smaller, well-controlled systems inform the modelling of larger and more complex networks.

Data-Driven Scenario Construction: By employing data-driven methods, the computational burden of large-scale stochastic optimisation is significantly reduced. This ensures that the essential characteristics of environmental variability are retained without excessive computational complexity.

Surrogate Modelling for Computation Efficiency: The application of Kriging and other surrogate models bridges the gap between high-fidelity simulations (e.g., OpenFAST) and optimisation algorithms. This enables thousands of operational scenarios to be evaluated efficiently, supporting realistic and computationally tractable planning.

Cross-Domain Integration: The synthesis of electrical, hydrogen, and environmental subsystems represents a cross-domain integration that goes beyond traditional energy optimisation frameworks. It demonstrates how physical modelling, data analytics, and optimisation can be coherently combined to support resilient energy system design.

Policy and Practical Implications

Beyond the methodological contributions, the results of this thesis carry several policy-relevant implications that align with ongoing decarbonisation and energy transition objectives.

Support for Low-Carbon Operation: The robust scheduling strategies developed in the first two studies provide practical mechanisms for achieving low-carbon operation in both local and regional energy systems. By optimising the interaction between energy carriers and integrating carbon constraints, the framework directly contributes to emission reduction goals under national and EU-level energy policies.

Enhanced System Resilience: The environmental integration in the third study reveals how incorporating extreme weather considerations can strengthen system resilience. For microgrids and offshore platforms alike, adaptive control and flexible storage are critical to maintaining reliability under fluctuating environmental conditions.

Economic and Infrastructural Planning: The techno-economic evaluations of the offshore energy island highlight the long-term investment value of hybrid systems that co-produce electricity and hydrogen. Policymakers and investors can leverage these insights to prioritise projects with higher energy utilisation efficiency and reduced curtailment losses.

Scalability and Transferability: The integrated framework is not limited to a specific location or system type. Its modular architecture allows adaptation to different energy mixes, regional resource availabilities, and policy contexts. This scalability ensures that the framework remains relevant across diverse national energy transition pathways.

6.2 Summary of Main Contributions

This thesis has systematically investigated the operational optimisation and long-term planning of integrated renewable energy systems under uncertainty. Motivated by the rapid expansion of renewable energy sources (RESs) and the resulting challenges of intermittency, system coordination, and offshore sustainability, the research developed a series of modelling, optimisation, and simulation frameworks that progressively expand in both scope and depth—from local microgrids to large-scale offshore energy island planning. Together, these studies constitute a coherent research trajectory that bridges short-term operational control with long-term strategic planning. The main contributions can be summarised and elaborated as follows.

Low-carbon operational framework for multi-energy microgrids (MMGs): The first part of this research introduced a novel data-driven distributionally robust optimisation (DRO) model for the day-ahead and intra-day operation of multi-energy microgrids. The framework explicitly considers uncertainties in solar radiation, wind power generation, and electrical demand through data-based ambiguity sets, allowing the system to maintain cost-effectiveness while reducing carbon emissions. Through clustering-based scenario generation and multi-temporal scheduling, the model achieves an intelligent balance between operational cost, emission penalties, and reliability. Simulation results demonstrated a significant improvement in operational efficiency—achieving up to 10.6% carbon reduction—and validated the method's ability to adapt to varying levels of renewable uncertainty. This contribution establishes the methodological foundation for subsequent coordination and integration studies.

Coordinated operation of transmission and distribution systems with hydrogen storage: Building upon the robust scheduling principles of the first study, the second study formulated a coordinated transmission–distribution optimisation model that embeds hydrogen storage and electrolyser operation across both system levels. The proposed TSO–DSO coordination mechanism employs a mixed-integer linear programming (MILP) formulation that captures the physical and operational constraints of electricity–hydrogen conversion, transportation, and storage. The model enables sector coupling between electricity and hydrogen systems, effectively reducing renewable energy curtailment and improving flexibility. Case studies showed that coordinated hydrogen management increased total system revenues by up to 9.3% compared to uncoordinated configurations, demonstrating the economic and technical benefits of joint optimisation. This study represents a key step from localised microgrid operation toward multi-layer energy coordination.

Techno-economic framework for floating offshore energy islands: The final study proposed an integrated techno-economic framework for evaluating floating offshore energy islands, combining life-cycle profit assessment, structural fatigue analysis, and optimal location selection. A Kriging-

based surrogate model was developed to approximate the relationship between environmental conditions and turbine responses, allowing efficient computation of power output and fatigue damage under large-scale environmental datasets. The framework achieved both computational efficiency and decision reliability, demonstrating that optimised siting could increase life-cycle profits by 44.47%. Furthermore, by integrating flexible energy conversion between electricity and hydrogen, the framework enhances the long-term adaptability and sustainability of offshore systems. This final contribution consolidates the methodological developments of earlier chapters into a comprehensive, practical decision-support tool for offshore renewable energy planning.

Taken together, the three studies collectively present a holistic pathway from robust multi-energy scheduling at the distribution level, through multi-layer coordination between system operators, toward environmentally adaptive offshore implementation. The thesis therefore contributes both theoretical innovations in optimisation and surrogate modelling, and practical insights for the design of low-carbon, resilient, and economically viable energy systems supporting the global transition to sustainable offshore infrastructures.

6.3 Limitations and Lessons Learned

While the research presented in this thesis advances several methodological and practical aspects of renewable energy optimisation, several limitations should be acknowledged to contextualise the findings and identify opportunities for further refinement.

Modelling simplifications: The optimisation models—especially the MILP formulations—are based on linearised representations of nonlinear system dynamics. Although this improves computational tractability and enables large-scale simulation, certain physical behaviours such as turbine aerodynamics, nonconvex storage losses, and nonlinear hydrogen production efficiencies were simplified. These approximations may limit model fidelity when applied to real-time control or highly dynamic conditions.

Data dependency: Both the DRO framework and Kriging surrogate models rely heavily on the quality and representativeness of the training and historical datasets. In offshore contexts where measurements are sparse, biased data or limited sampling may reduce the robustness and generalisability of the results. Hence, future work should incorporate uncertainty quantification for the data sources themselves and utilise probabilistic validation against real operational records.

Hydrogen value chain assumptions: The hydrogen production and storage models primarily focus on energy system integration and revenue optimisation, without extending to downstream logistics such as transportation networks, storage terminals, and end-use market uncertainties. Excluding these factors limits the assessment of the hydrogen economy's complete value chain and

its interaction with evolving market mechanisms or regulatory policies.

Computational scalability: Despite significant efficiency gains achieved through surrogate modelling and scenario clustering, the computational complexity of integrated optimisation across multiple systems (e.g., multi-island or cross-border operations) remains challenging. As the model size and temporal resolution increase, advanced decomposition and parallelisation methods will be required to maintain solution efficiency.

Environmental and socio-economic scope: Although the offshore framework included lifecycle assessment and fatigue analysis, other critical sustainability aspects—such as extreme weather risks, marine ecosystem effects, or socio-economic trade-offs—were not fully captured. These omissions highlight the need for more interdisciplinary integration between engineering optimisation, environmental science, and policy analysis.

In summary, these limitations reflect the intrinsic trade-offs between tractability and realism in system-level optimisation, while offering valuable insights into future research directions for improving robustness, scalability, and interdisciplinary comprehensiveness.

6.4 Future Research Directions

Building upon the methodological advancements and lessons learned, several promising research avenues are identified to extend the current work and further contribute to the development of resilient and sustainable energy systems.

Advanced uncertainty modelling: Future studies could enhance the DRO framework by incorporating spatio-temporal correlations among renewable resources and demand profiles, as well as hybridising robust optimisation with machine learning methods for more adaptive scenario generation. Bayesian inference and physics-informed neural networks could be explored to reduce the conservatism of current ambiguity sets while preserving robustness.

Real-time and multi-scale coordination: The next step in TSO–DSO integration should focus on hierarchical and real-time optimisation strategies, where distributed control and reinforcement learning can dynamically adjust energy and hydrogen flows in response to market fluctuations and grid contingencies. This would improve adaptability and enable seamless coordination between operational and planning timescales.

Integrated hydrogen economy modelling: Extending beyond the current system-level perspective, future research should develop end-to-end hydrogen supply chain models, encompassing production, transport, storage, and end-use applications in mobility and industry. Such integration would facilitate a more realistic assessment of hydrogen's long-term economic and strategic roles in decarbonised energy systems.

Resilience under extreme events: As climate and oceanic conditions become more unpredictable, incorporating extreme event scenarios and climate change impacts into offshore energy island optimisation is essential. Coupling techno-economic models with environmental hazard simulations (e.g., hurricanes, wave surges) will enhance the understanding of system resilience and inform robust design strategies.

Multi-objective sustainability assessment: Future frameworks should adopt multi-objective optimisation that simultaneously considers techno-economic, environmental, and social dimensions. Integrating biodiversity impacts, life-cycle emissions, and policy constraints will provide a more holistic foundation for decision-making in offshore renewable developments.

Digital twins and high-fidelity simulations: Finally, the deployment of digital twin technologies can bridge the gap between model-based optimisation and real-world operation. By integrating real-time monitoring, predictive maintenance, and adaptive control into offshore energy islands, digital twins can enable continuous performance improvement and long-term system reliability.

Collectively, these future research directions point toward the evolution of a new generation of integrated, intelligent, and sustainable multi-energy systems. Through the combination of robust optimisation, data-driven modelling, and interdisciplinary design, future work will continue to advance the theoretical and practical frontiers of the low-carbon energy transition.

6.5 Closing Remarks

In conclusion, this thesis has provided a unified methodological and conceptual foundation for understanding, modelling, and optimising the operation, coordination, and long-term sustainability of renewable energy systems across multiple spatial and temporal scales. Through the systematic integration of robust optimisation, data-driven modelling, and offshore energy planning, the research establishes a coherent framework that bridges the gap between theoretical modelling and practical implementation. This integrated approach not only enhances the technical efficiency and economic viability of renewable energy systems but also strengthens their resilience to environmental and operational uncertainties.

The thesis contributes to the ongoing academic discourse by demonstrating how advanced optimisation and surrogate-based modelling techniques can be effectively applied to the planning and operation of complex, multi-energy infrastructures. By capturing the interactions between offshore generation, hydrogen storage, and distribution-level energy management, the work highlights the critical importance of coordination and flexibility in achieving reliable and sustainable system performance. Furthermore, by incorporating extreme weather considerations and long-term environmental variability into the optimisation process, the proposed frameworks offer valuable insights

into the design of adaptive and robust energy systems capable of supporting future decarbonised grids.

Beyond its theoretical contributions, the outcomes of this research carry important practical and policy implications. The developed models and optimisation strategies can inform future decision-making on the deployment of offshore energy islands, hydrogen integration, and multi-energy microgrids. They provide a foundation upon which policymakers, industry practitioners, and researchers can collaboratively advance the sustainable transformation of the energy sector.

Overall, the frameworks, findings, and insights presented in this thesis are expected to serve not only as a reference for further academic exploration but also as a cornerstone for the next generation of industrial applications and energy policies. By bridging methodological innovation with real-world relevance, this work contributes to the collective global endeavour of building a resilient, low-carbon, and economically efficient energy future.

Bibliography

[1] D. Gielen, F. Boshell, D. Saygin, M. D. Bazilian, N. Wagner, R. Gorini, The role of renewable energy in the global energy transformation, Energy strategy reviews 24 (2019) 38–50.

[2] J. Rogelj, M. Den Elzen, N. Höhne, T. Fransen, H. Fekete, H. Winkler, R. Schaeffer, F. Sha, K. Riahi, M. Meinshausen, Paris agreement climate proposals need a boost to keep warming well below 2 c, Nature 534 (7609) (2016) 631–639.

[3] I. R. E. Agency, Weto energy transition key performance indicators tracker, https://www.irena.org/Data/View-data-by-topic/Energy-Transition/WETO-Energy-Transition-Key-Performance-Indicators-Tracker, accessed: 2025-10-28 (2024).

[4] N. T. Mbungu, R. M. Naidoo, R. C. Bansal, M. W. Siti, D. H. Tungadio, An overview of renewable energy resources and grid integration for commercial building applications, Journal of Energy Storage 29 (2020) 101385.

[5] J. Subtil Lacerda, J. C. Van den Bergh, International diffusion of renewable energy innovations: Lessons from the lead markets for wind power in china, germany and usa, Energies 7 (12) (2014) 8236–8263.

[6] M. DeCastro, S. Salvador, M. Gómez-Gesteira, X. Costoya, D. Carvalho, F. J. Sanz-Larruga, L. Gimeno, Europe, china and the united states: Three different approaches to the development of offshore wind energy, Renewable and Sustainable Energy Reviews 109 (2019) 55–70.

[7] E. P. Soares-Ramos, L. de Oliveira-Assis, R. Sarrias-Mena, L. M. Fernández-Ramírez, Current status and future trends of offshore wind power in europe, Energy 202 (2020) 117787.

[8] J. Zhang, J. Yan, D. Infield, Y. Liu, F.-s. Lien, Short-term forecasting and uncertainty analysis of wind turbine power based on long short-term memory network and gaussian mixture model, Applied Energy 241 (2019) 229–244.

[9] M. Ahmed, S. Mirsaeidi, M. A. Koondhar, N. Karami, E. M. Tag-Eldin, N. A. Ghamry, R. A. El-Sehiemy, Z. M. Alaas, I. Mahariq, A. Sharaf, Mitigating uncertainty problems of renewable energy resources through efficient integration of hybrid solar pv/wind systems into power networks, IEEe Access 12 (2024) 30311–30328.

[10] J. Oyekale, M. Petrollese, V. Tola, G. Cau, Impacts of renewable energy resources on effectiveness of grid-integrated systems: Succinct review of current challenges and potential solution strategies, Energies 13 (18) (2020) 4856.

[11] H. Quan, D. Srinivasan, A. M. Khambadkone, A. Khosravi, A computational framework for uncertainty integration in stochastic unit commitment with intermittent renewable energy sources, Applied energy 152 (2015) 71–82.

[12] P. Mancarella, Mes (multi-energy systems): An overview of concepts and evaluation models, Energy 65 (2014) 1–17.

[13] P. Mancarella, G. Andersson, J. Peças-Lopes, K. R. Bell, Modelling of integrated multi-energy systems: Drivers, requirements, and opportunities, in: 2016 Power Systems Computation Conference (PSCC), IEEE, 2016, pp. 1–22.

[14] L. Canale, A. R. Di Fazio, M. Russo, A. Frattolillo, M. Dell'Isola, An overview on functional integration of hybrid renewable energy systems in multi-energy buildings, Energies 14 (4) (2021) 1078.

[15] M. Mohammadi, Y. Noorollahi, B. Mohammadi-Ivatloo, H. Yousefi, Energy hub: From a model to a concept–a review, Renewable and Sustainable Energy Reviews 80 (2017) 1512–1527.

[16] D. Bertsimas, V. Gupta, N. Kallus, Data-driven robust optimization, Mathematical Programming 167 (2018) 235–292.

[17] F. Shen, L. Zhao, W. Du, W. Zhong, F. Qian, Large-scale industrial energy systems optimization under uncertainty: A data-driven robust optimization approach, Applied Energy 259 (2020) 114199.

[18] R. A. Verzijlbergh, L. J. De Vries, Z. Lukszo, Renewable energy sources and responsive demand. do we need congestion management in the distribution grid?, IEEE Transactions on Power Systems 29 (5) (2014) 2119–2128.

[19] F. Najibi, D. Apostolopoulou, E. Alonso, Tso-dso coordination schemes to facilitate distributed resources integration, Sustainability 13 (14) (2021) 7832.

[20] F. Zhang, P. Zhao, M. Niu, J. Maddy, The survey of key technologies in hydrogen energy storage, International journal of hydrogen energy 41 (33) (2016) 14535–14552.

[21] S. K. Afridi, M. A. Koondhar, M. I. Jamali, Z. M. Alaas, M. H. Alsharif, M.-K. Kim, I. Mahariq, E. Touti, M. Aoudia, M. Ahmed, Winds of progress: an in-depth exploration of offshore, floating, and onshore wind turbines as cornerstones for sustainable energy generation and environmental stewardship, Ieee Access 12 (2024) 66147–66166.

[22] R. Chitteth Ramachandran, C. Desmond, F. Judge, J.-J. Serraris, J. Murphy, Floating wind turbines: marine operations challenges and opportunities, Wind Energy Science 7 (2) (2022) 903–924.

[23] A. Garcia-Teruel, G. Rinaldi, P. R. Thies, L. Johanning, H. Jeffrey, Life cycle assessment of floating offshore wind farms: An evaluation of operation and maintenance, Applied Energy 307 (2022) 118067.

[24] H. J. Poremski, Life cycle assessment-development planning through decommissioning, in: Offshore Technology Conference, OTC, 1998, pp. OTC–8788.

[25] A. Bonou, A. Laurent, S. I. Olsen, Life cycle assessment of onshore and offshore wind energy-from theory to application, Applied Energy 180 (2016) 327–337.

[26] W. Huang, E. Du, T. Capuder, X. Zhang, N. Zhang, G. Strbac, C. Kang, Reliability and vulnerability assessment of multi-energy systems: An energy hub based method, IEEE Transactions on Power Systems 36 (5) (2021) 3948–3959.

[27] V. Alevizos, I. Georgousis, A. Kapodistria, Toward climate neutrality: A comprehensive overview of sustainable operations management, optimization, and wastewater treatment methods, Pollutants 3 (4) (2023) 521–543.

[28] L. J. Nilsson, F. Bauer, M. Åhman, F. N. Andersson, C. Bataille, S. de la Rue du Can, K. Ericsson, T. Hansen, B. Johansson, S. Lechtenböhmer, et al., An industrial policy framework for transforming energy and emissions intensive industries towards zero emissions, Climate Policy 21 (8) (2021) 1053–1065.

[29] S. Bresciani, F. Rizzo, A. Deserti, Toward a comprehensive framework of social innovation for climate neutrality: a systematic literature review from business/production, public policy, environmental sciences, energy, sustainability and related fields, Sustainability 14 (21) (2022) 13793.

[30] H. Scheuing, J. Kamm, The eu on the road to climate neutrality–is the 'fit for 55'package fit for purpose?, Renewable Energy Law and Policy Review 10 (3-4) (2022) 4–18.

[31] G. Resch, L. Liebmann, J. Geipel, F. H.-T. Wien, D. Hendricks, J. Vollmer, D. Fouquet-EREF, Study on 2030 renewable energy and energy efficiency targets in the european union, European Renewable Energies Federation: Brussels, Belgium (2023).

[32] M. J. O'Malley, M. B. Anwar, S. Heinen, T. Kober, J. McCalley, M. McPherson, M. Muratori, A. Orths, M. Ruth, T. J. Schmidt, et al., Multicarrier energy systems: shaping our energy future, Proceedings of the IEEE 108 (9) (2020) 1437–1456.

[33] F. Wang, Y. Xue, A review of the development of the energy storage industry in china: Challenges and opportunities, Energies 18 (6) (2025) 1512.

[34] H. Lund, Large-scale integration of wind power into different energy systems, Energy 30 (13) (2005) 2402–2412.

[35] L. Gorroño-Albizu, Ownership models for renewable smart energy systems: Insights from denmark and sweden regarding onshore wind farms and district heating systems (2021).

[36] D. Scamman, B. Solano-Rodríguez, S. Pye, L. F. Chiu, A. Z. Smith, T. Gallo Cassarino, M. Barrett, R. Lowe, Heat decarbonisation modelling approaches in the uk: An energy system architecture perspective, Energies 13 (8) (2020) 1869.

[37] R. Lusby, L. F. Muller, B. Petersen, A solution approach based on benders decomposition for the preventive maintenance scheduling problem of a stochastic large-scale energy system, Journal of Scheduling 16 (6) (2013) 605–628.

[38] A. Jacobson, F. Pecci, N. Sepulveda, Q. Xu, J. Jenkins, A computationally efficient benders decomposition for energy systems planning problems with detailed operations and time-coupling constraints, INFORMS Journal on Optimization 6 (1) (2024) 32–45.

[39] J. J. Torres, C. Li, R. M. Apap, I. E. Grossmann, A review on the performance of linear and mixed integer two-stage stochastic programming software, Algorithms 15 (4) (2022) 103.

[40] T. Ding, Q. Yang, X. Liu, C. Huang, Y. Yang, M. Wang, F. Blaabjerg, Duality-free decomposition based data-driven stochastic security-constrained unit commitment, IEEE Transactions on Sustainable Energy 10 (1) (2018) 82–93.

[41] R. Chen, Z. Bao, L. Lu, M. Yu, An extended c&cg algorithm for solving two-stage robust optimization of economic and feasible scheduling, Journal of Optimization Theory and Applications 205 (2) (2025) 24.

[42] Z. Liu, P. Tang, K. Hou, L. Zhu, Q. Li, F. Zhao, H. Jia, A lagrange-multiplier-based fast planning method for integrated community energy systems considering multiple uncertainties, CSEE Journal of Power and Energy Systems (2025).

[43] Z. Lei, T. L. Lei, Solving spatial optimization problems via lagrangian relaxation and automatic gradient computation, ISPRS International Journal of Geo-Information 14 (1) (2025) 15.

[44] L. Lanza, T. Faulwasser, K. Worthmann, Distributed optimization for energy grids: A tutorial on admm and aladin, arXiv preprint arXiv:2404.03946 (2024).

[45] A. Aydinoglu, M. Posa, Real-time multi-contact model predictive control via admm, in: 2022 International Conference on Robotics and Automation (ICRA), IEEE, 2022, pp. 3414–3421.

[46] A. Board, Stochastic modelling and applied probability, Springer, 2005.

[47] K. Najim, E. Ikonen, A.-K. Daoud, Stochastic processes: estimation, optimisation and analysis, Elsevier, 2004.

[48] J. Acevedo, E. N. Pistikopoulos, Stochastic optimization based algorithms for process synthesis under uncertainty, Computers & Chemical Engineering 22 (4-5) (1998) 647–671.

[49] H. Wu, I. Krad, A. Florita, B.-M. Hodge, E. Ibanez, J. Zhang, E. Ela, Stochastic multi-timescale power system operations with variable wind generation, IEEE Transactions on Power Systems 32 (5) (2016) 3325–3337.

[50] A. J. Keith, D. K. Ahner, A survey of decision making and optimization under uncertainty, Annals of Operations Research 300 (2) (2021) 319–353.

[51] V. Gabrel, C. Murat, A. Thiele, Recent advances in robust optimization: An overview, European journal of operational research 235 (3) (2014) 471–483.

[52] D. Bertsimas, D. B. Brown, C. Caramanis, Theory and applications of robust optimization, SIAM review 53 (3) (2011) 464–501.

[53] G. Liu, M. Starke, B. Xiao, K. Tomsovic, Robust optimisation-based microgrid scheduling with islanding constraints, IET Generation, Transmission & Distribution 11 (7) (2017) 1820–1828.

[54] A. Mehdizadeh, N. Taghizadegan, Robust optimisation approach for bidding strategy of renewable generation-based microgrid under demand side management, IET Renewable Power Generation 11 (11) (2017) 1446–1455.

[55] H. Haider, Y. Jun, G. I. Rashed, F. Peixiao, S. Kamel, Y. Li, A robust optimization model for microgrid considering hybrid renewable energy sources under uncertainties, Environmental Science and Pollution Research 30 (34) (2023) 82470–82484.

[56] R. A. Jabr, I. Džafić, B. C. Pal, Robust optimization of storage investment on transmission networks, IEEE Transactions on Power Systems 30 (1) (2014) 531–539.

[57] S. A. Mansouri, M. S. Javadi, A robust optimisation framework in composite generation and transmission expansion planning considering inherent uncertainties, Journal of ExpErimEntal & thEorEtical artificial intElligEncE 29 (4) (2017) 717–730.

[58] L. Baringo, A. Baringo, A stochastic adaptive robust optimization approach for the generation and transmission expansion planning, IEEE Transactions on Power Systems 33 (1) (2017) 792–802.

[59] D. Coppitters, W. De Paepe, F. Contino, Robust design optimization and stochastic performance analysis of a grid-connected photovoltaic system with battery storage and hydrogen storage, Energy 213 (2020) 118798.

[60] O. L. Oyewole, N. I. Nwulu, E. J. Okampo, Optimal design of hydrogen-based storage with a hybrid renewable energy system considering economic and environmental uncertainties, Energy Conversion and Management 300 (2024) 117991.

[61] A. M. Asim, A. S. Awad, M. A. Attia, Integrated optimization of energy storage and green hydrogen systems for resilient and sustainable future power grids, Scientific Reports 15 (1) (2025) 25656.

[62] H. Rahimian, S. Mehrotra, Distributionally robust optimization: A review, arXiv preprint arXiv:1908.05659 (2019).

[63] J. Blanchet, J. Li, S. Lin, X. Zhang, Distributionally robust optimization and robust statistics, arXiv preprint arXiv:2401.14655 (2024).

[64] D. Kuhn, S. Shafiee, W. Wiesemann, Distributionally robust optimization, Acta Numerica 34 (2025) 579–804.

[65] X. Lu, K. W. Chan, S. Xia, B. Zhou, X. Luo, Security-constrained multiperiod economic dispatch with renewable energy utilizing distributionally robust optimization, IEEE Transactions on Sustainable Energy 10 (2) (2018) 768–779.

[66] S. Dawn, A. Ramakrishna, M. Ramesh, S. S. Das, K. D. Rao, M. M. Islam, T. Selim Ustun, Integration of renewable energy in microgrids and smart grids in deregulated power systems: a comparative exploration, Advanced Energy and Sustainability Research 5 (10) (2024) 2400088.

[67] Y. Qiu, Q. Li, Y. Ai, W. Chen, M. Benbouzid, S. Liu, F. Gao, Two-stage distributionally robust optimization-based coordinated scheduling of integrated energy system with electricity-hydrogen hybrid energy storage, Protection and Control of Modern Power Systems 8 (2) (2023) 1–14.

[68] M. Ma, Z. Long, X. Liu, K. Y. Lee, Distributionally robust optimization of electric–thermal–hydrogen integrated energy system considering source–load uncertainty, Energy 316 (2025) 134568.

[69] Q. Jiang, M. Xue, G. Geng, Energy management of microgrid in grid-connected and stand-alone modes, IEEE transactions on power systems 28 (3) (2013) 3380–3389.

[70] H. Kanchev, F. Colas, V. Lazarov, B. Francois, Emission reduction and economical optimization of an urban microgrid operation including dispatched pv-based active generators, IEEE Transactions on sustainable energy 5 (4) (2014) 1397–1405.

[71] L. Meng, E. R. Sanseverino, A. Luna, T. Dragicevic, J. C. Vasquez, J. M. Guerrero, Microgrid supervisory controllers and energy management systems: A literature review, Renewable and Sustainable Energy Reviews 60 (2016) 1263–1273.

[72] Z. Li, Y. Xu, Optimal coordinated energy dispatch of a multi-energy microgrid in grid-connected and islanded modes, Applied Energy 210 (2018) 974–986.

[73] Z. Chen, Y. Zhang, W. Tang, X. Lin, Q. Li, Generic modelling and optimal day-ahead dispatch of micro-energy system considering the price-based integrated demand response, Energy 176 (2019) 171–183.

[74] Z. Tan, S. Yang, H. Lin, G. De, L. Ju, et al., Multi-scenario operation optimization model for park integrated energy system based on multi-energy demand response, Sustainable Cities and Society 53 (2020) 101973.

[75] Z. Li, Y. Xu, Dynamic dispatch of grid-connected multi-energy microgrids considering opportunity profit, in: 2017 IEEE Power & Energy Society General Meeting, IEEE, 2017, pp. 1–5.

[76] L. He, Z. Lu, L. Geng, J. Zhang, X. Li, X. Guo, Environmental economic dispatch of integrated regional energy system considering integrated demand response, International Journal of Electrical Power & Energy Systems 116 (2020) 105525.

[77] Z. Li, B. Zhao, Z. Chen, C. Ni, J. Yan, X. Yan, X. Bian, N. Liu, Low-carbon operation method of microgrid considering carbon emission quota trading, Energy Reports 9 (2023) 379–387.

[78] X. Zhong, W. Zhong, Y. Liu, C. Yang, S. Xie, Optimal energy management for multi-energy multi-microgrid networks considering carbon emission limitations, Energy 246 (2022) 123428.

[79] A. Coelho, J. Iria, F. Soares, J. P. Lopes, Real-time management of distributed multi-energy resources in multi-energy networks, Sustainable Energy, Grids and Networks 34 (2023) 101022.

[80] X. Guan, Z. Xu, Q.-S. Jia, Energy-efficient buildings facilitated by microgrid, IEEE Transactions on smart grid 1 (3) (2010) 243–252.

[81] S. E. Ahmadi, D. Sadeghi, M. Marzband, A. Abusorrah, K. Sedraoui, Decentralized bi-level stochastic optimization approach for multi-agent multi-energy networked micro-grids with multi-energy storage technologies, Energy 245 (2022) 123223.

[82] Z. Li, Y. Xu, Temporally-coordinated optimal operation of a multi-energy microgrid under diverse uncertainties, Applied energy 240 (2019) 719–729.

[83] A. A. Lekvan, R. Habibifar, M. Moradi, M. Khoshjahan, S. Nojavan, K. Jermsittiparsert, Robust optimization of renewable-based multi-energy micro-grid integrated with flexible energy conversion and storage devices, Sustainable Cities and Society 64 (2021) 102532.

[84] Z. Shi, T. Zhang, Y. Liu, Y. Feng, R. Wang, S. Huang, Optimal design and operation of islanded multi-microgrid system with distributionally robust optimization, Electric Power Systems Research 221 (2023) 109437.

[85] J. Jin, P. Zhou, C. Li, X. Guo, M. Zhang, Low-carbon power dispatch with wind power based on carbon trading mechanism, Energy 170 (2019) 250–260.

[86] X. Zhang, Z. Liang, S. Chen, Optimal low-carbon operation of regional integrated energy systems: A data-driven hybrid stochastic-distributionally robust optimization approach, Sustainable Energy, Grids and Networks 34 (2023) 101013.

[87] S. C. Obiora, O. Bamisile, Y. Hu, D. U. Ozsahin, H. Adun, Assessing the decarbonization of electricity generation in major emitting countries by 2030 and 2050: Transition to a high share renewable energy mix, Heliyon 10 (8) (2024).

[88] A. Ashraf, M. Sagheer, Renewable energy capacity and technological innovations: A review of global trends and future directions, Environmental Progress & Sustainable Energy (2025) e70071.

[89] E. Marino, M. Gkantou, A. Malekjafarian, S. Bali, C. Baniotopoulos, J. van Beeck, R. P. Borg, N. Bruschi, P. Cardiff, E. Chatzi, et al., Offshore renewable energies: A review towards floating modular energy islands—monitoring, loads, modelling and control, Ocean engineering 313 (2024) 119251.

[90] J. Chilvers, T. J. Foxon, S. Galloway, G. P. Hammond, D. Infield, M. Leach, P. J. Pearson, N. Strachan, G. Strbac, M. Thomson, Realising transition pathways for a more electric, low-carbon energy system in the united kingdom: Challenges, insights and opportunities, Proceedings of the Institution of Mechanical Engineers, Part A: Journal of Power and Energy 231 (6) (2017) 440–477.

[91] P. Xiao, W. Hu, X. Xu, W. Liu, Q. Huang, Z. Chen, Optimal operation of a wind-electrolytic hydrogen storage system in the electricity/hydrogen markets, International Journal of Hydrogen Energy 45 (46) (2020) 24412–24423.

[92] A. Alzahrani, S. K. Ramu, G. Devarajan, I. Vairavasundaram, S. Vairavasundaram, A review on hydrogen-based hybrid microgrid system: Topologies for hydrogen energy storage, integration, and energy management with solar and wind energy, Energies 15 (21) (2022) 7979.

[93] H. Gerard, E. I. R. Puente, D. Six, Coordination between transmission and distribution system operators in the electricity sector: A conceptual framework, Utilities Policy 50 (2018) 40–48.

[94] H. G. M. Valente, E. Lambert, J. Cantenot, Transmission system operator and distribution system operator interaction, in: Local Electricity Markets, Elsevier, 2021, pp. 107–125.

[95] B. Uzum, Y. Yoldas, S. Bahceci, A. Onen, Comprehensive review of transmission system operators–distribution system operators collaboration for flexible grid operations, Electric Power Systems Research 227 (2024) 109976.

[96] A. Ioanid, D. Palade, The role of distribution system operators in the decentralized power system, REVUE ROUMAINE DES SCIENCES TECHNIQUES—SÉRIE ÉLECTROTECHNIQUE ET ÉNERGÉTIQUE 69 (1) (2024) 33–38.

[97] A. Cabrera-Tobar, E. Bullich-Massagué, M. Aragüés-Peñalba, O. Gomis-Bellmunt, Review of advanced grid requirements for the integration of large scale photovoltaic power plants in the transmission system, Renewable and Sustainable Energy Reviews 62 (2016) 971–987.

[98] C. Medina, C. R. M. Ana, G. González, Transmission grids to foster high penetration of large-scale variable renewable energy sources–a review of challenges, problems, and solutions, International Journal of Renewable Energy Research (IJRER) 12 (1) (2022) 146–169.

[99] I. Pérez-Arriaga, T. Gómez, L. Olmos, M. Rivier, Transmission and distribution networks for a sustainable electricity supply, in: Handbook of Sustainable Energy, Edward Elgar Publishing, 2011.

[100] L. Lind, R. Cossent, J. P. Chaves-Ávila, T. Gómez San Román, Transmission and distribution coordination in power systems with high shares of distributed energy resources providing balancing and congestion management services, Wiley Interdisciplinary Reviews: Energy and Environment 8 (6) (2019) e357.

[101] P. G. Thakurta, J. Maeght, R. Belmans, D. Van Hertem, Increasing transmission grid flexibility by tso coordination to integrate more wind energy sources while maintaining system security, IEEE Transactions on Sustainable Energy 6 (3) (2014) 1122–1130.

[102] S. Y. Hadush, L. Meeus, Dso-tso cooperation issues and solutions for distribution grid congestion management, Energy policy 120 (2018) 610–621.

[103] M. Tolls, The role of low voltage distribution systems and digital tools in the electricity markets of the future (2024).

[104] D. Fernández Valderrama, Energy management systems for demand response in power distribution systems including prosumers and market participants (2025).

[105] P. Arboleya, M. A. Kippke, S. Kerscher, Flexibility management in the low-voltage distribution grid as a tool in the process of decarbonization through electrification, Energy Reports 8 (2022) 248–256.

[106] T. Alazemi, M. Darwish, M. Radi, Tso/dso coordination for res integration: a systematic literature review, Energies 15 (19) (2022) 7312.

[107] R. Silva, E. Alves, R. Ferreira, J. Villar, C. Gouveia, Characterization of tso and dso grid system services and tso-dso basic coordination mechanisms in the current decarbonization context, Energies 14 (15) (2021) 4451.

[108] C. Gu, J. Wang, L. Wu, Distributed energy resource and energy storage investment for enhancing flexibility under a tso-dso coordination framework, IEEE Transactions on Automation Science and Engineering 21 (3) (2023) 2961–2973.

[109] R. Dzikowski, Dso–tso coordination of day-ahead operation planning with the use of distributed energy resources, Energies 13 (14) (2020) 3559.

[110] L. Bagherzadeh, I. Kamwa, A. Delavari, Coupling energy management of power systems with energy hubs through tso-dso coordination: a review, International Journal of Emerging Electric Power Systems 26 (2) (2025) 183–222.

[111] A. Scheibe, R. Poudineh, Regulating the future European hydrogen supply industry: A balancing act between liberalization, sustainability, and security of supply?, no. 26, OIES Paper: ET, 2023.

[112] K. Oureilidis, K.-N. Malamaki, K. Gallos, A. Tsitsimelis, C. Dikaiakos, S. Gkavanoudis, M. Cvetkovic, J. M. Mauricio, J. M. Maza Ortega, J. L. M. Ramos, et al., Ancillary services market design in distribution networks: Review and identification of barriers, Energies 13 (4) (2020) 917.

[113] G. Tsaousoglou, R. Junker, M. Banaei, S. S. Tohidi, H. Madsen, Integrating distributed flexibility into tso-dso coordinated electricity markets, IEEE Transactions on Energy Markets, Policy and Regulation 2 (2) (2023) 214–225.

[114] R. Wang, S. Bu, C. Chung, Real-time joint regulations of frequency and voltage for tso-dso coordination: A deep reinforcement learning-based approach, IEEE Transactions on Smart Grid 15 (2) (2023) 2294–2308.

[115] A. Moretti, C. Pitas, G. Christofi, E. Bué, M. G. Francescato, Grid integration as a strategy of med-tso in the mediterranean area in the framework of climate change and energy transition, Energies 13 (20) (2020) 5307.

[116] A. Gabash, Energy market transition and climate change: A review of tsos-dsos c+++ framework from 1800 to present, Energies 16 (17) (2023) 6139.

[117] M. EL-Azab, W. Omran, S. Mekhamer, H. Talaat, Congestion management of power systems by optimizing grid topology and using dynamic thermal rating, Electric Power Systems Research 199 (2021) 107433.

[118] L. H. R. C. M. R. S. Bañales, Assessing the impact of renewable energy penetration and geographical allocation on transmission expansion cost: A comparative analysis of two large-scale systems, Sustainable Energy, Grids and Networks 38 (2024) 101349.

[119] M. Daraei, P. E. Campana, E. Thorin, Power-to-hydrogen storage integrated with rooftop photovoltaic systems and combined heat and power plants, Applied Energy 276 (2020) 115499.

[120] H. Haggi, P. Brooker, W. Sun, J. M. Fenton, Hydrogen and battery storage technologies for low-cost energy decarbonization in distribution networks, Journal of The Electrochemical Society 169 (6) (2022) 064501.

[121] G. Pan, W. Gu, Y. Lu, H. Qiu, S. Lu, S. Yao, Optimal planning for electricity-hydrogen integrated energy system considering power to hydrogen and heat and seasonal storage, IEEE Transactions on Sustainable Energy 11 (4) (2020) 2662–2676.

[122] D. Jang, K. Kim, K.-H. Kim, S. Kang, Techno-economic analysis and monte carlo simulation for green hydrogen production using offshore wind power plant, Energy Conversion and Management 263 (2022) 115695.

[123] A. H. Schrotenboer, A. A. Veenstra, M. A. uit het Broek, E. Ursavas, A green hydrogen energy system: Optimal control strategies for integrated hydrogen storage and power generation with wind energy, Renewable and Sustainable Energy Reviews 168 (2022) 112744.

[124] Q. Hassan, P. Viktor, T. J. Al-Musawi, B. M. Ali, S. Algburi, H. M. Alzoubi, A. K. Al-Jiboory, A. Z. Sameen, H. M. Salman, M. Jaszczur, The renewable energy role in the global energy transformations, Renewable Energy Focus 48 (2024) 100545.

[125] P. M. Soares, D. C. Lima, M. Nogueira, Global offshore wind energy resources using the new era-5 reanalysis, Environmental Research Letters 15 (10) (2020) 1040a2.

[126] G. W. E. Council, Global offshore wind report 2020, GWEC: Brussels, Belgium 19 (2020) 10–12.

[127] I. Sorrenti, T. B. H. Rasmussen, S. You, Q. Wu, The role of power-to-x in hybrid renewable energy systems: A comprehensive review, Renewable and Sustainable Energy Reviews 165 (2022) 112380.

[128] D. Niblett, M. Delpisheh, S. Ramakrishnan, M. Mamlouk, Review of next generation hydrogen production from offshore wind using water electrolysis, Journal of Power Sources 592 (2024) 233904.

[129] Q. Zhao, A. Basem, H. O. Shami, K. Mausam, M. Alsehli, A. I. Hameed, A. Alshamrani, H. Rajab, M. Ahmed, A. El-Shafay, Conceptual design and optimization of integrating renewable energy sources with hydrogen energy storage capabilities, International Journal of Hydrogen Energy 79 (2024) 1313–1330.

[130] A. C. Gonçalves, X. Costoya, R. Nieto, M. L. Liberato, Extreme weather events on energy systems: a comprehensive review on impacts, mitigation, and adaptation measures, Sustainable Energy Research 11 (1) (2024) 4.

[131] S. J. Price, R. B. Figueira, Corrosion protection systems and fatigue corrosion in offshore wind structures: current status and future perspectives, Coatings 7 (2) (2017) 25.

[132] M. Rezaei, A. Akimov, E. M. A. Gray, Techno-economics of offshore wind-based dynamic hydrogen production, Applied Energy 374 (2024) 124030.

[133] L. F. Gusatu, C. Yamu, C. Zuidema, A. Faaij, A spatial analysis of the potentials for offshore wind farm locations in the north sea region: challenges and opportunities, ISPRS International Journal of Geo-Information 9 (2) (2020) 96.

[134] J. Schulz-Stellenfleth, S. Emeis, M. Dörenkämper, J. Bange, B. Cañadillas, T. Neumann, J. Schneemann, I. Weber, K. Zum Berge, A. Platis, et al., Coastal impacts on offshore wind farms—a review focussing on the german bight area, Meteorol. Z 31 (2022) 289–315.

[135] O. C. Spro, R. E. Torres-Olguin, M. Korpås, North sea offshore network and energy storage for large scale integration of renewables, Sustainable Energy Technologies and Assessments 11 (2015) 142–147.

[136] W. Musial, B. Ram, Large-scale offshore wind power in the united states: Assessment of opportunities and barriers, Tech. rep., National Renewable Energy Lab.(NREL), Golden, CO (United States) (2010).

[137] S. Heier, Grid integration of wind energy: onshore and offshore conversion systems, John Wiley & Sons, 2014.

[138] J. Zhang, I. Fowai, K. Sun, A glance at offshore wind turbine foundation structures, Brodogradnja: An International Journal of Naval Architecture and Ocean Engineering for Research and Development 67 (2) (2016) 101–113.

[139] M. van Wijngaarden, Concept design of steel bottom founded support structures for offshore wind turbines, Delft University of Technology, The Netherlands: Faculty of Civil Engineering and Geosciences (2013).

[140] C. V. Amaechi, A. Reda, H. O. Butler, I. A. Ja'e, C. An, Review on fixed and floating offshore structures. part i: Types of platforms with some applications, Journal of Marine Science and Engineering 10 (8) (2022) 1074.

[141] D. Gao, X. Pan, B. Liang, B. Yang, G. Wu, Z. Wang, A review and design principle of fixed-bottom foundation scour protection schemes for offshore wind energy, Journal of Marine Science and Engineering 12 (4) (2024) 660.

[142] D. Matha, F. Lemmer, M. Muskulus, Offshore turbines with bottom-fixed or floating substructures, Wind energy modeling and simulation. Volume 2: Turbine and system (2019).

[143] S. Bashetty, S. Ozcelik, Review on dynamics of offshore floating wind turbine platforms, Energies 14 (19) (2021) 6026.

[144] M. Hmedi, E. Uzunoglu, C. Zeng, J. Gaspar, C. Guedes Soares, Experimental challenges and modelling approaches of floating wind turbines, Journal of Marine Science and Engineering 11 (11) (2023) 2048.

[145] M. Leimeister, M. Collu, A. Kolios, A fully integrated optimization framework for designing a complex geometry offshore wind turbine spar-type floating support structure, Wind Energy Science 7 (1) (2022) 259–281.

[146] N. Bento, M. Fontes, Emergence of floating offshore wind energy: Technology and industry, Renewable and Sustainable Energy Reviews 99 (2019) 66–82.

[147] A. Moore, J. Price, M. Zeyringer, The role of floating offshore wind in a renewable focused electricity system for great britain in 2050, Energy strategy reviews 22 (2018) 270–278.

[148] C. Pérez-Collazo, D. Greaves, G. Iglesias, A review of combined wave and offshore wind energy, Renewable and sustainable energy reviews 42 (2015) 141–153.

[149] K. Ha, H. V. A. Truong, T. D. Dang, K. K. Ahn, Recent control technologies for floating offshore wind energy system: A review, International Journal of Precision Engineering and Manufacturing-Green Technology 8 (1) (2021) 281–301.

[150] P. Katare, S. Bopche, P. Tamkhade, R. Gurav, S. Nalavade, M. M. Awad, Technological feasibility and challenges of hybrids: wave, hydro, offshore-wind and floating solar energy harnessing, Multidisciplinary Reviews 7 (3) (2024) 2024054–2024054.

[151] H. Dorotić, B. Doračić, V. Dobravec, T. Pukšec, G. Krajačić, N. Duić, Integration of transport and energy sectors in island communities with 100% intermittent renewable energy sources, Renewable and Sustainable Energy Reviews 99 (2019) 109–124.

[152] K. L. Yates, C. J. Bradshaw, Offshore energy and marine spatial planning, Routledge London, 2018.

[153] V. Battaglia, L. Vanoli, Optimizing renewable energy integration in new districts: Power-to-x strategies for improved efficiency and sustainability, Energy 305 (2024) 132312.

[154] M. Flikkema, M. Breuls, R. Jak, R. de Ruijter, I. Drummen, A. Jordaens, F. Adam, K. Czapiewska, F. Y. Lin, D. Schott, et al., Floating island development and deployment roadmap, Technical Report No. 774253 (2021).

[155] B. Zhou, Z. Zhang, G. Li, D. Yang, M. Santos, Review of key technologies for offshore floating wind power generation, Energies 16 (2) (2023) 710.

[156] J. Wang, J. Liu, Y. Lu, H. Li, X. Zhang, Machine learning-driven high-fidelity ensemble surrogate modeling of francis turbine unit based on data-model interactive simulation, Engineering Applications of Artificial Intelligence 133 (2024) 108385.

[157] A. Keprate, N. Bagalkot, M. S. Siddiqui, S. Sen, Reliability analysis of 15mw horizontal axis wind turbine rotor blades using fluid-structure interaction simulation and adaptive kriging model, Ocean Engineering 288 (2023) 116138.

[158] M. Scolaro, N. Kittner, Optimizing hybrid offshore wind farms for cost-competitive hydrogen production in germany, International Journal of Hydrogen Energy 47 (10) (2022) 6478–6493.

[159] M. Fischetti, J. R. Kristoffersen, T. Hjort, M. Monaci, D. Pisinger, Vattenfall optimizes offshore wind farm design, INFORMS Journal on Applied Analytics 50 (1) (2020) 80–94.

[160] H. Mohammed, Developing control strategies for variable hydrogen production from offshore wind: enabling power to x applications, Master's thesis, Universitat Politècnica de Catalunya (2024).

[161] S. Fadaei, F. F. Afagh, R. G. Langlois, A survey of numerical simulation tools for offshore wind turbine systems, Wind 4 (1) (2024) 1–24.

[162] M. Maali Amiri, M. Shadman, S. F. Estefen, A review of numerical and physical methods for analyzing the coupled hydro–aero–structural dynamics of floating wind turbine systems, Journal of Marine Science and Engineering 12 (3) (2024) 392.

[163] S. Jawalageri, S. Bhattacharya, S. Jalilvand, A. Malekjafarian, A comparative study on load assessment methods for offshore wind turbines using a simplified method and openfast simulations, Energies 17 (9) (2024) 2189.

[164] N. R. E. L. (NREL), Openfast, available online (2022).
URL `https://github.com/OpenFAST/openfast`

[165] P. Martynowicz, P. Ślimak, G. M. Katsaounis, Tlp-supported nrel 5mw floating offshore wind turbine tower vibration reduction under aligned and misaligned wind-wave excitations, Energies 18 (8) (2025) 2092.

[166] R. O. Cruz, F. N. Correa, B. S. de Lima, B. P. Jacob, Integration of a coupled offshore system code with openfast for mooring dynamic analysis of floating offshore wind turbines, in: ISOPE International Ocean and Polar Engineering Conference, ISOPE, 2025, pp. ISOPE–I.

[167] S. Zhou, C. Li, Y. Xiao, X. Wang, W. Xiang, Q. Sun, Evaluation of floating wind turbine substructure designs by using long-term dynamic optimization, Applied Energy 352 (2023) 121941.

[168] S. C. Pryor, R. J. Barthelmie, M. S. Bukovsky, L. R. Leung, K. Sakaguchi, Climate change impacts on wind power generation, Nature Reviews Earth & Environment 1 (12) (2020) 627–643.

[169] E. Faraggiana, A. Ghigo, M. Sirigu, E. Petracca, G. Giorgi, G. Mattiazzo, G. Bracco, Optimal floating offshore wind farms for mediterranean islands, Renewable Energy 221 (2024) 119785.

[170] M. Martín-Betancor, J. Osorio, A. Ruíz-García, I. Nuez, Technical-economic limitations of floating offshore wind energy generation in small isolated island power systems without energy storage: Case study in the canary islands, Energy Policy 188 (2024) 114056.

[171] O. A. Adelekan, B. S. Ilugbusi, O. Adisa, O. C. Obi, K. F. Awonuga, O. F. Asuzu, N. L. Ndubuisi, Energy transition policies: a global review of shifts towards renewable sources, Engineering Science & Technology Journal 5 (2) (2024) 272–287.

[172] Q. Gao, R. Yuan, N. Ertugrul, B. Ding, J. A. Hayward, Y. Li, Analysis of energy variability and costs for offshore wind and hybrid power unit with equivalent energy storage system, Applied Energy 342 (2023) 121192.

[173] M. Esteban, D. Leary, Current developments and future prospects of offshore wind and ocean energy, Applied Energy 90 (1) (2012) 128–136.

[174] C. J. Crabtree, D. Zappalá, S. I. Hogg, Wind energy: Uk experiences and offshore operational challenges, Proceedings of the Institution of Mechanical Engineers, Part A: Journal of Power and Energy 229 (7) (2015) 727–746.

[175] A. Myhr, C. Bjerkseter, A. Ågotnes, T. A. Nygaard, Levelised cost of energy for offshore floating wind turbines in a life cycle perspective, Renewable energy 66 (2014) 714–728.

[176] S.-Y. Chou, T. H.-K. Yu, et al., Developing an exhaustive optimal maintenance schedule for offshore wind turbines based on risk-assessment, technical factors and cost-effective evaluation, Energy 249 (2022) 123613.

[177] E. E. Ambarita, A. Karlsen, O. Osen, A. Hasan, Towards fully autonomous floating offshore wind farm operation & maintenance, Energy Reports 9 (2023) 103–108.

[178] L. Chen, J. Yang, C. Lou, Characterizing ramp events in floating offshore wind power through a fully coupled electrical-mechanical mathematical model, Renewable Energy 221 (2024) 119803.

[179] M. Bilgili, H. Alphan, Global growth in offshore wind turbine technology, Clean Technologies and Environmental Policy 24 (7) (2022) 2215–2227.

[180] Q. Fan, X. Wang, J. Yuan, X. Liu, H. Hu, P. Lin, A review of the development of key technologies for offshore wind power in china, Journal of Marine Science and Engineering 10 (7) (2022) 929.

[181] B. Desalegn, D. Gebeyehu, B. Tamrat, T. Tadiwose, A. Lata, Onshore versus offshore wind power trends and recent study practices in modeling of wind turbines' life-cycle impact assessments, Cleaner Engineering and Technology 17 (2023) 100691.

[182] M. Barooni, T. Ashuri, D. Velioglu Sogut, S. Wood, S. Ghaderpour Taleghani, Floating offshore wind turbines: Current status and future prospects, Energies 16 (1) (2022) 2.

[183] E. Uzunoglu, D. Karmakar, C. Guedes Soares, Floating offshore wind platforms, in: Floating offshore wind farms, Springer, 2016, pp. 53–76.

[184] W. Musial, S. Butterfield, B. Ram, Energy from offshore wind, in: Offshore technology conference, OTC, 2006, pp. OTC–18355.

[185] A. Al Mowafy, S. Lotfian, F. Brennan, Decommissioning offshore wind fixed steel pile foundations: a critical review, Energies 17 (21) (2024) 5460.

[186] A. R. Henderson, D. Witcher, Floating offshore wind energy—a review of the current status and an assessment of the prospects, Wind Engineering 34 (1) (2010) 1–16.

[187] M. Esteban, B. Couñago, J. López-Gutiérrez, V. Negro, F. Vellisco, Gravity based support structures for offshore wind turbine generators: Review of the installation process, Ocean Engineering 110 (2015) 281–291.

[188] A. Khosravi, T. Yeong, A. Parvez, J. Jaganathana, T. Lau, W. Elleithy, A comparative study between three-legged and tripod substructures in design of offshore wind turbines in the transition water depth, International Journal of Engineering & Technology 7 (3.36) (2018) 23–33.

[189] F. Tom, et al., Study of dynamic cables layout of floating wind turbines to optimize installation and cost (2024).

[190] A. Campanile, V. Piscopo, A. Scamardella, Mooring design and selection for floating offshore wind turbines on intermediate and deep water depths, Ocean Engineering 148 (2018) 349–360.

[191] J. E. Halkyard, Status of spar platforms for deepwater production systems, in: ISOPE International Ocean and Polar Engineering Conference, ISOPE, 1996, pp. ISOPE–I.

[192] Y. Liu, S. Li, Q. Yi, D. Chen, Developments in semi-submersible floating foundations supporting wind turbines: A comprehensive review, Renewable and Sustainable Energy Reviews 60 (2016) 433–449.

[193] R. D. McDonald, The design and field testing of the" triton" tension-leg fixed platform and its future application for petroleum production and processing in deep water, in: Offshore Technology Conference, OTC, 1974, pp. OTC–2104.

[194] N. Dimitrov, M. C. Kelly, A. Vignaroli, J. Berg, From wind to loads: wind turbine site-specific load estimation with surrogate models trained on high-fidelity load databases, Wind Energy Science 3 (2) (2018) 767–790.

[195] A. G. Gonzalez-Rodriguez, J. Serrano-Gonzalez, M. Burgos-Payan, J. Riquelme-Santos, Multi-objective optimization of a uniformly distributed offshore wind farm considering both economic factors and visual impact, Sustainable Energy Technologies and Assessments 52 (2022) 102148.

[196] S. Rodrigues, C. Restrepo, G. Katsouris, R. Teixeira Pinto, M. Soleimanzadeh, P. Bosman, P. Bauer, A multi-objective optimization framework for offshore wind farm layouts and electric infrastructures, Energies 9 (3) (2016) 216.

[197] J. Weinzettel, M. Reenaas, C. Solli, E. G. Hertwich, Life cycle assessment of a floating offshore wind turbine, Renewable Energy 34 (3) (2009) 742–747.

[198] J. Chipindula, V. S. V. Botlaguduru, H. Du, R. R. Kommalapati, Z. Huque, Life cycle environmental impact of onshore and offshore wind farms in texas, Sustainability 10 (6) (2018) 2022.

[199] B. Poujol, A. Prieur-Vernat, J. Dubranna, R. Besseau, I. Blanc, P. Pérez-López, Site-specific life cycle assessment of a pilot floating offshore wind farm based on suppliers' data and geo-located wind data, Journal of Industrial Ecology 24 (1) (2020) 248–262.

[200] L. Tsai, J. C. Kelly, B. S. Simon, R. M. Chalat, G. A. Keoleian, Life cycle assessment of offshore wind farm siting: effects of locational factors, lake depth, and distance from shore, Journal of Industrial Ecology 20 (6) (2016) 1370–1383.

[201] V. J. Ferreira, G. Benveniste, J. I. Rapha, C. Corchero, J. L. Domínguez-García, A holistic tool to assess the cost and environmental performance of floating offshore wind farms, Renewable Energy 216 (2023) 119079.

[202] C. Zhang, H.-P. Chen, K. F. Tee, D. Liang, Reliability-based lifetime fatigue damage assessment of offshore composite wind turbine blades, Journal of Aerospace Engineering 34 (3) (2021) 04021019.

[203] J. Gao, B. Sweetman, S. Tang, Multiaxial fatigue assessment of floating offshore wind turbine blades operating on compliant floating platforms, Ocean Engineering 261 (2022) 111921.

[204] X. Li, W. Zhang, Long-term fatigue damage assessment for a floating offshore wind turbine under realistic environmental conditions, Renewable Energy 159 (2020) 570–584.

[205] A. Saenz-Aguirre, A. Ulazia, G. Ibarra-Berastegi, J. Saenz, Floating wind turbine energy and fatigue loads estimation according to climate period scaled wind and waves, Energy Conversion and Management 271 (2022) 116303.

[206] O. Gaidai, V. Yakimov, F. Wang, F. Zhang, R. Balakrishna, Floating wind turbines structural details fatigue life assessment, Scientific Reports 13 (1) (2023) 16312.

[207] Y. Shui, J. Liu, H. Gao, S. Huang, Z. Jiang, A distributionally robust coordinated dispatch model for integrated electricity and heating systems considering uncertainty of wind power, Proceedings of the CSEE 38 (24) (2018) 7235–7247.

[208] T. Ding, Q. Yang, Y. Yang, C. Li, Z. Bie, F. Blaabjerg, A data-driven stochastic reactive power optimization considering uncertainties in active distribution networks and decomposition method, IEEE Transactions on Smart Grid 9 (5) (2017) 4994–5004.

[209] B. Zeng, L. Zhao, Solving two-stage robust optimization problems using a column-and-constraint generation method, Operations Research Letters 41 (5) (2013) 457–461.

[210] Y. He, Z. Li, J. Zhang, G. Shi, W. Cao, Day-ahead and intraday multi-time scale microgrid scheduling based on light robustness and mpc, International Journal of Electrical Power & Energy Systems 144 (2023) 108546.

[211] J. Wang, J. Sui, H. Jin, An improved operation strategy of combined cooling heating and power system following electrical load, Energy 85 (2015) 654–666.

[212] C. Zhang, Y. Xu, Z. Y. Dong, K. P. Wong, Robust coordination of distributed generation and price-based demand response in microgrids, IEEE Transactions on Smart Grid 9 (5) (2017) 4236–4247.

[213] M. A. Kashem, V. Ganapathy, G. Jasmon, M. Buhari, A novel method for loss minimization in distribution networks, in: DRPT2000. International conference on electric utility deregulation and restructuring and power technologies. Proceedings (Cat. No. 00EX382), IEEE, 2000, pp. 251–256.

[214] W. Gu, J. Wang, S. Lu, Z. Luo, C. Wu, Optimal operation for integrated energy system considering thermal inertia of district heating network and buildings, Applied energy 199 (2017) 234–246.

[215] L. Ma, N. Liu, J. Zhang, W. Tushar, C. Yuen, Energy management for joint operation of chp and pv prosumers inside a grid-connected microgrid: A game theoretic approach, IEEE Transactions on Industrial Informatics 12 (5) (2016) 1930–1942.

[216] C. Zhang, Y. Li, Thermodynamic performance of cycle combined large temperature drop heat exchange process: Theoretical models and advanced process, Energy 150 (2018) 1–18.

[217] S. Lu, Y. Li, W. Gu, Y. Xu, S. Ding, Economy-carbon coordination in integrated energy systems: Optimal dispatch and sensitivity analysis, Applied Energy 351 (2023) 121871.

[218] K. R. Shahapure, C. Nicholas, Cluster quality analysis using silhouette score, in: 2020 IEEE 7th International Conference on Data Science and Advanced Analytics (DSAA), 2020, pp. 747–748. doi:10.1109/DSAA49011.2020.00096.

[219] Scottish power tariff information.
URL https://www2.scottishpower.co.uk/tariff-information.process?execution=e1s8

[220] A. Martens, The energetic feasibility of chp compared to the separate production of heat and power, Applied thermal engineering 18 (11) (1998) 935–946.

[221] L. Zhang, F. Li, B. Sun, C. Zhang, Integrated optimization design of combined cooling, heating, and power system coupled with solar and biomass energy, Energies 12 (4) (2019) 687.

[222] S. K. Thompson, Sampling, Vol. 755, John Wiley & Sons, 2012.

[223] V. Walter, L. Göransson, M. Taljegard, S. Öberg, M. Odenberger, Low-cost hydrogen in the future european electricity system–enabled by flexibility in time and space, Applied Energy 330 (2023) 120315.

[224] ENTSO-E, Entso-e transparency platform, https://transparency.entsoe.eu/dashboard/show, accessed: 2024-05-24.

[225] M. T. Baumhof, E. Raheli, A. G. Johnsen, J. Kazempour, Optimization of hybrid power plants: When is a detailed electrolyzer model necessary?, in: 2023 IEEE Belgrade PowerTech, IEEE, 2023, pp. 1–10.

[226] G. Sdanghi, G. Maranzana, A. Celzard, V. Fierro, Towards non-mechanical hybrid hydrogen compression for decentralized hydrogen facilities, Energies 13 (12) (2020) 3145.

[227] M. Handwerker, J. Wellnitz, H. Marzbani, Comparison of hydrogen powertrains with the battery powered electric vehicle and investigation of small-scale local hydrogen production using renewable energy, Hydrogen 2 (1) (2021) 76–100.

[228] X. Xu, Dynamic analysis of a spar-type offshore floating wind turbine and its mooring system (2020).

[229] Y. Huang, D. Wan, Investigation of interference effects between wind turbine and spar-type floating platform under combined wind-wave excitation, Sustainability 12 (1) (2019) 246.

[230] M. Scalera, Assessment and analysis of accidental and ultimate load cases in the design of floating offshore wind turbines (2024).

[231] J. Jonkman, Definition of a 5-mw reference wind turbine for offshore system development, National Renewable Energy Laboratory (2009).

[232] M. Shinozuka, C.-M. Jan, Digital simulation of random processes and its applications, Journal of sound and vibration 25 (1) (1972) 111–128.

[233] D. N. V. GL, Dnvgl-rp-c203: Fatigue design of offshore steel structures, DNV GL: Oslo, Norway (2016).

[234] M. I. Kvittem, T. Moan, Time domain analysis procedures for fatigue assessment of a semi-submersible wind turbine, Marine Structures 40 (2015) 38–59.

[235] T. Li, Q. Yang, X. Zhang, Y. Ma, Efficient fatigue damage estimation of offshore wind turbine foundation under wind-wave actions, Journal of Constructional Steel Research 221 (2024) 108903.

[236] H. Li, Z. Hu, J. Wang, X. Meng, Short-term fatigue analysis for tower base of a spar-type wind turbine under stochastic wind-wave loads, International Journal of Naval Architecture and Ocean Engineering 10 (1) (2018) 9–20.

[237] C. Luan, T. Moan, On short-term fatigue analysis for wind turbine tower of two semi-submersible wind turbines including effect of startup and shutdown processes, Journal of Offshore Mechanics and Arctic Engineering 143 (1) (2021) 012003.

[238] C. Hübler, R. Rolfes, Analysis of the influence of climate change on the fatigue lifetime of offshore wind turbines using imprecise probabilities, Wind Energy 24 (3) (2021) 275–289.

[239] C. Li, J. M. Mogollón, A. Tukker, J. Dong, D. von Terzi, C. Zhang, B. Steubing, Future material requirements for global sustainable offshore wind energy development, Renewable and Sustainable Energy Reviews 164 (2022) 112603.

[240] T. Li, Z. Liu, S. Liu, Y. Fan, Q. Yang, H. Xiao, Numerical study on passive structural control of semi-submersible floating wind turbine considering non-collinear wind and waves, Ocean Engineering 266 (2022) 112745.

[241] I. E. Commission, et al., Wind energy generation systems-part 3-1: Design requirements for fixed offshore wind turbines, International standard IEC (2019) 61400–3.

[242] E. Cheynet, J. M. Diezel, H. Haakenstad, Ø. Breivik, A. Peña, J. Reuder, Tall wind profile validation using lidar observations and hindcast data, Wind Energy Science Discussions 2024 (2024) 1–29.

[243] W. contributors, Borssele offshore wind farm, `https://en.wikipedia.org/wiki/Borssele_Offshore_Wind_Farm`, accessed: 2025-01-30.

[244] W. contributors, Geography of the netherlands, https://en.wikipedia.org/wiki/Geography_of_the_Netherlands, accessed: 2025-01-30 (2025).

[245] E. Wayman, Coupled dynamic modeling of floating wind turbine systems, Massachusetts Institute of Technology and National Renewable Energy Laboratory (2006).

[246] Z. Han, Y. Zhao, J. Su, Y. He, Y. Xu, F. Wu, Z. Jiang, On the hydrodynamic responses of a multi-column tlp floating offshore wind turbine model, Ocean Engineering 253 (2022) 111262.

[247] J. Koto, J. A. Khair, A. Selamat, Ultra deep water pipeline design and assessment, Proceeding of Ocean, Mechanical, and Aerospace-Science Engineering 2 (2014).

[248] M. Carmo, D. L. Fritz, J. Mergel, D. Stolten, A comprehensive review on pem water electrolysis, International journal of hydrogen energy 38 (12) (2013) 4901–4934.

[249] A. Agostini, N. Belmonte, A. Masala, J. Hu, P. Rizzi, M. Fichtner, P. Moretto, C. Luetto, M. Sgroi, M. Baricco, Role of hydrogen tanks in the life cycle assessment of fuel cell-based auxiliary power units, Applied Energy 215 (2018) 1–12.

[250] TutorChase, How long do hydrogen fuel cells last? (2023).
URL https://www.tutorchase.com/answers/igcse/chemistry/how-long-do-hydrogen-fuel-cells-last

[251] E. Commission, Eu cordis project - h2020 fch-01-8-2016, accessed: 2024-01-13.
URL https://cordis.europa.eu/programme/id/H2020_FCH-01-8-2016

[252] ENTSO-e, Transparency platform, day-ahead prices, https://transparency.entsoe.eu/dashboard/show, accessed: 2025-01-07 (2022).

[253] M. Kausche, F. Adam, F. Dahlhaus, J. Großmann, Floating offshore wind-economic and ecological challenges of a tlp solution, Renewable Energy 126 (2018) 270–280.

[254] FINO1, Location information, https://www.fino1.de/en/location.html, accessed: 30 October 2023.